International
Progress Report

IPR-01-39

Äspö Hard Rock Laboratory

Prototype Repository

Hydraulic DFN model no:2

Martin Stigsson
Nils Outters
Jan Hermansson

Golder Assosiates

October 2001

Svensk Kärnbränslehantering AB
Swedish Nuclear Fuel
and Waste Management Co
Box 5864
SE-102 40 Stockholm Sweden
Tel +46 8 459 84 00
Fax +46 8 661 57 19

Äspö Hard Rock
Laboratory

Report no.	No.
IPR-01-39	F63K
Author	Date
Stigsson, Outters, Hermansson	01-10-31
Checked by	Date
Approved	Date
Christer Svemar	02-11-19

Äspö Hard Rock Laboratory

Prototype Repository

Hydraulic DFN model no:2

Martin Stigsson
Nils Outters
Jan Hermansson

Golder Assosiates

October 2001

Keywords: Prototype Repository, DFN model, modelling, groundwater flow

Abstract

The main objective of the present work is to perform the groundwater flow modelling in the Prototype Repository. The present modelling exercise starts with deriving DFN-parameters from the exploratory drill campaigns 2 and 3. The second phase of the work consists of the set-up of the DFN groundwater flow model, which requires a detailed statistical interpretation of the fracture flow and characteristics. After a sensitivity study the predictions of fracture characteristics and flow in the deposition holes of the Prototype Repository are made. Thereafter modelled tracemaps, inflow and head are compared to measured. To the last some improvements are discussed.

Main results are:

- Size variation of the deterministic features has a limited effect on the inflow to the deposition holes.
- The effect on the inflow to the deposition holes is limited when the transmissivity of the deterministic fractures is decreased. An increase of the transmissivity will on the other hand have a large effect on the inflow.
- Including more low-conductive fractures will not increase the inflow to the canister holes.
- Modelled average fracture trace intensity, P_{21}, is slightly smaller than measured. Modelled inflow is about 50 times larger than measured.
- The given heads, used for the boundaries, are afflicted with a systematic error.

The main source of uncertainty is the existence of a skin zone around the tunnels.

A major improvement could be a model with 3 distinct fracture sets and some background fracturing, which may result in a less connective fracture network and less inflow to cavities. Another improvement would be to apply new heads to the outer boundaries that reflect the current situation at Äspö.

Sammanfattning

Huvudsyftet med föreliggande arbete är att genomföra grundvattenmodelleringen i Prototypförvaret. I rapporten utvärderas DFN-parametrarna, utifrån mätta värden från undersökningshålen i 2:a och 3:e borrkampanjen, först. Därefter upprättas DFN-flödes-modellen, vilket kräver en detaljerad statistisk tolkning av sprickflödesnätverkets karaktär. Efter sensitivitetsanalysen vidtar beräkningar för förutsägande av sprickspårskaraktär i och inflöde till de sex depositionshålen. Därefter jämförs modellerade sprickkartor, inflöde och tryck med motsvarande uppmätta värden. Till sist diskuteras några möjliga förbättringar.

Huvudresultaten är:

- Storleken på de deterministiska sprickorna har liten påverkan på inflödet till depositionshålen
- En sänkning av transmissiviteten på de deterministiska sprickorna har liten påverkan på inflödet till depositionshålen. En ökning har däremot stor inverkan.
- Att lägga till fler lågkunduktiva sprickor ger ingen ökning i inflödet till depositionshålen
- Modellerad sprickspårsintensitet, P_{21}, är något lägre än uppmätt. Modellerat inflöde är ca 50 gånger större än uppmätt
- De givna trycken, använda som randvillkor, är inte i överensstämmelse med uppmätta värden.

Den största källan till osäkerhet är närvaron av ett eventuellt skin runt tunnlarna.

En stor förbättring skulle kunna vara att bygga en modell med tre distinkta sprickset samt ett fjärde mer diffust set för att reflektera bakgrundssprickigheten. Detta skulle resultera i mindre förbundna spricknätverk och därmed lägre inflöde till tunnlar och hål. En annan förbättring skulle kunna vara att applicera nya tryck på ränderna som motsvarar nuvarande tryckbild på Äspö.

List of content

List of Figures

List of tables

1 Introduction

1.1 Objectives of the prototype repository

In preparation for the underground disposal of spent nuclear fuel, SKB carry out an extensive work on research, development and demonstration in the Äspö Hard Rock Laboratory. The Prototype Repository Test is a project designed within the frame of the research program to test important components of SKB's deep repository system in full scale in a realistic environment. The Prototype Repository should simulate the physical processes encountered in a real repository and demonstrate the performance of the integrated function of the repository components. The characterisation program of the site is one of the early and major objectives of the test. It should provide a basis for the determination of the location of the deposition holes and permit to collect data on boundary and rock conditions to increase the confidence in understanding the experimental data.

The characterisation of the site is done in three stages; the fracture mapping of the tunnel, the study of fracture and hydraulic data from pilot and exploration holes and the excavation of the deposition holes.

1.2 Objectives of the present work

One of the general objectives of the Prototype Repository is to provide a full-scale reference for testing numerical models. The validation of the performance of numerical models depends of several factors among which the quality and quantity of experimental data is essential for the model set-up and the comparison between measured and modelled data. The main objective of the present work is to perform the groundwater flow modelling in the Prototype Repository. The modelling task consists of several phases that are presented below.

A first modelling exercise have been performed and presented in Hermanson *et al.* (1999). This exercise was based on data from boreholes drilled in the TRUE Block Scale project, tunnel fracture mapping of the TBM tunnel and data from exploratory holes of the volume. A prediction of inflow and fracture characteristics in the deposition holes and the 2nd drill campaign was made. The present modelling exercise starts with deriving DFN-parameters from the exploratory drill campaigns 2 and 3. The statistics from the latter drill campaigns are then compared to what was derived by Hermanson *et al.* (1999)

The second phase of the work consists of the set-up of the DFN groundwater flow model. It requires a detailed statistical interpretation of the fracture flow and characteristics such as fracture frequency, orientation, size and hydraulic properties.

The third phase of the work consists of the prediction of fracture characteristics and flow in the deposition holes of the Prototype Repository in a similar manner as it was made by Hermanson *et al.* (1999). This time however, the model is be based on all available data up to Spring 1999 from drill campaigns 1, 2 and 3 and evaluated deterministic features.

The fourth phase consist of comparison between modelled and measured tracemaps and inflow to the deposition holes and also head in packer sections. To the last some improvements are discussed.

The analysis of the fracture statistics and flow properties is carried out with a suite of computer programs developed by Golder Associates. The modelling concepts will be presented in details below. The modelling of the groundwater flow in the Prototype Repository will be performed using a Discrete Fracture Network (DFN) approach with the computer modelling codes FracMan and MAFIC.

2 Concepts of DFN modelling

A brief survey of the DFN concept is discussed below, for more details see Appendix A.

Discrete Fracture Network (DFN) hydrogeology is based on two fundamental empirical observations that flow and transport in geological materials are controlled by structural features and that the hydraulic conductivity of geological materials tends to follow a log normal or similarly skewed distribution.

As a result of the first observation, it is desirable to have a hydrogeological model that can model structural features to as fine level of detail as possible. As a result of the second observation, it can be assumed that the vast majority of the geological materials will not contribute significantly to the effective hydraulic properties, and can therefore be ignored. This leads to the use of a DFN approach which concentrates on an accurate representation of conductive structures and flow barriers, sacrificing accuracy in the representation of smaller scale or less transmissive features.

The conceptual model used in the DFN approach assumes that discrete fractures provide the primary hydraulic flow paths and connections, and that accurate representation of flow path geometry is a key to successful hydrogeologic analysis. Discrete fractures may be fractures, faults, karsts, or paleochannels, depending on the scale and geology. Discrete fractures may be one, two, or three-dimensional features, but are generally modelled as infinitely thin polygons. Discrete fractures are generated in realistic three-dimensional networks based on the structural geology and statistical information of the fracturing, and can be conditioned to local measurements. Interaction between discrete fractures and the rock matrix will be ignored in the present work.

The key assumptions of the DFN approach as applied in this project may be summarised as follows:

1. A range of scales of discrete features can be used to represent flow and transport behaviour at any scale.
2. Discrete feature geometric and hydraulic properties can be derived from structural information and hydraulic tests.
3. Discrete features can be represented by a combination of two-dimensional structures such as plates.
4. Flow in discrete features can be described by the same laws as used for continuum approaches (i.e., the Navier-Stokes and Darcy equations).
5. Meaningful boundary conditions can be defined and assigned to discrete features at the edge of the model.
6. Discrete features that have not been intersected or measured can be described statistically based on those features that have been intersected and characterised.
7. Practical problems can be described by a limited number of stochastic realisations of the fracture pattern.

The key limitations of the DFN approach as applied in this project may be summarised as follows:

1. The number of discrete features that can be modelled is limited by available computational power.
2. Data may be insufficient to provide appropriate statistics for stochastically generated features.
3. Hydraulically significant features may have different properties from the geologically identified features used to generate statistics.
4. More complex geological structures may be difficult to represent by simple geometric features.

In fractured rock, the geometry of flow paths is controlled by the characteristics of the fracture networks. The FracMan program package is used here to analyse and model the geometry of discrete features. It provides an integrated environment for the entire process of statistical analysis of data to modelling the network geometry in stochastic simulations and solving the flow field and transport pathways. The characteristics of fractures are successively analysed with different programs of the FracMan package.

Below follows a summary of what fracture parameters are needed in the construction of the DFN model. The FracMan data analysis package used for deriving these parameters are summarised in Table 2-1.

Fracture set orientation

It is attractive if fractures with the same spatial orientation can be sorted in fracture sets. Estimates of statistical models for each set can then be synthetically generated. FracMan comes with the ability to fit statistical models on orientation distributions. The determination of fracture set orientation is carried out with the program ISIS. ISIS defines fracture sets from field data using an adaptive, probabilistic pattern recognition algorithm. ISIS allows the user to select the fracture properties of concern and define their relative significance for the analysis. The premise of the ISIS approach for definition of fracture sets is that the sets should be groups of fractures with similar properties. Orientation does not need to be the only property defining sets; size, termination, fillings and other properties can identify sets as well. In the present study, properties defining set have been limited to the spatial orientation of two types of fractures; “natural” and “sealed”. On a basis of borehole logs and fracture trace maps, ISIS calculates the distribution of orientation for the fractures assigned to each set, then re-assigns fractures to sets according to probabilistic weights proportional to their similarity to other fractures in the set. The orientations of the sets are then recalculated and the process is repeated until the set assignment is optimised. The optimisation measure of this test is a Chi-Squared (χ^2) goodness.

Fracture size

The FracSize data analysis module is used to determine the distribution of fracture radii that gives the best match to the observed trace length data. FracSize uses simulated sampling to take into account censoring, truncation and sampling bias.

FracSize starts with an .ORS file containing measured fracture traces, a corresponding .SAB file containing the specification of the sampling process used to collect each of the fractures in the .ORS file and an assumed distribution of fracture radii provided by the user. FracSize then simulates the sampling process, compares the simulated sample to the actual data in the .ORS file and displays a graphical and statistical summary of the comparison.

Two optimisation algorithms are available to provide an automated search of the fracture radius distribution. For the simulated annealing and conjugate gradient optimisation algorithms, FracSize varies the assumed distribution of fracture radius to improve the match between simulated and measured trace results, as measured by either Kolmogorov-Smirnov (K-S) or Chi-Squared (χ^2) statistics. For each iteration, FracSize carries out five realisations of a specific fracture radius distribution and calculates the mean K-S and χ^2 statistics as the measure of the goodness-of-fit provided by that fracture radius distribution. As a result of the analysis, the fracture radius distributions are given in the form of probability density functions of the following types: Normal, Exponential, Lognormal, Normal of Log, Constant, Uniform or Power Law.

Fractures clustering (spatial model)

Fracture trace maps can present different aspects that are not necessarily dependent of the fracture size or orientation. This aspect mainly depends on the spatial distribution of the fracture traces within a given surface. Fractures can be heavily clustered and regularly dispersed within the surface or can be located in small groups. A spatial analysis of a trace map permits to characterise the clustering of fractures. This analysis is carried out with the program module HeterFrac. The trace map is overlain by a grid and the number of traces within each grid cell is calculated. The probability density function of the number of traces in each grid cell when changing the cell size is calculated. Simulated trace maps are matched to the observed data until a 99% significance level is reached for the χ^2 –test. If then the box dimension (i.e. slope of the curve on a plot of number of grid cells versus cell size) is close to 2 the spatial model is Poisson distributed. If the box dimension is larger than 2 the model needs to be more clustered and purely fractal if the box dimension is 3.

Fracture set intensity and transmissivity distribution

Fracture set intensity can be expressed as linear frequency, trace length density and fracture area density. The linear frequency (P_{10}) is the average number of discontinuities intersected by a unit length of a sampling line. The simplest method to express the frequency of discontinuities is to use a scanline mapping and measure the linear frequency of the fractures. Scanline mapping consists in measuring the frequency of all fracture traces intersecting a scanline; a measuring tape applied on the rock face. Priest (1993) recommends the sampling zone to contain between 150 to 350 discontinuities, of which about 50% should have one end visible. This method can also be applied for rock cores from diamond drilling. Linear frequency analysis may be carried out on all fractures or on a specified set of fractures.

Trace length density (P_{21}) consists in determine the sum of fracture traces per unit area on a rock exposure. Planar mapping is not frequently used since it usually requires a picture of the rock exposure for analysis of the fractures. So far, image analysis methods, which uses pictures of rock exposures, do not permit the measurement of orientation of the fractures. The trace length density is expressed in m/m^2.

Fracture area density (P_{32}) is the most realistic description of the fracture set frequency in space and it is defined as the area of fractures per unit volume of rock. The main drawback on the fracture area density is that it does not give any indication about the size of the fractures. For this reason, the trace length density is sometimes preferred to the fracture area density. The fracture area density is expressed in m^2/m^3.

The hydraulic behaviour of a fracture network depends mainly on the transmissivity of the fractures. The transmissivity T of a single fracture in a borehole section of 1 m length in an impermeable rock is equivalent to the conductivity K of the same 1 m long borehole section in a continuous porous material. Transmissivity distribution and frequency of conductive fractures from packer test data is determined by the OxFilet module ("**O**snes E**x**traction from **F**ixed-**I**nterval-**L**ength **E**ffective **T**ransmissivities") by using an approach adapted from Osnes *et al.* (1988).

The method assumes that the fracture network transmissivity of a packed borehole section is equal to the sum of the transmissivities of the conductive fractures that intersect that test zone:

$$T_1 = \sum_{j=1}^{n_i} T_{ij}$$

Where T_i is the apparent transmissivity of the *ith* packer interval, n_i is the number of conductive fractures in the *ith* interval and T_{ij} is the transmissivity of the *jth* conductive fracture within the *ith* interval. Within any given interval, the number of conductive fractures, n_i, is assumed to be a random number defined by a Poisson distribution (Benjamin and Cornell, 1970):

$$f_n(n) = \frac{\bar{n}^n e^{-\bar{n}}}{n!}$$

Where $\bar{n}$ is the Poisson process rate, which is equal to the expected value of n. The conductive fracture frequency is given by $f_c = n/L_i$, where L_i = the length of the test zone.

The distribution of fracture transmissivities is assumed to be independent within each packer interval, with a given distributional form. The distribution of T_i is the sum of a random number of random events and is therefore a compound Poisson process (Feller, 1971). In this approach, the mean number of fractures in a given interval is defined by the Poisson distribution rate parameter, *n*, and the distribution of fracture transmissivities T_{ij} is described by a log normal distribution with a mean and standard deviation (m_{logT} and s_{logT}).

For any given set of parameters describing the distribution of fracture transmissivity $f(T_{ij})$ and conductive fracture frequency f_c, the distribution of packer interval transmissivities $f(T_i)$ are found by Monte Carlo simulation, with the best fit value found by a simulated annealing search routine. Simulated intervals that contain no conductive fractures or that have values of T_i less than $T_{threshold}$, the lowest threshold transmissivity that could be reliably measured in the field, are assigned a transmissivity equal to $T_{threshold}$.

The intensity and transmissivity distributions for the conductive fractures are then estimated by finding the best match between the observed distribution of packer interval transmissivities $f(T_i)$ and the distribution of test zone transmissivities found by simulation for given fracture frequency and single-fracture transmissivity distributions. This match is found both visually and by comparison of Kolmogorov-Smirnov (K-S) or Chi-Squared (χ^2) statistics.

The values of n, $\mu_{log\ T}$ and $\sigma_{log\ T}$ that provided the best K-S or χ^2 are taken to be the best estimates of those parameters.

Table 2-1. FracMan data analysis package

Program name	***Input***	***Output***
ISIS	Borehole logs Fracture trace maps (Orientation, mineral filling, terminations, size, etc.)	Fracture set assignment and orientation
FracSize	Fracture trace maps (trace length)	Fracture set size statistical distribution
HeterFrac	Fracture trace maps (trace co-ordinates)	Fractures clustering characterisation: spatial model
OxFilet	Packer test interval Transmissivities and borehole fracture mapping	Fracture sets frequency and transmissivity statistical distribution

When experimental data are well characterised in a statistical manner, FracWorks is used to generate stochastic discrete features. Deterministic features, tunnels, packer sections etc can be included in the model. Fracture statistics can be extracted from the three dimensional fracture networks for calibration with observed fracture data in boreholes, outcrops or tunnels.

When the DFN model is properly calibrated, the hydraulic behaviour of the model is calculated by the program MAFIC. MAFIC (**Ma**trix/**F**racture **I**nteraction **C**ode) is a finite element program used to simulate transient flow and solute transport through three-dimensional rock masses. MAFIC handles all types of network geometry's and objects modelled by FracMan such as tunnels, deterministic objects, deposition holes etc.

The principle of DFN modelling is based on Monte Carlo simulations. This means that the hydraulic behaviour of a fracture network is modelled by several stochastic realisations (fracture networks) with the same statistical distribution. The confidence in the hydraulic behaviour of a fracture network is built on the statistical analysis of the results of the multiple realisations.

3 Analysis of available data

3.1 Overview

This chapter describes the statistical analysis and description of the fracture parameters of interest in the conception of a DFN model.

The general approach when simulating inflow using the DFN concept is to derive the fracture parameters that are relevant for solving flow in the rock mass. The basic assumption is that flow in crystalline bedrock occurs in fractures whereas the bedrock itself is considered impermeable. Further, the fracture network necessary to include in the DFN model is generally only considered to be a subset of all the fractures in the rock mass. To find out which proportion conductive fractures we need to implement we need to investigate and analyse certain aspects of the fracture and flow properties of the rock mass. Luckily, the prototype repository characterisation provides the necessary fracture data and flow properties from a large amount of boreholes and tunnels surrounding the location of the deposition holes.

The analysis of the fracture data is also aimed at comparing previously evaluated input parameters to the first DFN model (no. 1) of the prototype repository reported by Hermanson *et al.* (1999). The comparison between the parameters in the two DFN models are presented in chapter 4

The investigation of the prototype experimental volume has been performed in campaigns where a number of exploratory boreholes have been drilled and sampled in batches. The exploratory drillings, reported in three campaigns by Rhén & Forsmark (1998a, 1998b and Forsmark & Rhén 1999), forms the basis for deriving the DFN parameters in this report.

The previously reported work concerning DFN model no.1 constructed by Hermanson *et al.* (1999) uses data from drill campaign 1 (Rhén & Forsmark 1998a) to make predictions of fracture intersection data and inflow to exploratory boreholes in drill campaign 2 and to the deposition holes. The DFN model presented in this report (no. 2) focuses on data from drill campaign 2 and 3 presented by Rhén & Forsmark (1998b) and Forsmark & Rhén (1999) and makes predictions of inflow to the deposition holes. The fracture analysis presented below describes the derivation of DFN parameters for DFN model no.2 from drill campaign 2 and 3 data.

3.2 Fracture statistics from the 1st, 2nd and 3rd drill campaigns and the TBM tunnel

3.2.1 Fracture and flow data

The analysed fracture data comes from the three drill campaigns reported by Rhén & Forsmark (1998a, 1998b) and Forsmark & Rhén (1999) and from mappings of the TBM tunnel drift reported in Follin & Hermanson (1996).

The boreholes are drilled in the walls and the floor of the TBM tunnel around the planned deposition holes and in the G-tunnel in the Äspö HRL, see Figure 3-1. The data monitored in the exploratory boreholes are of two general types: geometric fracture data and hydraulic inflow data.

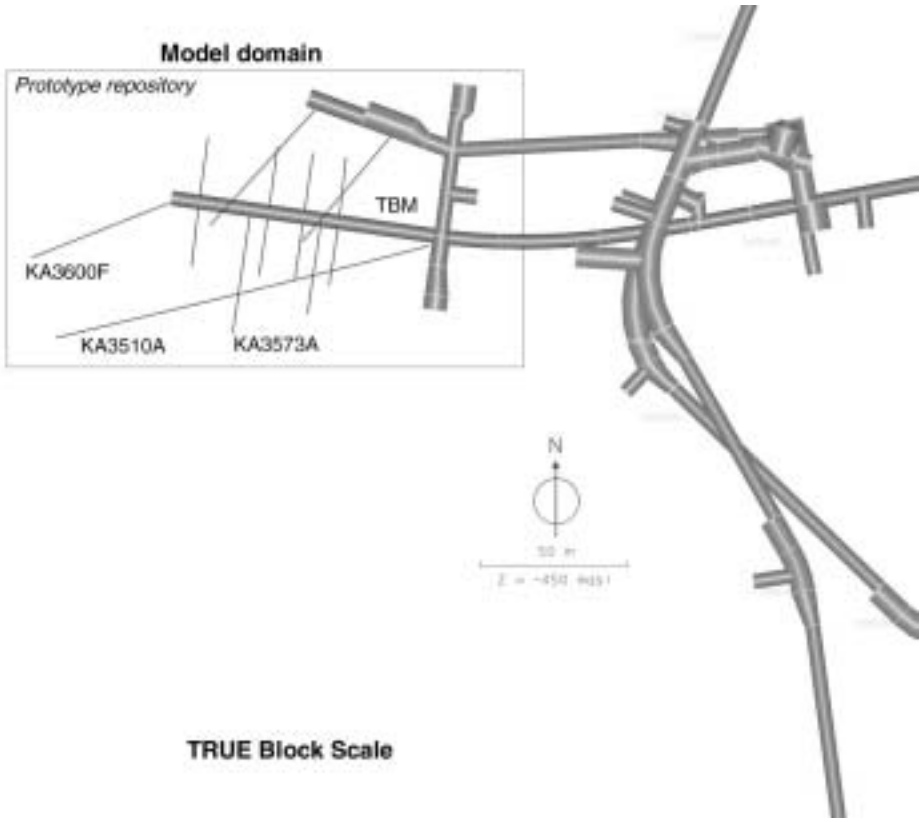

Figure 3-1*. Localisation of the Prototype Repository.*

The geometric data consist of the exact location of each fracture and its orientation and its geologic characteristics. Based on this information it is possible to compute the fracture frequency along the boreholes and the fracture orientation distribution. The TBM tunnel drift data contains information of the two-dimensional fracture trace length on the tunnel surface and the orientations of the individual traces. This information is used for estimating the three-dimensional fracture size distribution in the fracture network surrounding the tunnel system. The overall fracture intensity in the rock mass can be calculated both from borehole and tunnel data. The conductive fracture frequency is better estimated from hydraulic measurements in the boreholes.

Hydraulic data are based on hydraulic tests in the boreholes. These tests were carried out in sections of boreholes sealed with inflatable packers in section of 1 m and 3 m length.

The borehole data from drill campaigns 2 and 3 (Rhén & Forsmark 1998b; Forsmark & Rhén 1999) contains 36 exploratory boreholes with lengths varying from 8 to 90 m. To interpret the data from these boreholes Forsmark & Rhén (1999) have sorted the boreholes in subclasses defined by the inclination of the boreholes. Subclass 2 contains the sub vertical holes, subclass 3 the sub horizontal holes, subclass 4 the southerly inclined holes and subclass 5 the northerly inclined holes. Subclass 1 is the sum of all the subclasses 2, 3, 4 and 5. This classification is summarised by Figure 3-2 below.

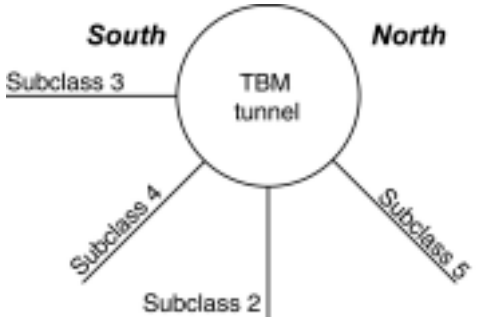

Figure 3-2. *Borehole subclass definition (after Forsmark & Rhén 1999).*

Table 3-1 below presents the list of the exploratory boreholes from drill campaign 2 and 3 that have been used in the process of deriving the DFN parameters in this study.

Table 3-1. Length and orientation of the exploratory boreholes used in the data analysis.

Name	Bearing	Inclination	Length [m]	Name	Bearing	Inclination	Length [m]
KA3539G	274.20	80.50	30.01	KA3576G01	213.70	89.20	12.01
KA3542G01	188.70	45.00	30.04	KA3578G01	252.60	89.00	12.58
KA3542G02	6.30	44.20	30.01	KA3579G	296.60	89.40	22.65
KA3544G01	0.00	90.00	12.00	KA3584G01	212.50	89.30	12.00
KA3546G01	194.00	89.80	12.00	KA3586G01	298.61	88.57	8.00
KA3548A01	188.40	3.10	30.00	KA3588G01	230.71	89.19	8.00
KA3548G01	75.70	89.80	12.01	KA3590G01	186.70	44.40	30.06
KA3550G01	249.00	89.20	12.03	KA3590G02	7.94	43.82	30.05
KA3552G01	130.60	89.50	12.01	KA3593G	252.20	79.90	30.02
KA3554G01	188.20	45.00	30.01	KA3600F	248.40	1.70	50.10
KA3554G02	8.20	45.00	30.01	KG0021A01	220.11	-17.69	48.82
KA3557G	271.20	81.50	30.04	KG0048A01	222.37	-13.98	54.69
KA3563G	277.90	79.90	30.00	KA3545G	270.00	81.20	8.04
KA3566G01	188.80	44.90	30.01	KA3551G	269.36	79.63	8.04
KA3566G02	7.72	43.80	30.01	KA3569G	269.66	80.27	8.04
KA3572G01	225.00	89.60	12.00	KA3575G	-79.82	80.88	8.04
KA3573A	188.30	2.10	40.07	KA3581G	-83.31	81.60	8.04
KA3574G01	249.00	89.20	12.00	KA3587G	-82.91	79.75	8.04

3.2.2 Orientation

Fractures in crystalline pre-cambrian granitoids usually show complex patterns with orientations in many directions. The deformation history is long and contains several phases, which has left tectonic imprint in the form of mylonites, faults, sealed and brittle fractures with complex mineralogies. To help understanding of the brittle structures, fractures in the rock mass can be grouped into a number of fracture sets with different orientations and different properties. It is sometimes possible to correlate the fracture properties to the sets they belong to. This may be helpful when interpreting the DFN parameters for each fracture set. Previous studies of the Äspö HRL tunnel (LaPointe *et al.*, 1993, 1995; Munier, 1995) have put great efforts in statistically separating fractures into sets based on fracture mineralogy, orientation, trace length, termination mode, surface roughness, kinematical evidence etc. The main conclusion from these studies is that the geological fracture properties are weakly correlated to the fracture orientation. The only significant coupling is the increase in trace length for water bearing fractures mapped in the tunnel drift.

The sources of data for the estimation of fracture orientations are the fracture mapping of the TBM tunnel and the 36 bore- and exploratory holes drilled from the TBM tunnel drift. The exploratory holes are grouped in the sub-classes according to Table 3-2.

Fracture data from the TBM drift consist of less than 300 fractures. Although the sample is small, the data are considered to be of high quality since it covers a large volume and is therefore less affected by an orientation bias. The orientations of fractures in the exploratory boreholes consist of almost 1500 data points.

Table 3-2. The pilot and exploratory holes used for fracture set identification.

Sub vertical holes Sub Class 2		*Sub horizontal Sub Class 3*	*Dipping South Sub Class 4*	*Dipping North Sub Class 5*
KA3539G	KA3574G01	KA3548A01	KA3542G01	KA3542G02
KA3544G01	KA3575G	KA3573A	KA3554G01	KA3554G02
KA3545G	KA3576G01	KA3600F	KA3566G01	KA3566G02
KA3546G01	KA3578G01	KG0021A01	KA3590G01	KA3590G02
KA3548G01	KA3579G	KG0048A01		
KA3550G01	KA3581G			
KA3551G	KA3584G01			
KA3552G01	KA3586G01			
KA3557G	KA3587G			
KA3563G	KA3588G01			
KA3569G	KA3593G			
KA3572G01				

The projections of the poles of all the fractures of all exploratory boreholes are plotted on an equal area lower hemisphere projection in Figure 3-3. The plot shows at least two fracture sets, one sub-horizontal and one steep north-west set. There is also indications of a third set with steep fractures in the north-east direction. The latter fracture set is diffuse, but this may be a visual bias due to the fact that most of the boreholes are in the same plane. The bias can be corrected using the Terzaghi correction method (Terzaghi, 1965) which compensates for fractures that are sub-parallel to the borehole axis. In this study a maximum correction factor of 5 is used based on previous experience from LaPointe *et al.* (1995) and Dershowitz *et al.* (1996).

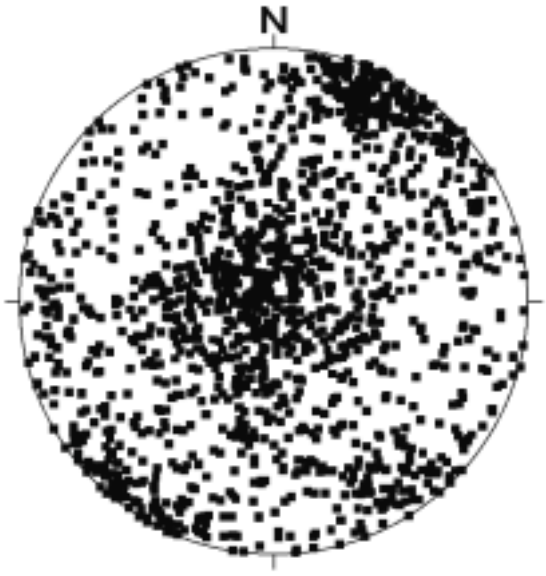

Figure 3-3. *Lower hemisphere projection of poles to fracture planes in the 36 bore- and exploratory holes.*

Fractures intersecting boreholes are defined as either “sealed” or “natural” in SICADA. Based on this the analysis of the fracture orientation can be refined using the information if the intersecting fracture is “sealed” or “natural”. The general assumption is that “sealed” fractures can not be water bearing, at least not in the intersection with the borehole. “Natural” fractures are possibly water bearing but does not necessarily take part in the conductive network. Figure 3-4 shows the poles of the “natural” fracture planes.

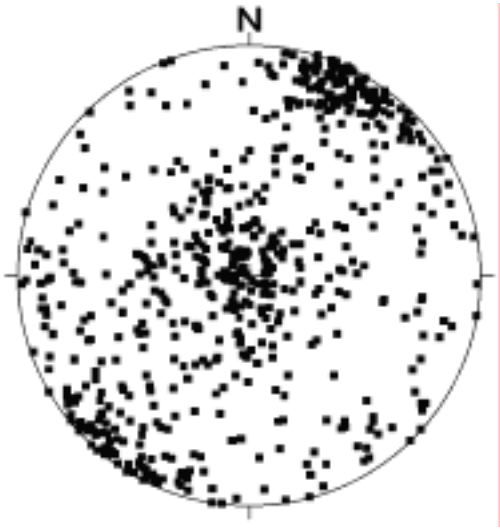

Figure 3-4. *Lower hemisphere projection of poles to fracture planes for “natural” fractures in the 36 exploratory holes.*

At least two different fracture sets can be visually discerned from the “natural” fractures group. As a complement to the visual observations a set identification algorithm can be used to fit a statistical distribution to each fracture set. This is attractive as the knowledge of the distribution of each set makes it possible to simulate orientations according to a statistical model. In this case the ISIS software of the FracMan package

is used for the set identification. Based on the visual investigation it is assumed that the fractures shall be divided into three sets. The ISIS algorithm then tries to fit statistical distributions to the data. Several statistical distributions have been tested for the three fracture set assumptions. The Fisher distribution was the most successful in all tests and is used as statistical model in all fracture sets both in this model and in the previously analysed data from Hermanson *et al.* (1999). The results from the ISIS analysis are shown in Table 3-3. It is clear that the statistics shows similar results for both "all" fractures as for "natural" fractures respectively. The major difference is that set 2 has a larger proportion of "natural" fractures than the other two sets. This indicates that we have fractures in the north-west direction that have gone through a more recent brittle deformation phase and are thus more likely to conduct water than the other two fracture sets. This is also the dominating direction of fracturing at Äspö.

Table 3-3. Statistical separation of fracture sets of the 36 pilot and exploratory holes. The Fisher distribution is used for all fracture sets.

SET 1	**Prototype DFN 2**		**Prototype DNF 1**
	All	Natural	True BS
Strike	219	212.8	207.9
Dip	83.7	83.7	77.1
K	4.84	3.96	5.64
%-fractures	26.50%	23.20%	12%
KS-%	0.050;15.7%	0.075;26.6%	0.16;38.5%

SET 2	**Prototype DFN 2**		**Prototype DFN 1**
	All	Natural	True BS
Strike	127	126.9	290.4
Dip	84.2	86.8	88
K	8.35	10.53	15.75
%-fractures	35.60%	43.30%	46%
KS-%	0.040;23.4%	0.069;8.3%	0.163;4.6%

SET 3	**Prototype DFN 2**		**Prototype DFN 1**
	All	Natural	True BS
Strike	20.6	17.9	276.5
Dip	6	7.5	8.9
K	8.33	9.32	13.6
%-fractures	37.90%	33.50%	42%
KS-%	0.043;14.4%	0.068;19.2%	0.095;79.7%

The orientation analysis based on the data from drill campaigns 2 and 3 show that the assumption of three fracture sets is nicely approximated by Fisher statistical distributions. A comparison with the statistics from DFN model no.1 (Hermanson *et al.* 1999) is presented in chapter 4.

3.2.3 Size

The general shape of a fracture in three dimensions is essentially unknown. We can observe traces and cuts on walls and outcrops but the complete shape of the fracture remains invisible. For conceptual purposes, fractures can be simplified as disks, and their sizes[1] can be estimated by looking at the trace length on outcrops and tunnel walls.

Follin and Hermanson (1996) performed size estimates based on two data sources from the innermost section of the TBM tunnel drift. The method they used is described by LaPointe *et al.* (1993) and is based on the probability that a fracture trace that is mapped all the way around the tunnel surface is a function of fracture size. Size can thus be estimated by defining how large part of a tunnel surface a fracture intersects.

The methodology allows testing several statistical distributions to the observed trace length distribution. However, the method is time consuming and testing of distributions have been limited to the lognormal size distributions due to the following reasoning: Two different hypotheses of fracture size distributions dominate in the literature; lognormal and power law distributions. It is by many authors such as LaPointe and Follin (1999), Castaing *et al.* (1996) and Oillon *et al.* (1996) considered that fractures mapped on unlimited outcrops could best be approximated with the fractal power law size distribution whereas others such as Priest (1993) conclude that the lognormal distribution is a valid assumption. Upon review of the different hypotheses it is clear that scale is important when trying to make an estimate of the three dimensional size distribution from two-dimensional outcrops. Castaing *et al.* (1996) concluded that fault traces following the power law size distribution on large scales had different behaviour when mapped in small observation windows in the same outcrop. It was shown that the distribution of the smaller observation windows matched better the lognormal distribution than power law. LaPointe and Follin (1999) have drawn the same conclusion using synthetic trace map samples.

The TBM tunnel drift is a limited outcrop along a tunnel with a limited amount of fracture traces. Based on the findings that traces in small observation windows better match lognormal size distributions it is assumed that this is valid also for the relatively small size of the outcrop in the TBM tunnel. It is also considered valid to use lognormally distributed fractures as long as the model domain is relatively small compared to the estimated mean fracture size radius. The model domain around the prototype repository is less than 200 m long. The lognormal assumption have previously been advocated by other authors (LaPointe *et al.*, 1995; Dershowitz *et al.*, 1996; Priest 1993, Kulatilake and Wu 1984).

Data source - Trace length from TBM tunnel

There exist two different databases of fracture trace lengths from the last section of the TBM tunnel. Traces on the tunnel walls have been mapped by site geologists through visual inspection just after blasting of a new section. The two data measurement sets origin from the mapping technique by the geologists. The first data set consists of hand drawn maps of the traces in the tunnel. These maps have then been digitised at the site, and later converted by VBB Viak to 3D co-ordinates as reported by Follin and

[1] In FracMan, fracture size is expressed as the equivalent radius of a circular disk with the same area as the fracture, independent of shape.

Hermanson (1996). These sketched traces are here referred to as the VBB Viak data set. The second measurement set origins from the estimation of the trace length performed by the same geologist simultaneously as he draws the trace map. This estimate is then recorded in SICADA, and is here referred to as the SICADA data set. Ideally they should be identical. However, estimating the length of an object by sketching is generally easier than estimating with numbers. This can be seen by looking at the average trace lengths from these different data sets:

- SICADA data set, mean trace length 5.5 m.
- VBB Viak data set, mean trace length 8.3 m

The TBM tunnel is circular and has fracture traces all around its perimeter. Unfortunately, when the original mapping was performed in the tunnels of the HRL, fracture traces less than one meter was not recorded. This trace truncation implies that fractures with a radius less than 0.5 m intersecting the tunnel can not be analysed as traces are not measured. It also implies that traces of larger fractures, which are just intersecting a small part of the tunnel wall (< 1 m) are truncated.

Size estimate

By means of exploration simulation and sampling with a 16-sided "TBM tunnel" in a stochastic network model, intersection statistics on the tunnel walls have been compared to observed intersections in the real TBM tunnel. The three fracture sets have been analysed separately with regard to their size distribution(s). The procedure used in the performed analysis is described by LaPointe *et al.* (1993) and in detail by Follin and Hermanson (1996) and is shortly summarised below:

1. Intersection statistics from the field observations was produced using 16 panels on the walls of the TBM tunnel (i.e. resembling a 16 sided tunnel)
2. A DFN model was generated with parameters according to Table 3-4.
3. A 16-sided tunnel resembling the shape, size and orientation of the TBM tunnel was inserted into each network realisation of the DFN models.
4. For each trace the number of panel intersections were calculated.
5. A correlation analysis of the 16 panel intersection statistics between the simulations and the observations show in which mean size window there is best correlation of trace statistics.

The input data in this analysis is the VBB Viak data set. The analysis was subjected to the following rationale. Sampled traces shorter than a meter was discarded from the analysis as the observations are subjected to such a truncation. However, a non-truncated size distribution was used in the stochastic network realisations, as truncation of traces does not necessarily imply that fractures of sizes less than 0.5 m in radius does not exist. The latter is most likely true as can be observed on tunnel walls. But by using a non-truncated size distribution and only truncating the traces on the tunnel wall, we may enhance our possibility to recreate what has been observed also in the more fractured drill cores.

The analysis is based on calculating the number of panels intersected by fractures and comparing the observed panel intersections with simulated panel intersections. There may be several weaknesses to such a method, such as correlation to a small observed sample with an uneven distribution, and lack of panel intersection statistics for fracture sets with an extremely acute angle to the tunnel axis. One may also argue that small samples are always subject to weak statistical significance.

Table 3-4. Network parameters used in the exploration simulations. After Follin and Hermanson (1996)

Spatial model	Enhanced Baecher
Orientation	According to previous findings for Set 1 - 3
Size distribution	Lognormal
Size	Mean = 1 - 12 m, Std. Dev = 1 - 5 m
No. of fractures/realisation	10 000
No. of realisations	10 realisations for each combination

The simulations have been carried out in two steps. In the first step a large number of possible fracture mean sizes have been tested for each fracture set to establish a window of well correlated sizes. Acceptable mean size intervals are: 2 – 4 m for Set 1, 5-10 m for Set 2 and at least 4 – 7 m for Set 3. Secondly, a more detailed analysis was performed using these mean size intervals. The standard deviation was altered between 1 – 5 for each mean size, a number of realisations where run (10 for each combination), and the correlation analyses were repeated once more. The results from these latter analyses are shown in Figure 3-5 to Figure 3-7 and in Table 3-5. In Table 3-6 is the chosen distributions presented.

Table 3-5. Lognormal fracture size estimates of the three orientation sets. After Follin and Hermanson (1996).

Orientation	***Lognormal size distribution***
Set 1 (NE)	Mean 1-3 m , Standard deviation 1-2 m
Set 2 (NW)	Mean 6-9 m , Standard deviation 1-2 m
Set 3 (Sub-horizontal)	Mean 4-7 m , Standard deviation 2-4 m

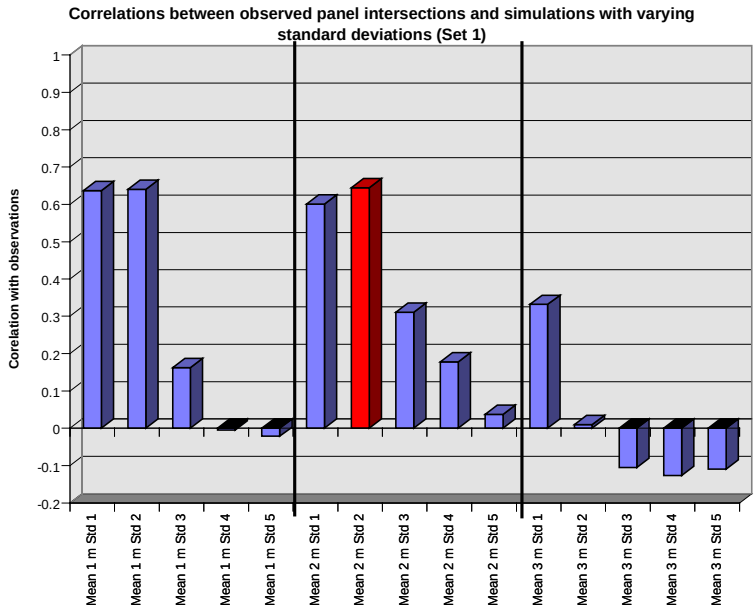

Figure 3-5. *Correlation between observed and simulated traces for orientation set 1 (NE-trending). To optimise the previous size analysis, a simulated size distribution in the estimated mean window is varied in standard deviation. The best fit estimation is observed for lognormally distributed fracture sizes of mean size 2 m with a standard deviation of 2 m. After Follin and Hermanson (1996).*

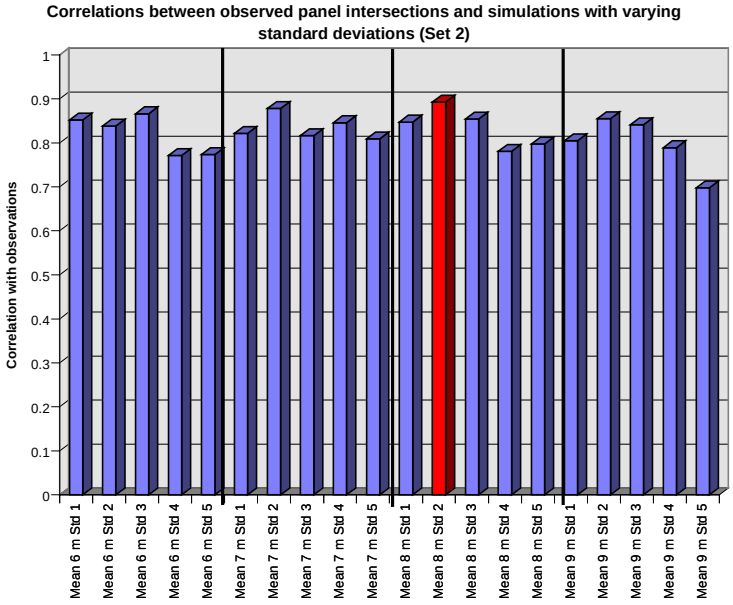

Figure 3-6. *Set 2 (N-W trending) correlation between observed and simulated traces in the mean size interval 6 to 9 m. The standard deviation is varied between 1 and 5. The best-fit estimation is similar within the whole observed interval. An estimate of lognormally distributed fractures of mean size of 8 m with a standard deviation of 2 is chosen to represent fracture set 2. After Follin and Hermanson (1996).*

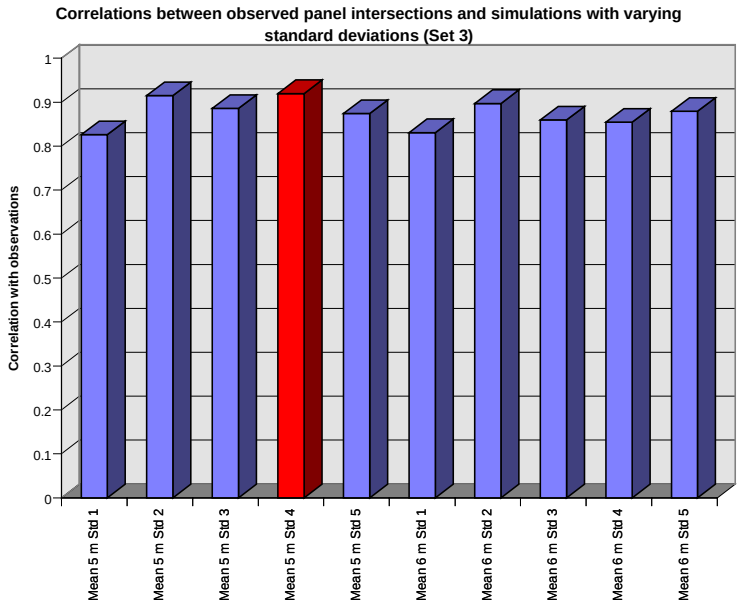

Figure 3-7. *Set 3 (Sub-horizontal). The correlation between observed and simulated traces in the mean size interval 5 to 6 m (lognormal distribution) reveal that one cannot make more exact statements than the first estimate of a best fit estimate of mean size 4 to 7 m. A variation in standard deviation makes little difference. After Follin and Hermanson (1996).*

Table 3-6. The chosen lognormal fracture radius distribution for each fracture set.

Fracture set	***Strike***	***Dip***	***Mean radius***	***Standard deviation***
Set1	219	83.7	2 m	2 m
Set2	127	84.2	8 m	2 m
Set3	20.6	6	5 m	4 m

3.2.4 Fracture frequency

The fracture frequency is an important parameter for estimating the intensity of fractures in the DFN model. The fracture frequencies in the exploratory boreholes in the prototype repository are shown in Figure 3-8. The figure shows all measured fractures and fractures that are defined as “natural”. The fracture statistics are divided into the 4 subclasses to show the frequency in the different groups. Subclass 2 contains the sub vertical holes, subclass 3 the sub horizontal holes, subclass 4 the southerly inclined holes and subclass 5 the northerly inclined holes, see Figure 3-2.

In subclass 2 (sub-vertical boreholes) the fracture frequency, for all measured fractures, varies between 0.62 and 5.10 fractures/m and the arithmetic average is 1.59 fractures/m. Most of the boreholes have a fracture frequency between 1 and 2 fractures/m. The intensity increases slightly towards the east in the TBM tunnel. The frequency for the “natural” fractures varies between 0.12 and 1.62 fractures/m and the arithmetic average is 0.54 fractures/m. About one third of all fractures in subclass 2 is defined as “natural”.

Subclass 3 (sub-horizontal boreholes) contains fracture frequencies that vary between 1.2 to 3 fractures/m and 0.6 to 1.4 “natural” fractures/m. The arithmetic average of all and “natural” fractures is 1.0 and 1.8 fractures/m respectively. It is worth noting that these boreholes sample mostly steep fractures.

The fracture frequency in subclass 4 (southerly inclined boreholes) increases from 1.77 fractures/m at the west end to 3.50 fractures/m at the east end of the TBM tunnel. The “natural” fracture frequency also increases to the east but not as much as for all fractures. The arithmetic average for all fractures is 2.65 fractures/m and 1.29 fractures/m for “natural” fractures, i.e. half of the measured fractures is defined as “natural”.

The boreholes that are inclined towards the north, subclass 5, have a decreasing fracture frequency towards the east, i.e. the opposite of subclass 2 and 4. The intensity for all fractures varies between 0.87 and 1.37 fractures/m. The arithmetic average for all fractures is 2.22 fractures/m, and 1.05 fractures/m for the “natural”, i.e. slightly lower than for subclass 4, but roughly the same relation between all and the “natural” fractures.

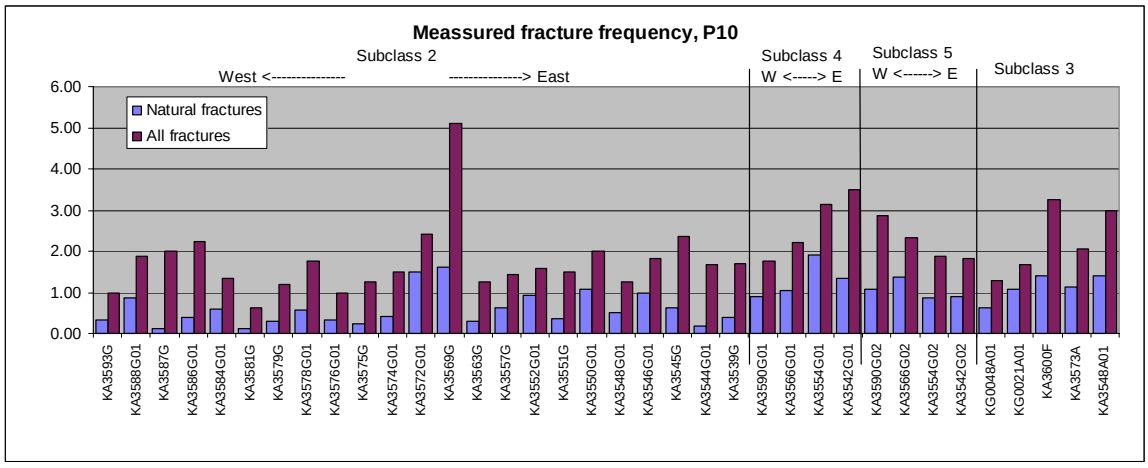

Figure 3-8. *Fracture frequency in the 36 pilot and exploratory holes in the vicinity of the Prototype repository of the TBM tunnel.*

3.2.5 Fracture intensity

The fracture frequency along boreholes does not by itself explain how fractured the rock mass is as boreholes are only line samples. Maps of outcrops and tunnel walls show two-dimensional intersections with fractures in the network and are also subject of sampling bias. From a DFN point of view, intensity is best described by a three-dimensional measure, fracture area per unit volume (m^2/m^3), P_{32}. The fracture intensity measure, P_{32}, cannot be measured directly in the field. However, Dershowitz and Herda (1992) have shown that P_{21} and P_{10} is linearly correlated to P_{32} according to the equations:

$$P_{32} = C_{21} \cdot P_{21}$$

or

$$P_{32} = C_{10} \cdot P_{10}$$

Where *C* is an unknown constant of proportionality. This constant depends only upon the orientation and size distribution of the fractures in the rock mass, and the orientation of the surface (P_{21}) or along the line (P_{10}) in which the fractures have been mapped. Applying its linear relationship with P_{10}, P_{32} can be calculated from borehole data by means of generating a DFN model based on the orientation and size distributions derived in the previous chapters with a hypothetical $P_{32,sim}$. The methodology is performed as follows:

A number of realisations of the DFN model are generated, and simulated $P_{10,sim}$ values are calculated by sampling a simulated borehole, equivalent in size and orientation to the Prototype exploratory boreholes. The fracture intensity value for the simulation, $P_{32,sim}$ is then varied until the ratio $P_{10,sim}$ and $P_{10,obs}$ are equal (ratio=1).

Performing the simulation with input data from the "all" fracture data set and the previously derived orientation and size distributions reveals a global P_{32} of 3.41 m^2/m^3. The average observed fracture frequency (P_{10}) in different subclasses is shown together with the sampled P_{10} in Figure 3-9. The simulations mimic fairly well the observed fracture frequency in all subclasses with a slight difference in the inclined boreholes. Each of the three different fracture sets contribute to the global P_{32} according to Table 3-7.

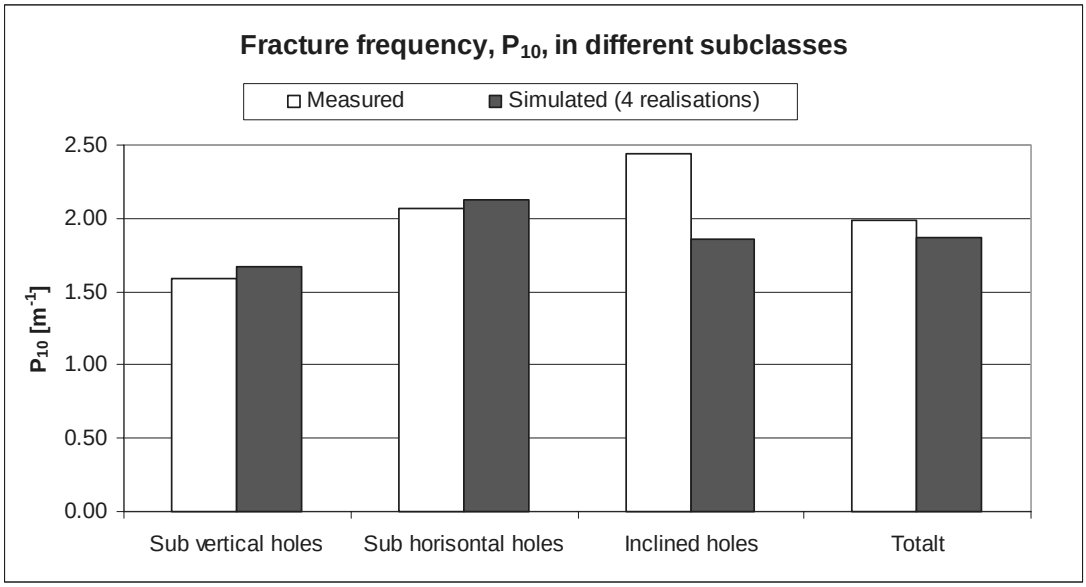

Figure 3-9. *Comparison between measured and simulated fracture frequency in different subclasses of exploratory boreholes.*

Table 3-7. P_{32} for the three sets used in the DFN –model. The contribution of each set is based on the relative contribution of fractures given in Table 3-3.

	Set 1	***Set 2***	***Set 3***	***Σ***
P_{32}	0.85	1.59	0.97	3.41

3.2.6 Spatial model

The clustering and spread of the fractures throughout the network volume has under certain geological conditions large impact on the flow properties in sub volumes. For example, the fracture network in stratified sedimentary formations may be very clustered in fold hinges and in certain strata. An ideal DFN model would try to mimic that type of fracturing by using either statistical models for the spatial distribution or simply by generating fractures with different orientations, sizes and intensities in different strata. The situation is perhaps more simple in crystalline, pre-cambrian rock with approximately the same material characteristics throughout the whole rock mass, fracture zones excluded. The Prototype DFN model will contain deterministic structures that may locally influence the fracturing. The rest of the volume is assumed to contain stochastically generated "background" fractures. A spatial analysis is performed to see if the fractures mapped the TBM tunnel show any signs of clustering or if we can assume that they are more or less evenly distributed in the volume.

A spatial analysis of the trace maps from the TBM tunnel has been done by Follin and Hermanson (1996). The spatial model is estimated by analysing the pattern of fracturing along an outcrop such as the end of the TBM tunnel, c.f. Figure 3-10. The trace map is overlain by a grid and the number of traces within each grid cell is calculated.
Figure 3-11 shows a plot of the probability density function of number of traces in each grid cell when changing the cell size. Simulated trace maps are matched to the observed data until a 99% significance level is reached for the χ^2 –test. If then the box dimension (i.e. slope of the curve on a plot of number of grid cells versus cell size) is close to 2 the spatial model is Poisson distributed. If the box dimension is larger than 2 the model needs to be more clustered and purely fractal if the box dimension is 3. The analysis indicates that a Poisson distributed model for the observed data is appropriate. For more detailed explanations, see Appendix A.

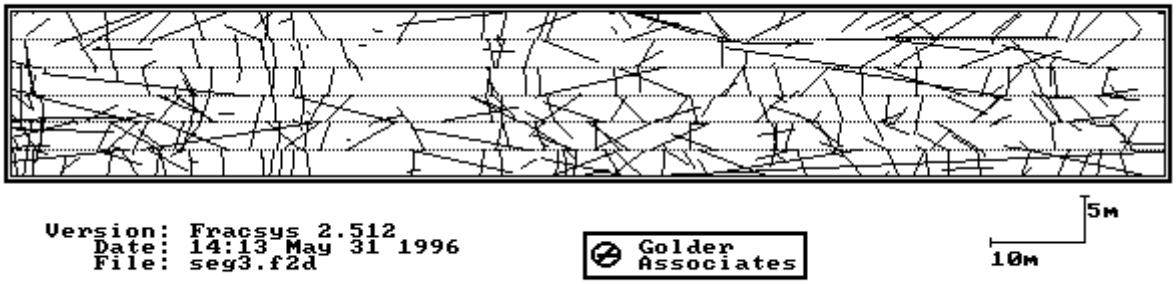

Centre line characteristics: L =122.03 m, Trend = 277.16, Plunge = -0.94
x = 1,984.84, y = 7,262.33, z = –447.768
P_{21} = 0.656 m/m^2

Figure 3-10. *Trace map over the last 120 m of the TBM tunnel after Follin and Hermanson (1996).*

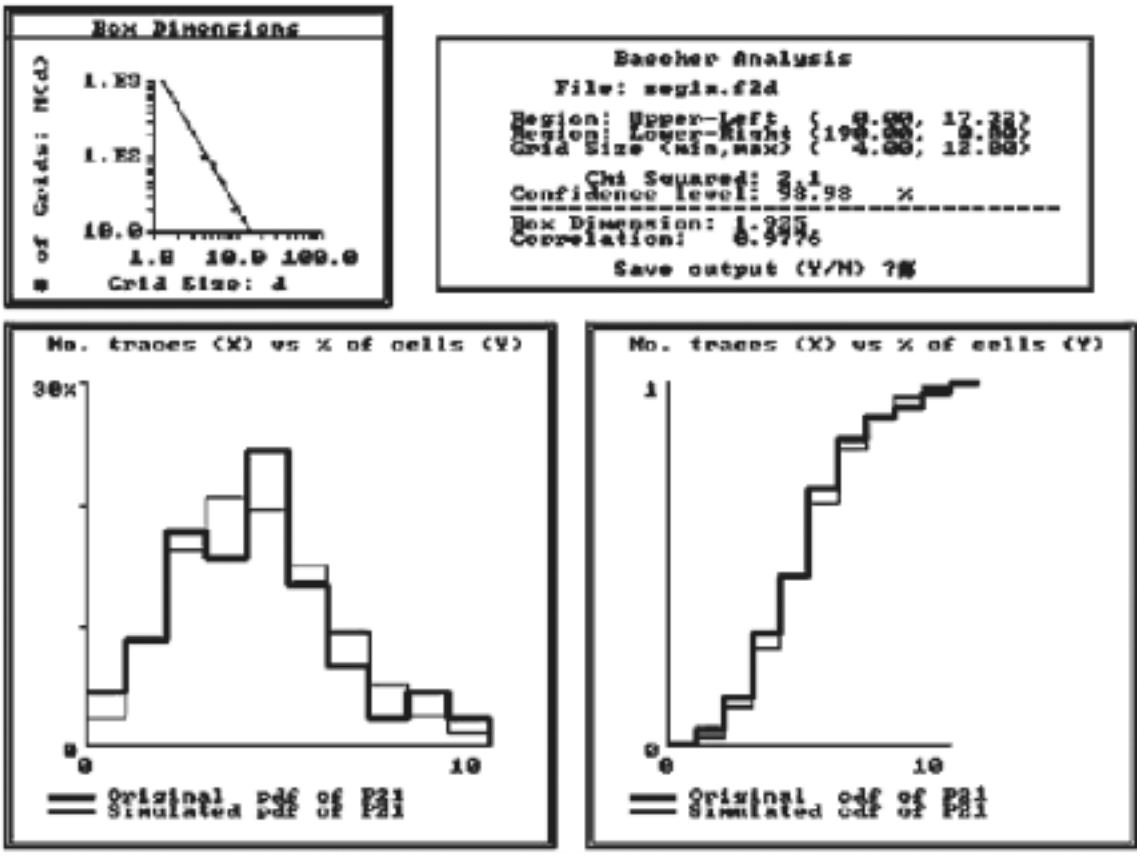

Figure 3-11*. A spatial analysis of the trace maps from the TBM suggests that a Poisson distributed spatial model with a homogeneous space filling may be appropriate. Analysis from Follin and Hermanson (1996).*

3.2.7 Analysis of transmissivity in borehole section

There are two approaches to analyse the hydraulic behaviour of a rock mass; the fracture network transmissivity approach and the rock mass conductivity approach. The hydraulic conductivity is the capacity of a medium to conduct a fluid within the matrix while the transmissivity represents the capacity of a fracture to conduct a fluid. The relationship between transmissivity and hydraulic conductivity in a borehole is described by:

$T_{sec} = e_{sec} \cdot K_{sec}$

Where

T_{sec} = Equivalent transmissivity of the section [m^2/s]
K_{sec} = Hydraulic conductivity of the section [m/s]
e_{sec} = Length of the packed-off section [m]

The equivalent transmissivity of a packed-off section is the sum of the transmissivities of the fractures that intersects the section, i.e.:

$T_{sec} = \Sigma(T_f)$

Where

T_{sec}= Equivalent transmissivity of the section [m^2/s]
T_f = Transmissivity of one fracture [m^2/s]

This implies that the transmissivity of a packed-off section is dependent on the length of the section. The hydraulic conductivity is independent of the length for a homogeneous rockmass. Consequently if data from different section lengths are to be compared, it requires that the measured transmissivities are converted to equivalent hydraulic conductivity for the borehole section. The equivalent hydraulic conductivity is the measured transmissivity divided by the length of the packed-off section.

In the present work, the evaluation of the hydraulic properties was based on transmissivity measurements made in 34 monitored exploratory boreholes around the TBM tunnel. Two different lengths of packer sections were used; 1 m and 3 m. The 1 m data consist of 363 packer sections and the 3 m data consist of 88 packer sections.

Figure 3-12 shows the hydraulic conductivity as a function of the number of weighted and normalised sections. The total length of the 1 m sections is normalised to 100 m and so are the 3 m sections. This implies that the 3 m sections are weighted to be 3 times fewer than the 1 m packers. There is 363 m of 1 m sections, consequently the number of sections in each class have been divided by 3.63. In the same way the number of sections in each 3 m class has been divided by 2.64 since there is 264 m (3·88 m) 3 m sections. Figure 3-12 shows that there is about the same amount of packer sections that intersect highly transmissive fractures.

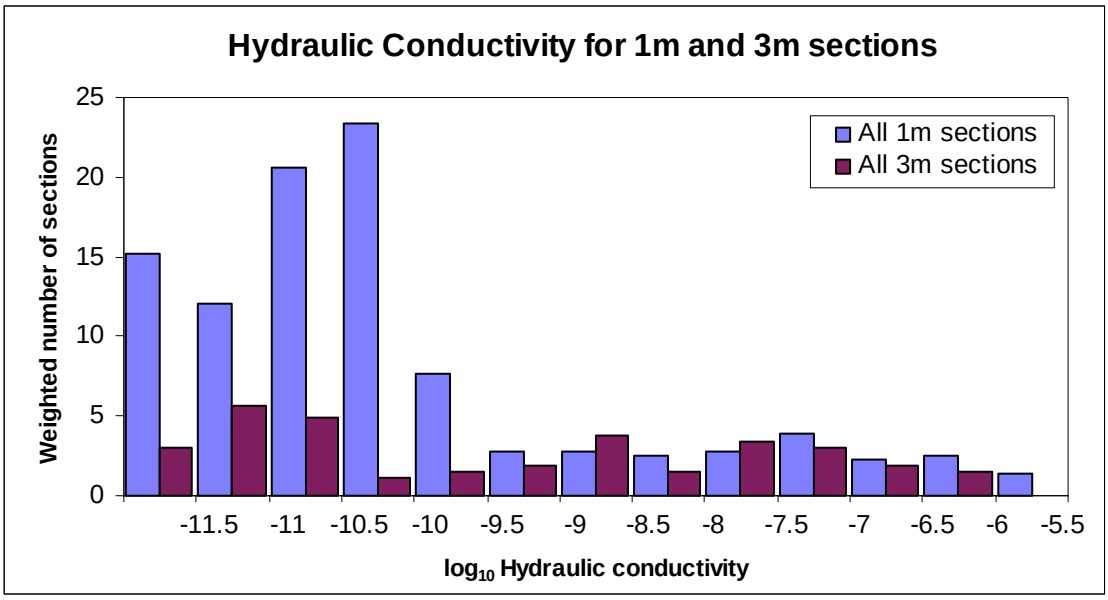

Figure 3-12. *Histogram of the hydraulic conductivity in 1m and 3m packer sections in 34 exploratory boreholes. Data comes from Forsmark and Rhén 1999.*

There are some similarities between the two data sets. Both sets show one peak for sections with low conductivity and one peak, somewhat smaller, with highly conductive sections. The observed two peaks indicate that there are different transmissivity distributions for different fracture sets in different directions. One fracture direction with few and highly transmissive fractures, and some other direction with many low transmissive fractures.

This observation of the coupling of transmissive fractures and the fracture orientation is also made by Rhén *et al.* (1997). In this report Rhén *et al.* couples the transmissivity with direction of fracture traces in a large amount of short pilot boreholes drilled at the front of the advancing access tunnel. The results revealed that the transmissivity is higher in sections that contain north-west striking fractures.

The probability plots for the subclasses are shown in Figure 3-13 and Appendix C. Average and standard deviation in log-space is shown in Table 3-8. The figure and the table show large differences in the transmissivity distribution in the different directions.

The sub-vertical boreholes, subclass 2, has the lowest median value for transmissivity, i.e. the boreholes intersect fractures with low transmissivity. This should correspond to the sub-horizontal fracture set, since the other fracture sets are sub-vertical.

Subclass 3, sub-horizontal boreholes, intersects with the two vertical sets. The orientation of the boreholes makes them intersect more of the north-west striking fractures than the north-east striking fractures. According to Rhén *et al.* (1997) the north-west striking set is the most transmissive set. The flat middle part for the data points in chart *c* and *h* in Figure 3-13 indicate that there is a tendency to a double peak in this subclass, probably due to the two different fracture sets that is intersected by the boreholes in subclass 3.

The orientation of the 8 boreholes of subclass 4 and 5 make them intersect with all three-fracture sets.

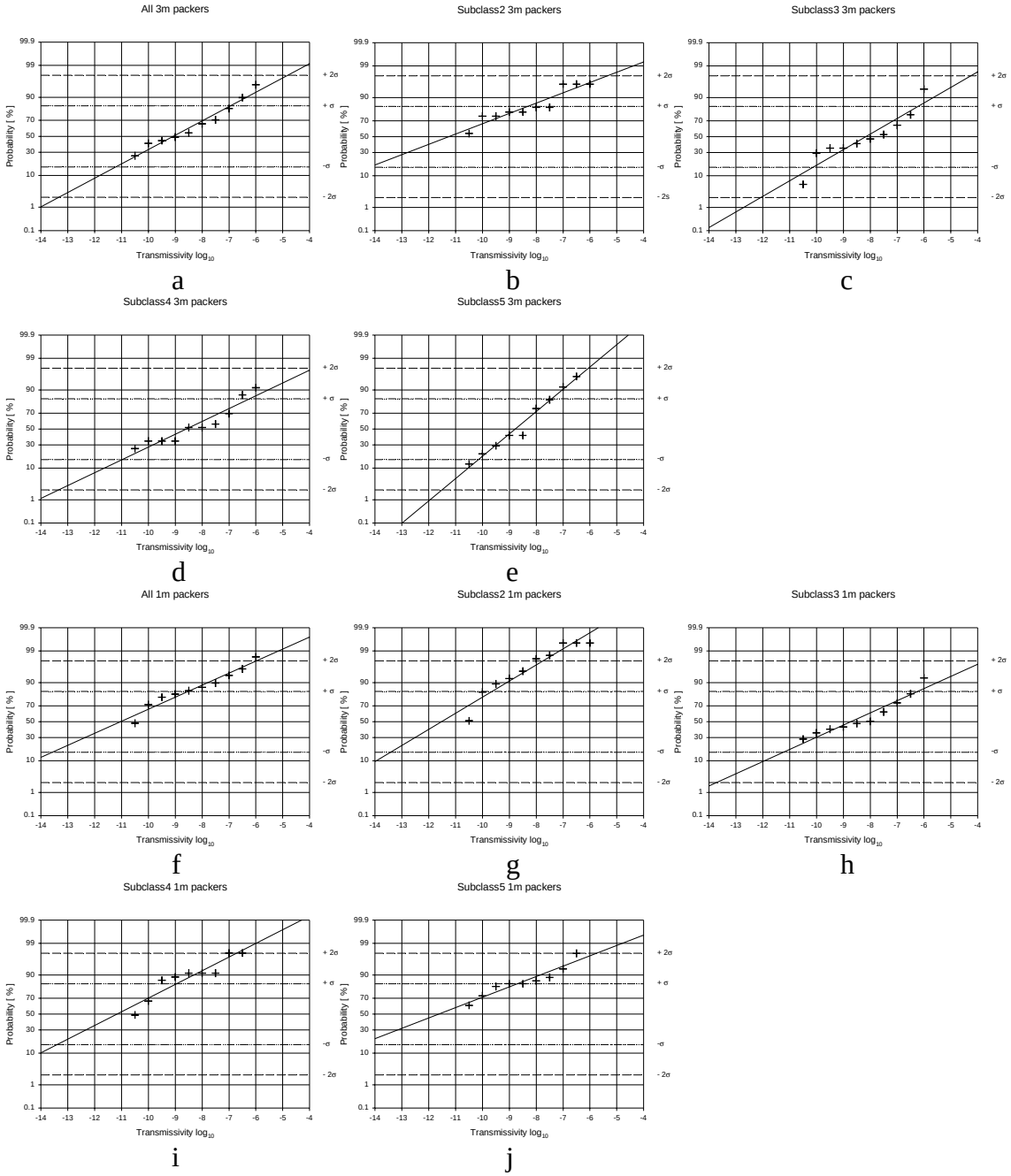

Figure 3-13*. Probability charts for transmissivity for the packed off sections divided into sub sets. The estimated average and standard deviation from the charts are shown in table 3-8.*

Table 3-8. Estimated average and standard deviation of measured transmissivities.

	1m packers			***3m packers***		
	$\bar{x}$	σ	# of data	$\bar{x}$	σ	# of data
All	-11.0	2.5	362	-9.1	2.1	88
subclass 2	-11.5	1.9	206	-11.2	2.9	24
subclass 3	-8.7	2.5	67	-8.2	2.0	17
subclass 4	-11.2	2.2	45	-8.6	2.4	23
Subclass 5	-11.6	2.9	44	-8.8	1.4	24

The data presented in Figure 3-13 is analysed by the FracWorks tool Oxfilet for estimation of the transmissivity distribution for each fracture set in the model. Oxfilet requires the length and the measured transmissivity for each section and a transmissivity cut-off value, i.e. the lowest possible transmissivity to measure. It is also required to estimate the conductive fracture frequency, P_{10C}, and a transmissivity distribution for the fractures intersecting the borehole. The last two parameters can be kept constant or be variable. A lognormal distribution is assumed for the transmissivity data.

The borehole flow measurement equipment can measure transmissivities lower than $1 \cdot 10^{-11}$ m^2/s, but in most cases, this limit is as high as $3 \cdot 10^{-11}$ m^2/s, especially for short packer sections (Rhén pers. com.1999). The truncation in the Oxfilet analysis is thus set to $3 \cdot 10^{-11}$ m^2/s.

There are two different approaches in building the DFN model. The first approach is to model only the waterbearing fractures and use a transmissivity distribution that is truncated so that no fractures will have a transmissivity below a limit. The second approach is to produce all fractures in the rockmass, both water conductive and non-conductive, and assign a non-truncated transmissivity distribution. Fractures that have a transmissivity below the limit of being waterbearing are then deleted before the flow-solver is used. The advantage of the second approach is that it is possible to produce fracture trace maps of not only waterbearing fractures but of all fractures.

The latter approach is used in this study. Fractures with a transmissivity below the truncation limit will be considered “sealed”. It will therefore be possible to make trace maps for all kind of fractures.

Transmissivity data come from the 34 exploratory boreholes where both the packer section lengths and the transmissivity are monitored. The cut-off transmissivity is assumed to be $3 \cdot 10^{-11}$ m^2/s, since the data contains many short 1 m sections.

As an initial assumption, P_{10C} is chosen according to measured P_{10} in the different subclasses. The deviation of best match $P_{10C,}$ derived from Oxfilet, and P_{10} observed, c.f.
Table 3-9, is due to that the observed transmissivity distribution in Figure 3-14 is better matched if P_{10C} is slightly adjusted.

Table 3-9. Measured fracture frequency for all fractures and the fracture frequency for the best match in Oxfilet.

Subclass	***2***	***3***	***4 & 5***
Measured all fractures	1.59 m^{-1}	2.07 m^{-1}	2.44 m^{-1}
Assumed fractures	1.5 m^{-1}	2 m^{-1}	2 m^{-1}

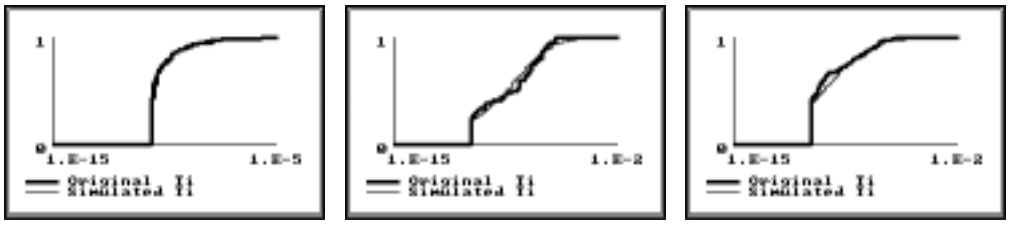

Subclass 2 Subclass 3 Subclass 4 & 5

Figure 3-14. *Oxfilet analysis of observed packer tests (1 and 3m) in the prototype volume. The bottom diagram shows T cut-off at $3 \cdot 10^{-11}$ m^2/s.*

Table 3-10 shows the transmissivity distribution parameters per borehole sub-class. Observe that the table does not show the statistic parameters for the evaluated 3 fracture sets, but rather shows the parameters for fractures that intersects only that subclass regardless of orientation. The assigning of transmissivity distributions to fracture sets are explained in below.

Table 3-10. Parameters for transmissivity distributions from Oxfilet

Subclass	***2***	***3***	***4 & 5***
$Log_{10}(T) \in N(\bar{x}, \sigma)$	-11.59, 1.47	-9.77, 2.07	-11.50, 2.30
$T \in log_{10}N(\bar{x}, \sigma)$	$7.9 \cdot 10^{-10}$, $2.4 \cdot 10^{-7}$	$1.5 \cdot 10^{-5}$, 1.2	$3.9 \cdot 10^{-6}$, 4.8

3.2.8 Assigning transmissivity to fracture sets

The statistics given in Table 3-10 is related to the borehole subclasses, and not to fracture sets, which makes interpretation of conductive fracture orientation complicated. Instead the transmissivity distribution can be assigned to the 3 fracture sets by comparison of the orientation of the mean pole for the sets and the orientation of the boreholes. If the mean pole of a particular fracture set is parallel to the borehole then it is likely that the borehole is intersected by most fractures from this set. In an analogous way it is not likely that sets with an acute angle to the boreholes will intersect them in large numbers.

In accordance to the discussion above, the fracture transmissivity distribution from fractures intersecting subclass 2 boreholes will be assigned to the sub-horizontal set, set 3. The sub-horizontal boreholes of subclass 3 most likely intersect with the north-west striking fracture set, and hence the fracture transmissivity distribution from those borehole are assigned to the north-west striking set, set 2. The inclined boreholes will be intersected by the fractures of all the 3 fracture sets. The north-east striking fracture set is assigned the transmissivity distribution assigned by Oxfilet to borehole subclasses 4 and 5. The assumptions above are confirmed by testing a model. The model uses the assumed transmissivity and orientation distributions and compares the simulated transmissivities in the different exploratory hole subclasses with the observed.

The assigned transmissivity distributions are censored in purpose to prevent the model to produce unlikely high transmissive fractures. The simulated data produces some more high transmissive fractures than is measured, c.f. Figure 3-14 to the middle and the right. The censoring is based on the following two assumptions. A fracture should not have higher transmissivity than the large zones that surround the modelled volume.

As a second guideline Forsmark and Rhén (1999) investigated the distance between fractures with transmissivity higher than given cut-off values, c.f. Figure 3-15. The assumption is that there are not two or more highly transmissive fractures within the same 1 m packer, which implies that there might be shorter distances than shown in Figure 3-15, for fractures with transmissivity lower than $1 \cdot 10^{-10}$. On the other hand the amount of data decreases and the uncertainty increases as the cut-off value increases. The DFN model size is 100·175·100 m, i.e. 100 m scale. Therefor the cut-off for the different fracture sets is the transmissivity where the trend line intersects the value of 100 m between the fractures. The cut-off transmissivity is set $1 \cdot 10^{-5}$ m^2/s for the north-west striking fractures, $1 \cdot 10^{-6}$ m^2/s for the north-east striking fractures, and $1 \cdot 10^{-7}$ m^2/s for the sub horizontal set. Different values in different directions is due to the orientation of the fracture sets and that the water conductance is different for each set.

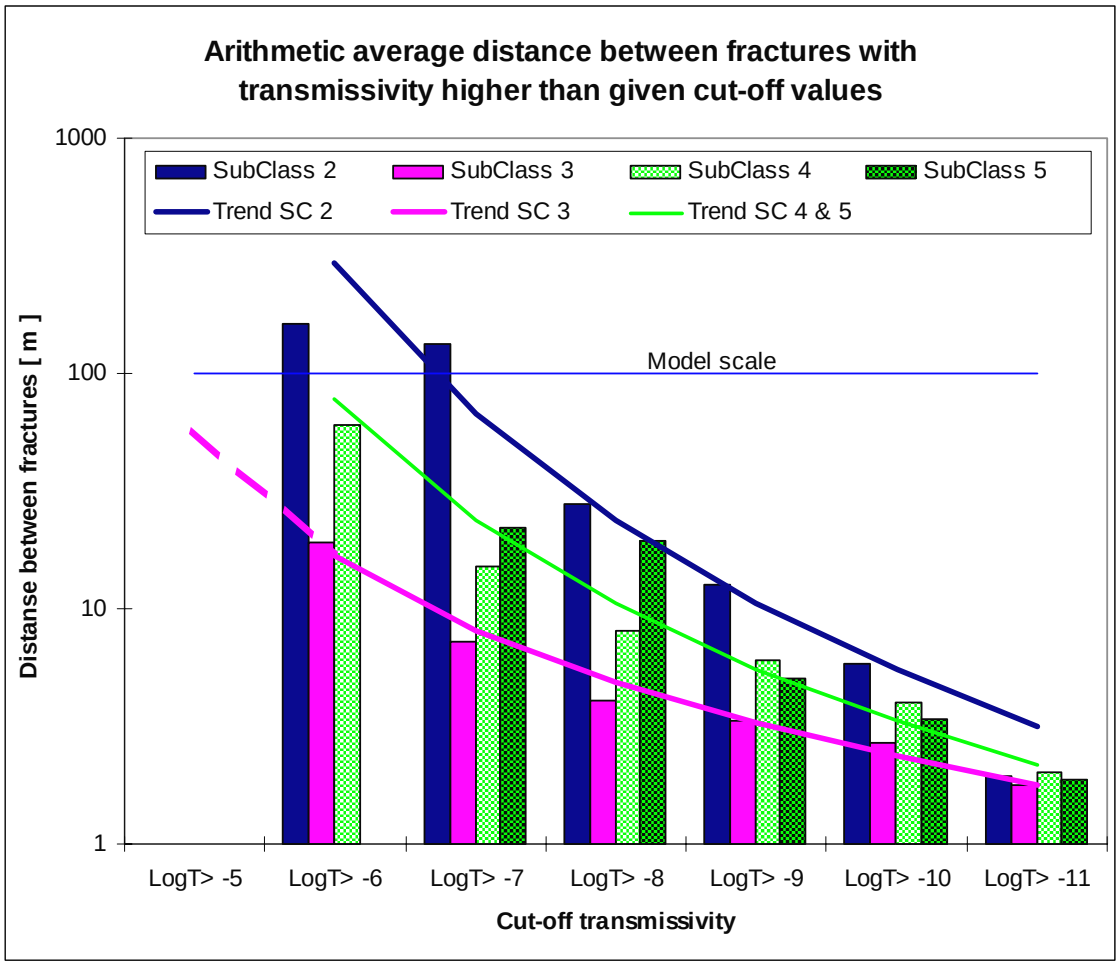

Figure 3-15. *The measured average distances between fractures with transmissivity higher than given cut-off values according to Forsmark and Rhén (1999).*

As suggested above a DFN model was generated and sampled with 1 m monitoring sections to validate the assumptions of transmissivity cut-offs for the different fracture sets. Simulations of pump tests were not made. Instead the transmissivities in each monitoring interval of 1 m length where assumed to be representative value for the section.

Figure 3-16 presents the cumulative transmissivity distribution per subclass. The truncation match is good for the sub-vertical holes, subclass 2. The simulated bore holes of subclass 2 are though intersected by too few fractures within the transmissivity range $5 \cdot 10^{-11}$ to $1 \cdot 10^{-10}$ m^2/s, and in the range $1 \cdot 10^{-10}$ to $1 \cdot 10^{-9}$ m^2/s the simulated subclass is intersected by too many fractures. The sub-horizontal holes, subclass 3, shows a good match up to $5 \cdot 10^{-10}$ m^2/s but then the simulated boreholes are intersected by too many fractures up to $1 \cdot 10^{-8}$ m^2/s. Between $5 \cdot 10^{-8}$ and $1 \cdot 10^{-6}$ m^2/s the simulated boreholes are intersected by too few fractures. The inclined boreholes, subclass 4 & 5, are intersected by too few fractures up to $5 \cdot 10^{-10}$ m^2/s and then have too many fractures up to $5 \cdot 10^{-8}$ m^2/s.

The model produces a bit too many fractures with transmissivities in the midrange. This is due to the "double peak" distribution in the measured data. It is impossible to match a lognormal distribution to such a sample, and to make a better match it is necessary to use another type of distribution. Another problem is that the horizontal holes demand more highly transmissive fractures while the inclined holes demands less high transmissive fractures. If the transmissivity is increased for the north-west striking set the inclined monitoring holes will also be intersected by more highly transmissive fractures.

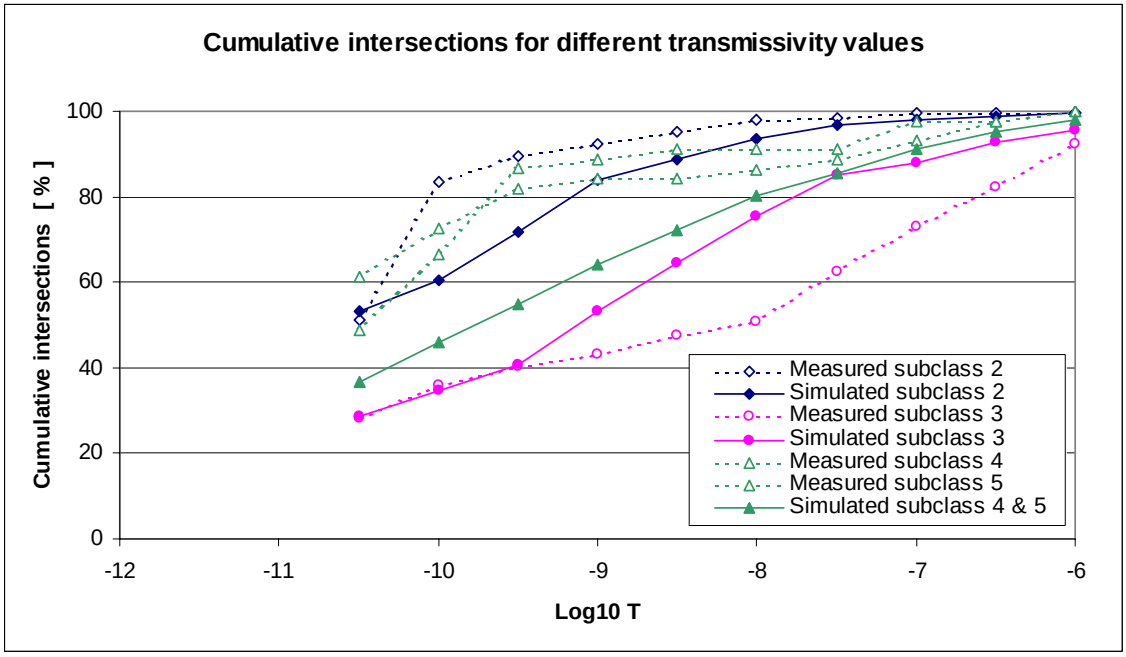

Figure 3-16. *Cumulative transmissivity distributions for 1 m packer sections.*

A statistical comparison between measured and simulated transmissivity in different borehole directions is presented in Table 3-11. The match is fair, within one order of magnitude, except for the inclined holes. On the other hand the 3 m packer sections in the inclined holes show very different transmissivities than in the 1 m sections, $\log(\bar{x}) = -8.7$ and $s = 2.9$. This may be due to large-scale heterogeneity in the rock, which is not taken into account in the DFN model.

Table 3-11. Mean and standard deviation of transmissivity in boreholes based on 1 m packer sections.

	Vertical holes		*Horizontal holes*		*Inclined holes*	
	$\bar{x}$	σ	$\bar{x}$	σ	$\bar{x}$	σ
Measured 1m	-11.5	1.9	-8.7	2.5	-11.4	2.5
Simulated 1m	-10.5	1.7	-9.2	1.9	-9.7	2.0

Fractures with low transmissivity have little influence on the flow solution but still require computer power to calculate the flow solution. In accordance to section 3.2.7 the assumed cut-off for T of "natural" fractures is $3 \cdot 10^{-11}$ m^2/s. This is the value that is assumed to be the cut-off for the simulated fractures that will be mapped as "natural" in the deposition holes. Fractures with a lower transmissivity are assumed to be "sealed". The "natural" fractures still contain fractures that are unnecessary for the flow solution, see Figure 3-17. The highest truncation value that is possible to use without loosing accuracy for the flow is $5 \cdot 10^{-10}$ m^2/s. Conductive fractures are defined as fractures with a transmissivity larger than or equal to $5 \cdot 10^{-10}$ m^2/s.

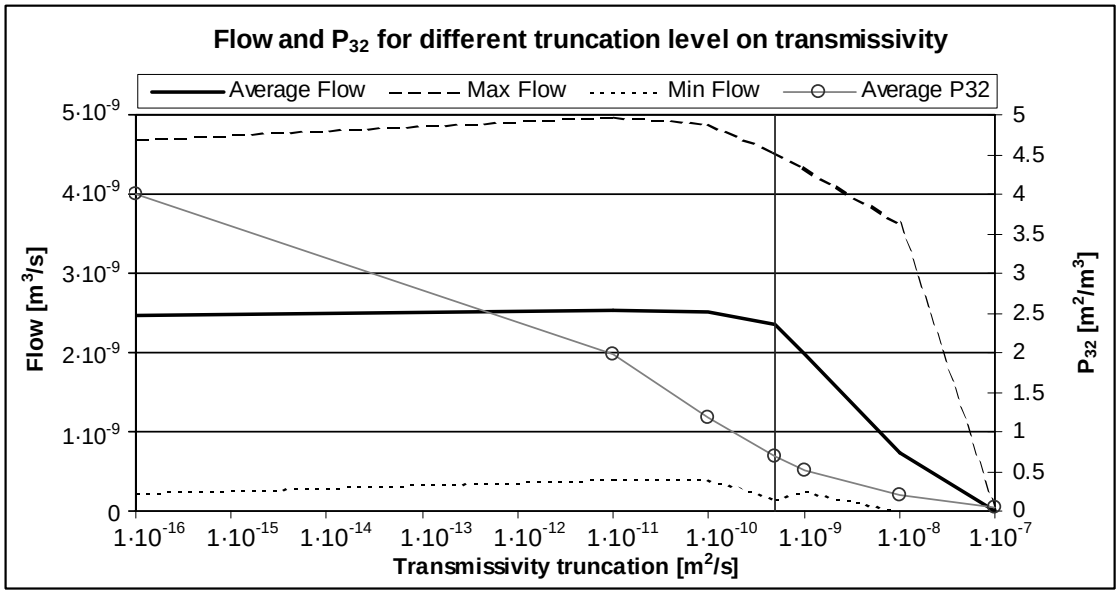

Figure 3-17. *The effect on the flow and the fracture intensity, P32, for different truncation levels on the transmissivity for a rock block with constant head boundaries.*

Table 3-12 shows the fracture intensity, P_{32}, for all, natural- and conductive fractures. The measured and simulated fracture frequency for different transmissivity cut-off is shown in Figure 3-18. One can see a good match for measured and simulated frequencies for the sub-vertical holes, sub-horizontal holes and holes inclined towards north, but the southerly inclined holes is intersected by approximately 30% too few fractures.

Table 3-12. P_{32} for the three different fracture sets with different truncation level.

	Set 1	*Set 2*	*Set 3*	*Σ*
$P_{32,\ all}$	0.85	1.59	0.97	3.41
$P_{32,\ natural}$	0.26	0.85	0.18	1.25
$P_{32,conductive}$	0.15	0.51	0.06	0.71

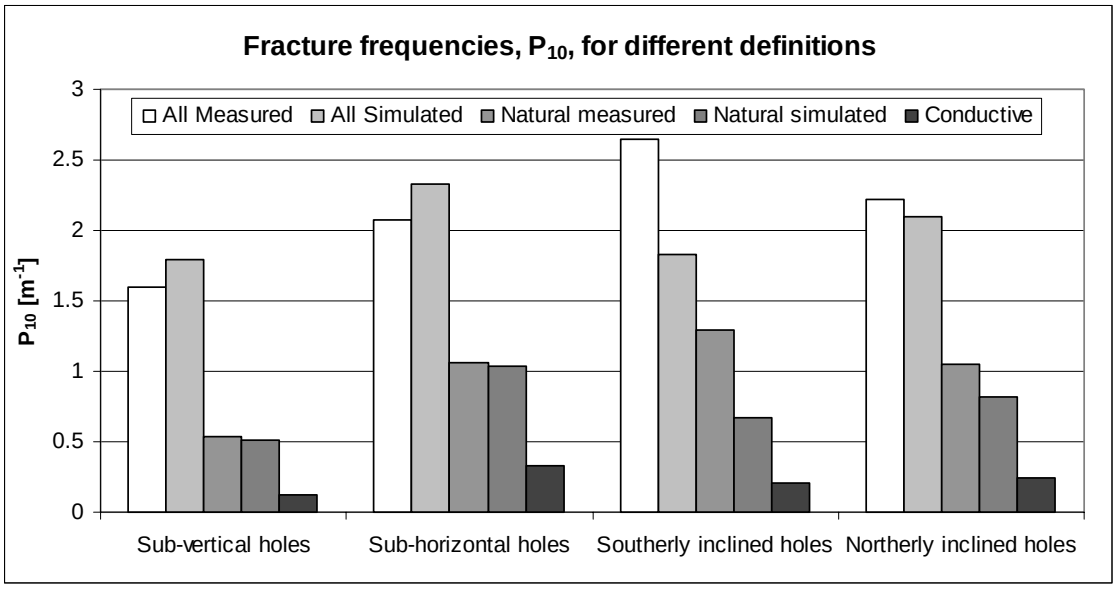

Figure 3-18. *The fracture frequency in different borehole directions for different transmissivity cut-off.*

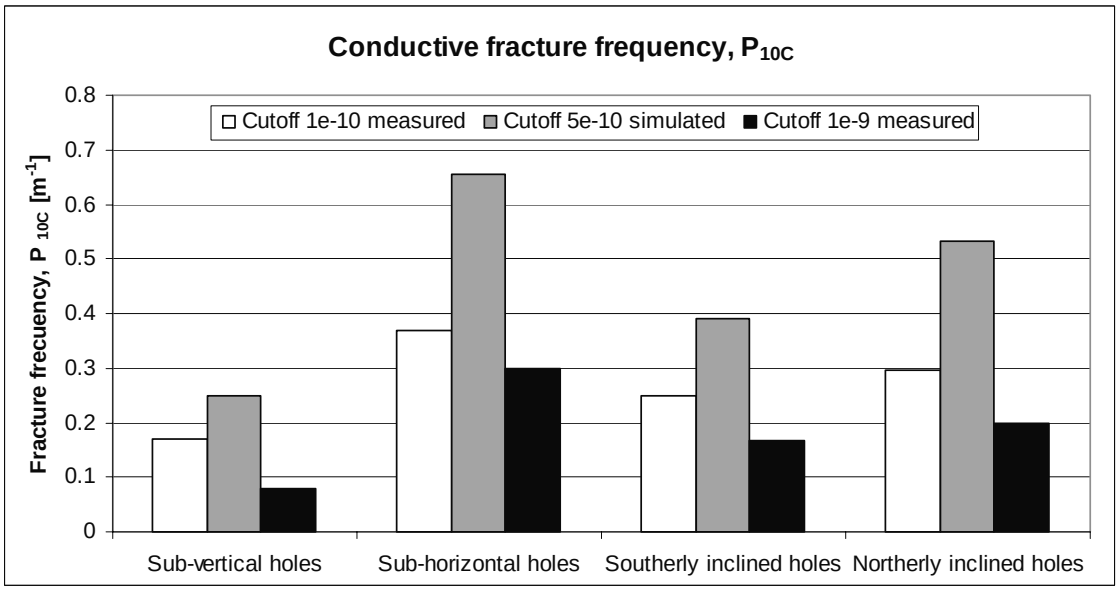

Figure 3-19. *Estimated conductive fracture frequencies by Forsmark and Rhén (1999) and simulated frequency.*

As mentioned above the flow solution is made with only the conductive fractures present in the model, i.e. a model with a P_{32C} equal to 0.71 m^2/m^3. As a comparison Hermanson *et al.* (1999), used a DFN model with a conductive P_{32C} of 0.7 m^2/m^3. A comparison with the estimated fracture frequency at different transmissivities done by Forsmark and Rhén (1999) shows that the DFN model produces twice as much fractures, see Figure 3-19. This can be an effect that Forsmark and Rhén (1999) assumed that there only was one fracture per packer section and that the DFN model simulate a bit to many fractures with transmissivity in the mid range, c.f. the double peak.

3.3 TBM tunnel inflow

Inflows in the HRL are measured at weirs collecting water in sections along the tunnel system. Inflow data come from the TBM tunnel (sections at 3521-3600 m) and the G tunnel. Inflow data for the TBM tunnel was sampled from the period of 18 August 1997 to 1 September 1997 and has been presented in Patel *et al.*, 1997.

The total flow measured in section 3521-3600 m in the TBM tunnel was 6.3 l/min. The modelled TBM tunnel section is 3509-3600 m, i.e. the inflow to the modelled TBM tunnel has to be scaled by a factor of 0.87 (=79/91) before it is compared with the measured inflow.

The inflow to the G tunnel is estimated from the inflow to the F tunnel. Measurements in the F tunnel gave different results depending on when measurements were made. Values of inflow per metre vary from 0.066 l/min to 0.087 l/min. The modelled G tunnel is 52 m long. The measured inflow for this tunnel section varies between 3.4 l/min and 4.5 l/min.

Table 3-13. Inflow in the TBM and G tunnels

Tunnel	*Inflow [l/min]*
TBM	6.3
G	4.5

4 Comparison of predictions from simulation of drill campaign 2 and field data from drill campaign 2 and 3

The prediction of the fracture parameters, fracture inflow and TBM tunnel inflow was presented in Hermanson *et al.*, 1999. All predictions were made with a DFN model built with fracture orientation data from the True Block Scale volume. The present chapter provides a comparison of the predicted results and the measured data of the 2nd drill campaign. The modelled 2nd drill campaign in Hermanson *et al.* (1999) consisted of twelve vertical boreholes, ten of 12 m length and two of 8 m length, located in the floor of the TBM tunnel. The actual 2nd drill campaign consists of ten vertical boreholes, eight of 12 m length and two of 8 m length, see Table 4-1. In Hermanson *et al.* (1999) the boreholes KA3574G01 and KA3576G01 are assumed to be parts of the 2nd drill campaign. Field data were measured in the 36 exploratory boreholes described in chapter 3.

Table 4-1. List of the boreholes of drill campaign 2.

Name	Length [m]
KA3544G01	12
KA3546G01	12
KA3548G01	12
KA3550G01	12
KA3552G01	12
KA3572G01	12
KA3578G01	12
KA3584G01	12
KA3586G01	8
KA3588G01	8

4.1 Comparison of fracture parameters

The comparison of the fracture parameters are made for the fracture orientation, size and frequency of the three fracture sub-sets with NW, NE and sub-horizontal orientations.

4.1.1 Orientation

Used and measured orientations of the three sub-sets in the Prototype repository area are presented in Table 4-2 below. The *"All fractures"* group of drill campaign might be too exhaustive to be compared with the used statistics since it is constituted by both "sealed" and "natural" fractures. Hermanson et al. (1999) showed that fractures could be sorted in three sets. A new comparison of "*Conductive fractures"* with "*Natural fractures"* statistics show only minor differences between the two groups regarding the orientation of the fracture sets. The comparison of the used True Block Scale results for the simulation of drill campaign 2 and field data from drill campaign 2 and 3 shows:

- The main trend of sub-vertical set 1 has a discrepancy of about 17^{o}. The used true block scale plunge of this set is in agreement with the field measurements.
- The trend of sub-vertical set 2 shows a difference of about 180^{o} between used and measured trend since fractures are near vertical.
- The sub-horizontal trend of set 3 is almost the same for true block scale data and measured during drill campaign 2. Since the inclination of set 3 is close to horizontal, discrepancies between predicted and measured are small.

Table 4-2. Used and measured for fracture orientation of Drill campaign 2. For more details see Hermanson et al (1999).

SET 1	**Used by Hermanson *et al.*, 1999**	**Drill campaign 2 measurements**	
	Conductive fractures	*All fractures*	*Natural fractures*
trend	117.9	129	135.1
plunge	12.9	6.3	23.5
k	5.64	4.84	4.7
%-fractures	12%	26.50%	35.30%
KS-%	0.16;38.5%	0.050;15.7%	0.059;12.4%

SET 2	**Hermanson *et al.*, 1999**	**Drill campaign 2**	
	Conductive fractures	*All fractures*	*Natural fractures*
trend	200.4	37	38.3
plunge	2	5.8	13.7
k	15.75	8.35	6.09
%- fractures	46%	35.60%	32.20%
KS-%	0.163;4.6%	0.040;23.4%	0.046;41.4%

SET 3	**Hermanson *et al.*, 1999**	**Drill campaign 2**	
	Conductive fractures	*All fractures*	*Natural fractures*
trend	186.5	290.6	280.7
plunge	81.1	84	77
k	13.6	8.33	8.7
%- fractures	42%	37.90%	32.50%
KS-%	0.095;79.7%	0.043;14.4%	0.064;9.3%

In Figure 4-1 is the lower hemisphere projection of the predicted poles of the conductive fractures and of the measured “natural” fractures that intersects the boreholes in drill campaign 2 shown.

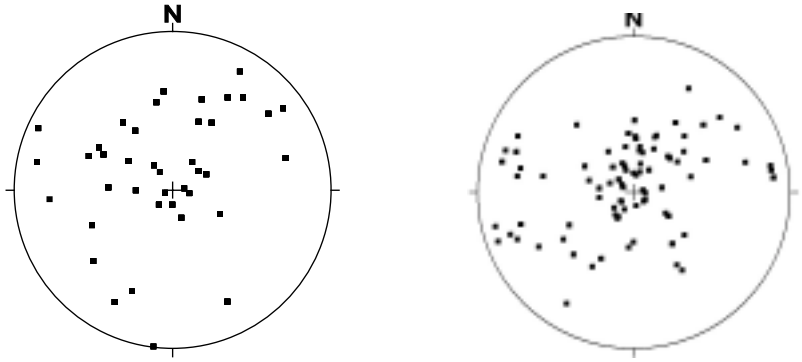

Figure 4-1. *Left: Lower hemisphere projection of the predicted poles of the conductive fractures that intersects the boreholes in drill campaign 2. Right: Lower hemisphere projection of the measured poles of the intersecting fractures in the boreholes from drill campaign 2.*

4.1.2 Size

No more fracture size analysis has been carried out since the set up of the modelling for prediction of fracture size of drill campaign 2. Drill campaign 2 only considers the borehole data that do not offer sufficient information to derive fracture size distribution. As a consequence, no comparison can be done between the predicted fracture set size distribution and additional data from drill campaign 2.

4.1.3 Frequency

The predicted statistics of the simulated fracture frequency of drill campaign 2 were based on ten stochastic realisations of the fracture network. Ten sub-vertical exploratory holes were sampled in each realisation. The list of the holes is presented above in Table 4-1.

The conductive fracture frequency was predicted to be on average 0.34 “conductive” fractures per metre. The observed “natural” fracture frequency from drill campaign 2 gave a value of 0.76 “natural” fractures per metre. A “natural” fracture is interpreted to be an open fracture, but it does not have to be waterbearing. Unfortunately the borehole data do not contain information if a “natural” fracture is waterbearing or not and Hermanson *et al.* (1999) only modelled conductive fractures. As shown in section 3.2.7 the relationship between modelled “natural” and modelled conductive fractures is a factor 2 to 3 in this model. It is most believable that the same ratio could be applied to the data in Hermanson et al. (1999).

4.2 Comparison of modelled and measured exploratory holes inflow

Hermanson et al. (1999) used ten stochastic realisations to get statistics for prediction of the inflow to ten exploratory holes in drill campaign 2. The exploratory holes of the TBM tunnel were implemented one at a time to simulate a real situation where each borehole is closed after drilling. The boundary condition of the exploratory holes was set to be atmospheric pressure. The average simulated inflow was 0.07 l/min, c.f. Figure 4-2.

Rhén and Forsmark (1998b) evaluated the measured inflow to the exploratory holes. During the flow tests a packer with a pipe system was put on top of each borehole so that the opening of the borehole was between 1.35 and 1.51 m above the tunnel floor. The average inflow for the ten exploratory holes was 0.013 l/min, c.f. Figure 4-2.

The simulations predict an average inflow that is about 5 times larger than the measured and a maximum inflow that is about 3 times larger than the measured. The minimum inflow is zero for both simulations and measurements, which corresponds to that no conductive fracture intersects the hole. Part of the discrepancies may be explained by the fact that a pressure exceeding atmospheric pressure of ca 1.4 m water was applied during the measurements of the exploratory holes while Hermanson et al. (1999) used atmospheric pressure during simulations. The simulated flow will be smaller if the boundary condition is changed to match the measurements. Another explanation could be that Hermanson et al (1999) used the same transmissivity distribution in all directions that might be more water bearing.

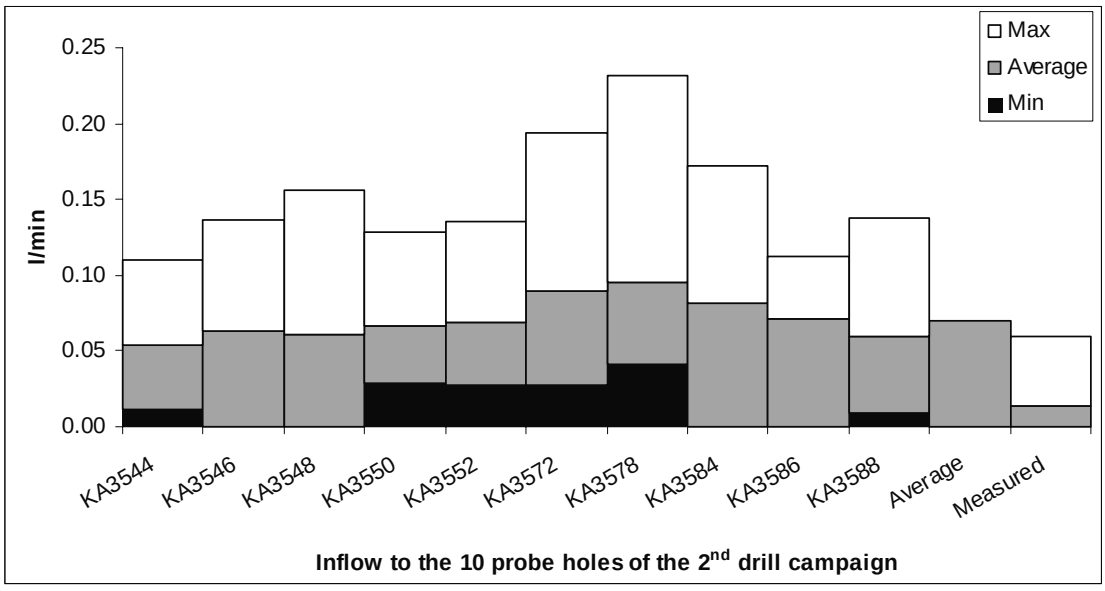

Figure 4-2. *Simulated and measured inflow to the ten exploratory holes in drill campaign 2. Unfortunately the simulated and measured inflow tests are made under different circumstances.*

5 Prototype DFN model II

5.1 Model geometry and location

The model has to cover a sufficient volume to be able to adequately predict the inflow to the deposition holes. It is preferable if the volume is so big that reasonable changes of the boundary will not affect the inflow to the studied volume. On the other hand the model volume has to be small to adapt to the existing computer power. Hermanson et al. (1999) used a model size of 100·150·100 m^3, In this study the volume is expanded 25 m westwards and covers a volume of 100·175·100 m^3. The model is a cube where the boundaries are parallel with the Äspö96 co-ordinate system. The Lower left co-ordinate of the cube is 1811, 7221, -498 (East, North, Up) and the upper right is 1986, 7321, -398. Figure 5-1 illustrates the model volume and some of the surrounding tunnels.

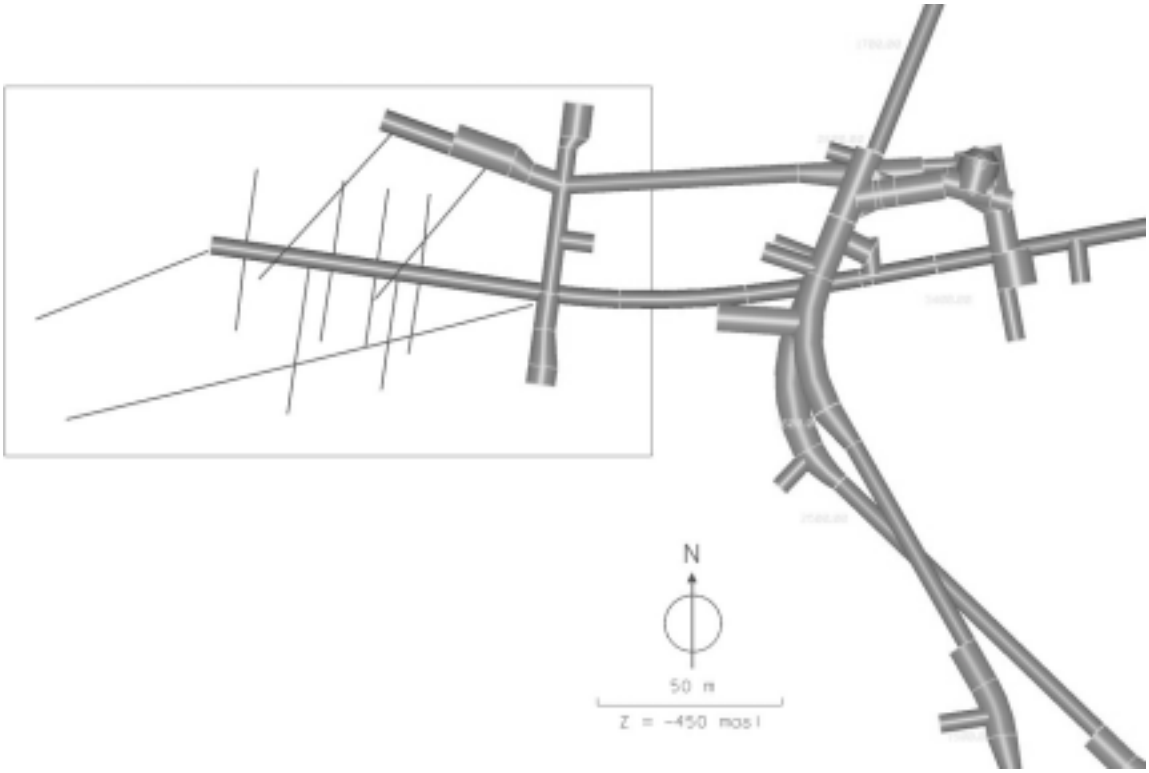

Figure 5-1. *Model volume. The outlined box shows the main boreholes and tunnels in the area.*

5.2 Boundary conditions

The boundaries of the model consist of outer and inner boundaries. The outer boundaries are the 6 surrounding surfaces of the simulation domain and inner boundaries are the tunnels and boreholes inside the domain. Conditions of the boundaries are discussed below.

5.2.1 Outer boundaries

Specified head is applied to all the 6 outer boundaries. The heads have been derived from the site scale finite difference flow solution presented in Svensson (1997). The pressure distribution results of Svensson's model is converted to fresh water head according to:

$$H = Z + p_{US} / (\rho_w \cdot g)$$

Where

- H = Fresh water head [m]
- Z = Current elevation in [m]
- p_{US} = Pressure from Svensson (1997) [Pa]
- ρ_w = density of fresh water [kg/m^3]
- g = Constant of gravity [m/s^2]

To get a smoother head field from Svensson's discrete 20 m blocks, a 3D interpolation has been performed using the 8 nearest values with a weighting factor that decreases with the square of the distance. Consequently the head field on the outer boundaries vary in space, but not in time.

The fact that Svensson (1997) modelled the A-tunnel but not the F-tunnel makes it inappropriate to incorporate this part of the Äspö tunnel system in the DFN model. The effect of taking the F-tunnel into account will result in a large flow into the F-tunnel from the east boundary in vicinity of the area where the tunnel intersects the outer boundary. It will not affect the volume around the vicinity of the prototype tunnel, but will give rise to dummy value for the flow over the east boundary. In Hermanson et al. (1999) it is shown that the flow into the prototype tunnel is increased by a factor 1.25 if all other tunnels are removed from the model, i.e. only the prototype tunnel and the deposition holes are kept in the model. The effect on the deposition holes is even smaller as the increasing factor varies between 1.15 and 1.02, with the smallest value for the most westward deposition hole. Consequently the F-tunnel is removed from the DFN model since there are still 4 tunnels left between the prototype repository and the F-tunnel. Obviously excluding the F-tunnel will affect the inflow to the G-tunnel by, approximately, a factor 1.25 to 1.5. This shall be kept in mind when the DFN model is calibrated against inflow to the G-tunnel.

5.2.2 Inner boundaries: tunnels, pilot holes and deposition holes

The tunnels included in the model are shown in Figure 5-2 and

Figure 5-4 and comprise segments from the last part of the A-tunnel (i.e. the TBM tunnel), and the G-, I-, and J-tunnels. The tunnels are implemented with a specified head boundary, which corresponds to atmospheric pressure to simulate the effect of open tunnels.

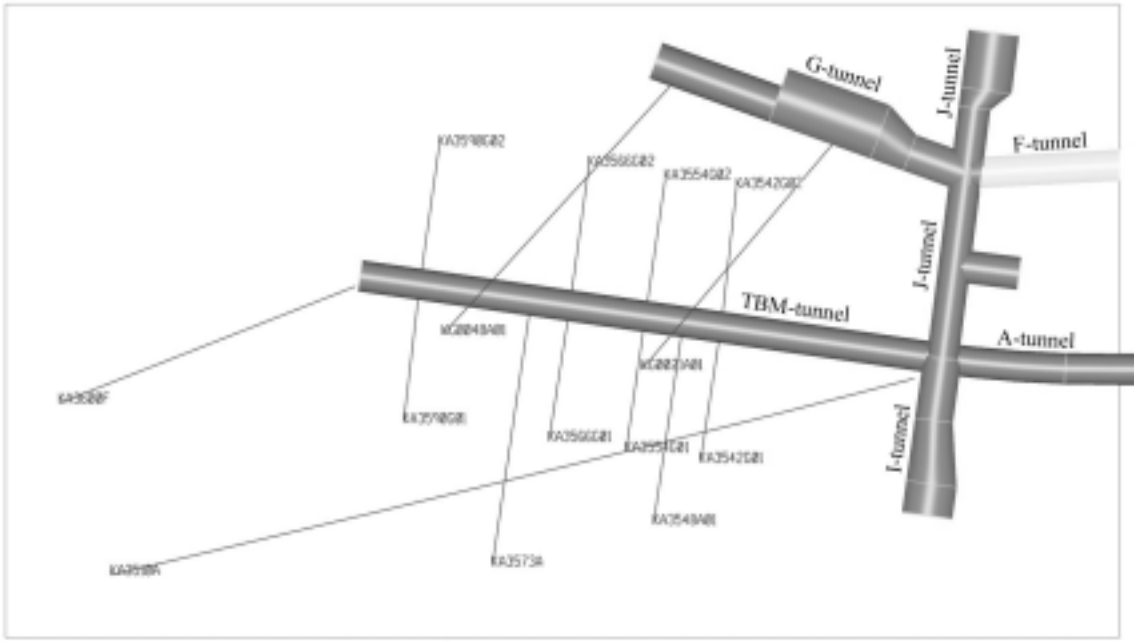

Figure 5-2. *Model domain showing sub-horizontal and inclined boreholes together with the included A-, G-, I-, and J-tunnels. The shaded F-tunnel is excluded.*

Packed off sections where no measurements are made in the boreholes are implemented in the model but not monitored. The boundary type is a variation of a specified flow boundary. It is called “groupflux” boundary. Groupflux boundaries allow the water to flow from one fracture to another through a packed off section, c.f.
Figure 5-3. The inflow to the section is equal to the outflow as mass balance is respected and the head remains constant in the packed off section.

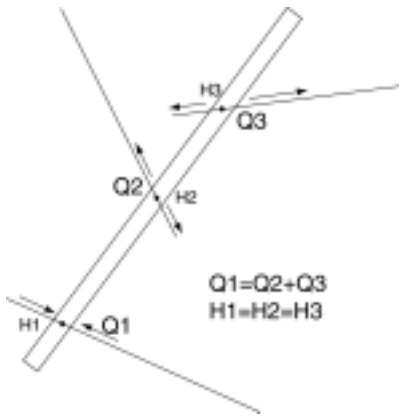

Figure 5-3. *Illustration of groupflux boundaries.*

Packed off sections where inflow measurements are made has a boundary that is as similar as possible to the conditions of the field-tests. During the field tests a tube was put on top of the borehole and the inflow was measured under atmospheric pressure plus the pressure of the water in the tube. The tube system was between 0.45 and 2 m above the tunnel floor, c.f. Forsmark and Rhén (1999). This implies that the simulated exploratory holes have to be implemented in a similar manner not to overestimate the possible inflow. The simulated exploratory holes are implemented in the model with a specified head boundary condition corresponding to atmospheric pressure plus a water pillar of the same height over the tunnel floor as was used during the measurements.

The deposition holes are numbered from the most inner part of the prototype tunnel and eastward. They are grouped in two groups, hole 1 to 4 is one group and hole 5 and 6 is one, see
Figure 5-4. The deposition holes are implemented in different ways depending on the purpose of the model. During the calibration phase all deposition holes are assumed to be closed, i.e. a no-flow boundary is applied.

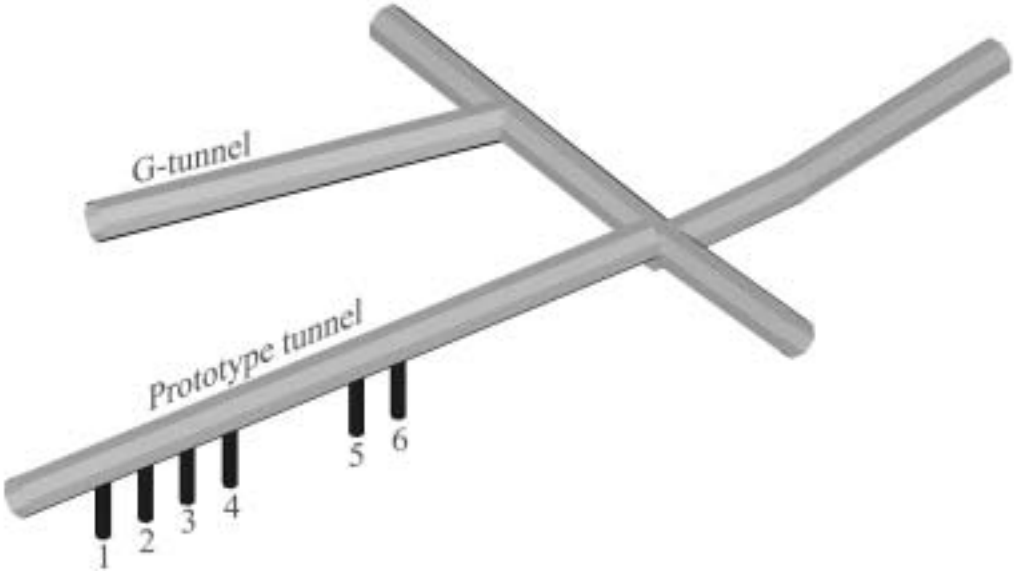

Figure 5-4. *The position and numbering of the 6 deposition holes in the Prototype repository tunnel.*

The sensitivity study is performed with all six holes open and drained, i.e. specific head corresponding to atmospheric pressure. The simulation of the excavation of the deposition holes is made in two phases. First, only deposition holes 1 to 4 are excavated, the most westward deposition holes. This implies that borehole 1 to 4 are assumed to be open and drained, i.e. specified head, while deposition holes 5 and 6 are modelled as a no-flow boundary, i.e. there are no in- or out-flow in those deposition holes. Consequently, the head-field is not affected by hole 5 and 6. The effect on the flow paths of a no-flow boundary is that the water has to flow around the deposition holes as sketched in Figure 5-5. Second, when all deposition holes 1 to 6 are drilled, the deposition holes are assumed to be open and drained, i.e. the deposition holes have a specified head corresponding to atmospheric pressure.

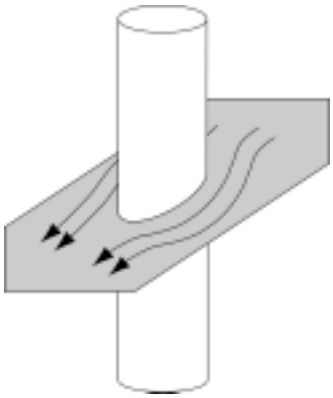

Figure 5-5. *Sketch of how a no-flow boundary affects the flow paths.*

For the transient simulations the excavated deposition holes are assumed to have atmospheric pressure, i.e. it simulates a case were all water in the excavated deposition holes immediately is removed. Non-excavated deposition holes is set to have no-flow boundary.

5.3 Summary of evaluated DFN parameters

5.3.1 Orientation distribution

The Prototype DFN model will be used for generation of both fracture maps and conductive fracture maps together with calculation of inflow to tunnels and deposition holes. Fracture statistics show small differences between the "all fractures" group and the "natural fractures" group, c.f. chapter 3.2.2. Table 5-1 shows the evaluated orientation data based on "natural" fractures.

Table 5-1. Orientation data used when generating the DFN-model

	Set 1	***Set 2***	***Set 3***
Strike [^{o}]	219	127	20.6
Dip [^{o}]	83.7	84.2	6
K	4.84	8.35	8.33

5.3.2 Size distribution

The fracture size distribution was estimated from TBM tunnel drift data. The fracture size estimates evaluated in chapter 3.2.3 vary in different orientations. The size distributions for sets 1, 2 and 3 were taken as the most probable distributions from Figure 3-5 to Figure 3-7. Data are summarised in Table 5-2 below.

Table 5-2. Most probable fracture set size for sets 1, 2 and 3.

	Set 1	*Set 2*	*Set 3*
Mean radius	2 m	8 m	5 m
Standard deviation	2 m	2 m	4 m

5.3.3 Spatial fracture model

In accordance to the discussion in chapter 3.2.6 an enhanced Baecher model is used .

5.3.4 Fracture intensity

A model based on the "all" fracture frequency together with the derived distributions for orientation and size is generated to estimate the fracture intensity. The result from the simulations gives a global P_{32} of 3.41m^2/m^3 where each fracture set contributes with a P_{32} of 0.85, 1.59 and 0.97 for fracture set 1, 2 and 3 respectively. This model intends to simulate the complete fracture network containing all fractures. The model will be used to predict trace maps from the deposition holes.

The fracture intensity of fractures that are considered to be "natural" and fractures that are estimated to be conductive is evaluated below. The conductive fracture frequency is critical for the flow simulation.

5.3.5 Transmissivity distribution

The assigned transmissivity distributions for the different fracture sets, shown in Table 5-3 is in accordance to the discussion in section 3.2.8.

Table 5-3. Transmissivity distribution for the three sets.

Set	*1*	*2*	*3*
$Log_{10}(T) \in N(\bar{x}, \sigma)$	-11.50, 2.30	-9.77, 2.07	-11.59, 1.47
$T \in log_{10}N(\bar{x}, \sigma)$	$3.9 \cdot 10^{-6}$, 4.8	$1.4 \cdot 10^{-5}$, 1.1	$7.7 \cdot 10^{-10}$, $2.3 \cdot 10^{-7}$

5.4 Deterministic structures

Eight fractures have been characterised during the field measurements of the prototype tunnel. These fractures are included into the DFN-model of the prototype repository as deterministic fractures. The size and the transmissivity values are in the range of the stochastic parameters and the fractures are therefore not treated in a different way during the evaluation of the field data.

Structures 1 and 2 have been characterised by interference test determined by Rhén (pers. com. 1999). Structure 1 is in contact with boreholes KG0048A01, KA3590G02 and KA3566G02. Structure 2 is in contact with boreholes KA3590G01 and KA3566G01. Structures 3 to 8 have been characterised out of exploratory hole drilling, flow logging, borehole pressure build up tests and interference test. These structures are suspected to be smaller than structures 1 and 2. They are located at the vicinity of

deposition holes. Structures 3, 7 and 8 have no particular connection with any borehole. Structures 4 and 5 show connections with boreholes KA3546G01, KA3548G01 and KA3550G01. Sizes and storativity of features 3 to 8 are very uncertain. The characteristics of the deterministic structures are summarised in Table 5-4 below.

Table 5-4. Characteristics of the deterministic features of the prototype DFN model as given by Rhén (pers. com. 1999).

Feature	*Trend [°]*	*Plunge[°]*	*Strike [°]*	*Dip[°]*	*Radius [m]*	*T [m^2/s]*	*S*
1	28	2	118	88	20	7E-08	2E-07
2	34	1	124	89	20	8E-08	5E-08
3	264	11	354	79	2	8E-09	3E-07
4	222	50	312	40	2	4.7E-09	3E-07
5	181	52	271	38	2	3.3E-09	2E-07
6	188	66	278	24	2	1.7E-09	2E-07
7	74	26	164	64	2	2.8E-10	9E-08
8	208	26	298	64	2	1.3E-08	4E-07

The location, orientation and size of the deterministic structures are presented Figure 5-6 below.

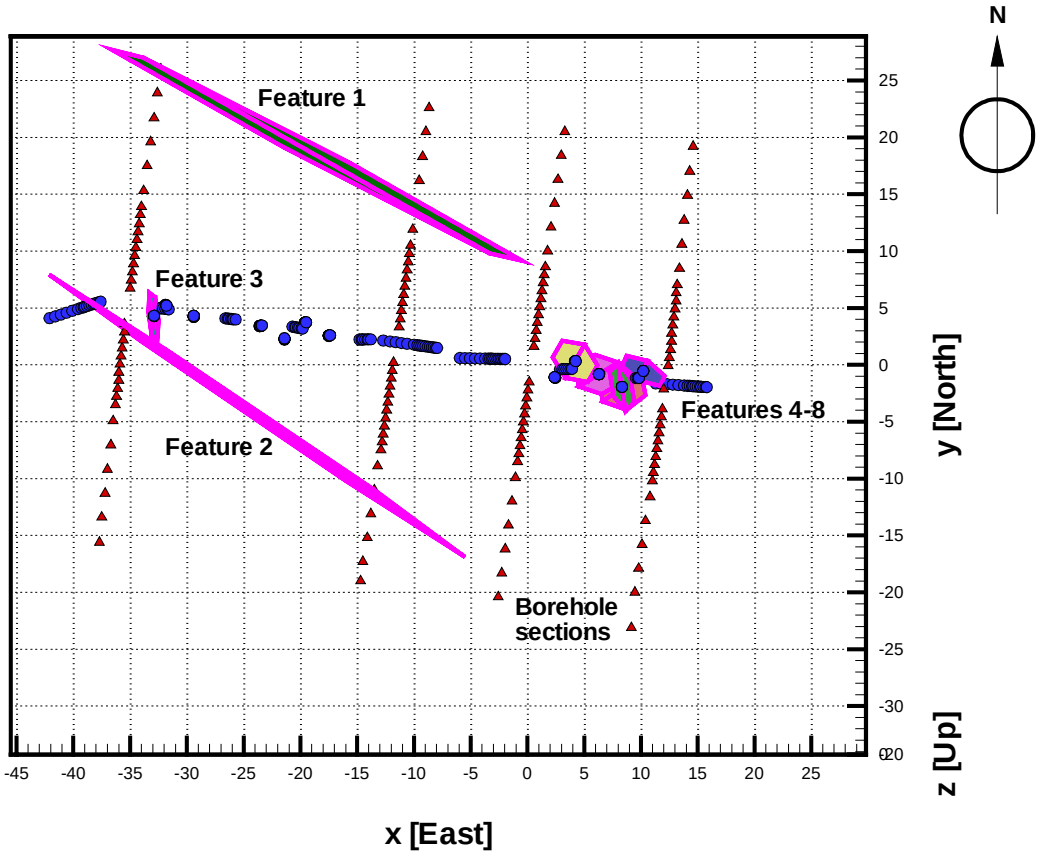

Figure 5-6. *Top view of the prototype repository area with borehole sections and deterministic fractures.*

6 Model calibration and sensitivity study

6.1 Calibration of the model against field data from the TBM tunnel and pilot holes

When constructing the DFN model, simplifications and assumptions are made of the input data. The model cannot handle the diversity of the nature and needs to be simplified. A consequence is that several uncertainties and differences remain between the behaviour of the DFN model and the observations. To overcome these discrepancies, the model can be calibrated to what is observed. The calibration of the DFN model is focused on calibrating flow properties through the network.

In the present work, the calibration is made against inflow data from the TBM tunnel, G-tunnel, and the exploratory boreholes listed in Table 6-1. The flow measurements in the boreholes were performed with a tube put on top of each borehole. The inflow was measured with atmospheric pressure plus the pressure of the water in the tube. Each hole was tested one at a time while the other holes were kept closed.

Table 6-1. Boreholes used for calibration

Borehole	*Level of measurements [m above tunnel floor]*
KA3539G	1.46
KA3542G01	1.01
KA3542G02	1
KA3548A	2
KA3554G01	0.92
KA3554G02	1.07
KA3557G	1.49
KA3563G	1.49
KA3566G01	1.01
KA3566G02	1.06
KA3574G01	1.47
KA3576G01	1.49
KA3579G	1.2
KA3590G01	1
KA3590G02	0.95
KA3593G	1.45
KG0021A01	0.71
KG0048A01	0.45

The first calibration model is based on the DFN parameters presented in section 5.3. This model simulated too high inflow to the TBM and G-tunnel, c.f. Table 6-2.

Table 6-2. Measured and simulated inflow from the first calibration model.

	TBM-tunnel	G-tunnel
Measured inflow [l/min]	6.3	3.4-4.5
Simulated inflow [l/min]	98	38

There are many possibilities to calibrate the modelled inflow to the tunnels, either the flow into the tunnels can be decreased by reducing the overall transmissivity distribution of the fracture sets or a skin could be applied around the tunnels. A skin is a volume of the model around the tunnels, which has a hydraulic conductivity different from the rest of the model. Other calibration tools can bee to decrease the dispersion of the highly conductive fractures so that the connectivity decreases.

The hypothesis of a skin around underground openings can be argued, but several authors have reported that either a reduction or increase of the hydraulic conductivity may exist. This can be due to change in stressfield, unsaturated flow or increased fracturing, c.f. Winberg (1995). The TBM-tunnel is drilled with a TBM-machine and not excavated by blasting, this implies that it is most believable that the hydraulic conductivity is reduced due to stressfield and unsaturated flow.

An overall decrease of the transmissivity will affect the whole model by giving less inflow to all inner boundaries, e.g. tunnels and boreholes. Using a skin will decrease the inflow to the parts that are surrounded by the skin but will increase the inflow to the parts that are not surrounded by skin. The results of the model still showed very large inflow to the tunnel system and in the boreholes where the flow measurements have been made, c.f. Table 6-3.

Table 6-3. Measured and simulated inflow from the first calibration model when a skin is applied around the tunnels.

	TBM-tunnel	G-tunnel
Measured inflow [l/min]	6.3	3.4-4.5
Simulated inflow, Skin T·0.1 [l/min]	67	19
Simulated inflow, Skin T·0.01 [l/min]	59	7

There are some uncertainties in assigning a lognormal transmissivity distribution to the fracture sets, c.f. the double peak nature in section 3.2.7. It is therefore possible that changing the mean and standard deviation for one fracture set could give better match for the inflow to the tunnels. The north-west striking set, set 2, was reduced half an order of magnitude of its original mean value to obtain a maximum effect on the tunnel system inflow with a minimum change in the fracture network hydraulic characteristics. The new transmissivity distribution of the north-west striking set was validated by an Oxfilet analysis made on the 3 m packers sections, see Figure 6-1.

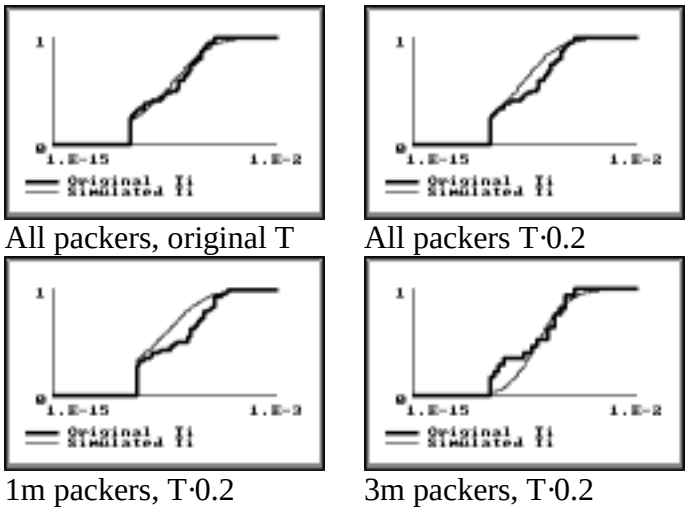

Figure 6-1. *Oxfilet analysis with a lower T-distribution.*

The estimated transmissivity statistics in the different borehole subclasses was affected by the change of the transmissivity distribution of the north-west striking set. The vertical and inclined holes statistics showed a better match with the measurements while the horizontal holes statistics showed a somewhat worse match with the measurements see Figure 6-2.

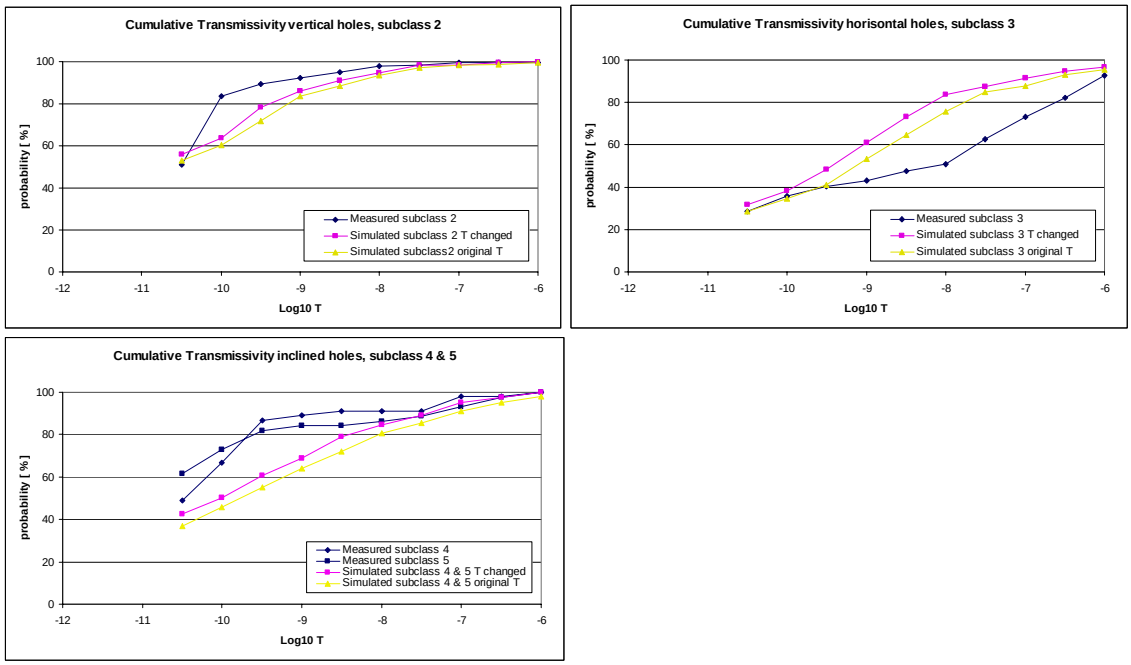

Figure 6-2. *Cumulative plots of transmissivity per borehole subclasses.*

It was observed that the reduction of the mean of the transmissivity distribution of the north-west striking set did not fully correct the inflow in the G and TBM tunnel, c.f. Table 6-4.

Table 6-4. Measured and simulated inflow from the first calibration model when the transmissivity distribution for the north-west striking set is reduced.

	TBM-tunnel	G-tunnel
Measured inflow [l/min]	6.3	3.4-4.5
Simulated inflow, reduced T_{set2}, [l/min]	33	36

As mentioned above, it is most likely that there will be a skin around the TBM tunnel. Therefore a model with skin around the tunnels and a reduced transmissivity for the north-west striking set is used. The result show good match for a skin-factor of 0.01, c.f. Table 6-5.

Table 6-5. Measured and simulated inflow from the first calibration model when a skin is applied around the tunnels and reduced transmissivity distribution for the north-west striking set.

	TBM-tunnel	G-tunnel
Measured inflow [l/min]	6.3	3.4-4.5
Simulated inflow, Skin T·0.1 & reduced T_{set2} [l/min]	14	17
Simulated inflow, T·0.01 & reduced T_{set2} [l/min]	6	7

Table 6-6 shows the inflow in the monitoring holes for the calibration model with skin around the tunnels and reduced transmissivity for the north-west striking set. Despite the small amount of data, the comparison shows good accordance between the measured inflow and the simulated except for the geometric mean for the inflow to the vertical holes.

Table 6-6. Measured and simulated inflow for different borehole directions

	Measured inflow [l/min]	*Simulated inflow [l/min]*	*Ratio sim/meas*
	All boreholes		
Max	87.20	41.11	0.47
Average	8.64	9.91	1.15
Geomean	0.26	2.47	9.64
Min	0.00	0.00	1.00
	Vertical boreholes, subclass 2		
Max	5.02	11.34	2.26
Average	0.84	2.54	3.01
Geomean	0.0032	0.1346	42.54
Min	0.00	0.00	1.00
	Horizontal boreholes, subclass 3		
Max	87.20	41.11	0.47
Average	40.40	22.14	0.55
Geomean	25.62	18.54	0.72
Min	7.20	10.38	1.44
	Inclined boreholes, subclass 4 & 5		
Max	8.24	15.86	1.93
Average	2.58	10.86	4.21
Geomean	1.23	10.32	8.36
Min	0.18	6.39	35.48

Table 6-7 is a summary of the calibrated parameters in the DFN model that will be used for the sensitivity analysis and the predictions.

Table 6-7. Summary of used parameters for the DFN model.

Parameter	*Used data*	*Data from*	*Reference*
Orientation	Set Strike Dip K 1 219 83.7 4.84 2 127 84.2 8.35 3 20.6 6 8.33	Pilot and Exploratory holes	This report
Size	Set mean Std dev 1 2 2 2 8 2 3 5 4	TBM tunnel	Follin & Hermanson (1996)
Location model	Poisson distributed Enhanced Baecher	TBM tunnel	Follin & Hermanson (1996)
Conductive intensity, P_{32c}	0.71	Exploratory holes 1 m and 3 m test	This report
Transmissivity distribution $\log_{10}(T)$	Set mean Std dev Upper trunc 1 -11.5 2.30 -5 2 -10.3 2.07 -6 3 -11.6 1.47 -7	Pilot and Exploratory holes	This report
Model size	100 x 175 x 100 m (North, East, Up)		
Centre point in Äspö96 Co-ordinates	North = 7271 m East = 1899 m Z = -448 m		
Outer boundary conditions	Specified head boundary	site scale model	Svensson (1997)
Inner boundaries	Tunnels as head simulating atmospheric pressure p = 0. Boreholes no flow or head according to performed tests	Performed tests	Gentzschein (personal communication 1998) and Forsmark and Rhén (1999)

6.2 Sensitivity study

6.2.1 Introduction

The sensitivity study is based on the change of inflow to the 6 deposition holes, see Figure 5-4. The studied sensitivity cases are the variation of the deterministic fracture size and transmissivity, the effect of a skin zone around the tunnel system and the effect of a lower truncation for the conductive fractures.

Hermanson et al. (1999) made a sensitivity study of the effects of changing the outer boundaries to zero head gradient, the presence of a nearby tunnel system, the correlation of fracture transmissivity with fracture size, and finally the effect of simulating only steep fractures. The results showed that a zero head boundary only changed the inflow by less than 8%. Removing the nearby tunnel system increased the inflow to the TBM tunnel by 25%. The increase was 15% to deposition hole 6 and 2% for deposition hole 1. The correlation of the fracture transmissivity with fracture size resulted in an increase of the inflow to the tunnel system of more than 100 times its original value, which was considered to be an unrealistic situation. Simulating only steep fractures in the model resulted in a decreased inflow to the deposition holes by 25% while the inflow to the TBM tunnel increased by less than 10%. This approach made it possible to simulate realistic inflows to boreholes, tunnels and deposition holes.

6.2.2 Strategy

One of the 20 performed realisations is selected as the base case model to compare the impact that different parameters will have on the inflow to deposition holes. The selected case is the one that has a tunnel-inflow closest to the average of all 20 realisations. Note that the base case model is based on the model after the calibration phase (see Table 6-7). The model contains the last part of the A-tunnel together with the G-, I- and J-tunnels and the deposition holes. All boreholes that take part in the hydraulic measurements have been included in the model. The deposition holes during the sensitivity analysis are assumed open and drained. Figure 6-3 shows the inflow to the tunnels and deposition holes using the base case model.

Below follows sensitivity studies of the effect of the size of the deterministic structures and their transmissivity. The sensitivity study also includes variations of the skin around the tunnel system.

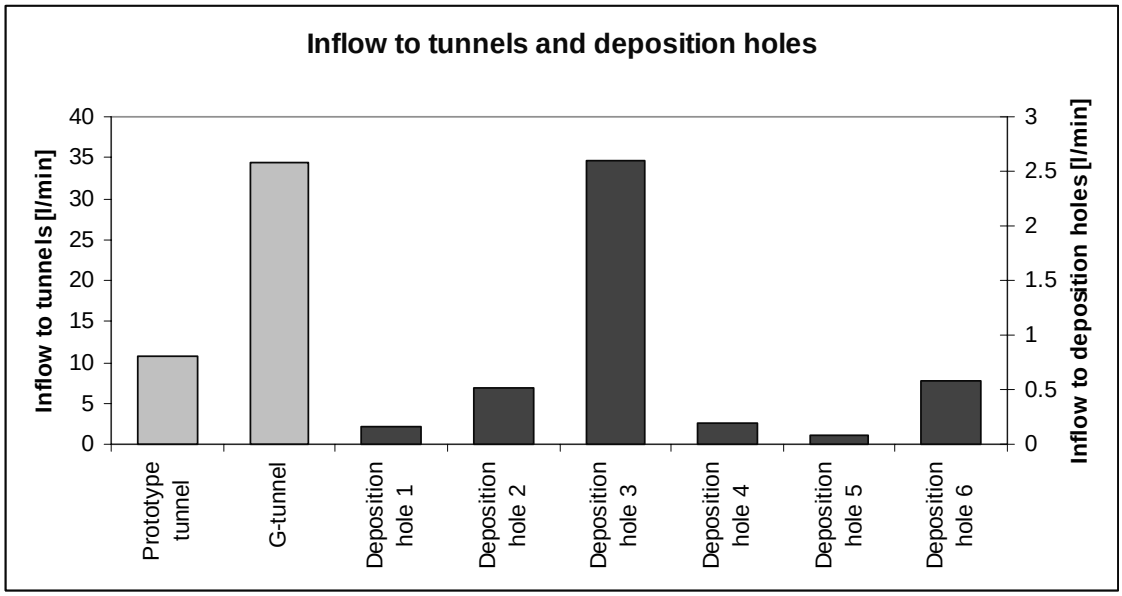

Figure 6-3. *Inflow to tunnels and deposition holes for the base case.*

6.2.3 Effect of deterministic fracture size variation

The size of the deterministic structures is an uncertain parameter that is difficult to measure in-situ. The hydraulic impact of the deterministic structures is large if the size and transmissivity are large compared to the stochastic network model volume. As size is difficult to measure, a sensitivity study is performed of the impact of increasing and decreasing the size of the deterministic structures in the model. The radii of the 8 deterministic structures are changed by ±50%.

Figure 6-4 shows the change relative to the base case when the sizes of the deterministic structures are reduced by 50%. The change in inflow is less than 10 % for all monitoring excavations except for deposition hole 5 for which the inflow is 47 % lower than in the base case.

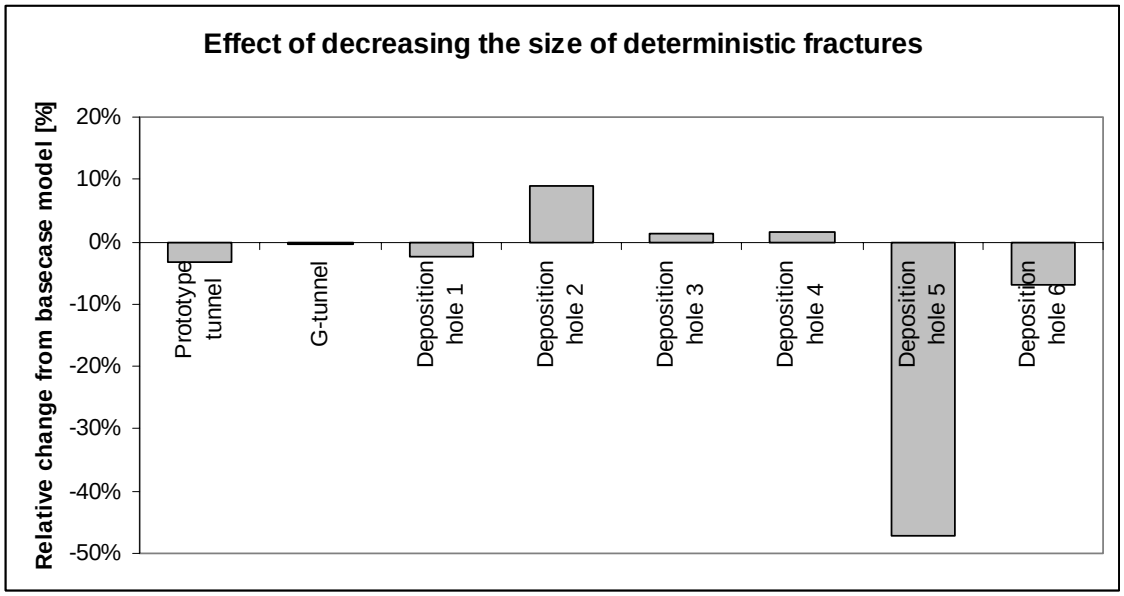

Figure 6-4. *The diagram shows the effect of decreasing the radius of the 8 deterministic structures by 50%.*

When the radius of the deterministic structures are increased by 50% the change of the inflow is significative for deposition hole 1 and 5, see Figure 6-5. The inflow increases by 58 % to deposition hole 1, 217 % to deposition hole 5 and 13 % to deposition hole 6. The effect on the other deposition holes and tunnels are less than 5 %.

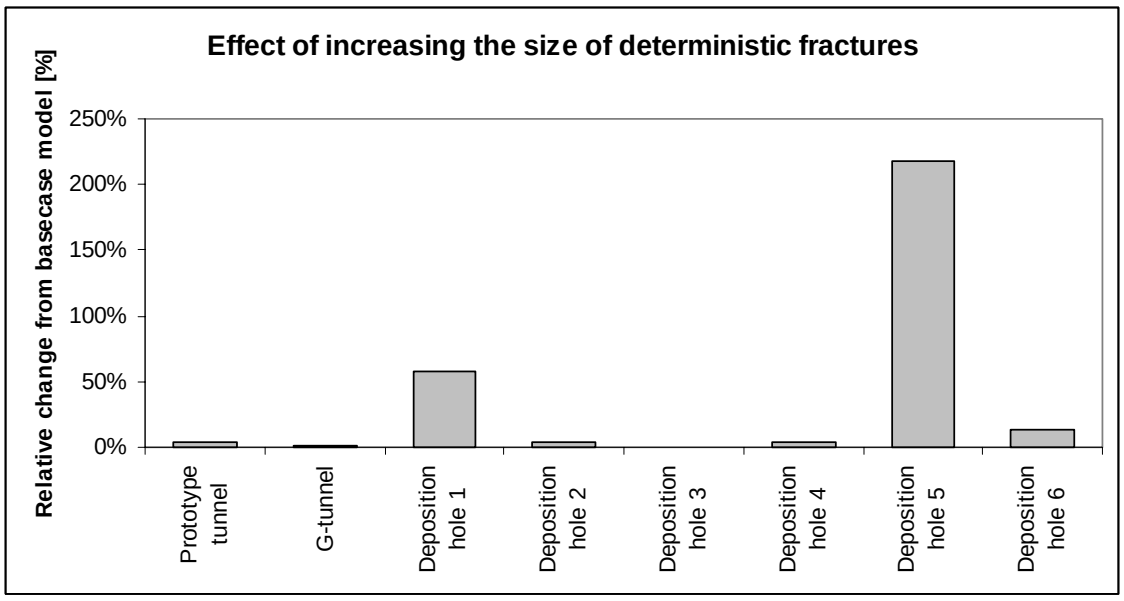

Figure 6-5. *The diagram shows the effect of increasing the radius of the 8 deterministic structures by 50%.*

Deposition hole 5 is largely affected by the variation of the size of the deterministic features. The reason is that the inflow to deposition hole 5 is the lowest in the base case, which means a high sensitivity to change in inflow, and the fact that some of the deterministic structures intersect this hole.

The inflow change in deposition hole 1 can be explained by the presence of the little deterministic structure, #3, between the deposition hole and the southerly large deterministic structure. When the size of this structure is small, it does not interact with the neigborhood more than in the base case. When its size is increased, it connects with the surrounding structures and becomes a major flow path between deposition hole 1 and the southerly large deterministic structure, #2, connected to a boundary, c.f. Figure 6-6.

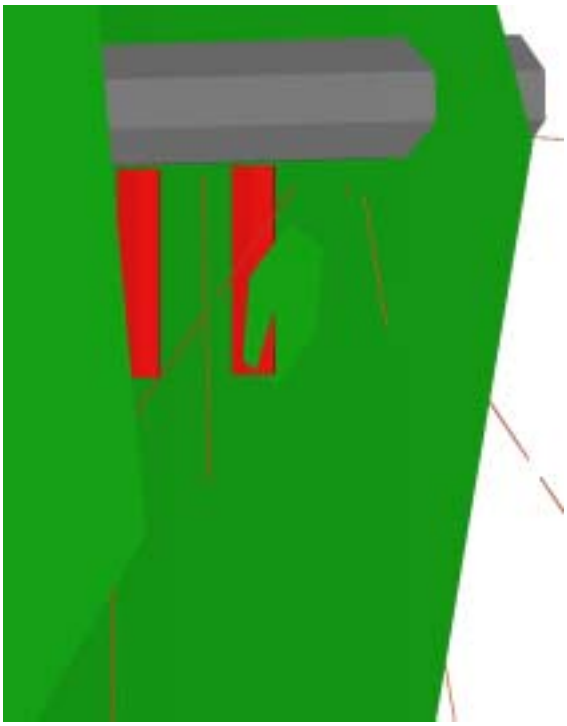

Figure 6-6. *The small deterministic fracture, #3, intersects both the deposition hole 1 and the southerly large deterministic fracture, #2.*

Deposition hole 6 is surrounded by most of the deterministic structures, see Figure 6-7. The lack of response due to size change depends on their low transmissivity.

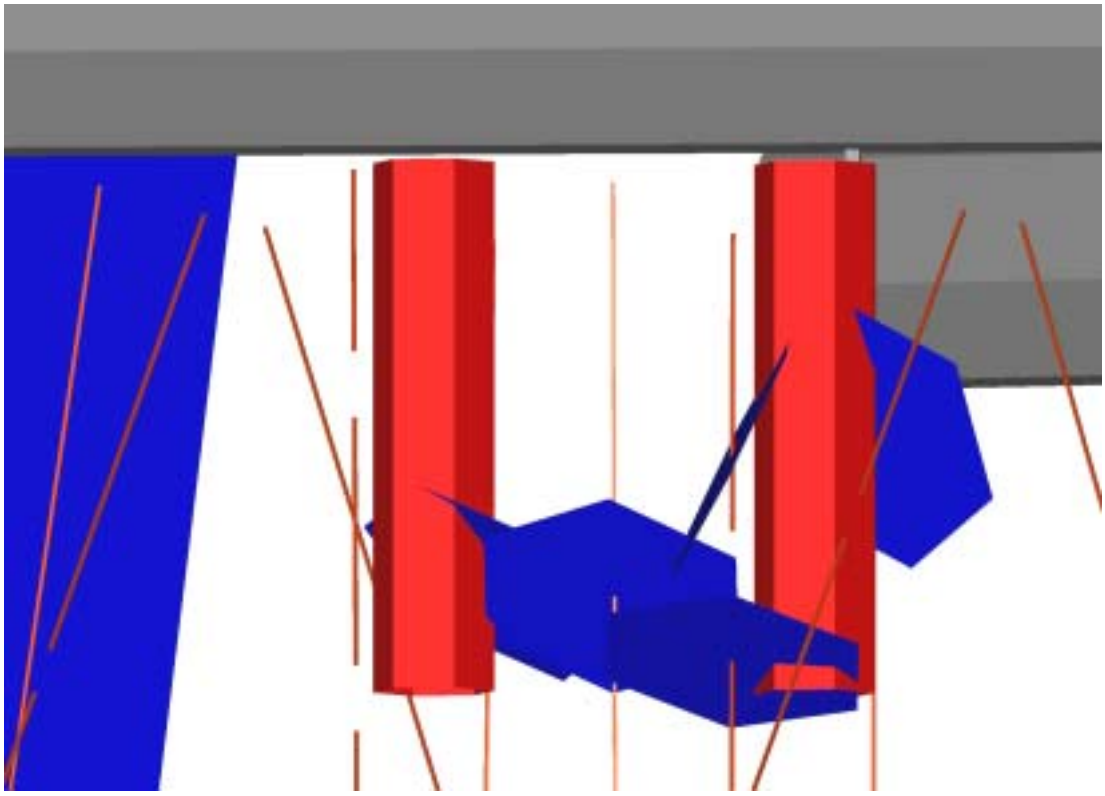

Figure 6-7. *Deposition holes 5 and 6 are surrounded by the blue deterministic structures. The brown lines are the packer sections.*

The following conclusions are drawn from the deterministic feature size variation study: Size variation of deterministic feature changes locally the connectivity of the DFN. A size increase has a negligible effect on the inflow to four of the deposition holes and the tunnels, only deposition hole 1 and 5 are affected.

6.2.4 Transmissivity of deterministic fractures

The transmissivities of the deterministic structures were characterised by double packer field tests (Forsmark and Rhén, 1999). The potential effect in the modelled flow field may be significant when varying the transmissivities in the deterministic structures. The parameter variations are based on a reduction and an increase of the transmissivity in these structures by a factor of 100.

When transmissivity values are decreased, the inflow in deposition hole 5 is reduced by 68 %. The variations of inflow in the other deposition holes are less than 10 % as seen Figure 6-8.

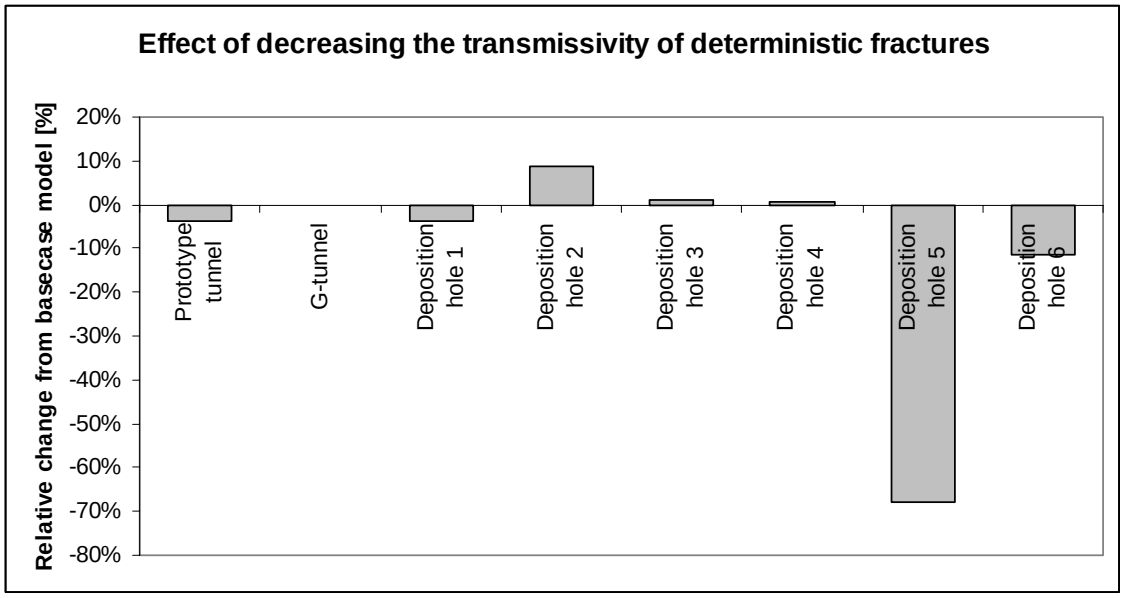

Figure 6-8. *The diagram shows the effect of reducing the transmissivity of the 8 deterministic features by a factor of 100.*

When the transmissivity is increased, a large increase in the inflow is observed in some deposition holes, c.f. Figure 6-9. The inflows to deposition holes 5 and 6 are increased by 227 % and 266 % respectively. At the same time the inflow to deposition holes 1, 2 and 4 is decreased by more than 50%.The relatively large increase in inflow in deposition holes 5 and 6 obviously diverts flow from other deposition holes.

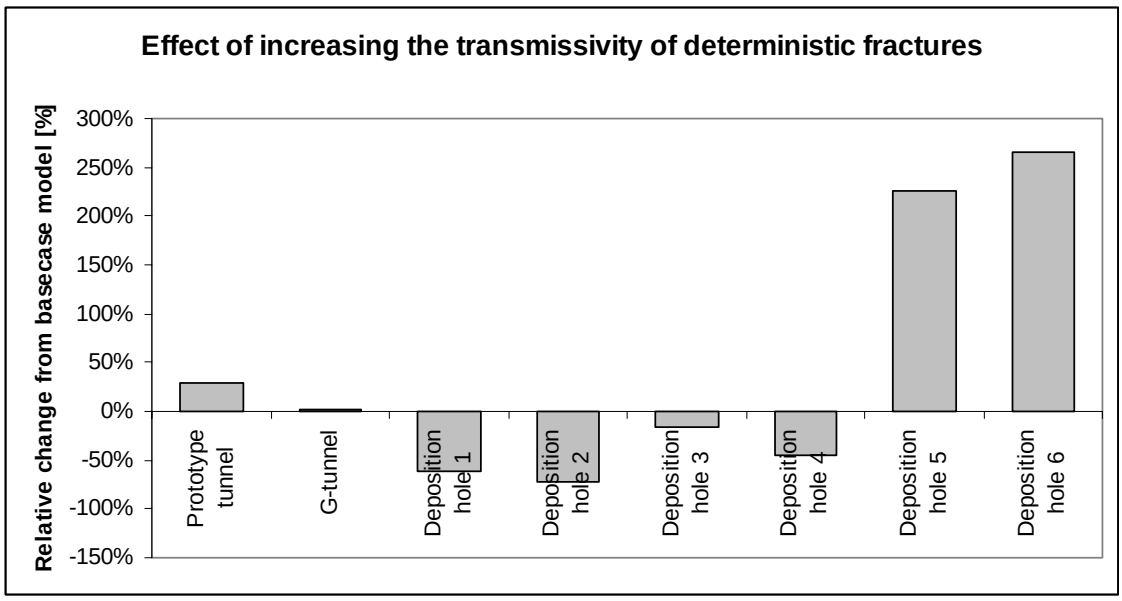

Figure 6-9. *The effect of increasing the transmissivity of the 8 deterministic features by a factor of 100.*

The main conclusion of the variation of transmissivity study is that the structures intersecting deposition holes 5 and 6 has a large impact on the predictive capabilities of the model. It is clear that changing either size or transmissivity in the structures intersecting deposition hole 5 has an effect of the flow situation in all the other boreholes. Deterministic features located deeper in the rock mass may have little effect on the inflow in the deposition holes or the tunnels.

6.2.5 Skin around the tunnel system

A skin zone around the tunnel system with reduced hydraulic conductivity is used to lower the water inflow into the tunnel. The natural explanation for having a skin zone in the model may be explained by different parameters: unsaturated flow in the rock mass, grouting or fracture closure due to increased compressive tangential stress around tunnels. The effect of varying the decrease of conductivity around the tunnel may be critical to the performance of the model. Using a skin will decrease the inflow to the parts that are surrounded by the skin but will increase the inflow to the parts that are not surrounded by skin due to less resistance. The thickness of the skin set to 2.5 m may permit water inflow in the lowest 5.5 m length of the deposition holes. The skin is modelled by reducing the transmissivity of the triangular elements of a fracture within a certain range around the tunnels. If one of the nodes of the element is outside the range, the element transmissivity remains unchanged. If all nodes are within the range, the transmissivity is scaled down. This technique is illustrated by Figure 6-10.

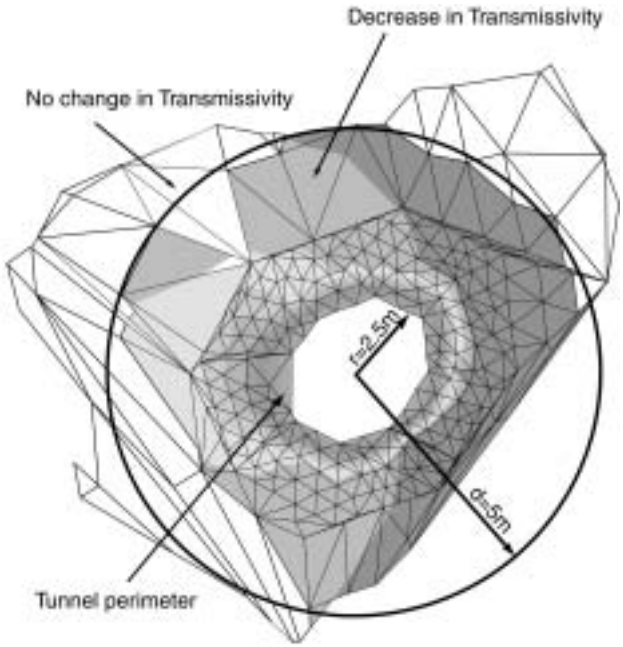

Figure 6-10. *Application of a skin effect to the elements of a fracture intersecting a tunnel in the DFN model.*

The skin effect is simulated for two cases. First, the transmissivity of the fractures within the skin zone is reduced by a factor of 10. Second, the skin reduces the transmissivity by a factor of 100. The results of the sensitivity analysis are presented in Figure 6-11 and Figure 6-12 below.

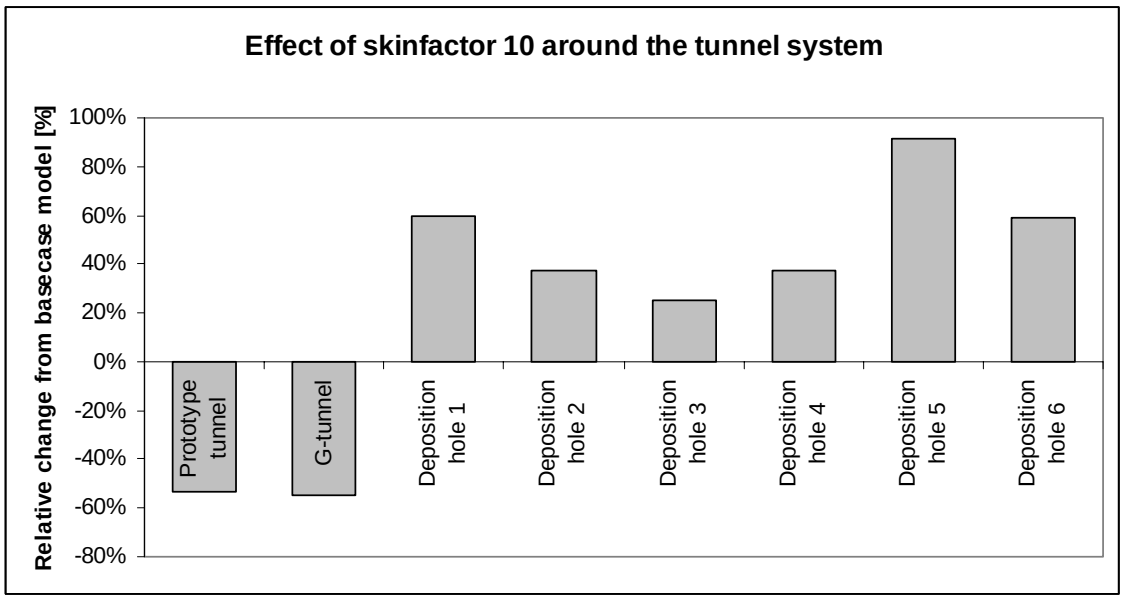

Figure 6-11. *Effect of the skin around the tunnel system on the flow. Transmissivity is reduced by a factor 10.*

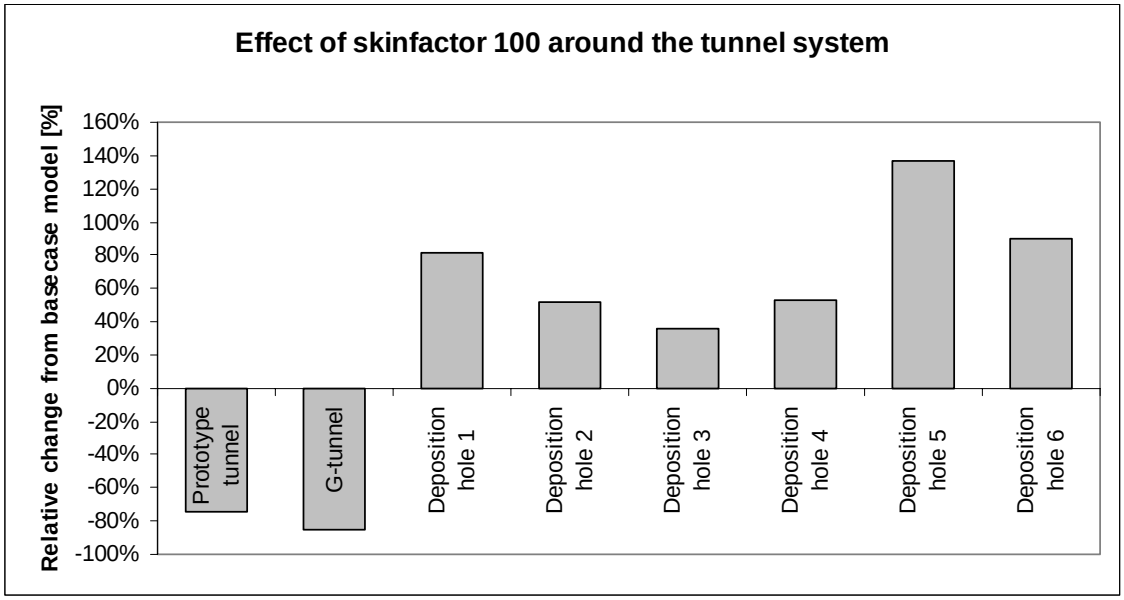

Figure 6-12. *Effect of the skin around the tunnel system on the flow. Transmissivity is reduced by a factor 100.*

When the transmissivity of the fractures within the skin zone is lowered by a factor of 10, the inflow to the tunnel system is reduced by about 50%. At the same time, the average inflow to the deposition holes is increased by about 50%.

The inflow to the tunnel system is reduced by about 80% when the transmissivity of the fractures within the skin zone is lowered by a factor of 100. At the same time, the average inflow to the deposition holes is increased by about 80%.

The variation of the hydraulic conductivity of the skin has a major effect on the inflow to the tunnel system, and consequently on the inflow into the deposition holes. The skin factor provides an effective tool for calibrating inflow to both tunnels and deposition holes. The weakness lies in the fact that the reason for and the width of the skin zone are poorly known.

6.2.6 Lower truncation for "natural" fractures

The effect of a different truncation for the transmissivity of the fractures is evaluated using the inflow to the deposition holes and the tunnels. To simulate this effect in the model a transmissivity truncation is implemented that is $1 \cdot 10^{-10}$ m^2/s instead of, in the basecase, $5 \cdot 10^{-10}$ m^2/s. Consequently the model now contains all fractures from the base case plus the fractures which have a transmissivity between $1 \cdot 10^{-10}$ m^2/s and $5 \cdot 10^{-10}$ m^2/s.

Adding fractures with low transmissivity should result in a minor increase of the average inflow to the cavities, approximately less than a percent. On the other hand including more fractures into the fracture network will increase the complexity and, as for all numerical methods, the risk for less efficiently shaped elements increases. Therefore there will be a risk that the numerical solution will produce results with large variability in flow, which is exemplified in Figure 3-17.

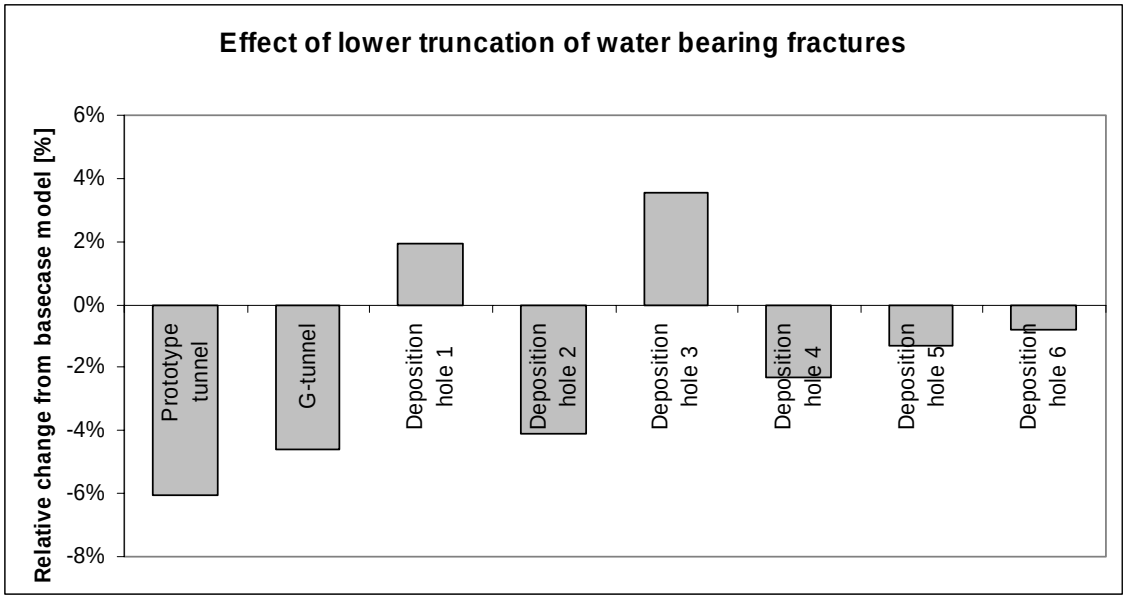

Figure 6-13. *Effect of including fractures with a transmissivity between $1 \cdot 10^{-10}$ and $5 \cdot 10^{-10}$ m^2/s.*

As can be seen in Figure 6-13 the inflow will, as an average, decrease in both tunnels and in 4 of the 6 deposition holes. The difference is explained by redistribution of the flow, since more fractures are added the flow will find new paths to the deposition holes. The effect is small, only 1 to 6%, compared to the other sensitivity studies. The difference in the global flow is negligible, see e.g. Figure 3-17.

6.3 Transient simulation

In all previous DFN sensitivity analysis and calibration phases, it has been assumed that steady state conditions prevail. However, the excavation process of the deposition holes is performed over a time period that suggests that transient conditions may exist for a limited time. A simulation of the inflow to the deposition holes is performed using the same time steps as indicated in ***Table 6-9*** to see if the results show significant difference to the steady state simulations. If steady state conditions are reached in inflow and head between each excavation of deposition hole, then it can be assumed that the head and flow fields can be predicted by a steady state approach.
The flow in deposition holes 1 to 4 and the freshwater head in 3 monitoring sections in the prototype repository area are modelled in a transient mode. The storativity S of the stochastic features was set according to the following equation (Rhén, pers. com. 1999):

$$\mathrm{Log}_{10}(S) = -2.13 + 0.59 \log_{10}(T)$$

The monitoring sections are presented in ***Table 6-8*** below.

Table 6-8. Name and description of the monitoring sections.

Name	*Section*	*Comment*
KA3584G01	Whole borehole	Subclass 2. Sub-vertical. Between deposition holes 1 and 2
KA3590G01	Section 17.3-30.03m from the top	Subclass 4. Inclined. South direction. Close to deposition hole 1
KA0048A01	Section 49-54.7m from the top	About 13m above the top of the deposition hole 1

The transient simulation is performed taking into account drill times and pauses between drilling periods. The excavation process of the deposition holes itself is not modelled in details. The deposition holes are assumed to be either non-excavated or totally excavated (open). A deposition hole is set to be excavated in the model at a time equal to half the real elapsed time of excavation. In Table 6-9 the recorded and assumed times for different events are shown. The transient simulation is based on 1 realisation of the stochastic fracture network only.

Table 6-9. Assumed times for different events during the transient simulation.

Date and Time	*Event:*
6/19/99 17:50	Start of excavation of deposition hole 1
6/21/99 7:41	Excavation modelling start: deposition hole 1 is open
6/22/99 21:32	Completion of excavation of deposition hole 1
6/30/99 8:05	Start of excavation of deposition hole 2
7/1/99 14:45	Deposition hole 2 set to open in the model
7/2/99 21:25	Completion of excavation of deposition hole 2
7/5/99 10:50	Start of excavation of deposition hole 3
7/6/99 23:10	Deposition hole 3 set to open in the model
7/8/99 11:30	Completion of excavation of deposition hole 3
7/13/99 10:00	Start of excavation of deposition hole 4
7/14/99 12:42	Deposition hole 4 set to open in the model
7/15/99 15:25	Completion of excavation of deposition hole 4
8/26/99 13:05	End date in the model

The results of the transient modelling of the excavation of deposition holes 1 to 4 is presented below in Figure 6-14.

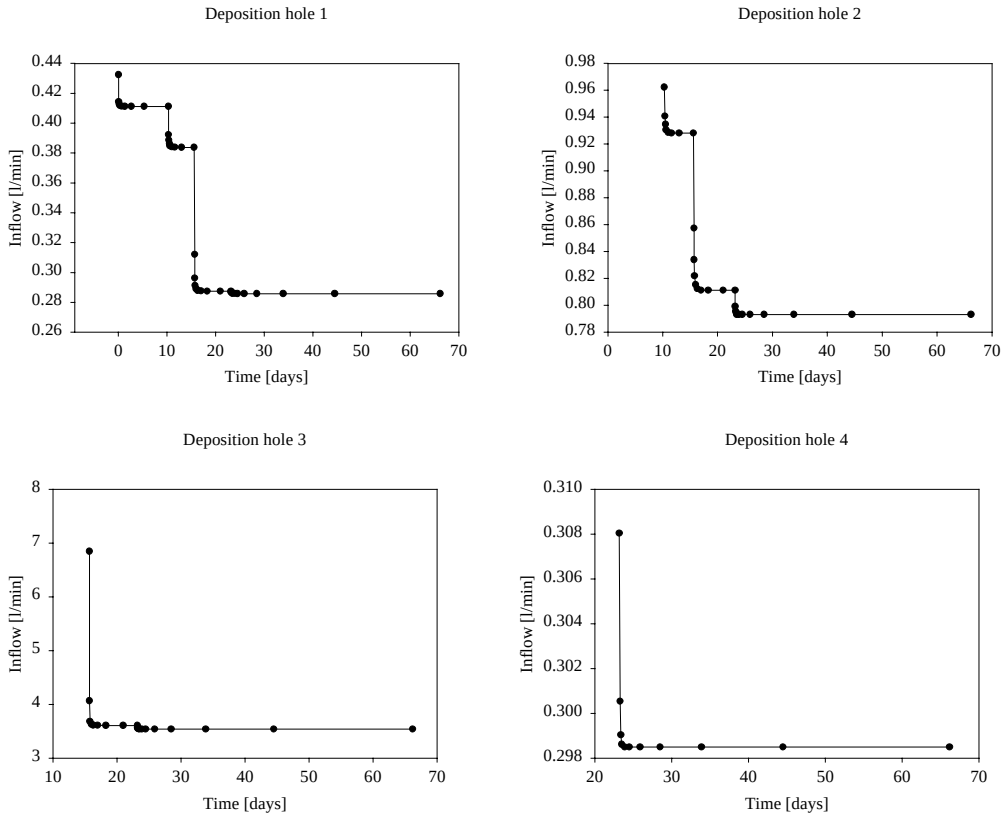

Figure 6-14. *Inflow in the deposition 1 to 4 during the excavation of the deposition holes.*

The inflow to deposition hole 1 starts at 0.432 l/min and decreases and stabilises 8 hours after excavation at 0.411 l/min.
When deposition hole 2 is excavated, inflow to hole 1 drops to 0.392 l/min. This inflow decreases and stabilises 16 hours after excavation of hole 2 to 0.384 l/min.
When deposition hole 3 is excavated, inflow to hole 1 drops to 0.312 l/min. This inflow decreases and stabilises 16 hours after excavation of hole 3 to 0.288 l/min.
When deposition hole 4 is excavated, inflow to hole 1 drops to 0.287 l/min. This inflow decreases and stabilises 16 hours after excavation of hole 4 to 0.286 l/min. The influence of the excavation of deposition hole 4 on the inflow to deposition hole 1 is negligible.

The inflow to the deposition hole 2 starts at 0.962 l/min and decreases and stabilises 32 hours after excavation at 0.928 l/min.
When deposition hole 3 is excavated, inflow to hole 2 drops to 0.857 l/min. This inflow decreases and stabilises 32 hours after excavation of hole 3 to 0.811 l/min.
When deposition hole 4 is excavated, inflow to hole 2 drops to 0.799 l/min. This inflow decreases and stabilises 8 hours after excavation of hole 4 to 0.793 l/min.

The inflow to the deposition hole 3 starts at 0.684 l/min and decreases and stabilises 16 hours after excavation at 0.361 l/min.
When deposition hole 4 is excavated, inflow to hole 3 drops to 0.356 l/min. This inflow decreases and stabilises 8 hours after excavation of hole 4 to 0.354 l/min.

The inflow to the deposition hole 4 starts at 0.308 l/min and decreases and stabilises 8 hours after excavation at 0.298 l/min.

It is observed that all the inflow to the deposition holes is of the same order of magnitude except for deposition hole 3 where the inflow is 10 times the inflow to the other holes. This large inflow to deposition hole 3 may be due to highly conductive pathways around the hole. Another stochastic realisation may provide different flowpaths and slightly different results.

Figure 6-15 below presents the cumulative inflow to the deposition holes. The global inflow to the deposition holes is increasing during the excavation of the deposition holes is made. The peak of the inflow diagram occurs when excavating deposition hole 3.

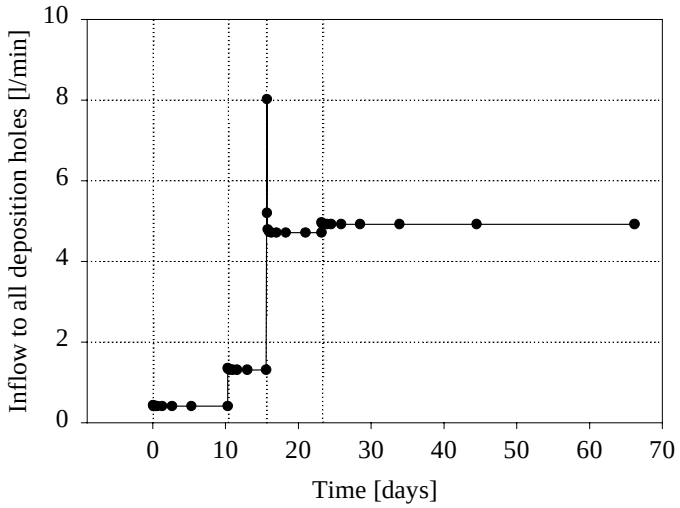

Figure 6-15. *Cumulative inflow to the deposition holes during the transient simulation.*

The head variation in the monitored borehole sections is presented in Figure 6-16 below. The water head is decreased successively by the excavation of the deposition holes 1 to 4. The head stabilises in all monitoring holes within 16 hours after the excavation of the deposition holes.

Borehole KA3584G01, located between deposition holes 1 and 2, shows a large drawdown when hole 3 is excavated. There is a large flowpath, possibly a single fracture between the borehole section and the deposition hole.
Borehole KA0048A01 located about 13m above deposition holes 1 and 2 shows little response to the excavation process. It is probably due to that the TBM tunnel is located between the monitoring section and the deposition holes.
The monitoring section in borehole KA3590G01 shows little response to the excavation process.

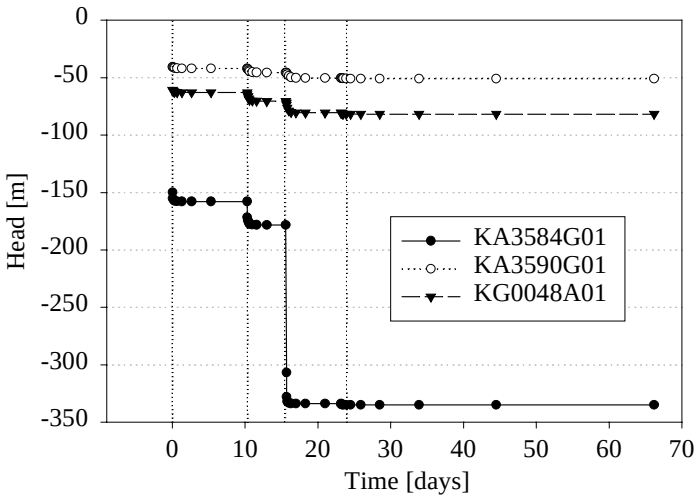

Figure 6-16. *Head variation during the excavation of the deposition holes 1 to 4. Vertical lines represents the excavation of deposition holes 1 to 4.*

The hydraulic response of the system to the excavation of deposition holes 1 to 4 shows that there is a quick stabilisation within the time frame of the excavation process. The assumption that the excavation process can be modelled using a steady state approach is therefore valid.

7 Predictions

The model of the repository is used for the prediction of fracture trace statistics in the deposition holes, inflow statistics to the deposition holes and TBM-tunnel, and drawdown in the observation packer sections. The calibrated DFN model, as presented in Table 6-7, has been used throughout the prediction process

7.1 Prediction of fracture traces in deposition holes

The fracture trace statistics are calculated from 20 stochastic realisations where minimum, maximum, average values and standard deviation has been calculated.

The DFN model can produce fracture trace maps for all, “natural” and conductive fractures in each of the 6 deposition holes, i.e. 18 trace maps for each stochastic realisation. The complete simulation consists of 20 stochastic realisations out of which 360 trace maps can be extracted. Figure 7-1 shows 6 examples of trace maps from realisation #1. However it is not meaningful to present all trace maps. Instead summary statistics from all sampled trace maps are given in Table 7-1. In appendix D is all data from the 20 realisations presented. The fracture statistics is calculated for the simulated “natural” fractures, which corresponds to open but not necessarily waterbearing fractures. A simulated “natural” fracture is a fracture with a transmissivity > $5 \cdot 10^{-11}$ m^2/s, as defined in section 3.2.8.

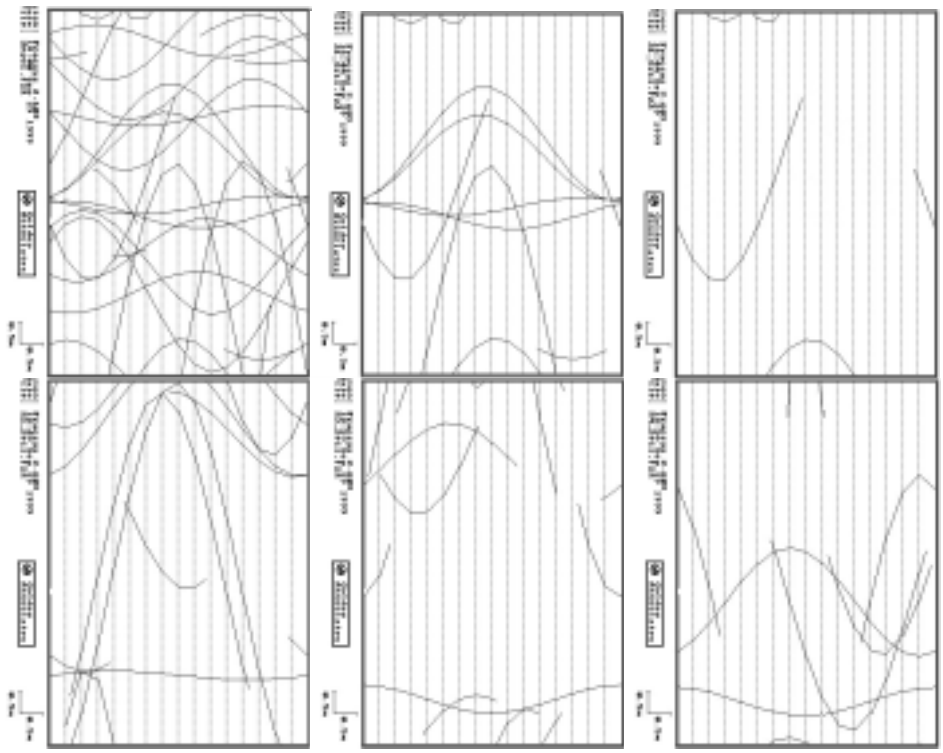

Figure 7-1. *Fracture traces on the wall of the deposition holes in realisation1. Upper row from left: all fractures, “natural” fractures ($T > 5 \cdot 10^{-11}$ m^2/s) and conductive fractures ($T > 5 \cdot 10^{-10}$ m^2/s) for deposition hole 1. Lower: “natural” fractures in deposition hole 2, 3 and 4.*

The number of "natural" fractures for the 6 deposition holes varies between 3 and 15 with an average around 8 "natural" fractures per deposition hole, see Table 7-1 and Figure 7-2.

The average trace length of one fracture is on average 5 m within all deposition holes and the trace lengths vary between 0.01 to 16.9 m, c.f. Table 7-1 and Figure 7-3. As a comparison the circumference in a deposition hole is 5.8 m which implies that a trace of 16.9 m corresponds to a fracture that is visible along the whole perimeter of the deposition hole at an angle of about 75°.

The density of fracture traces is given by P_{21} and varies between 0.22 and 1.76 m/m^2 with an average around 0.9 m/m^2, see Table 7-1 and Figure 7-4.

The transmissivity statistics of the fractures that intersects the deposition holes are shown in Table 7-1 and Figure 7-5. The average value is around $5 \cdot 10^{-8}$ m^2/s in all deposition holes. The minimum transmissivity is $5 \cdot 10^{-11}$ m^2/s which is the same value as the truncation for fractures that is assumed to be "natural". The maximum transmissivity is $6.6 \cdot 10^{-6}$ m^2/s which is half an order of magnitude lower than the upper limit for transmissivity for the north-west striking set. The sub-horizontal fracture set has the largest possibility to intersect the deposition holes and at the same time it has the lowest transmissivity distribution. The steeply dipping north-west striking set has the highest transmissivity distribution and also the lowest possibility of intersecting a deposition hole. This explains how the minimum transmissivity value equals the truncation, but that the highest is half an order of magnitude lower than the upper transmissivity limit.

Table 7-1. Statistics of the "natural" fracture traces around the perimeter of deposition holes 1 to 6 based on 20 realisations of the calibrated DFN model. The min and maximum values for trace length and transmissivity is for a single trace in the deposition hole, other values are calculated for a whole hole.

Canister	*1*	*2*	*3*	*4*	*5*	*6*
Average number of traces	7.5	7.7	9.3	8.9	8.85	8.6
Minimum number of traces	3	3	5	4	3	4
Maximum number of traces	11	12	14	15	13	12
Average trace length [m]	4.91	5.31	5.53	4.79	4.85	5.00
Std dev trace length [m]	3.98	3.98	4.03	3.26	2.99	3.47
Minimum trace length [m]	0.09	0.01	0.09	0.08	0.07	0.01
Maximum trace length [m]	16.7	16.9	16.4	16.0	16.3	16.2
Average P_{21} [m/m^2]	0.79	0.88	1.08	0.89	0.93	0.90
Minimum P_{21} [m/m^2]	0.25	0.33	0.51	0.22	0.27	0.41
Maximum P_{21} [m/m^2]	1.48	1.47	1.76	1.66	1.74	1.36
log(Average T) [m^2/s]	-7.48	-7.24	-7.21	-7.09	-7.17	-7.59
log(Std dev T) [m^2/s]	-7.10	-6.85	-6.74	-6.63	-6.77	-7.20
log(Minimum T)[m^2/s]	-10.29	-10.29	-10.29	-10.30	-10.29	-10.30
log(Maximum T)[m^2/s]	-5.99	-5.43	-5.18	-5.18	-5.30	-6.10

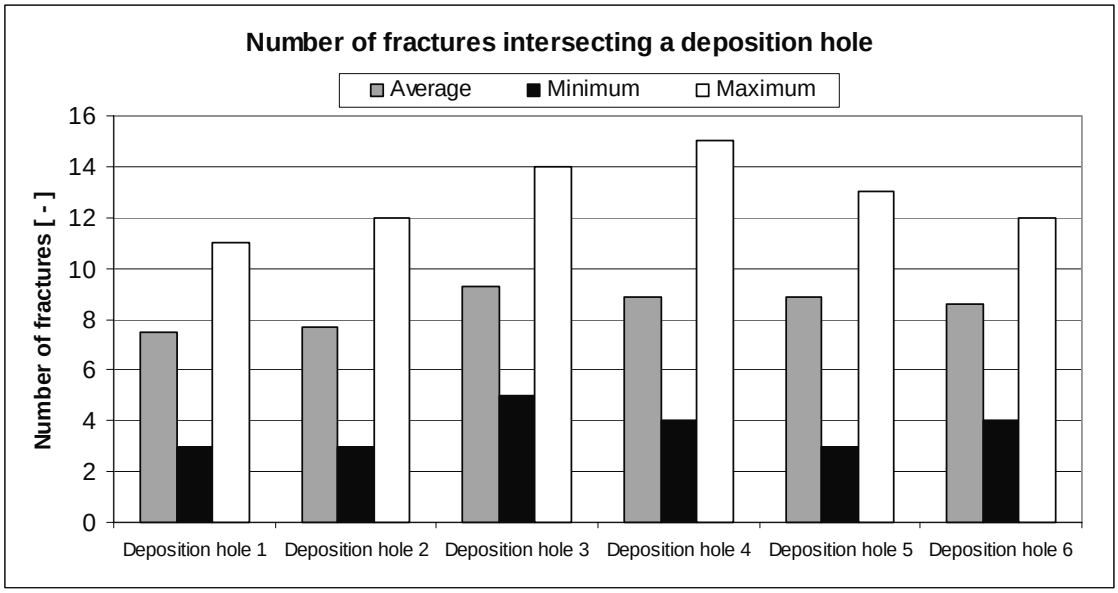

Figure 7-2. *Number of "natural" fracture traces per deposition hole. Summary statistics based on 20 realisations of the calibrated DFN model.*

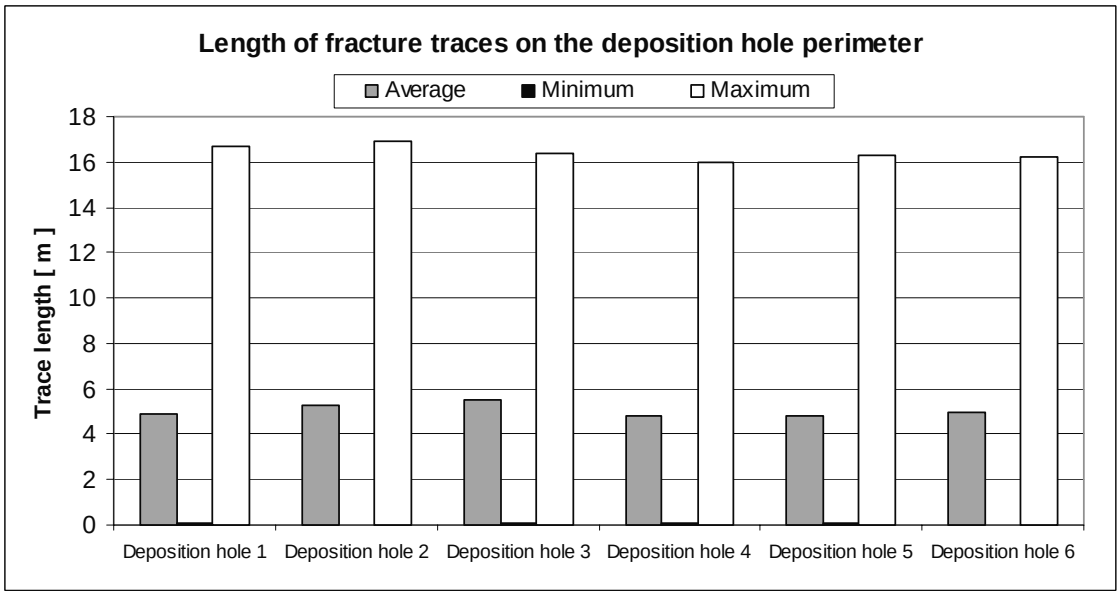

Figure 7-3. *Trace length of individual "natural" fractures per deposition hole. Summary statistics based on 20 realisations of the calibrated DFN model.*

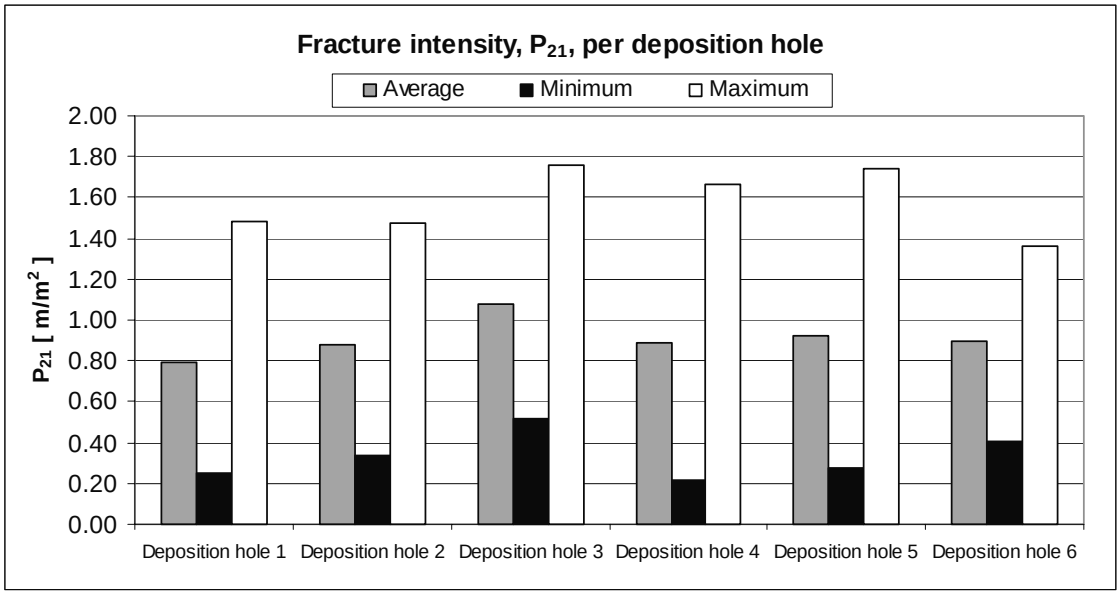

Figure 7-4. *Fracture intensity, P_{21} (m/m^2), for "natural" fractures on the deposition hole walls. Summary statistics based on 20 realisations of the calibrated DFN model.*

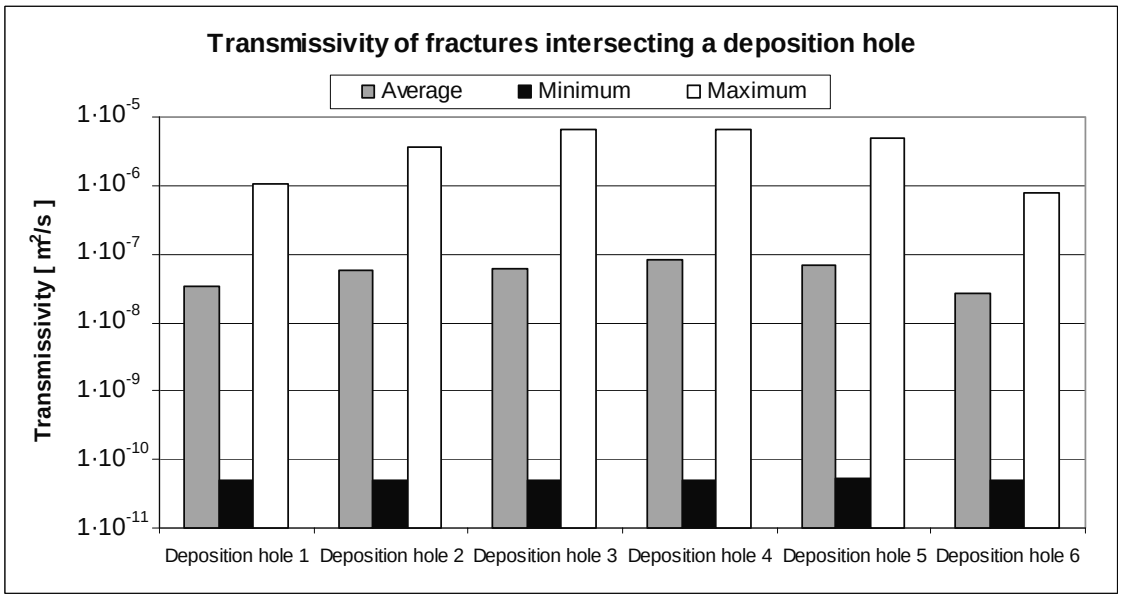

Figure 7-5*. Transmissivity of individual conductive fractures intersecting the deposition holes. Summary statistics based on 20 realisations of the calibrated DFN model.*

7.2 Prediction of inflow in the deposition holes – Steady state condition

The DFN model is used to predict the inflow to the 6 deposition holes, the TBM tunnel and the G-tunnel. The input parameters for the DFN model is summarised in Table 6-7, with the extra condition that a skin factor of 0.01 is applied to the fracture elements that is fully inside a radius of 5 m from the tunnel centre.

The predictions are calculated for a steady state solution, i.e. there are no changes for the pressure or flow in time. The prediction are calculated for two different steady state cases; case one corresponds to that boreholes 1 to 4 is excavated and case two corresponds to that all 6 deposition holes are excavated. In both cases all surrounding tunnels are present, except the F-tunnel see section 5.2.1. Flow statistics are calculated from 20 stochastic realisations for each case. Minimum, maximum, average, geometric mean and median is calculated for each depositionhole and tunnel and are presented in Table 7-2.

Table 7-2. Summary of inflow [l/min] for the tunnels and deposition holes.

Boundary:	***TBM tunnel***	***G tunnel***	***Hole 1***	***Hole 2***	***Hole 3***	***Hole 4***	***Hole 5***	***Hole 6***
min (1-4)	1.400	0.792	0.075	0.000	0.000	0.008	-	-
min (1-6)	1.307	0.788	0.075	0.000	0.000	0.008	0.092	0.006
Average (1-4)	6.084	4.720	1.167	1.109	1.189	3.145	-	-
Average (1-6)	5.777	4.688	1.141	1.069	1.112	2.966	3.529	1.431
Geomean (1-4)	4.940	3.638	0.614	0.581	0.466	0.879	-	-
Geomean (1-6)	4.699	3.611	0.604	0.563	0.441	0.807	1.253	0.532
Median (1-4)	5.067	3.812	0.556	0.614	1.016	0.853	-	-
Median (1-6)	4.876	3.796	0.553	0.607	0.943	0.695	1.678	0.934
max (1-4)	14.064	11.412	5.653	5.666	4.087	18.666	-	-
max (1-6)	13.974	11.370	5.619	5.590	4.030	18.168	17.664	6.708
Std dev (1-4)	3.896	3.306	1.484	1.452	1.159	4.903	-	-
Std dev (1-6)	3.745	3.295	1.453	1.418	1.097	4.779	4.953	1.663

Figure 7-6 shows the flow statistics for the case where deposition hole 1 to 4 is excavated, and Figure 7-7 shows the statistics for the case where all 6 deposition holes are excavated.

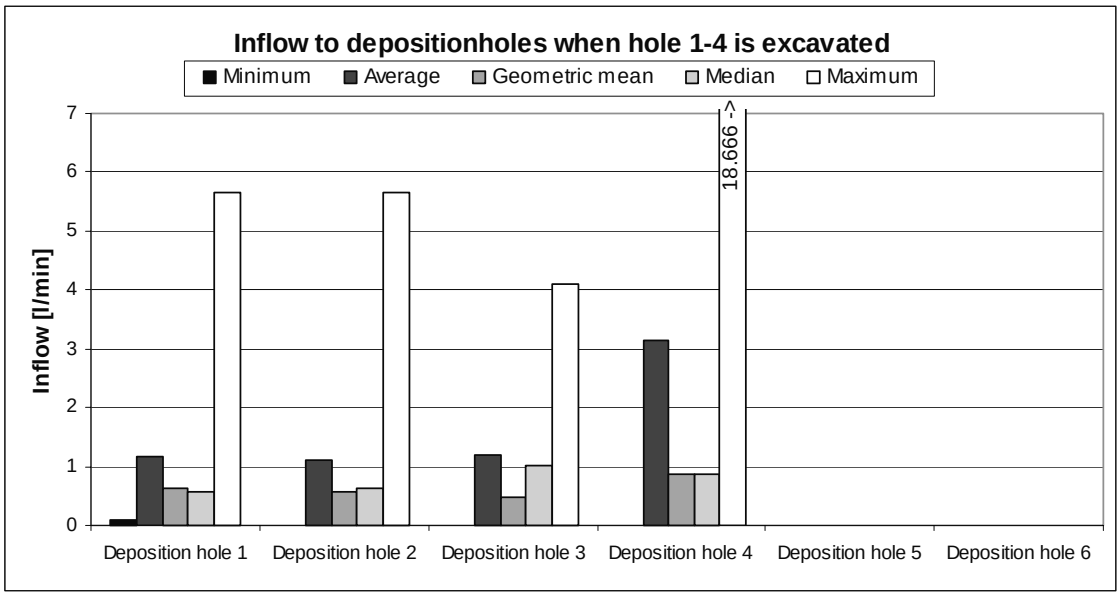

Figure 7-6. *Predicted inflow to the deposition holes, average, min, max, median and geometric mean values from 20 realisations. The graph is constrained to show a max value of inflow of 7 l/min.*

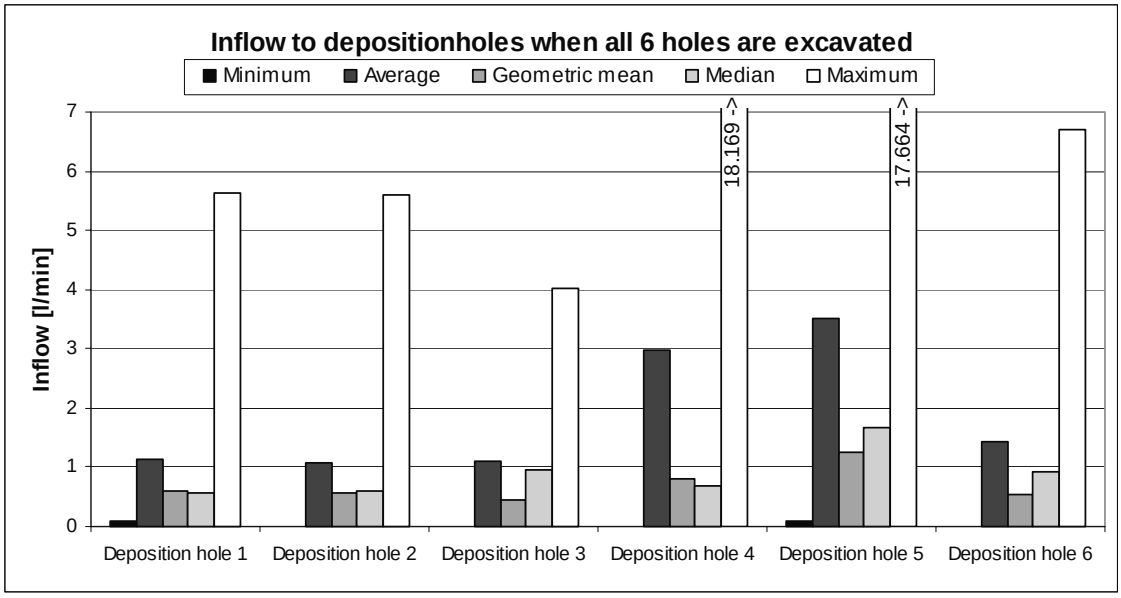

Figure 7-7. *Predicted inflow to the deposition holes, average, min, max, median and geometric mean values from 20 realisations. The graph is constrained to show a max value of inflow of 7 l/min.*

One can notice that the flow into deposition holes 4 and 5 is larger than in the other deposition holes. The large average, geometric mean and maximum inflow into deposition hole 4 is due to a well-connected high transmissive fracture in realisation # 7, c.f. appendix D and E. In Table 7-1 and appendix D it is shown that both deposition hole 3 and 4 are intersected by a highly transmissive fracture, $6.6 \cdot 10^{-6}$ m^2/s (realisation # 9). This fracture is probably isolated from the rest of the network why the inflow to deposition hole 3 and 4 is small in this realisation.

The maximum inflow in deposition hole 5 is in the same range as in deposition hole 4 but occur in realisation #12. The conclusion is that if an infinity number of realisation were made, every one of the 6 deposition holes would show high inflow in some realisations. Both deposition hole 5 and 6 have a high median inflow which may be explained by the 5 deterministic fractures that is in the vicinity of these two deposition holes.

As expected, the effect of the excavation of deposition hole 5-6 is a reduction of the inflow in the deposition holes 1-4 and G and TBM tunnels. The reduction decreases with the distance from deposition hole 5 and 6, thus the smallest reduction of the average inflow is in deposition hole # 1, 2%, and the largest in deposition hole # 4, 8%.

The scale of the inflow is given by Figure 7-8. The frequency analysis is made for the inflow to each of the six holes for all 20 realisation, i.e. there is 120 values in the frequency plot. The most probable inflow into one deposition hole is predicted to be between 0.3 and 3 l/min.

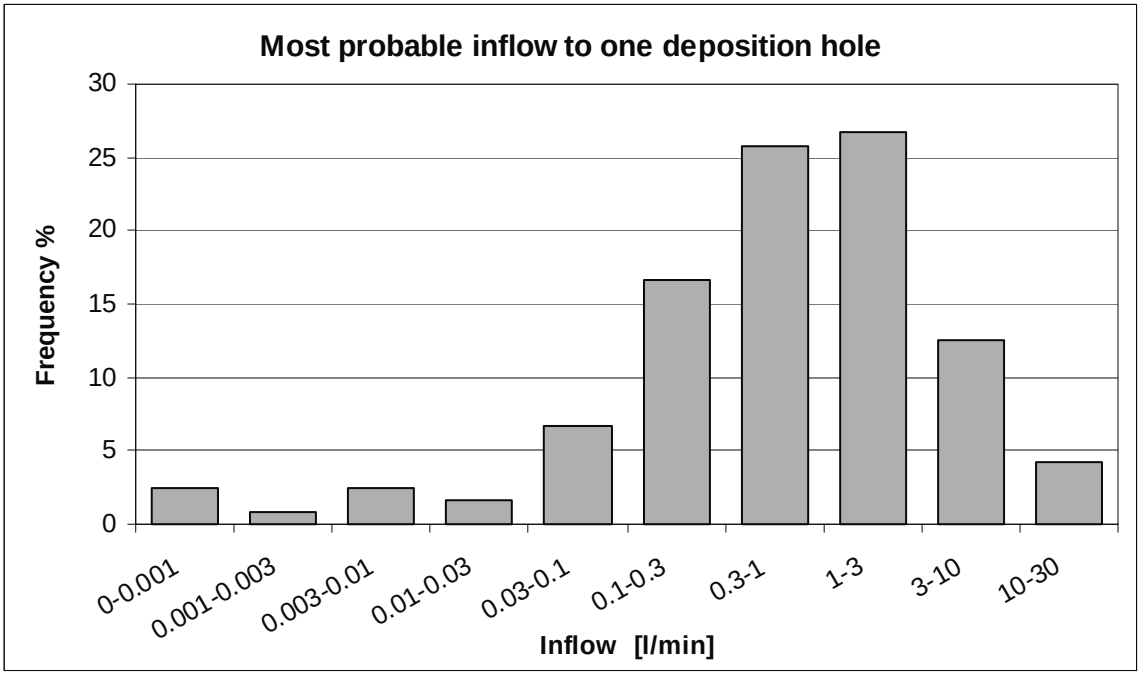

Figure 7-8. *Frequency plot of the flow into each deposition hole.*

7.3 Pressure distribution in the observation holes

The same model as for the flow predictions is used for the drawdown predictions, i.e. the model with input parameters according to Table 6-7 with the extra condition that a skin factor of 0.01 is applied to fracture elements that is fully within 5 m from the tunnel centre.

Drawdown is the piezometric head change and is expressed in metres. It is calculated for a steady state solution, i.e. there are no changes for pressure or flow with time. The head-field is calculated for three separated stages for the 20 stochastic realisations; in stage 1 there are no deposition holes excavated, in stage 2 holes #1-4 are excavated and in stage 3 all 6 deposition holes are excavated. The drawdown is then calculated as the difference in head between stage 1 and 2, stage 1 and 3 and stage 2 and 3. This corresponds to the expected drawdown due to the excavation of deposition holes 1 to 4, the expected drawdown due to the excavation of all the 6 deposition holes and the expected drawdown when excavating deposition holes 5 and 6 respectively.

There are 31 observation holes included in the DFN model, listed in Table 7-3, and totally 76 sections where head have been monitored. The sections are located in the surrounding rock mass of the TBM tunnel. Some of the pressure gauges in the monitoring boreholes were moved after excavation of deposition holes 1 to 4.

Table 7-3. Boreholes used for the observation of pressure changes as given by Rhén (pers. com. 1999)

KA3539G	KA3572G01
KA3542G01	KA3573A
KA3542G02	KA3574G01
KA3544G01	KA3576G01
KA3546G01	KA3578G01
KA3548A01	KA3579G
KA3548G01	KA3584G01
KA3550G01	KA3590G01
KA3552G01	KA3590G02
KA3554G01	KA3593G
KA3554G02	KA3600F
KA3557G	KA3510a
KA3563G	KG0021A01
KA3566G01	KG0048A01
KA3566G02	

The minimum, maximum, and average drawdown in each section for the 20 stochastic realisations are calculated and presented in Table 7-4. The drawdown from each realisation is presented in appendix F.

Table 7-4. The simulated drawdown (m), due to the excavation of the deposition holes, in the monitoring sections based on 20 stochastic realisations.

Borehole/monitoring section	Max (1-4)	Max (1-6)	Max (5-6)	Average (1-4)	Average (1-6)	Average (5-6)	Min (1-4)	Min (1-6)	Min (5-6)
KA3539G (1.3-8.8 m)			-243.2			-97.0			-6.5
KA3539G (9.8-18.3 m)			-184.2			-70.3			-6.3
KA3539G (19.3-30.01 m)			-96.7			-48.0			-2.9
KA3542G01 (1.3-7.8 m)			-232.7			-133.6			-7.8
KA3542G01 (8.8-24.8 m)			-242.0			-67.8			-1.9
KA3542G01 (25.8-30.04 m)			-55.8			-19.9			-1.4
KA3542G02 (1.3-7.8 m)			-179.4			-59.6			-13.6
KA3542G02 (8.8-12.8 m)			-142.4			-42.1			-7.9
KA3542G02 (13.8-21.3 m)			-104.5			-28.1			-4.6
KA3542G02 (22.3-30.01 m)			-69.0			-12.6			-0.7
KA3544G01 (1.3-5.3 m)			-452.9			-316.2			-128.1
KA3544G01 (6.3-12 m)			-415.6			-220.9			-8.8
KA3546G01 (1.3-5.8 m)			-359.8			-247.8			-86.5
KA3546G01 (6.8-12 m)			-456.8			-267.6			-63.9
KA3548A01 (10-14 m)	-97.2	-234.2		-20.7	-64.9		-2.9	-15.9	
KA3548A01 (15-30 m)	-63.0	-72.0		-15.0	-25.4		-2.0	-4.2	
KA3548G01 (0.3-12.01 m)			-368.0			-250.5			-65.9
KA3550G01 (1.3-5.3 m)			-364.5			-276.5			-110.5
KA3550G01 (6.3-12.03 m)			-387.1			-301.2			-158.2
KA3552G01 (0.3-3.05 m)			-170.2			-70.4			-4.2
KA3552G01 (4.05-7.8 m)			-372.7			-308.3			-188.5
KA3552G01 (8.8-12.01 m)			-343.7			-203.0			-10.6
KA3554G01 (1.3-11.3 m)			-227.1			-67.9			-1.8
KA3554G01 (12.3-21.3 m)			-182.1			-36.9			-1.5
KA3554G01 (22.3-30.01 m)			-85.8			-16.0			-0.9
Table 7-4 continued									

Borehole/monitoring section	Max (1-4)	Max (1-6)	Max (5-6)	Average (1-4)	Average (1-6)	Average (5-6)	Min (1-4)	Min (1-6)	Min (5-6)
KA3554G02 (1.3-9.3 m)			-257.3			-84.5			-12.3
KA3554G02 (10.3-21.3 m)			-189.4			-52.3			-2.7
KA3554G02 (22.3-30.01 m)			-92.4			-19.9			-2.4
KA3557G (0.30-8 m)			-249.3			-52.8			-2.7
KA3563G (1.3-2.8 m)	-209.8			-25.9			-2.2		
KA3563G (3.8-8.3 m)	-279.0			-119.2			-12.9		
KA3563G (9.3-30.00 m)	-370.8			-79.9			-8.4		
KA3566G01 (1.3-6.3 m)	-252.1	-274.3		-113.5	-124.7		-17.4	-23.0	
KA3566G01 (7.3-11.3 m)	-164.7	-186.7		-68.4	-87.8		-10.9	-22.0	
KA3566G01 (12.3-19.8 m)	-256.8	-261.2		-62.5	-72.1		-3.5	-5.5	
KA3566G01 (20.8-30.01 m)	-128.1	-132.9		-33.6	-42.0		-3.1	-5.7	
KA3566G02 (1.3-6.8 m)	-265.6	-268.2		-91.2	-118.0		-6.7	-26.1	
KA3566G02 (7.8-11.3 m)	-110.9	-208.2		-51.5	-80.4		-3.8	-22.5	
KA3566G02 (12.3-18.3 m)	-87.1	-145.2		-30.3	-62.7		-3.5	-13.2	
KA3566G02 (19.3-30.01 m)	-62.3	-90.4		-16.9	-35.0		-2.0	-6.0	
KA3572G01 (1.3-5.3 m)	-375.2			-255.2			-31.8		
KA3572G01 (6.3-12.00 m)	-374.8			-254.9			-29.6		
KA3573A (4.5-17.0 m)	-180.5	-184.3		-44.7	-52.2		-3.9	-5.4	
KA3573A (18.0-40.07 m)	-44.9	-50.7		-12.6	-16.1		-1.0	-1.5	
KA3574G01 (8.8-12.00 m)	-364.9			-281.3			-34.6		
KA3576G01 (1.3-2.8 m)	-192.1			-147.5			-120.6		
KA3576G01 (3.8-7.8 m)	-395.6			-325.2			-218.7		
KA3576G01 (8.8-12.01 m)	-343.2			-211.7			-98.6		
KA3578G01 (1.3-5.8 m)	-359.9			-261.4			-156.7		
KA3578G01 (6.8-12.58 m)	-363.9			-197.1			-43.0		
KA3579G (1.3-4.3 m)	-358.6			-261.9			-104.1		
KA3579G (5.3-8.3 m)	-386.3			-339.3			-225.0		
KA3579G (9.3-22.65 m)	-340.7			-159.6			-31.1		
KA3584G01 (0.3-12.00 m)	-455.2			-210.9			-49.4		
KA3590G01 (1.3-6.8 m)	-127.4			-55.3			-5.5		
KA3590G01 (7.8-16.3 m)	-166.0			-49.7			-2.4		
KA3590G01 (17.3-30.06 m)	-67.2			-22.7			-2.6		
KA3590G02 (1.3-7.3 m)	-166.0			-78.5			-25.7		
KA3590G02 (8.3-16.3 m)	-305.8			-67.6			-13.2		
KA3590G02 (17.3-22.3 m)	-90.5			-38.8			-9.8		
KA3590G02 (23.3-30.05 m)	-82.9			-25.4			-4.5		
KA3593G (1.3-7.3 m)	-201.6			-86.8			-11.2		
KA3593G (8.3-30.02 m)	-158.6			-44.8			-7.1		
KA3600F (4.5-21.00 m)	-15.9	-17.5		-6.8	-7.9		-1.1	-1.5	
KA3600F (22.00-50.10 m)	-7.7	-8.2		-1.8	-2.1		-0.3	-0.3	
KA3510a (4.52-113.02 m)	-10.1	-138.4		-5.0	-21.6		-0.7	-4.8	
KG0021A01 (4-16 m)	-36.1	-39.7		-4.5	-12.1		-0.4	-2.6	
KG0021A01 (17-24 m)	-35.1	-62.1		-7.0	-20.2		-0.8	-4.7	
KG0021A01 (25-34 m)	-43.8	-66.8		-9.7	-23.2		-0.7	-4.0	
KG0021A01 (35-41.5 m)	-39.7	-80.3		-11.1	-24.3		-1.4	-4.2	
KG0021A01 (42.5-48.8 m)	-41.6	-68.8		-13.0	-25.1		-2.2	-4.3	
KG0048A01 (4-12 m)	-50.0	-52.5		-8.0	-14.5		-0.8	-2.2	
KG0048A01 (13-29 m)	-68.0	-135.4		-19.8	-34.9		-3.1	-8.5	
KG0048A01 (30-40 m)	-73.7	-100.6		-26.1	-35.2		-4.0	-6.9	
KG0048A01 (41-48 m)	-99.3	-103.9		-23.4	-28.2		-4.1	-8.2	
KG0048A01 (49-54.7 m)	-100.7	-104.5		-24.6	-29.0		-3.0	-4.1	

As an example, the drawdown in the monitoring holes is illustrated in Figure 7-9. The blue area in the figure shows the effect of the excavation of deposition holes 1 to 6. This qualitative representation of the drawdown is based on the interpolation of the drawdown in the monitoring sections (white circles) to a vertical plane containing the axis of the TBM tunnel and the vertical monitoring holes.

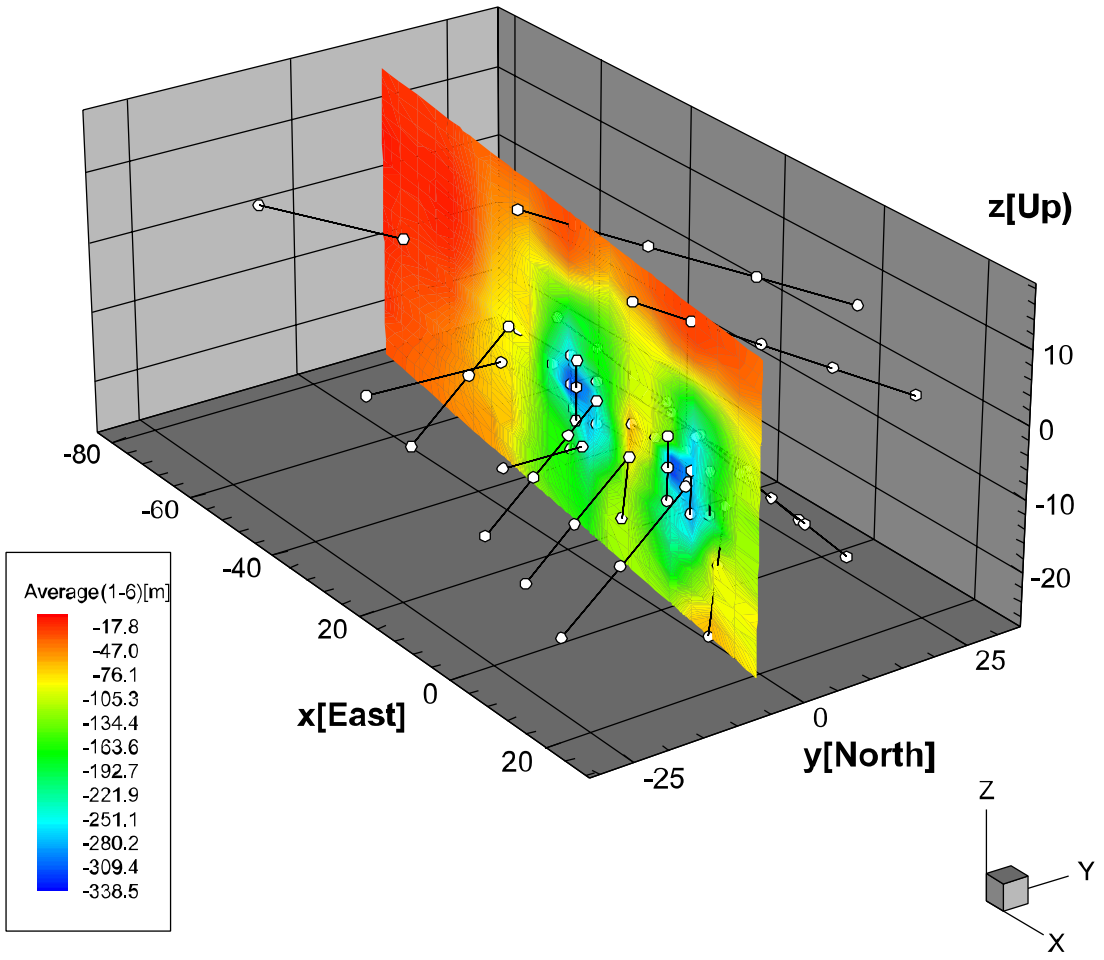

Figure 7-9. *Average of predicted drawdown in the monitoring holes from 20 realisations after excavation of deposition holes 1 to 6.*

8 Comparison to measured data

During the analysis and the prediction stages the result from the Prototype Repository experiment where not known to the modelling group. However after the modelling was accomplished the measured data were presented and a comparison between measured and simulated data was possible. This chapter presents a comparison of simulated and observed data.

The results that are presented are fracture trace maps in deposition holes, inflow to deposition holes and pressure in packer sections.

8.1 Fracture traces

Fracture trace maps are scale dependent, i.e. working in a small scale will result in lots of small fracture traces, while working in a large scale will result in few and long traces. The fracture size distribution in the DFN-model is based on trace maps with a truncation limit of 1 m from the TBM-tunnel. The truncation limit for the trace maps in the deposition holes is, unfortunately, 0.25 m. However the intensity, P_{21} (m fracture trace/m^2 rock wall), is not as dependent as the length are on the scale and can be used for a better comparison. The measured P_{21}, in a small scale, will only be slightly larger than the modelled due to that the long traces will be divided in smaller segment (that will decrease the intensity), but there will also be more short traces (that will increase the intensity).

In ***Table 8-1*** is a brief summary of the statistics from the measured and the modelled trace maps shown. All data is shown in Appendix D. The P_{21} for the modelled deposition holes is a bit small and have a larger dispersion than the measured trace maps. As expected the average trace length for the modelled trace maps are longer than the measured. The reasons for the low modelled P_{21} can be that the orientation statistics of the fractures or the relative fracture density for the 3 sets is not fully understood.

Table 8-1. Comparison of measured and modelled fracture trace length statistics for all fractures.

	P_{21} max [m/m^2]	P_{21} min [m/m^2]	P_{21} ave [m/m^2]	Trace length ave [m]
Measured	4.23	2.74	3.38	1.88
Modelled	4.56	0.64	2.77	4.84

One modelled and one measured trace map are shown in
Figure **8-1**. Trace maps from all 6 deposition holes for 2 realisations are shown in Appendix D. Apart from that the modelled traces are longer and therefore fewer to maintain the correct P_{21} ratio, the trace maps show a similar picture.

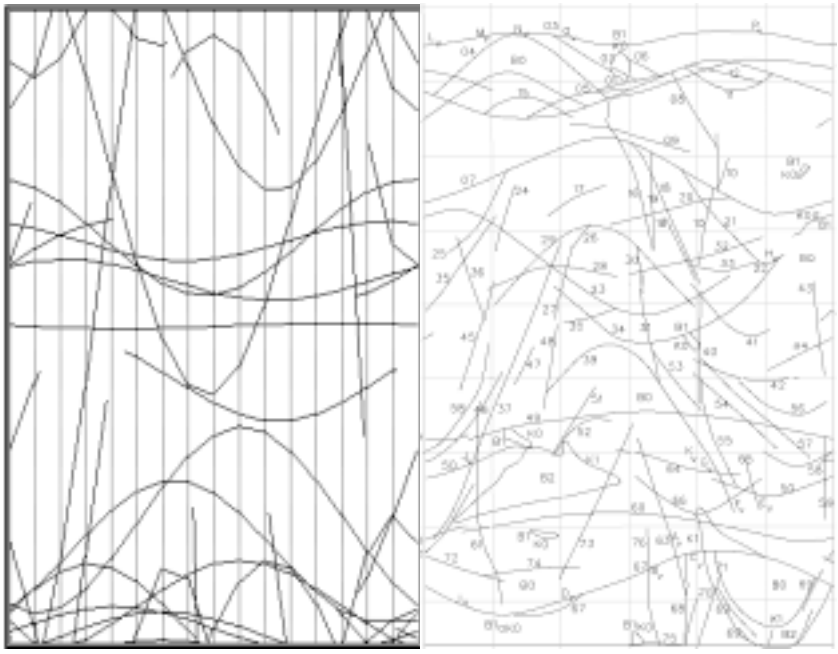

Figure 8-1. *Example of modelled (left) and measured (right) trace maps. The modelled traces are fewer but longer compared to the measured.*

An attempt to compare the transmissivity of the measured waterbearing fractures is made through a rough estimate. For 14 fractures the inflow and the length of the fractures traces are measured. Under the assumption that the flow in the fracture and the headfield is linear, see Figure 8-2, the following equation is valid:

$$Q = -K \cdot A \frac{dH}{dx}$$

Where

Q	=	flow [m^3/s]
K	=	Hydraulic conductivity [m/s]
A	=	Area [m^2]
$\frac{dH}{dx}$	=	Gradient [-]

Since A = b · L, i.e. the area equals the length of the fracture trace times the aperture, and T = b · K, i.e. the transmissivity equals the hydraulic conductivity times the aperture, the equation above can be written as:

$$T = -\frac{Q}{L \cdot \frac{dH}{dx}}$$

The head drop from cavities and 4 m out in the rockmass is about 100 m, see Figure 8-4 and Figure 8-5, hence the gradient is assumed 25 m/m.

The estimation is very rough but gives a hint in which order the transmissivity should be. As can be seen in ***Table 8-2*** the modelled transmissivities is one to two orders of magnitude to high.

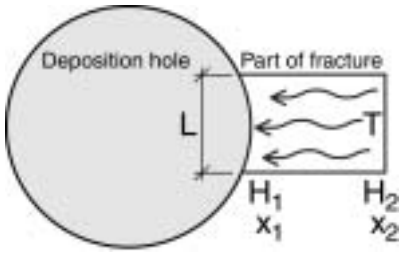

Figure 8-2. *Assumptions to estimate the transmissivity of a fracture intersecting a deposition hole.*

Table 8-2. Comparison of transmissivity between modelled and estimated from measurements.

Transmisivity	max	min	Average
Measured	$6.8 \cdot 10^{-10}$	$1.3 \cdot 10^{-12}$	$1.6 \cdot 10^{-10}$
Modelled	$6.6 \cdot 10^{-6}$	$5.0 \cdot 10^{-11}$	$5.1 \cdot 10^{-8}$

8.2 Inflow to canisters

In previous sections the statistics has been evaluated for the inflow to the deposition holes. In ***Table 8-3*** is modelled average values compared to the measured. The match is poor as can be seen in the table. The inflow is overestimated by two orders of magnitude. The reason is that there is no skin around the deposition holes, which there are around the tunnels in the model or that the measured transmissivity distribution is difficult to model, see section 5.3.5.

Table 8-3. Comparison of measured and calculated inflow to deposition holes

Boundary	Average	Geomean	Median	Measured
Hole 1	1.141	0.604	0.553	0.0800
Hole 2	1.069	0.563	0.607	0.0016
Hole 3	1.112	0.441	0.943	0.0028
Hole 4	2.966	0.807	0.695	0.0007
Hole 5	3.529	1.253	1.678	0.0027
Hole 6	1.431	0.532	0.934	0.0061
Sum inflow	11.248	4.200	5.410	0.094
Factor	120	45	58	1

The simulated inflow to the Prototype tunnel cannot be compared to the measured inflow since the tunnel is used for calibration of the model.

8.3 Head in packers

The pressure is measured at 12 different times during the excavation. The flow solution in the model is only calculated at 3 different times with assumption of steady state conditions. The 3 times corresponds to the following moments in time; before excavation, after excavation of deposition holes 1 to 4 and after excavation of all 6 deposition holes.

Comparisons can be made between:

- the modelled steady state before excavation and the measurements before drilling, 15 June 1999
- the modelled steady state after excavation of deposition holes 1 to 4 and the measurements after drilling deposition hole 4, 15 July 1999
- the modelled steady state after excavation of deposition holes 1 to 4 and the measurements after re-instrumentation but before drilling deposition hole 5, 26 August 1999
- the modelled steady state after excavation of all 6 deposition holes and the measurements of the undisturbed situation after drilling deposition hole 6, 1 December 1999

In the Prototype tunnel the pressure is measured, while the head is simulated. It is easier to compare heads since they, in the hydrostatic case, are independent of depth. The pressure in every packer section were recalculated to head in accordance to

$$H = Z + p / (\rho_w \cdot g)$$

Where

H = Fresh water head [m]
Z = Current elevation in [m]
p = Measured pressure [Pa]
ρ_w = density of fresh water [kg/m^3]
g = Constant of gravity [m/s^2]

8.3.1 Simulated head versus measured

The simulated heads are plotted as a function of the measured head, as seen in Figure 8-3. The upper left diagram in REFMERGEFORMAT shows that the average of the simulated heads are higher than the measured, especially for low values of measured heads which corresponds to the case with no drilled deposition holes. Only a few minimum heads are lower than the measured values.

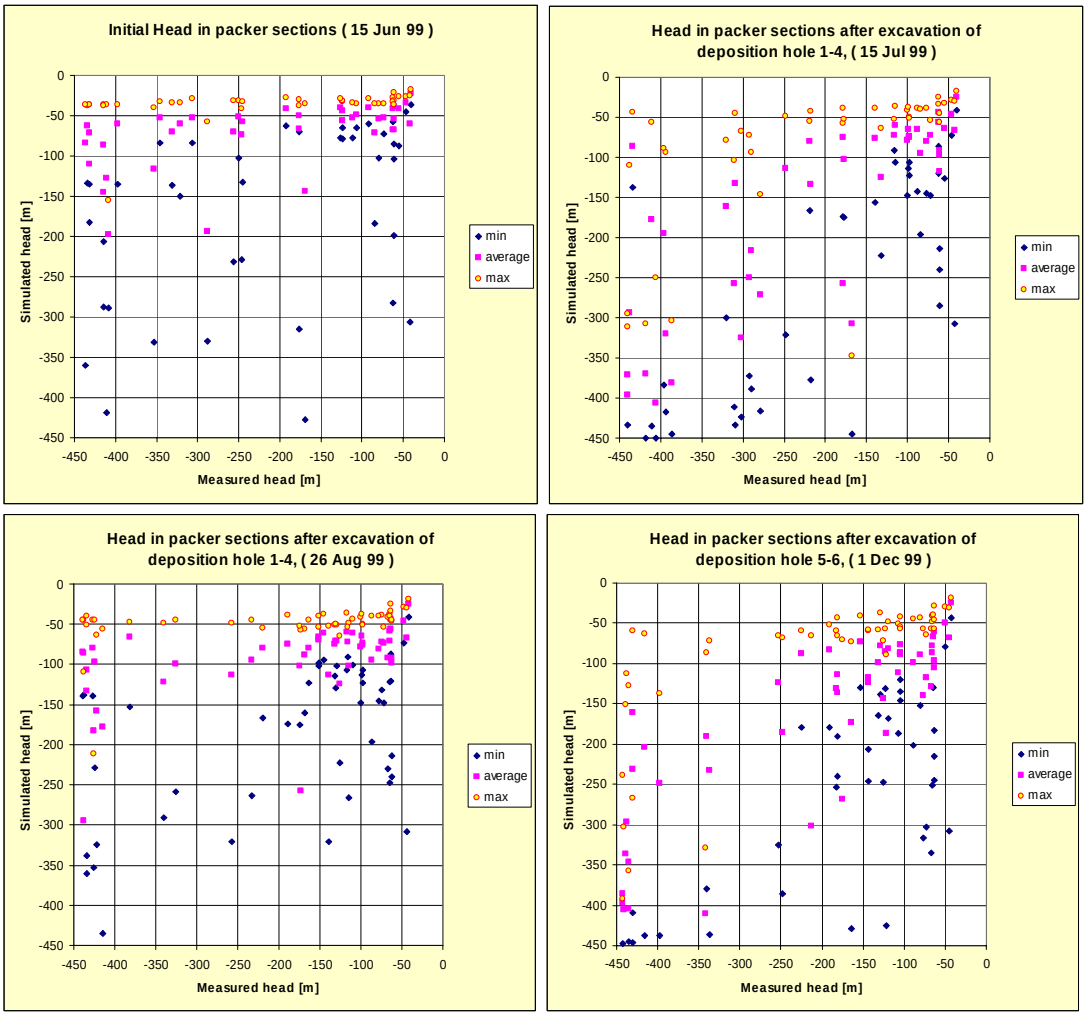

Figure 8-3. *Simulated heads versus measured heads.*

When the first 4 deposition holes are excavated the cross-plot shows a better correlation to measured values of head, but still the simulated heads are too high for the lowest measured heads as can be seen upper right chart in Figure 8-3.

After the re-instrumentation but before the start of excavating deposition holes 5 and 6 the plot looks worse again, this is explained by the re-instrumentation, i.e. that the instruments in boreholes near deposition hole 1-4 are moved to boreholes near deposition hole 5 and 6.

The cross plot when all deposition holes are excavated and a steady state situation is assumed is shown in the lower right chart in Figure 8-3. The simulated average heads is still too high for the lowest measured values, but is good for the high heads. Since the model is a discrete fracture network model it is naturally that there will be a large difference between the maximum and minimum values due to connections between the fractures. The poor match for the initial state is a result of the skin on the tunnels.

8.3.2 Head versus distance from tunnels

By studying the head versus the distance from a tunnel it is possible to check how the head drops in the vicinity of the tunnel. The distance, in this study, is calculated as the distance from the midpoint of the packer section to any tunnel or deposition hole. This implies that some vertical boreholes in the vicinity of a deposition hole can have the distance of 8 m in the initial case, 15 June 1999, and only 1 m at the end of the measuring, 1 December 1999.

In Figure 8-4 is the max, average and minimum values from the simulation and the measured values plotted as a function of distance to any excavated tunnel. The maximum modelled value almost form a straight line at –40 m. This corresponds to an occasion were there is no, or small, contact for the modelled packer section to the nearest tunnel or good connection to the outer boundaries. The modelled minimum values correspond to an occasion where the contact between the packer section and the tunnel is good. There is a tendency for the minimum values to follow a logarithmic curve.

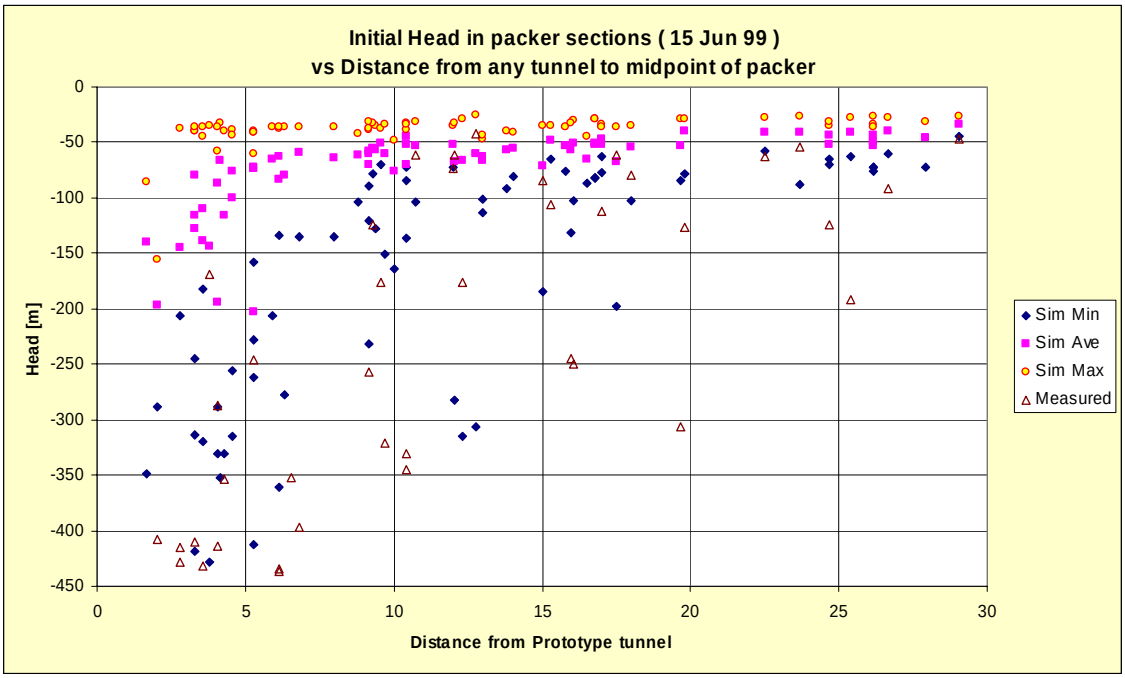

Figure 8-4. *The initial heads versus distance from any excavated tunnel or hole.*

The modelled average values only have a slight decrease in head as the distance to any cavity decrease until about 2 m where the head decreases more rapidly. The measured heads are widely spread, due to the fact that discrete fractures are the water bearing medium. The head drop almost forms a logarithmic function of the distance to the tunnel.

In Figure 8-5 the simulated and measured heads are plotted for the time where it is assumed that the volume around the prototype repository has come into a steady state, i.e. after excavating the 6 deposition holes. A logarithmic trend is added to make it easier to see the match between measured and simulated head. The modelled head shows a smaller dispersion than the measured and it is a bit higher than the measured.

Another way of presenting the head as a function of distance is to draw a line between the minimum and maximum distance for every packer section at the level of the modelled and measured head. The head as a functon of both minimum and maximum distance is shown in Figure 8-6.

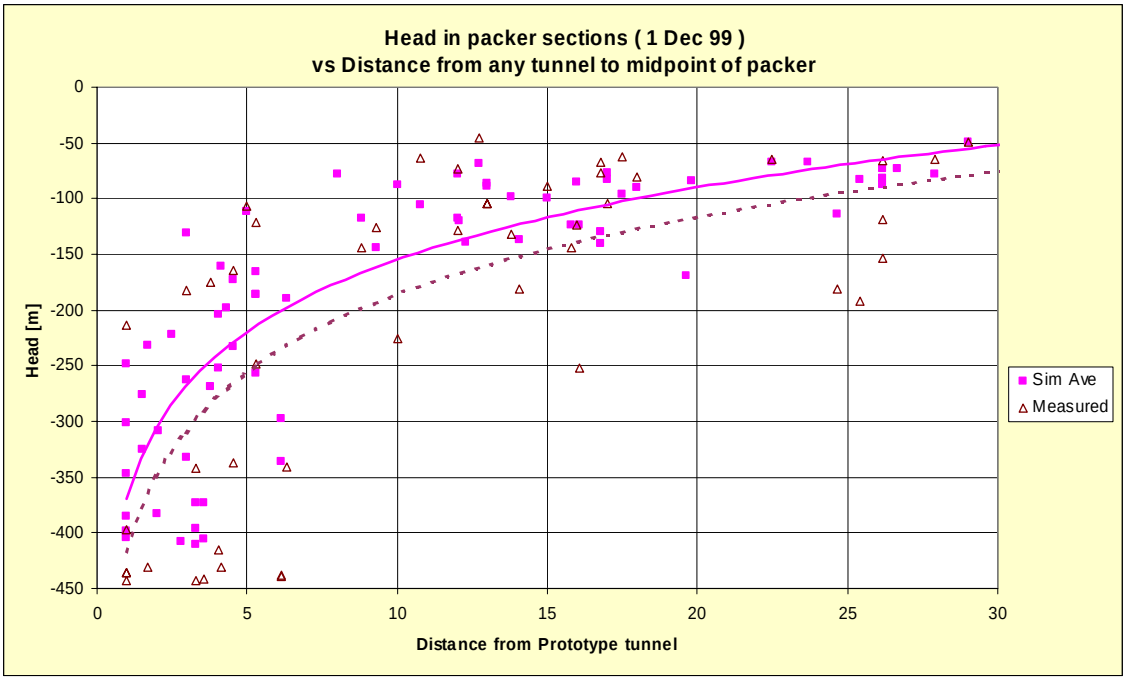

Figure 8-5. *Simulated and measured head as a function of distance from midpoint of packer section to any cavity.*

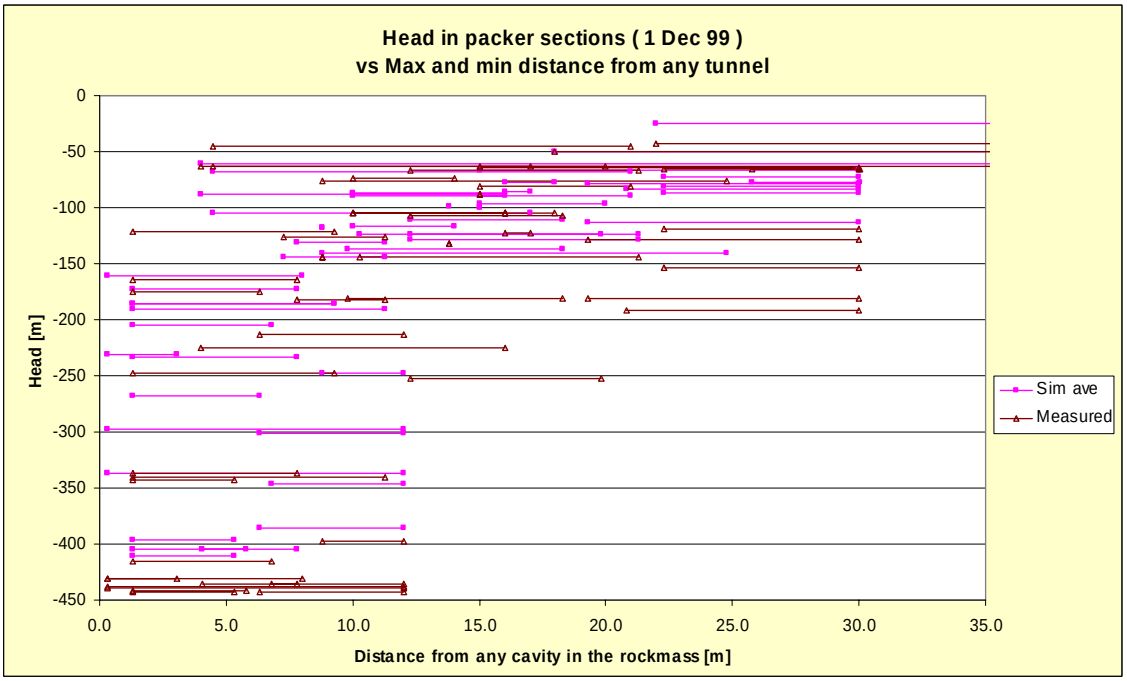

Figure 8-6. *Simulated and measured head as a function of minimum and maximum distance from packer section to any cavity.*

8.3.3 Head on boundaries

The given head values from Svensson (1997) can in some points be compared to the measured heads. In ***Table 8-4*** is the head in 4 points compared. The first point is near the west boundary of the modelled volume, the second near the south, the third near the bottom, and the last is as far as possible from the tunnel system.

There is a systematic error of about 20 m head from measured values and the modelled values by Svensson (1997). The differences may depend on that the model was calibrated for the conditions 1997. The boundary conditions for the DFN-model are based on the head from Svensson (1997) c.f. section 5.2.1.

Table 8-4. Measured heads compared to given heads from Svensson (1997)

Near west boundary (1850, 7270,-450)			
	1999-06-15	1999-07-15	1999-12-01
measured	-37	-38	-40
Svensson 97		-18	

Near south boundary (1890, 7230, -450)			
	1999-06-15	1999-07-15	1999-12-01
measured	-47	-48	-49
Svensson 97		-22	

Near bottom boundary (1850, 7230, -510)			
	1999-06-15	1999-07-15	1999-12-01
measured	-37	-38	-39
Svensson 97		-15	

Far from tunnels 1830, 7230, -510			
	1999-06-15	1999-07-15	1999-12-01
measured	-35	-35	-
Svensson 97		-15	

8.3.4 Conclusions from Head comparisons

The dispersion is large for maximum and minimum values when simulated head is plotted as a function of measured. This is naturally since it is a DFN-model and not a continuum model. At the initial state the simulated average head is too high, but after excavating all deposition holes the head decreases and is better correlated to the measured.

The same behaviour is observed when the head is plotted as a function of distance to the nearest tunnel, i.e. that the match is better when all 6 deposition holes are excavated. The better match is a result of not having a skin around the deposition holes and therefore the skin around the prototype tunnel can be questioned.

Another question is whether the head field from Svensson (1997) is a good approximation of the headfield for the volume. The impact will probably be minor since the systematic error only is 20 m, see Hermanson *et al*. (1999).

9 Conclusions

The following conclusions can be drawn from the project. The conclusions are divided into 3 parts concerning main results, source of uncertainty, and improvements

9.1 Main results

- Fracture orientation of the 3 fracture sets was estimated with confidence.
- The fracture statistics from drill campaigns 1, 2 and 3 shows similar behaviours. The fracture network can be characterised from a smaller number of boreholes.
- The most probable modelled inflow to a deposition hole was predicted to be between 0.3 to 3 l/min.
- Large inflows to a deposition hole is not only dependent on a high transmissive fracture intersecting the deposition hole but also needs to be connected to the conductive network of fractures.
- When new deposition holes are drilled the inflow to old deposition holes will decrease. The effect decreases by distance.
- Transient simulation of the excavation of deposition holes 1 to 4 shows that flow and pressure changes stabilise within a maximum of two days. The modelling of the hydraulic behaviour of the prototype repository with a steady state approach is therefore valid.
- Size variation of the deterministic features has a limited effect on the inflow to the deposition holes. The variation changes the connectivity of the DFN at the vicinity of the deposition holes.
- The effect on the inflow to the deposition holes is limited when the transmissivity of the deterministic fractures is decreased. An increase of the transmissivity will on the other hand have a large effect on the inflow.
- A skin zone around the tunnels will have large effect on the inflow to both tunnels and deposition holes.
- Including more low-conductive fractures will not increase the inflow to the canister holes.
- Modelled average fracture trace intensity, P_{21}, is slightly smaller than measured.
- The modelled average tracelength is longer than measured due to different scale for mapping fractures
- Modelled inflow is about 50 times larger than measured.
- The modelled head drop towards the tunnel is small due to the assigned skin when no deposition holes are excavated. The skin should be considered to be uncertain.
- When all deposition holes are excavated the modelled headfield shows a better match to measured.
- The headfield from Svensson (1997) shows a systematic error of about 20 m.

9.2 Source of uncertainty

- Almost all observation boreholes are drilled within parallel planes. These planes are perpendicular to the TBM tunnel axis. This particular orientation makes it difficult to characterise the fractures parallel to these planes.
- TBM fracture mapping is of good quality but the level of truncation of the trace size is too high. As a consequence, there is no data available for the size of the fracture below the truncation level chosen.
- The rock mass hydraulic behaviour around the prototype repository is difficult to reproduce and is not fully understood.
- A skin zone may exist around the TBM tunnel. Its thickness and magnitude has not been accurately characterised. The sensitivity analysis showed that the model is very sensitive to the skin zone hydraulic characteristics.
- The head field used as outer boundary is not calibrated for the current situation at Äspö.
- What role does the packer sections play for making “short cuts” for the water in the model?
- The fracture size distribution is assumed to be lognormal, but there is an uncertainty whether other distribution would fit better.

9.3 Improvements

9.3.1 Improvements of the characterisation of the Prototype Repository

The measurement program has been ambitious and provides the right kind of data necessary for flow simulations using the DFN approach. However, to better optimise the knowledge of how the rock mass around the repository behaves, one could expand and spread the investigations more evenly in all directions. The prototype repository is located in a straight tunnel where most exploratory boreholes are drilled in more or less one plane. The short holes could well be somewhat more inclined to sample fractures with less bias.

The detailed geological characterisation of the repository identified a small number of deterministic features out of which only a couple was of significant size. The impact of implementing these structures into the model was of limited significance. From a modelling perspective, it may not be necessary to implement such small structures deterministically into the model for future simulations.

9.3.2 Improvements of the model

The model is sensitive to the applied skin. The skin factor could be better estimated as well as the natural explanation, width and persistence of the skin zone. A better understanding of the EDZ (Excavation Damage Zone) and the effect of the injected grout would be helpful. To use measured pressures in the immediate surroundings of the tunnel may improve the estimation of the skin zone effect.
It was difficult to match the measured transmissivity to a lognormal transmissivity distribution. A better understanding of which fractures are playing the dominant role in the conductive network may help to estimate the transmissivity distribution.
More effort to match the different transmissivity data to fracture sets divided not only by their orientation, but also by their geological characteristics, e.g. joints or faults.

A key issue could be to do a new analysis of the fracture orientation using 3 sets that has a low dispersion in orientation and properties, and 1 extra set that reflect the background fracturing with some more or less constant properties. This will probably decrease the connectivity in the fracture network, and as a consequence the inflow will decrease without a skin around the tunnels. The modelled and measured heads will probably show a better match if the skin is removed.

New boundary heads on the outer boundary that reflects the current situation at Äspö will also decrease the driving force for the water flow.

The correlation between observed and modelled traces is low for the NE-trending set and there is no distinct peak for the other 2 sets, see section 3.2.3. This might reflect, as mentioned above, that there should be a 4^{th} fracture set to take care of a background fracturing. It also raises the question to test different size distributions, e.g. powerlaw. This would affect the connectivity and the flow and maybe get a better understanding of the hydraulic behaviour.

Another interesting topic to study could be to correlate the transmissivity of the fractures to the radii together with a fractal distribution of the transmissivity over the fracture plane to make “channels” for the water.

References

Benjamin, J.R. and C.A. Cornell, 1970. "Probability, Statistics and Decision for Civil Engineers," McGraw Hill Book Company, New York.

Castaing C., M. A. Halawi, F. Gervais, J. P. Chilés, A. Genter, B. Bourgine, G.Ouillon, J. M. Brosse, P. Martin, A. Genna and D. Janjou ,1996. Scaling relationships in intraplate fracture systems related to Red Sea rifting. Tectonophysics, Vol. 26, 291-314.

Dershowitz, W. S. and H.H. Herda, 1992. Interpretation of fracture spacing and intensity. In proceedings of the 33rd US symposium on Rock Mechanics, A.A. Balkema, Roterdam p.757-766.

Dershowitz, W., A.Thomas and R. Busse (1996) Discrete fracture network analysis in support of the Äspö Tracer Retention Understanding Experiment (TRUE-1), SKB ICR 96-05, Swedish Nuclear Fuel and Waste Management Company, Stockholm.

Feller, W., 1971. "An Introduction to Probability Theory and Its Applications." John Wiley and Sons, New York.

Follin, S. and J. Hermanson (1996) A discrete fracture network model of the Äspö TBM Tunnel Rock Mass, SKB AR D-97-001, Swedish Nuclear Fuel and Waste Management Company, Stockholm.

Forsmark, T. and I. Rhén (1999). Äspö Hard Rock Laboratory PrototypeRepository. Hydrogeology – Drill Campaign 3A and 3B. VBB Viak, Göteborg. Under revision.

Hermanson, J., M. Stigsson and A. Pringle. (1999) Äspö Hard Rock Laboratory. Prototype repository DFN Model No. 1, SKB IPR-99-09, Swedish Nuclear Fuel and Waste Management Company, Stockholm.

Kulatilake, P. H. S. W. and T. H. Wu, (1984) Estimation of mean trace length of discontinuities, Rock Mechanics and Rock Engineering, 17, pp. 215-32.

LaPointe, P., P. Wallman and W. Dershowitz. (1993) Stochastic estimation of fracture size through simulated sampling. Int. J. Rock Mech. Min Sci. & Geomech. Abstr. Vol 30, No. 7, pp. 1611-1617.

LaPointe, P., P. Wallmann, and S. Follin (1995). Estimation of effective block conductivities based on discrete network analyses using data from the Äspö site, SKB TR 95-15, Swedish Nuclear Fuel and Waste Management Company, Stockholm.

LaPointe, R. P. and S. Follin 1999. Calculation of displacements on fractures intersecting canisters induced by earthquakes: Aberg, Beberg and Ceberg examples. Tachnical Report TR-99-03. , Swedish Nuclear Fuel and Waste Management Company, Stockholm.

Munier, R. (1995) Studies of geological structures at Äspö - Comprehensive summary of results, SKB PR 25-95-21, Swedish Nuclear Fuel and Waste Management Company, Stockholm.

Oillon, G., C. Castaing and D. Sornette, 1996. Hierarchical geometry of faulting. J. Geophysical Res., Vol. 101, No. B3, 5477-5487.

Osnes, J.D., A. Winberg and J. Andersson, 1988. "Analysis of Well Test Data -- Application of Probabilistic Models to Infer Hydraulic Properties of Fractures," Topical Report RSI-0338, RE/SPEC Inc., Rapid City, South Dakota

Patel, S., L.O. Dahlström and L. Stenberg, 1997. Characterisation of the rockmass in the prototype repository at Äspö HRL, stage 1. Progress report HRL-97-24. Swedish Nuclear Fuel and Waste management Company.

Priest, S. D. (1993) Discontinuity analysis for rock engineering, p. 473 Chapman & Hall, London.

Rhén, I. and T. Forsmark (1998a). Äspö Hard Rock Laboratory Prototype repository. Hydrology – Drill Campaign 1. Progress Report PR HRL 98-12. Swedish Nuclear Fuel and Waste management Company.

Rhén, I. and T. Forsmark (1998b). Äspö Hard Rock Laboratory Prototype repository. Hydrology – Drill Campaign 2. Progress Report PR HRL 98-22. . SKB TR 97-06. Swedish Nuclear Fuel and Waste management Company.

Rhén, I., G. Gustavsson, R. Stanfors and P. Wikberg, 1997. Äspö HRL-Geoscientific Evaluation 1997/5, models based on site characterisation 1986-1995. SKB TR 97-06. Swedish Nuclear Fuel and Waste management Company.

Svensson, U. (1997) Asite scale analysis of groundwater flow and salinity distribution in the Äspö area. SKB TR 97-17. Swedish Nuclear Fuel and Waste management Company.

Terzaghi, R. D. (1965) Sources of error in joint surveys. Geotechnique, 15, pp. 287-304.

Winberg, A., 1995. Overview and review of experiments on the excavation disturbed zone (EDZ). SKB PR 25-95-17. Swedish Nuclear Fuel and Waste management Company.

Appendix A

Excerpt From the FracMan and MAFIC User Documentation

A.1 FracMan

FracMan is a software package developed by Golder Associates Inc. to model the geometry of discrete features, including faults, fractures, paleochannels, karsts and stratigraphic contacts. For convenience, all discrete features will be frequently referred to as fractures in this manual, although the tools provided in FracMan are equally useful for all types of discrete features.

FracMan is designed to provide geologists and engineers with an easy-to-use tool for modelling fractured rock masses, rock mechanics and hydrologic applications in hazardous and nuclear waste management, underground construction, mining and petroleum reservoir engineering. FracMan provides an integrated environment for the entire process of discrete feature data analysis and modelling. FracMan provides:

- **data analysis features** to allow transformation of raw data into the formats needed for discrete fracture modelling,

- **stochastic simulation** of fracture patterns to facilitate three-dimensional visualisation,

- **exploration simulation,** to improve the design and interpretation of site characterisation programs for collection of fracture data,

- **finite element mesh generation and output post-processing,** to facilitate flow and transport modelling in networks of fractures and

- **macro** support, to facilitate **Monte Carlo** stochastic simulation.

FracMan's data analysis capabilities include new techniques for analysing fracture orientation, size, intensity and transmissivity. These techniques provide the data needed for fracture geometric modelling from data which are frequently collected as part of comprehensive site investigations, but are rarely used in hydrologic or mechanical modelling.

FracMan's geometric modelling features include nine conceptual models for fracture heterogeneity. These models provide users with the flexibility to include fractal, non-stationary Poisson point process and correlated fracture locations. Geometric realism is enhanced by the ability to model terminations at fracture intersections, plus dislocation and rotation on faults.

A.1.1 FracSys: Fracture Data Analysis

FracMan discrete fracture modelling is useful for modelling possible geological conditions when there is little or no data. It is also useful for modelling *in situ* conditions when data is available. Unfortunately, FracMan requires information in formats which are frequently not available as part of conventional data collection programs, although these formats can be derived by appropriate procedures. The FracSys module provides those procedures.

A.1.1.1 ISIS: Interactive Set Identification System

ISIS defines fracture sets from field data using an adaptive, probabilistic pattern recognition algorithm. ISIS allows the user to select the fracture properties of concern and define their relative significance for the analysis. Unlike conventional approaches to fracture set definition, which define sets by contouring orientations on stereoplots, ISIS is as powerful for overlapping fracture sets as for clearly defined sets. The premise of the ISIS approach for definition of fracture sets is that the sets should be groups of fractures with similar properties. Orientation does not need to be the only property defining sets; size, termination, fillings and other properties can identify sets as well.

ISIS identifies fracture sets using multiple fracture properties. ISIS calculates the distribution of properties for the fractures assigned to each set, then re-assigns fractures to sets according to probabilistic weights proportional to their similarity to other fractures in the set. The properties of the sets are then recalculated and the process is repeated until the set assignment is optimised.

Assigning fractures to sets

The goal of the ISIS approach is to assign groups of fractures which are similar geologically or hydrogeologically to sets which are statistically homogenous . This is achieved by deriving the statistical properties of each set from the statistical properties of the fractures assigned to the set and then removing and reassigning fractures which have a low probability of being part of the set. The ISIS algorithm begins by requiring the user to select and assign weighting factors w_j to each of the n_j fracture characteristics of concern and to provide initial guesses for the properties of the each set *k*. In addition, the user must specify the convergence method, either hard sector, soft sector, sector preconditioning or none (see below). For each fracture *i*, ISIS then calculates a probability that the fracture belongs to that set. During the first iteration, this probability is calculated using the value of the probability density function for that property and set, taken at the value of the fracture.

$$P[i \in k] = C\ p_{w,k}$$

$$p_{w,k} = \sum_{j=1}^{n_j} W_j\, f_j(k_i) P_{si} + f_{si}$$

$$C = \frac{1}{\sum_{k=1}^{n_k} p_w}$$

where $P[i \in k]$ is the probability that fracture i is an element of set *k*, $p_{w,k}$ is the weighted probability density function of set *k* for property *j*, $f_k(k_i)$ is the probability density function of set *k* for property *j* evaluated for fracture *i*, w_j is the user-assigned weighting for property I and P_{si} and f_{si}; are sector factors, (see below) and C is a proportionality constant defined to ensure that the sum of probabilities for all set equals 1. ISIS does not require complete information on every fracture property *j* for all fractures *i*.

When a piece of information about fracture *i* is missing, $f_k(k_i)$ is set at 0 for that fracture over all sets *k*, such that only those properties for which values are specified are used in the assigning that fracture to a set.

The probability density functions $f_k(k_i)$ for each property of each set are provided by the user for the first iteration. For subsequent iterations, they are calculated using the distributional forms specified by the user, with moments calculated using the fractures assigned to sets during the previous iteration. The form of the probability density function $f_k(k_i)$ is also determined by the user and may be Fisher (for orientation), normal, lognormal, exponential or a histogram and is dependent on the property.

The factors P_{si} and f_{si} depend on the user-specified convergence method. Sectors are defined by the closest mean pole (or dip vector) as defined by the fracture set mean pole (or dip vector).

Table 3-2 Convergence Factors and Sectoring in ISIS

	Fracture *i* in same sector as set *k* mean pole (or dip)	Fracture *i* in different sector from set *k* mean pole (or dip)
Hard Sector	$P_{si} = 1$ $f_{si} = 0$	$P_{si} = 0$ $f_{si} = 0$
Soft Sector	$P_{si} = 1$ $f_{si} = 0.25$	$P_{si} = 1$ $f_{si} = 0$
No Sector	$P_{si} = 1$ $f_{si} = 0$	$P_{si} = 1$ $f_{si} = 0$
Sector Preconditioning	Same as Hard Sector first iteration Same as No Sector afterwards	

Once the probability $P[i \in k]$ has been calculated for each fracture and set, the fractures are reassigned to sets by Monte Carlo simulation, such that the each fracture is assigned to set *k* with probability $P[i \in k]$.

When all fractures have been reassigned to sets, the set distribution parameters are recalculated for each property j using the fractures assigned to that set. For orientation statistics, the mean pole vector or mean dip vector and the Fisher dispersion parameter *k* (Fisher et al., 1987) are calculated. For continuous distributions such as lognormal and normal, the mean and standard deviation are recalculated and for histogram distributions the percentages for each class are calculated. For example, for rock type histogram distributions, the property statistics for rock-type for set *k* are set to the percentage of each rock type among the fractures currently assigned to set *k*.

When the distributions of fracture properties for each set have been recalculated, ISIS repeats the process, reassigning sets to fractures. In order to speed convergence, a relaxation factor $\gamma$is used in calculating the probability $P[i \in k]$. This relaxation factor controls the rate of change in $P[i \in k]$ using a weighted average of probability density functions for the fractures current and previous set assignments:

$$P[i \in k] = Cp_{w,k}$$

$$p_{w,k} = \sum_{j=1}^{n_j}(1-\gamma_j)W_j f_j(k_i) + \sum_{j=1}^{n_j}\lambda_j W_j f_j^{(old)}(k_i)$$

$$C = \frac{1}{\sum_{k=1}^{n_k} p_w}$$

where $f_j^{(old)}$ is the probability density function from the previous iteration. For each property *j*, a relaxation factor of 0 calculates the probability $P[i \in k]$ based solely upon the current assignment of fractures to sets and a relaxation factor of 1 calculates the probability $P[i \in k]$ without an change as fractures are reassigned and as set-properties change. A value of approximately 0.5 is appropriate for most properties.

ISIS also uses damping factors in the calculation of updated mean directions and dispersion parameters for each set using the equation

$$\kappa^{(updated)} = (1-d_\kappa)\kappa^{(old)} + d_\kappa\kappa^{(new)}$$

$$\upsilon^{(updated)}(\bar{\varphi},\bar{\theta}) = \frac{(1-d\upsilon)\,\upsilon^{(old)}(\bar{\varphi},\bar{\theta}) + d\upsilon\,\upsilon^{(new)}(\bar{\varphi},\bar{\theta})}{\left|(1-d\upsilon)\,\upsilon^{(old)}(\bar{\varphi},\bar{\theta}) + d\upsilon\,\upsilon^{(new)}(\bar{\varphi},\bar{\theta})\right|}$$

where

d_κ	=	is the damping parameter for Fisher dispersion
d_υ	=	the damping parameter for mean orientation
$\kappa^{(old)}$	=	the Fisher dispersion parameter from the previous iteration.
$\kappa^{(new)}$	=	the Fisher dispersion parameter based on the fractures currently assigned set
$\kappa^{(updated)}$	=	the Fisher dispersion parameter to be used by the set in the next iteration.
υ	=	the unit vector for mean orientation (φ,θ).

This process is repeated for a number of iterations specified by the user. When the analysis is complete, ISIS calculates the Kolmogorov-Smirnov goodness-of-fit statistics for each of the properties and distributions used in the analysis, based upon the fractures assigned to the sets at the end of the analysis. This process of regrouping the fractures is repeated until the distribution parameters of the sets stabilise.

This algorithm has been verified utilising one, two and three overlapping Fisher distributed fracture sets.

Terzaghi Correction
ISIS includes the option to apply a modified Terzaghi correction (Terzaghi, 1965), to partially compensate for orientation bias of planar (trace plane) and linear (scan line and borehole) sampling. When the Terzaghi correction option is selected, the data set is modified so that for each original fracture data record, N records are added according to:

$$N = min(\lfloor R / cos\beta \rfloor, U)$$

where

R	=	a uniform, random deviate between 0 and 1,
β	=	the angle between the normal to the fracture plane and the borehole or scanline direction.
U	=	User-specified maximum correction.

This correction increases the number of records for fractures that have normal vectors at high angle to the direction of the borehole or scanline by a quantity that is inversely proportional to the probability of intersecting those fractures with the borehole or scanline.

A maximum value of N = 7 will avoid excessively strong correction for fractures that are nearly parallel to the boreholes or scanlines.

A.1.1.2 HeterFrac

HeterFrac geologic structure analysis allows the evaluation of single trace planes containing both linear and curved fracture traces.

HeterFrac derives statistics for seven of the geologic conceptual models implemented in FracMan/FracWorks for geologic simulation: Baecher Model, BART Model, geostatistical, POCS, Nearest Neighbour Model, Fractal ("Levy-Lee") Model and War-Zone Model. This section describes the models analysed and the statistical tests used for evaluation of the appropriateness of the different models.

HeterFrac Trace Analysis can be carried out using either trace centres or random points on the trace as measures for fracture location. HeterFrac prompts the user for specification of the trace using either trace centre or random point(s) before proceeding to analyse options. In general, no more than one random point should be used.

HeterFrac then provides six alternative selections:

- **Statistics** produces statistical analysis of trace maps, except for the calculations and goodness of fit tests for the Enhanced Baecher Model Poisson (uniform location) assumption and the box fractal dimension.

- **Baecher Analysis** calculates the box fractal dimension and uses the χ^2 test and the correlation coefficient to test the statistical significance of the Enhanced Baecher model's Poisson assumption and the box fractal dimension fit. When running the Baecher analysis, the user must specify the region to be analysed and the grid size to be used in calculating local fracture intensity P_{22}.

- **Geostatistical POCS** calculates the variogram for local fracture intensity P_{22} and determines the variogram fractal dimension D_v and the spherical variogram correlation length λ, for the random field of local intensities. A non-linear least-squares algorithm is used to derive D_v and λ,. The variogram fractal dimension D_v can be used with the POCS geometric conceptual model. The variogram correlation length λ, can be used with the POCS and geostatistical conceptual models.

- **Nearest Neighbour Analysis** calculates the relationship between fracture intensity P_{22} and the distance to user-defined major fractures using the χ^2 test and the correlation coefficient to determine the significance of the fit.

- **Levy-Lee Analysis** calculates the log-linear intensity P_{21} versus circle radius relationship for the box fractal dimension and uses the χ^2 test and correlation coefficient to determine the significance of the fit. The Levy-Lee analysis requires specification of the centre of the area to be analysed and the radiis of the smallest and largest circle to be used.

- **War Zone Analysis** calculates the relationship between the war zone criterion W_z and relative fracture intensity factor W_f. The region to be analysed and the grid cell size are specified as in the Baecher analysis. In addition, the user must specify values of war zone coefficients z_L, z_p and z_c. For deterministic war zone analysis, the user have to define the perimeter of a war zone. The program will then display the war zone intensity W_f and war zone criteria W_z for regions selected.

The determination of which spatial model that is most appropriate is accomplished in FracMan by means of statistical tests and geometrical measures such as the χ^2 -test and the box fractal dimension. For example, a χ^2 -test can be used to compare the observed distribution of fracture centres to a theoretical Poisson distribution. A significance of 85% or greater generally indicates a good fit to the Poisson distribution and a high probability that the Beacher model is appropriate. The box fractal dimension is a measure of how completely the fracture pattern fills the trace plane surface. A fractal dimension near 1 indicates a very strongly clustered, heterogeneous pattern, whereas a dimension close to 2 indicates a more homogeneous, space filling pattern. Large fractal dimensions indicate Poisson type models whereas smaller dimensions indicate clustered models such as the Nearest neighbour , War zone or Levy-Lee fractal models.

A.1.1.3 FracSize Tracelength Simulation Module

The FracSize data analysis module is used to determine the distribution of fracture radii that gives the best match to the observed tracelength data. FracSize uses simulated sampling to take into account censoring, truncation and sampling bias.

FracSize starts with an .ORS file containing measured fracture radii, a .SAB file containing the specification of the sampling process used to collect each of the fractures in the .ORS file and an assumed distribution of fracture radii provided by the user. FracSize then simulates the sampling process, compares the simulated sample to the actual data in the .ORS file and displays a graphical and statistical summary of the comparison.

Two optimisation algorithms are available to provide an automated search of the fracture radius distribution. For the simulated annealing and conjugate gradient optimisation algorithms, FracSize varies the assumed distribution of fracture radius to improve the match between simulated and measured trace results, as measured by either Kolmogorov-Smirnov (K-S) or Chi-Squared (χ^2)/statistics. For each iteration, ' FracSize carries out five realisations of a specific fracture radius distribution and calculates the mean K-S and χ^2 statistics as the measure of the goodness-of-fit provided by that fracture radius distribution.

A.1.1.4 Oxfilet

The OxFilet ("**O**snes E**x**traction from **F**ixed-**I**nterval-**L**ength **E**ffective **T**ransmissivities") module is used to determine the transmissivity distribution and frequency of conductive fractures from packer test data by using an approach adapted from Osnes et al. (1988).

The method assumes that the net transmissivity of a test zone is equal to the sum of the transmissivities of the conductive fractures that intersect that test zone:

$$T_i = \sum_{j=1}^{n_j} T_{ij}$$

where T_{ij} is the apparent transmissivity of the ith packer interval, n_i is the number of conductive fractures in the ith interval, and T_{ij} is the transmissivity of the jth conductive fracture within the ith interval. Within any given interval, the number of conductive fractures, n_i, is assumed to be a random number defined by a Poisson distribution (Benjamin and Cornell, 1970):

$$f_n(n) = \frac{\bar{n}^n e^{-\bar{n}}}{n!}$$

where $\bar{n}$ is the Poisson process rate, which is equal to the expected value of n. The conductive fracture frequency is given by $f_c = n/L_i$, where L_i = the length of the test zone. The distribution of fracture transmissivities is assumed to be independent within each packer interval, with a given distributional form. The distribution of T_i is the sum of a random number of random events, and is therefore a compound Poisson process (Feller,

1971). In this approach, the mean number of fractures in a given interval is defined by the Poisson distribution rate parameter, n, and the distribution of fracture transmissivities T_{ij} is described by a lognormal distribution with a mean and standard deviation, m_{logT} and s_{logT}.

For any given set of parameters describing the distribution of fracture transmissivity $f(T_{ij})$ and conductive fracture frequency f_c, the distribution of packer interval transmissivities $f(T_i)$ are found by Monte Carlo simulation, with the best fit value found by a simulated annealing search routine. Simulated intervals that contain no conductive fractures, or that have values of T_i less than $T_{threshold}$, the lowest threshold transmissivity that could be reliably measured in the field, are assigned a transmissivity equal to $T_{threshold}$.

The intensity and transmissivity distributions for the conductive fractures are then estimated by finding the best match between the observed distribution of packer interval transmissivities $f(T_i)$ and the distribution of test zone transmissivities found by simulation for given fracture frequency and single-fracture transmissivity distributions. This match is found both visually and by comparison of Kolmogorov-Smirnov (K-S) or Chi-Squared statistics (χ^2).

The values of n, $\mu_{\log T}$ and $\sigma_{\log T}$ that provided the best K-S or χ^2 minimise D are taken to be the best estimates of those parameters.

MAFIC flow and transport simulations require that the fracture transmissivity used be the effective transmissivity through a fracture between the fractures intersecting the fracture ("cross-fracture transmissivity", T_{fi}). OxFilet provides three alternative interpretations for the relationship between T_{fi} and T_{ij}, the transmissivity seen in the fixed interval packer test.

- The packer test influences one fracture at a time, such that the transmissivity seen for each fracture T_{ij} is equal to the cross fracture transmissivity, T_{fi}.

The packer test is strongly influenced by the local fracture aperture near the borehole. In this case the transmissivity seen by the packer test is a small scale ("at-borehole") transmissivity, and the cross-fracture transmissivity T_{ij} must be found using a correlation of the form,

$$T_{ij} = \left(\frac{1}{B_f}\right) T_{fi}$$

In OxFilet, the proportionality constant Bf is described as a normally distributed random variable with mean and standard deviation provided by the user.

- The packer test influences a network with a number of interconnected fractures. In this case, the transmissivity seen by the packer test, T_{ij}, is a network transmissivity related to the cross-fracture transmissivity of a number of fractures. Assuming series flow through the n fractures influenced by the packer test, the relationship between T_{ij} and T_{fi} could be given approximately by,

$$T_{ij} = \frac{\overline{m}}{\sum_{i=1}^{\overline{m}} \frac{1}{T_{fi}}} \qquad (3\text{-}1)$$

For this option, an additional parameter $\underline{m}$, the mean number of fractures per network seen by packer tests must be specified. The distribution of $\underline{m}$ may be constant or Poisson.

A.1.2 FracWorks

The FracMan package idealises fractures as planar and polygonal. The planarity simplification is adopted for three reasons: firstly, because little field data is available on non-planar fractures; secondly, because planar fractures are computationally far more tractable than undulating fractures; and thirdly, because for problems of concern the effects of fracture undulation can be approximated in a more tractable manner, e.g., as an increased coefficient of friction for mechanical problems, or as an adjusted transmissivity for hydrological problems.

The assumption of polygonal fractures is both realistic and useful, as it allows the approximate representation of a wide variety of fracture shapes by a single mathematical form. Considerations from fracture mechanics suggest that in homogeneous rock the general shape of an isolated fracture should be elliptical, as is assumed in the Baecher model (Baecher et al, *1977).* However, since rock is generally heterogeneous, perfectly elliptical fractures are unlikely, and in a practical sense no error is introduced by representing the ideal, elliptical fracture by a many-sided polygon of equivalent area. Dershowitz (1984) has noted, moreover, that observed fractures are generally polygonal due to terminations of the fractures at intersections with other fractures. The Veneziano model (Veneziano, 1979) and the Dershowitz model (Dershowitz, 1984) both treat fractures as polygons.

The current version of FracMan contains nine conceptual models for fractures:

- the Enhanced Baecher model, an extension of the Baecher model which provides for termination of fractures at intersections with pre-existing fractures;

- the Levy-Lee Fractal model, a stochastic model which uses a Levy Flight fractal process to produce clusters of smaller fractures around widely scattered, larger fractures;

- the Nearest Neighbour model, a semi-stochastic, pattern-based model which simulates the tendency of fractures to be clustered around major joints and faults by preferentially producing new fractures in the vicinity of earlier fractures; and
- the War Zone model, a semi-stochastic, pattern-based model which imitates the geometry of shear zones by preferentially producing fractures in the regions between subparallel, neighbouring fractures.

- the Non-Planar zone model, a semi-stochastic model which generates fractures with location and orientation varying according to a user defined non-planar surface.

- the Fractal Box model which uses a self-similar fractured field to define fracture initiation points, which may be either centres or random surface points.

- the Fractal POCS (Projection Onto Convex Sets) model which generates a random field of fracture initiation points (centers or surface points) (a) consistent with a user specified fatal dimension, (b) consistent with a user specified variogram, and (c) conditioned to intensities at specified locations.

- the Geostatistical model, which generates a random field of fracture initiation points (centre or surface points) according to a specified spherical, exponential, or null variogram.

- the Poisson Rectangle model, simple version of the Enhanced Baecher Model, in which fractures are represented by rectangles with prescribed length and width, rather than as polygonal disks with an "effective radius". Location and termination are treated the same way as in the Enhanced Baecher model.

- the BART model, a version of the Enhanced Baecher model in which the fracture termination process is modified to improve computational efficiency.

The first four of these models are described in Geier, Lee, and Dershowitz, 1989. These models all generate polygonal fractures that may or may not terminate at intersections with other fractures. The models differ from one another only with regard to the spatial distribution of the fractures, and the interrelationship of fracture size and fracture location.

A.2 MAFIC

MAFIC (Matrix/Fracture Interaction Code) was developed by Golder Associates to simulate transient flow and solute transport through three-dimensional rock masses with discrete fracture networks. Flow and solute transport are simulated in both the fractures and the rock matrix. MAFIC is part of the FracMan discrete feature analysis package. MAFIC provides flow and transport simulation for hydrogeological conceptual models generated under FracMan/FracWorks. Input files for MAFIC can be generated by FracMan/MeshMaker and FracMan/MeshMonster, and edited by FracMan/EdMesh.

MAFIC simulates flow in fractures using three-dimensional networks of triangular finite elements. MAFIC simulates flow in the rock matrix using either a fully discretized multi-dimensional Galerkin finite element approach, or a generic matrix block scheme.

The matrix block scheme can use either one-dimensional finite elements or a pseudo steady-state analytical approximation. The matrix block approach reduces computational effort significantly, and is preferred for most applications, even though it does not model flow between non-intersecting fractures by matrix interconnection.

MAFIC simulates solute transport using a connective particle tracking approach. Solute dispersion is simulated stochastically using orthogonal, normally distributed, lateral and transverse dispersion vectors. MAFIC solute transport includes matrix diffusion, mineral-specific retardation, and sorption features.

MAFIC was designed to simplify input data requirements while providing maximum flexibility for the designation of boundary conditions. Input files may be specified by the user or generated by the FracMan fracture network simulation package. An efficient iterative matrix solver is provided to maximise solution efficiency and minimise matrix storage requirements.

Initial development of MAFIC was funded by BatteIle's Office of Waste Technology Development (OWTD). Development of the current version of MAFIC was funded primarily Golder Associates.

Several researchers have shown that, in many cases, flow and solute transport through fracture networks cannot be accurately modelled with equivalent porous media models (Long, et. al., 1982; Robinson, 1984; Anderson and Deverstorp, 1987; Smith and Schwartz, 1984). To provide for more realistic simulations of fractured rock masses, flow models incorporating networks of discrete fractures are required. MAFIC is a finite element flow model designed to simulate transient flow and solute transport in a rock mass with a discrete fracture network.

MAFIC models fracture flow through a network of interconnecting "plates," and matrix flow through a three-dimensional volume. MAFIC is capable of handling very general fracture network geometries. Both constant and time-dependent Dirichlet (prescribed head) and Neumann (prescribed flux) flow boundary conditions can be specified at any network node. Time-varying solute source strengths may be prescribed as a specified concentration at a given fracture element node or boundary surface.

MAFIC provides a number of special features including:

1. Choice of linear or quadratic elements using the same input data. Linear elements are transformed into quadratic elements by automated insertion of midside nodes.
2. Simulation of matrix flow using either a fully discretized finite element procedure, or a generic matrix block scheme which can accommodate a variety of fracture geometries. The matrix block approach can reduce computation time by orders of magnitude.
3. Specification of nodal groups with identical time-varying head or flux boundary conditions. An option also exists for simulating wells (or other prescribed flux boundaries) containing several fracture and matrix nodes for which only the **total** time-varying well flux is known.
4. An efficient incomplete Choleskii conjugate gradient equation solver, which significantly reduces memory and computation time requirements.

5. Creation of a restart input file using nodal heads from the last timestep as initial heads to allow for changes in boundary condition type and location.
6. Capacity for multiple simulations with different fracture network geometries but identical problem parameters and boundary conditions to accommodate stochastically generated fracture networks.
7. Solute transport modelling with either steady-state or transient flow conditions and stochastic emulation of convective dispersion, matrix diffusion, radioactive decay, and mineral-specific retardation.

Appendix B

Transformations of the Log-Normal Distribution

The log-normal distribution is given by the function

$$f(x) = \frac{1}{x\ln(10)y_\alpha\sqrt{2\pi}}\exp\{-\frac{1}{2}(\frac{\log x - \bar{y}}{y_\alpha})^2\}$$

Where $\bar{y}$ and y_α is mean and standard deviation in $\log_{10}$ space. In FracMan the logarithmic distribution is defined by the mean and standard deviation in real space (arithmetic). This is to provide a mean in units of meters which is a comprehensible measure of fracture size. This is despite the fact that the standard deviation in real space is more complex to understand. There exists simple conversion formulas between $\log_{10}$ space and real space. Given the $\bar{y}$ and y_α the arithmetic mean $\bar{x}$, and standard deviation x_α is:

$$\bar{x} = e^{(c\bar{y}+1/2(cy_\alpha)^2}$$

and

$$x_\alpha = \bar{x}\sqrt{e^{(cy_\alpha)^2} - 1}$$

and vice versa, i.e. given $\bar{x}$ and x_α

$$\bar{y} = \frac{1}{c}(\ln(\bar{x}) - \frac{(cy_\alpha)^2}{2})$$

$$y_\alpha = \frac{1}{c}\sqrt{\ln(1+(\frac{x_\alpha}{\bar{x}})^2)}$$

where c is the natural log of 10 (≈ 2.302).

Appendix C

Probability charts of measured transmissivities in 1 m and 3 m packers

All 3m packers

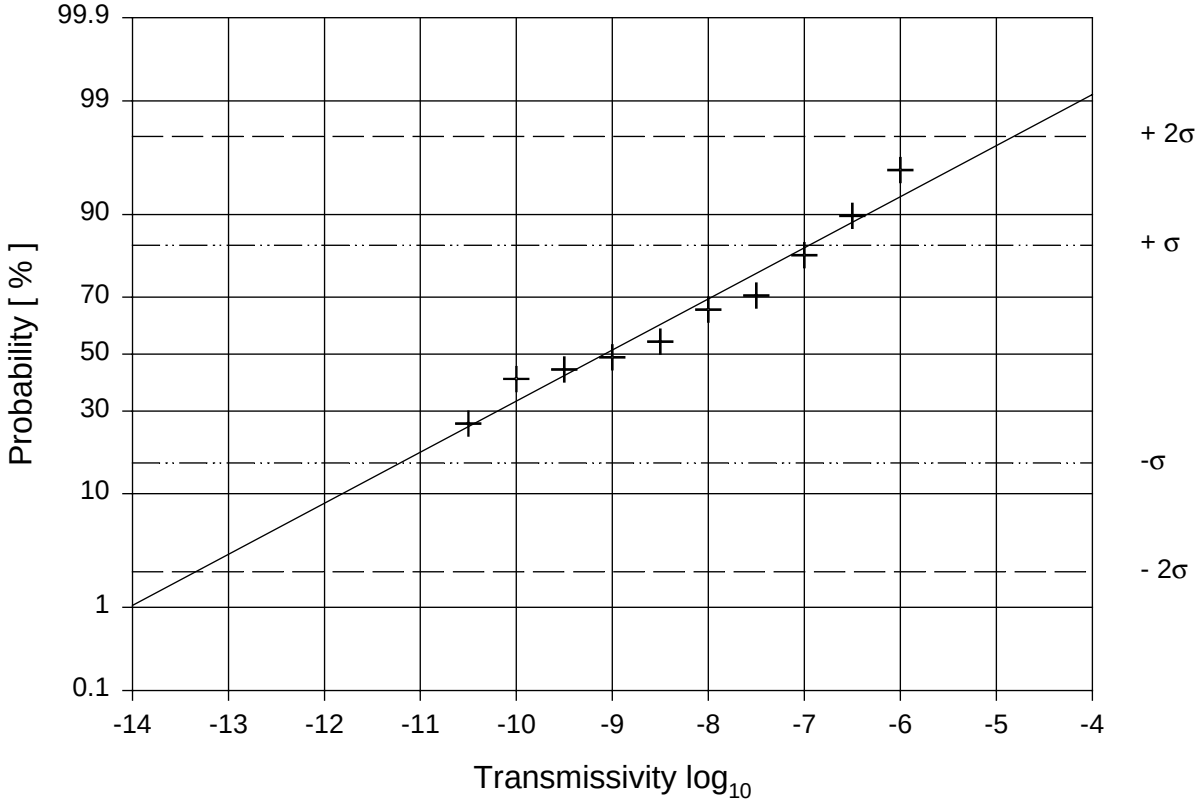

Subclass2 3m packers

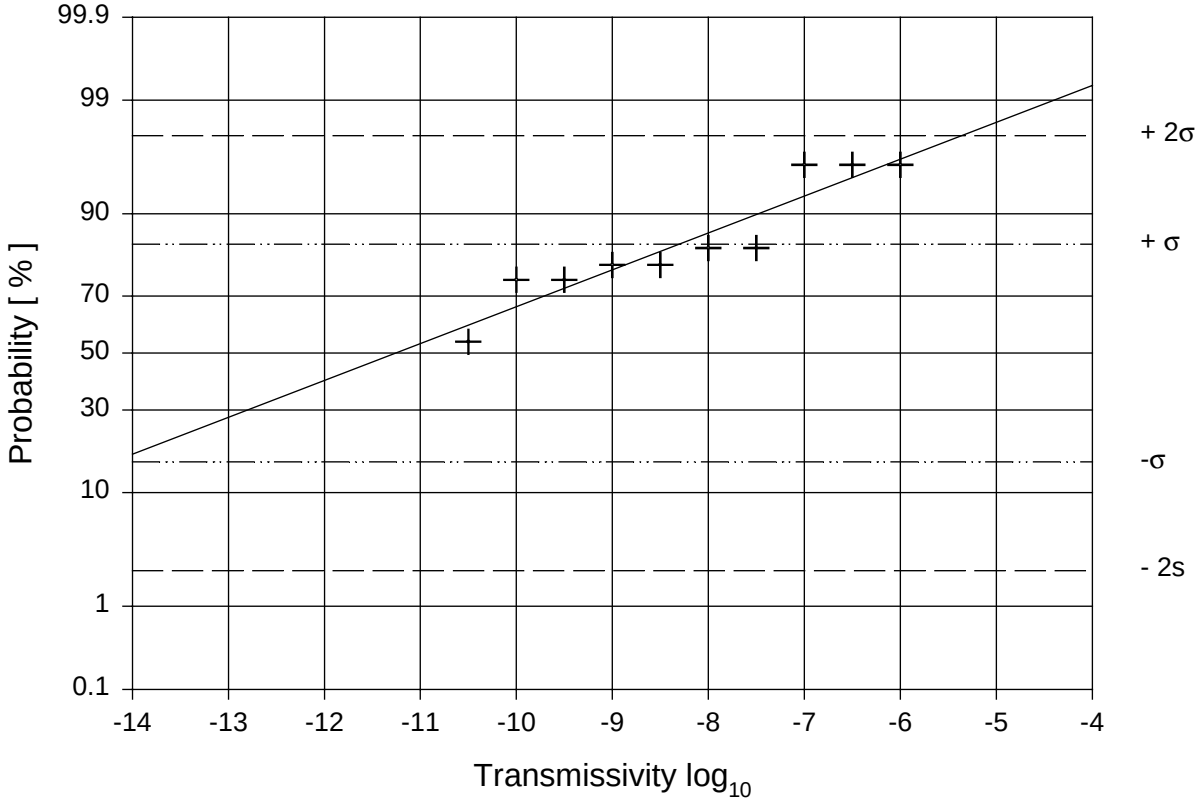

Subclass3 3m packers

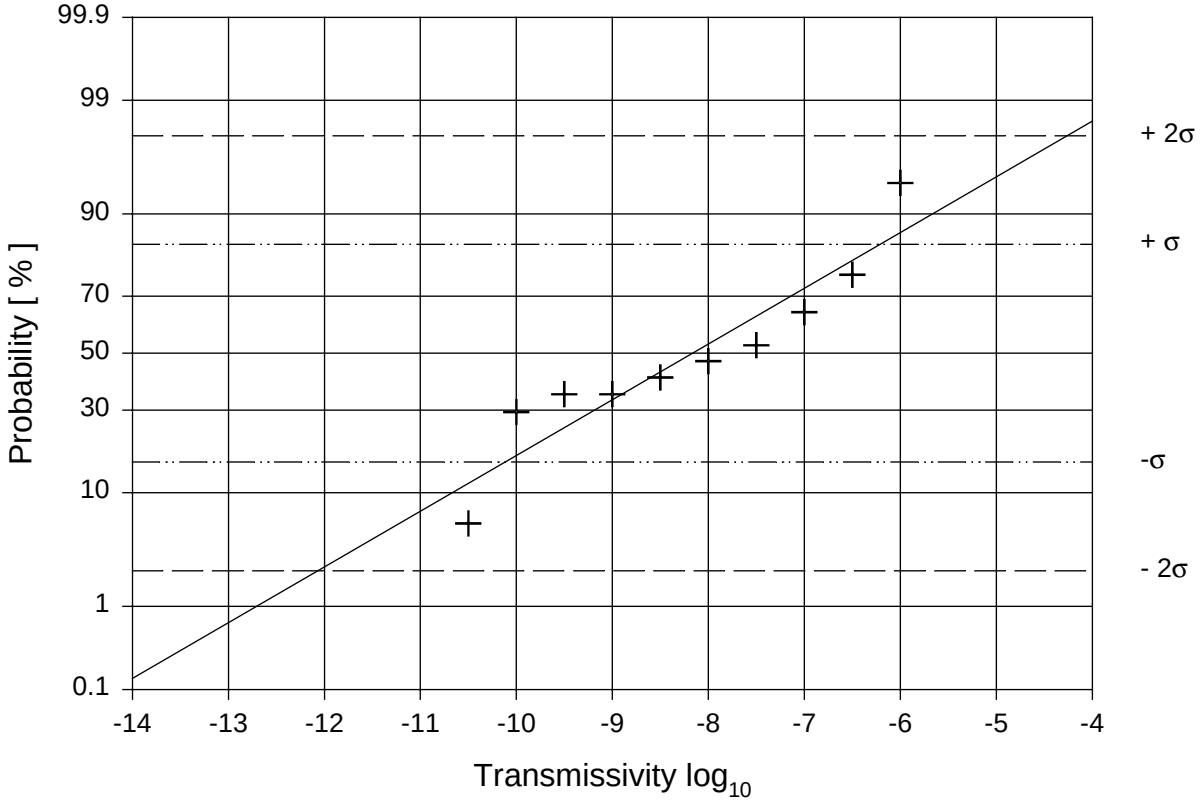

Subclass4 3m packers

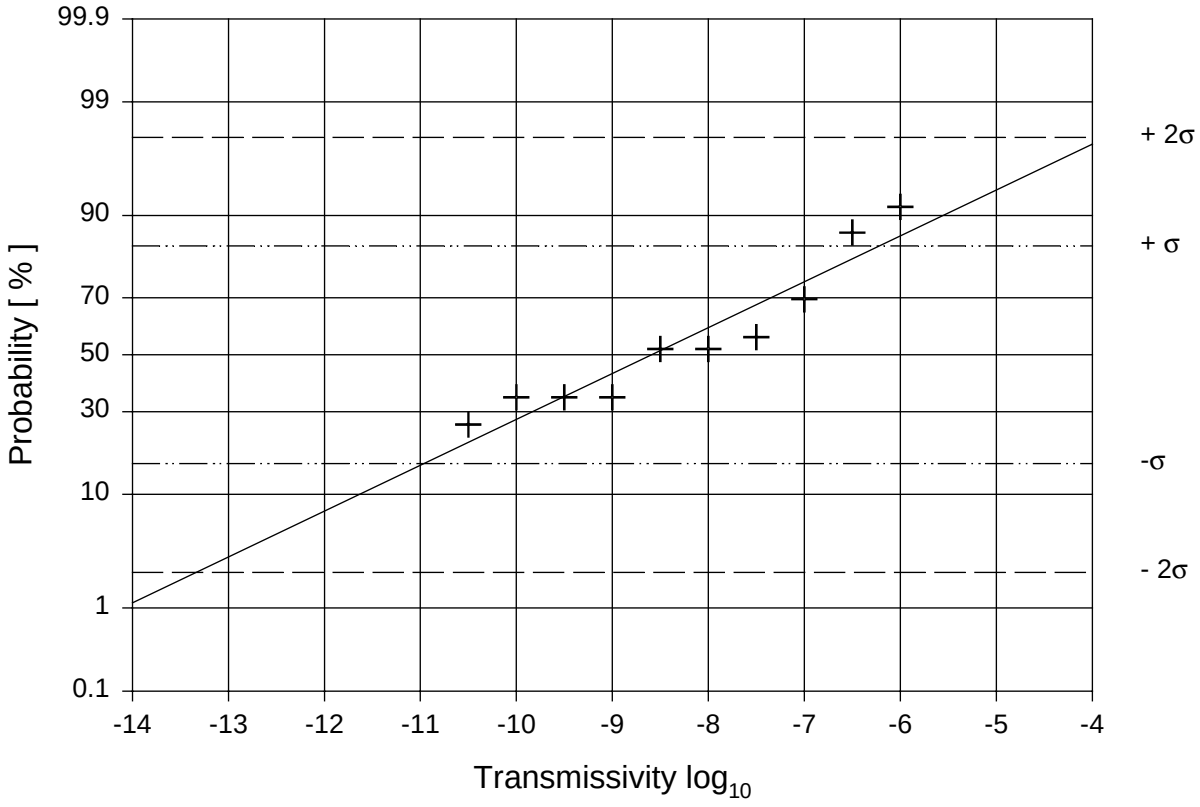

Subclass5 3m packers

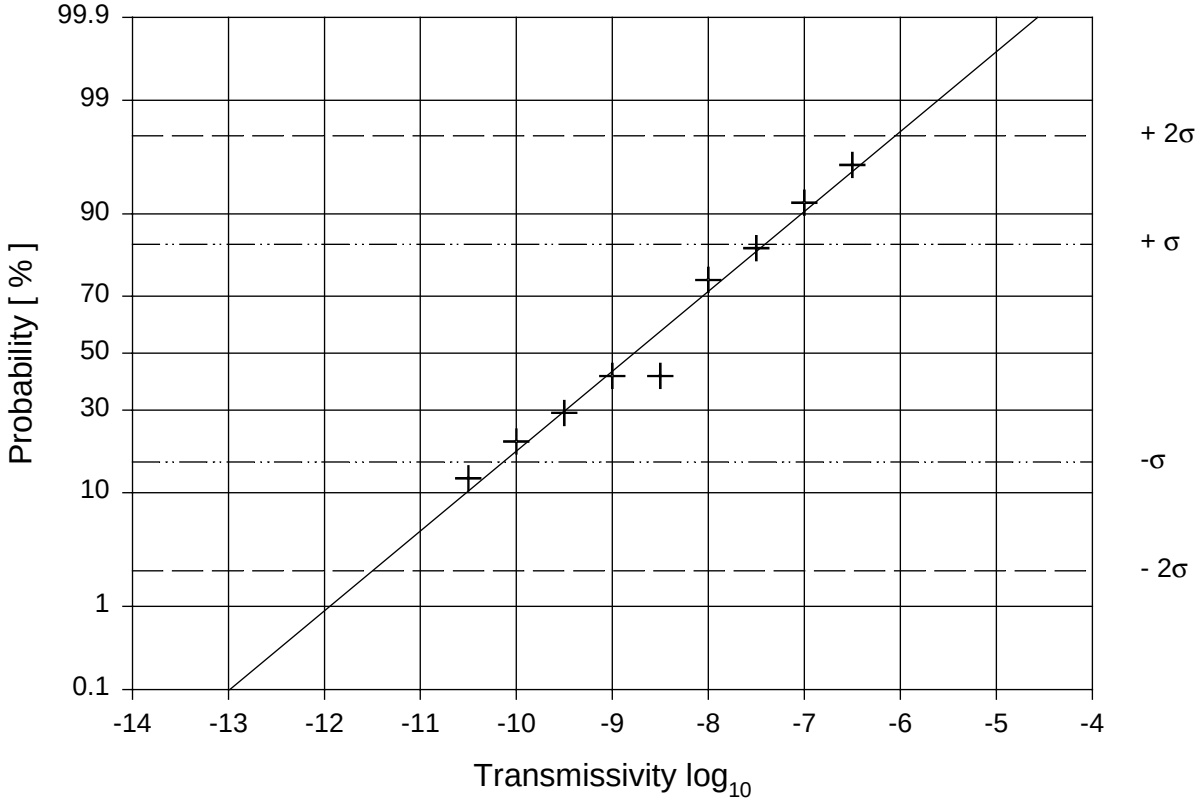

All 1m packers

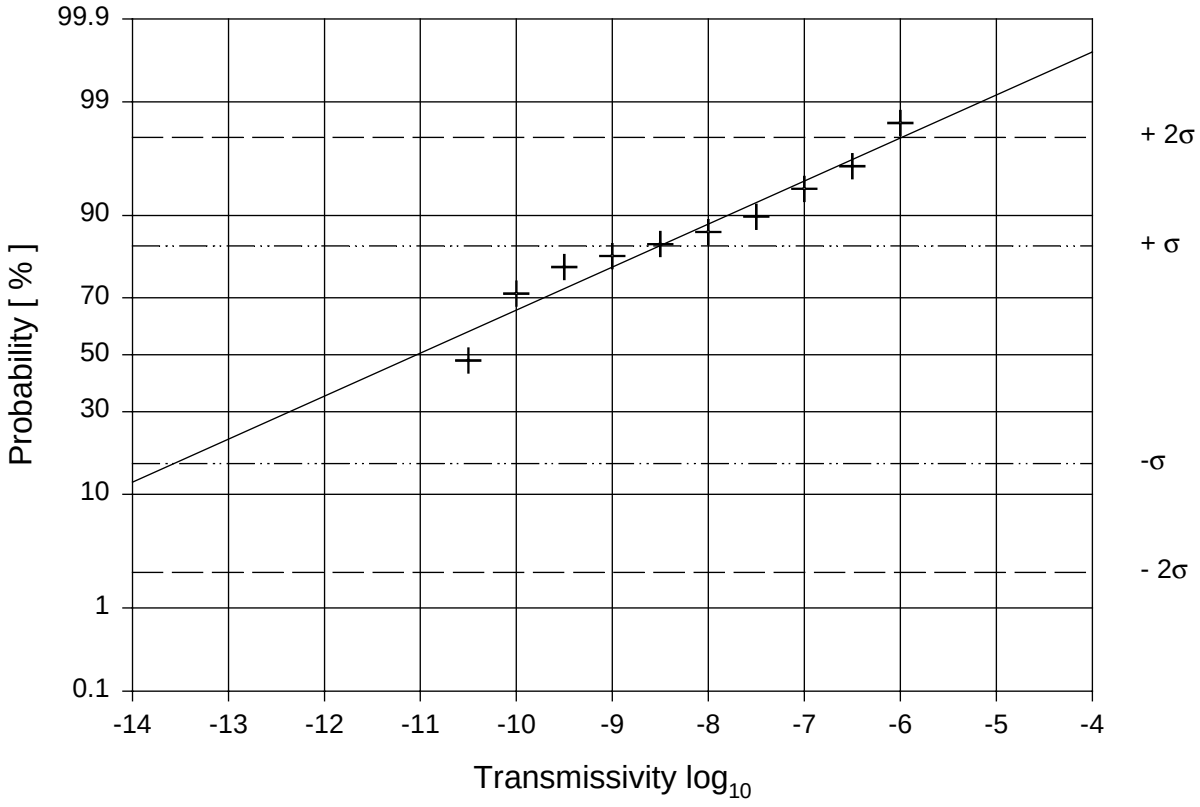

Subclass2 1m packers

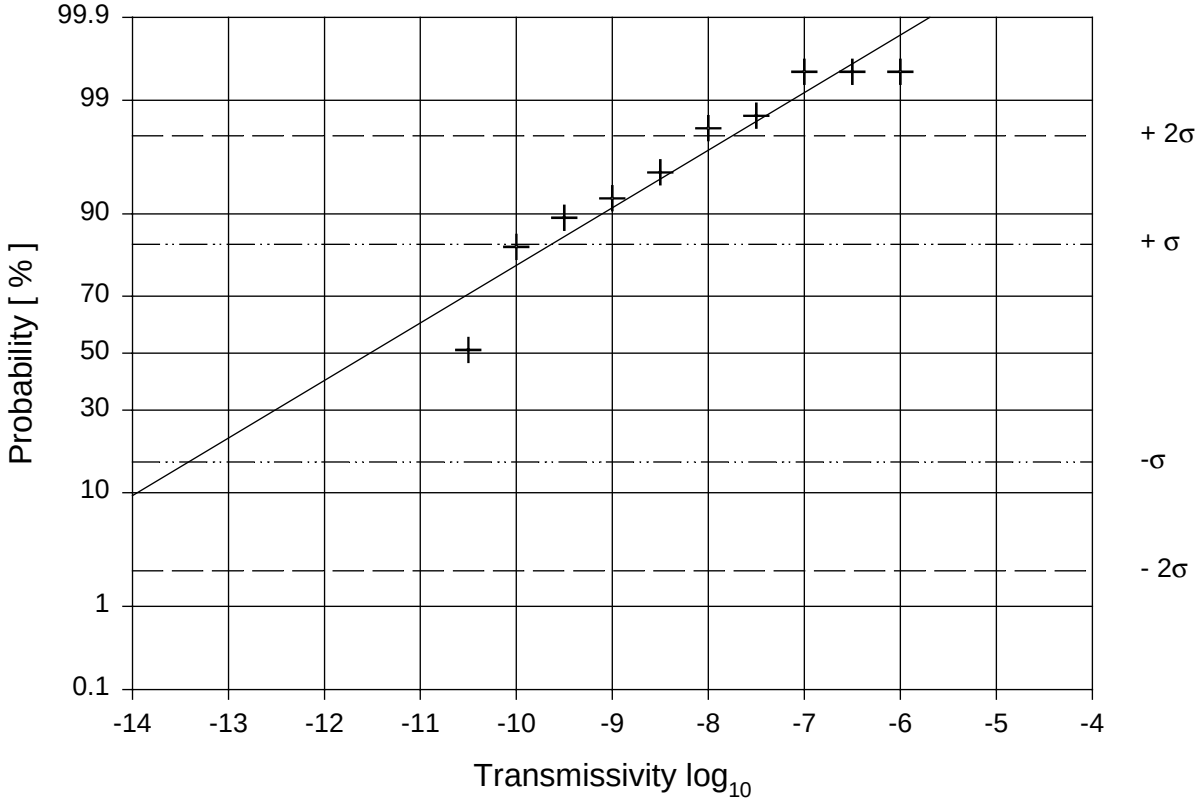

Subclass3 1m packers

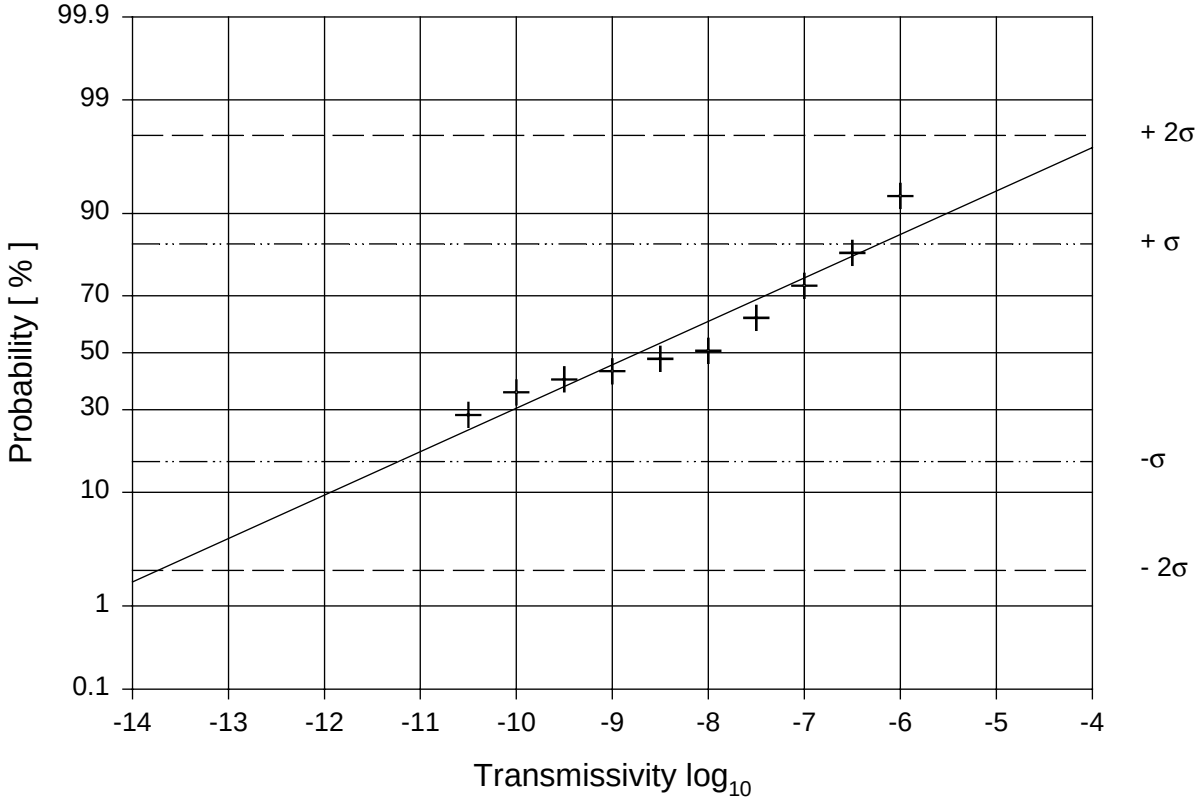

Subclass4 1m packers

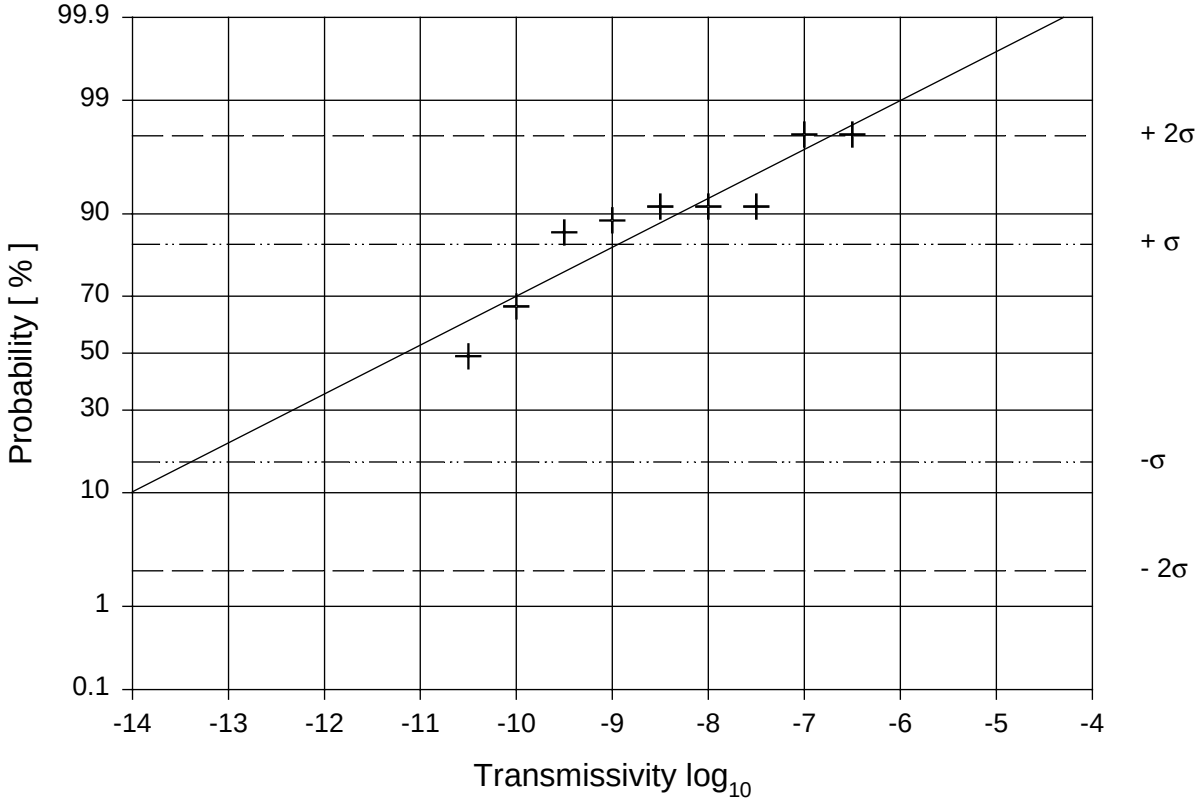

Subclass5 1m packers

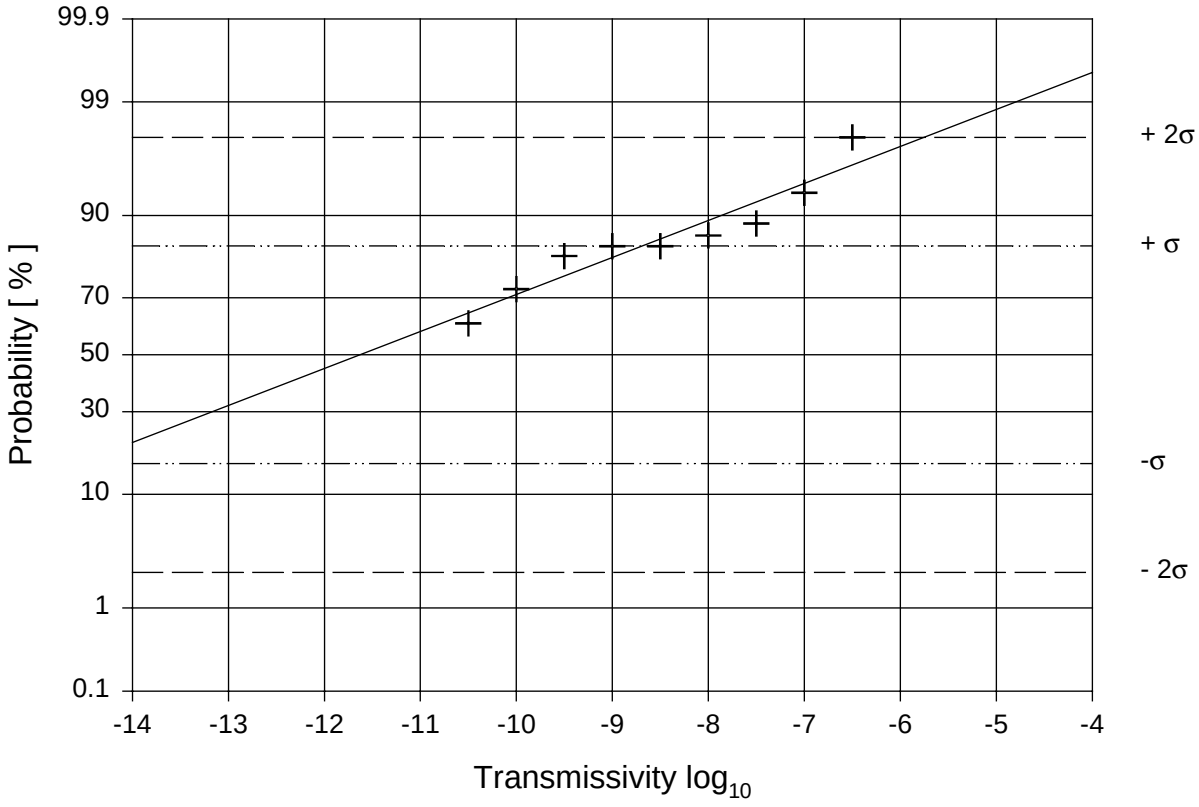

Appendix D

Statistics of fracture traces in deposition holes

Statistics from all 20 stochastic realisations for natural fractures, i.e. fractures with transmissivity larger than $5 \cdot 10^{-11}$ m^2/s and all fractures, tables D.1 to D.12.

Figures of the statistics from all fractures, figure D.1 to D.4.

Figures of modelled tracemaps for all fractures and all 6 deposition holes for 2 realisations, figure D.5 to D.16.

Figures of measured tracemaps for all 6 deposition holes, figure D.17-D.22.

Table D.1 Deposition hole #1, "natural fractures"

# of traces	P_{21} [m/m^2]	trace length [m]				Fracture transmissivity [m^2/s]			
		Average	Std dev	Min	Max	Average	Std dev	Min	Max
10	1.07	5.06	3.31	0.72	9.95	$8.00 \cdot 10^{-10}$	$1.37 \cdot 10^{-9}$	$5.73 \cdot 10^{-11}$	$4.52 \cdot 10^{-9}$
3	0.28	4.44	3.94	1.40	8.89	$7.77 \cdot 10^{-9}$	$1.07 \cdot 10^{-8}$	$3.00 \cdot 10^{-10}$	$2.00 \cdot 10^{-8}$
9	0.66	3.44	3.01	0.32	9.04	$2.73 \cdot 10^{-8}$	$6.70 \cdot 10^{-8}$	$1.99 \cdot 10^{-10}$	$2.05 \cdot 10^{-7}$
6	0.34	2.68	2.09	0.64	6.19	$2.53 \cdot 10^{-8}$	$6.10 \cdot 10^{-8}$	$7.79 \cdot 10^{-11}$	$1.50 \cdot 10^{-7}$
4	0.43	5.10	7.15	1.22	15.80	$7.80 \cdot 10^{-9}$	$1.34 \cdot 10^{-8}$	$1.17 \cdot 10^{-10}$	$2.78 \cdot 10^{-8}$
11	1.20	5.15	3.13	0.32	11.10	$3.53 \cdot 10^{-9}$	$1.04 \cdot 10^{-8}$	$7.18 \cdot 10^{-11}$	$3.49 \cdot 10^{-8}$
3	0.48	7.55	7.55	1.49	16.00	$9.31 \cdot 10^{-10}$	$1.25 \cdot 10^{-9}$	$1.16 \cdot 10^{-10}$	$2.37 \cdot 10^{-9}$
11	1.10	4.70	3.52	1.54	13.50	$1.06 \cdot 10^{-8}$	$3.29 \cdot 10^{-8}$	$5.36 \cdot 10^{-11}$	$1.10 \cdot 10^{-7}$
9	1.05	5.52	2.74	0.28	8.46	$8.20 \cdot 10^{-8}$	$2.38 \cdot 10^{-7}$	$2.46 \cdot 10^{-10}$	$7.16 \cdot 10^{-7}$
6	0.38	2.97	2.49	0.74	6.82	$7.19 \cdot 10^{-9}$	$6.89 \cdot 10^{-9}$	$1.64 \cdot 10^{-10}$	$1.57 \cdot 10^{-8}$
4	0.25	2.99	2.70	0.67	5.97	$6.14 \cdot 10^{-8}$	$1.21 \cdot 10^{-7}$	$7.65 \cdot 10^{-11}$	$2.42 \cdot 10^{-7}$
8	0.71	4.20	3.50	0.74	10.60	$5.30 \cdot 10^{-8}$	$1.38 \cdot 10^{-7}$	$5.87 \cdot 10^{-11}$	$3.93 \cdot 10^{-7}$
11	1.40	6.00	3.96	0.97	16.00	$8.35 \cdot 10^{-9}$	$1.46 \cdot 10^{-8}$	$5.09 \cdot 10^{-11}$	$4.63 \cdot 10^{-8}$
5	0.49	4.57	3.97	0.36	11.10	$3.78 \cdot 10^{-9}$	$6.04 \cdot 10^{-9}$	$2.46 \cdot 10^{-10}$	$1.43 \cdot 10^{-8}$
8	1.06	6.23	4.47	0.26	13.50	$1.05 \cdot 10^{-9}$	$1.21 \cdot 10^{-9}$	$1.13 \cdot 10^{-10}$	$3.13 \cdot 10^{-9}$
9	1.48	7.76	4.98	1.87	16.70	$1.21 \cdot 10^{-7}$	$3.37 \cdot 10^{-7}$	$1.02 \cdot 10^{-10}$	$1.02 \cdot 10^{-6}$
9	0.97	5.09	4.82	0.44	12.70	$1.14 \cdot 10^{-7}$	$3.03 \cdot 10^{-7}$	$7.71 \cdot 10^{-11}$	$9.16 \cdot 10^{-7}$
10	0.92	4.35	3.45	0.62	11.60	$1.59 \cdot 10^{-8}$	$4.02 \cdot 10^{-8}$	$1.18 \cdot 10^{-10}$	$1.29 \cdot 10^{-7}$
8	1.11	6.51	4.65	0.09	16.00	$7.10 \cdot 10^{-9}$	$1.33 \cdot 10^{-8}$	$9.79 \cdot 10^{-11}$	$3.81 \cdot 10^{-8}$
6	0.50	3.93	4.25	0.96	12.40	$1.08 \cdot 10^{-7}$	$1.71 \cdot 10^{-7}$	$5.26 \cdot 10^{-11}$	$3.90 \cdot 10^{-7}$

Table D.2 Deposition hole #2, "natural fractures"

# of traces	P_{21} [m/m^2]	trace length [m]				Fracture transmissivity [m^2/s]			
		Average	Std dev	Min	Max	Average	Std dev	Min	Max
11	1.32	5.64	5.16	0.00	16.90	$1.41 \cdot 10^{-8}$	$3.41 \cdot 10^{-8}$	$5.73 \cdot 10^{-11}$	$1.11 \cdot 10^{-7}$
9	0.66	3.47	2.98	0.47	9.48	$1.44 \cdot 10^{-8}$	$4.06 \cdot 10^{-8}$	$5.23 \cdot 10^{-11}$	$1.23 \cdot 10^{-7}$
3	0.33	5.22	6.75	0.48	12.90	$2.27 \cdot 10^{-9}$	$3.12 \cdot 10^{-9}$	$3.38 \cdot 10^{-10}$	$5.87 \cdot 10^{-9}$
7	1.17	7.88	2.98	5.96	14.10	$3.51 \cdot 10^{-9}$	$6.39 \cdot 10^{-9}$	$7.79 \cdot 10^{-11}$	$1.71 \cdot 10^{-8}$
8	1.27	7.47	5.89	1.35	16.20	$3.61 \cdot 10^{-8}$	$5.00 \cdot 10^{-8}$	$1.36 \cdot 10^{-10}$	$1.36 \cdot 10^{-7}$
10	1.07	5.02	2.67	1.23	8.82	$7.60 \cdot 10^{-10}$	$7.35 \cdot 10^{-10}$	$9.95 \cdot 10^{-11}$	$2.05 \cdot 10^{-9}$
5	0.47	4.38	6.60	0.18	16.10	$6.44 \cdot 10^{-10}$	$9.69 \cdot 10^{-10}$	$1.57 \cdot 10^{-10}$	$2.37 \cdot 10^{-9}$
7	0.66	4.47	4.97	0.60	15.20	$4.19 \cdot 10^{-8}$	$5.92 \cdot 10^{-8}$	$6.89 \cdot 10^{-11}$	$1.50 \cdot 10^{-7}$
8	0.42	2.48	1.51	0.52	4.41	$9.64 \cdot 10^{-9}$	$2.62 \cdot 10^{-8}$	$5.69 \cdot 10^{-11}$	$7.46 \cdot 10^{-8}$
6	0.62	4.85	4.01	0.46	11.40	$3.92 \cdot 10^{-9}$	$4.88 \cdot 10^{-9}$	$7.60 \cdot 10^{-11}$	$1.23 \cdot 10^{-8}$
8	1.02	6.00	4.58	1.87	16.10	$2.05 \cdot 10^{-7}$	$5.75 \cdot 10^{-7}$	$1.00 \cdot 10^{-10}$	$1.63 \cdot 10^{-6}$
7	0.73	4.91	4.12	0.83	10.30	$5.39 \cdot 10^{-7}$	$1.42 \cdot 10^{-6}$	$1.45 \cdot 10^{-10}$	$3.75 \cdot 10^{-6}$
8	0.99	5.85	3.23	0.94	10.70	$8.37 \cdot 10^{-9}$	$1.60 \cdot 10^{-8}$	$5.09 \cdot 10^{-11}$	$4.63 \cdot 10^{-8}$
12	1.45	5.70	4.12	0.91	16.10	$1.02 \cdot 10^{-8}$	$2.47 \cdot 10^{-8}$	$8.34 \cdot 10^{-11}$	$8.42 \cdot 10^{-8}$
6	0.40	3.11	1.88	0.48	5.61	$4.33 \cdot 10^{-9}$	$3.04 \cdot 10^{-9}$	$1.25 \cdot 10^{-9}$	$9.94 \cdot 10^{-9}$
6	0.61	4.76	2.55	2.58	9.16	$2.81 \cdot 10^{-8}$	$6.56 \cdot 10^{-8}$	$7.65 \cdot 10^{-11}$	$1.62 \cdot 10^{-7}$
8	1.33	7.82	5.21	0.00	14.60	$1.47 \cdot 10^{-7}$	$3.05 \cdot 10^{-7}$	$1.35 \cdot 10^{-10}$	$8.51 \cdot 10^{-7}$
10	1.47	6.92	4.27	1.46	15.20	$7.50 \cdot 10^{-10}$	$1.20 \cdot 10^{-9}$	$5.96 \cdot 10^{-11}$	$3.86 \cdot 10^{-9}$
9	0.72	3.78	2.43	0.79	8.01	$4.32 \cdot 10^{-8}$	$1.07 \cdot 10^{-7}$	$9.73 \cdot 10^{-11}$	$3.24 \cdot 10^{-7}$
6	0.81	6.37	3.66	2.06	11.30	$4.85 \cdot 10^{-8}$	$1.13 \cdot 10^{-7}$	$1.96 \cdot 10^{-10}$	$2.80 \cdot 10^{-7}$

Table D.3 Deposition hole #3, "natural fractures"

# of traces	P_{21} [m/m^2]	trace length [m]				Fracture transmissivity [m^2/s]			
		Average	Std dev	Min	Max	Average	Std dev	Min	Max
10	0.60	2.84	2.00	0.34	6.04	$1.57 \cdot 10^{-7}$	$4.38 \cdot 10^{-7}$	$9.74 \cdot 10^{-11}$	$1.40 \cdot 10^{-6}$
11	1.76	7.55	5.71	0.84	16.40	$2.92 \cdot 10^{-8}$	$6.34 \cdot 10^{-8}$	$5.23 \cdot 10^{-11}$	$1.86 \cdot 10^{-7}$
5	0.51	4.84	5.99	0.83	15.30	$5.71 \cdot 10^{-9}$	$7.48 \cdot 10^{-9}$	$1.39 \cdot 10^{-10}$	$1.46 \cdot 10^{-8}$
8	1.09	6.41	2.14	3.01	10.40	$4.65 \cdot 10^{-9}$	$1.04 \cdot 10^{-8}$	$6.88 \cdot 10^{-11}$	$2.98 \cdot 10^{-8}$
6	0.89	6.94	7.03	0.95	16.00	$1.71 \cdot 10^{-8}$	$3.41 \cdot 10^{-8}$	$9.51 \cdot 10^{-11}$	$8.64 \cdot 10^{-8}$
12	1.09	4.26	2.99	0.24	9.66	$3.92 \cdot 10^{-9}$	$9.27 \cdot 10^{-9}$	$1.56 \cdot 10^{-10}$	$3.27 \cdot 10^{-8}$
7	1.02	6.86	1.14	5.75	8.68	$1.41 \cdot 10^{-9}$	$2.35 \cdot 10^{-9}$	$1.47 \cdot 10^{-10}$	$6.57 \cdot 10^{-9}$
9	0.63	3.30	2.13	0.63	6.63	$1.36 \cdot 10^{-8}$	$3.04 \cdot 10^{-8}$	$5.39 \cdot 10^{-11}$	$9.02 \cdot 10^{-8}$
11	0.94	4.04	3.22	0.95	10.20	$5.97 \cdot 10^{-7}$	$1.98 \cdot 10^{-6}$	$5.54 \cdot 10^{-11}$	$6.56 \cdot 10^{-6}$
10	1.05	4.94	5.02	0.41	15.20	$6.03 \cdot 10^{-9}$	$9.06 \cdot 10^{-9}$	$5.92 \cdot 10^{-11}$	$2.89 \cdot 10^{-8}$
6	0.63	4.90	3.17	1.09	8.42	$4.79 \cdot 10^{-8}$	$1.14 \cdot 10^{-7}$	$5.24 \cdot 10^{-11}$	$2.81 \cdot 10^{-7}$
5	0.56	5.29	3.92	1.91	10.60	$5.96 \cdot 10^{-9}$	$1.29 \cdot 10^{-8}$	$1.42 \cdot 10^{-10}$	$2.90 \cdot 10^{-8}$
14	1.31	4.42	2.54	0.62	8.04	$5.32 \cdot 10^{-8}$	$1.95 \cdot 10^{-7}$	$6.57 \cdot 10^{-11}$	$7.32 \cdot 10^{-7}$
10	1.27	5.99	4.82	0.55	16.00	$1.55 \cdot 10^{-8}$	$3.15 \cdot 10^{-8}$	$8.10 \cdot 10^{-11}$	$8.42 \cdot 10^{-8}$
10	1.25	5.89	5.42	0.09	16.40	$8.07 \cdot 10^{-9}$	$1.71 \cdot 10^{-8}$	$5.79 \cdot 10^{-11}$	$5.58 \cdot 10^{-8}$
8	1.31	7.72	4.76	0.60	13.20	$1.49 \cdot 10^{-8}$	$3.15 \cdot 10^{-8}$	$7.69 \cdot 10^{-11}$	$8.98 \cdot 10^{-8}$
13	1.64	5.96	5.35	0.12	16.10	$8.00 \cdot 10^{-8}$	$2.37 \cdot 10^{-7}$	$5.15 \cdot 10^{-11}$	$8.51 \cdot 10^{-7}$
11	1.35	5.77	3.50	0.94	11.20	$5.06 \cdot 10^{-8}$	$1.32 \cdot 10^{-7}$	$5.96 \cdot 10^{-11}$	$4.35 \cdot 10^{-7}$
13	1.73	6.28	4.63	1.10	16.20	$1.14 \cdot 10^{-8}$	$2.40 \cdot 10^{-8}$	$9.59 \cdot 10^{-11}$	$8.96 \cdot 10^{-8}$
7	0.94	6.35	5.03	0.97	13.50	$1.08 \cdot 10^{-7}$	$2.82 \cdot 10^{-7}$	$5.10 \cdot 10^{-11}$	$7.47 \cdot 10^{-7}$

Table D.4 Deposition hole #4, "natural fractures"

# of traces	P_{21} [m/m^2]	trace length [m]				Fracture transmissivity [m^2/s]			
		Average	Std dev	Min	Max	Average	Std dev	Min	Max
8	0.81	4.79	3.49	0.08	9.09	$1.19 \cdot 10^{-9}$	$1.05 \cdot 10^{-9}$	$7.81 \cdot 10^{-11}$	$2.90 \cdot 10^{-9}$
11	0.99	4.26	2.20	0.93	7.76	$1.38 \cdot 10^{-8}$	$3.65 \cdot 10^{-8}$	$5.59 \cdot 10^{-11}$	$1.23 \cdot 10^{-7}$
7	0.70	4.71	2.22	0.81	7.61	$1.87 \cdot 10^{-8}$	$3.11 \cdot 10^{-8}$	$1.39 \cdot 10^{-10}$	$8.30 \cdot 10^{-8}$
11	0.74	3.17	2.27	0.24	8.00	$3.84 \cdot 10^{-9}$	$5.30 \cdot 10^{-9}$	$5.12 \cdot 10^{-11}$	$1.42 \cdot 10^{-8}$
11	1.13	4.85	3.77	0.09	12.70	$4.31 \cdot 10^{-8}$	$1.01 \cdot 10^{-7}$	$8.60 \cdot 10^{-11}$	$3.39 \cdot 10^{-7}$
12	1.22	4.79	3.96	0.83	14.10	$1.15 \cdot 10^{-8}$	$2.13 \cdot 10^{-8}$	$1.56 \cdot 10^{-10}$	$6.59 \cdot 10^{-8}$
9	0.91	4.77	3.44	0.56	9.90	$2.89 \cdot 10^{-7}$	$8.64 \cdot 10^{-7}$	$7.21 \cdot 10^{-11}$	$2.59 \cdot 10^{-6}$
11	0.87	3.74	2.31	1.11	8.14	$2.03 \cdot 10^{-8}$	$4.43 \cdot 10^{-8}$	$5.39 \cdot 10^{-11}$	$1.27 \cdot 10^{-7}$
10	1.66	7.81	5.59	0.94	16.00	$6.57 \cdot 10^{-7}$	$2.07 \cdot 10^{-6}$	$5.09 \cdot 10^{-11}$	$6.56 \cdot 10^{-6}$
5	0.79	7.42	3.81	2.14	11.20	$1.94 \cdot 10^{-9}$	$2.50 \cdot 10^{-9}$	$1.20 \cdot 10^{-10}$	$6.20 \cdot 10^{-9}$
15	1.21	3.80	2.29	0.80	7.79	$7.66 \cdot 10^{-9}$	$1.56 \cdot 10^{-8}$	$5.87 \cdot 10^{-11}$	$6.00 \cdot 10^{-8}$
6	0.60	4.74	3.39	0.99	9.28	$2.75 \cdot 10^{-8}$	$6.39 \cdot 10^{-8}$	$7.06 \cdot 10^{-11}$	$1.58 \cdot 10^{-7}$
7	0.89	5.95	1.41	3.25	8.06	$3.60 \cdot 10^{-10}$	$4.39 \cdot 10^{-10}$	$6.15 \cdot 10^{-11}$	$1.34 \cdot 10^{-9}$
7	0.52	3.47	2.39	0.48	6.56	$1.58 \cdot 10^{-8}$	$3.09 \cdot 10^{-8}$	$8.10 \cdot 10^{-11}$	$8.42 \cdot 10^{-8}$
6	0.59	4.64	3.46	0.61	10.10	$9.74 \cdot 10^{-9}$	$1.41 \cdot 10^{-8}$	$3.14 \cdot 10^{-10}$	$3.75 \cdot 10^{-8}$
6	0.82	6.47	5.46	1.33	14.00	$7.22 \cdot 10^{-8}$	$1.04 \cdot 10^{-7}$	$1.34 \cdot 10^{-10}$	$2.38 \cdot 10^{-7}$
9	1.02	5.33	4.94	0.78	15.90	$6.78 \cdot 10^{-9}$	$1.16 \cdot 10^{-8}$	$5.15 \cdot 10^{-11}$	$3.55 \cdot 10^{-8}$
4	0.22	2.58	1.76	0.37	4.66	$5.15 \cdot 10^{-9}$	$1.01 \cdot 10^{-8}$	$8.76 \cdot 10^{-11}$	$2.02 \cdot 10^{-8}$
12	0.95	3.73	2.98	0.97	10.10	$9.51 \cdot 10^{-10}$	$1.06 \cdot 10^{-9}$	$5.00 \cdot 10^{-11}$	$3.14 \cdot 10^{-9}$
11	1.12	4.79	4.04	0.81	15.00	$4.03 \cdot 10^{-7}$	$1.26 \cdot 10^{-6}$	$8.04 \cdot 10^{-11}$	$4.21 \cdot 10^{-6}$

Table D.5 Deposition hole #5, "natural fractures"

# of traces	P_{21} [m/m^2]	trace length [m]				Fracture transmissivity [m^2/s]			
		Average	Std dev	Min	Max	Average	Std dev	Min	Max
9	0.90	4.69	3.42	0.47	11.10	$1.59\cdot10^{-8}$	$3.50\cdot10^{-8}$	$5.11\cdot10^{-11}$	$1.03\cdot10^{-7}$
8	1.39	8.16	3.22	4.02	14.00	$6.33\cdot10^{-7}$	$1.78\cdot10^{-6}$	$7.70\cdot10^{-11}$	$5.03\cdot10^{-6}$
8	0.41	2.42	2.23	0.19	6.49	$5.80\cdot10^{-9}$	$1.23\cdot10^{-8}$	$5.25\cdot10^{-11}$	$3.54\cdot10^{-8}$
12	1.64	6.43	4.80	0.91	15.50	$6.41\cdot10^{-9}$	$1.10\cdot10^{-8}$	$8.38\cdot10^{-11}$	$3.71\cdot10^{-8}$
8	1.22	7.16	2.28	3.10	10.60	$5.10\cdot10^{-8}$	$1.24\cdot10^{-7}$	$5.57\cdot10^{-11}$	$3.57\cdot10^{-7}$
3	0.27	4.30	3.38	0.45	6.72	$1.24\cdot10^{-9}$	$1.67\cdot10^{-9}$	$1.90\cdot10^{-10}$	$3.16\cdot10^{-9}$
8	0.89	5.22	2.77	1.96	10.70	$8.89\cdot10^{-9}$	$2.14\cdot10^{-8}$	$7.24\cdot10^{-11}$	$6.18\cdot10^{-8}$
4	0.37	4.36	3.27	1.55	9.04	$1.90\cdot10^{-7}$	$3.76\cdot10^{-7}$	$1.11\cdot10^{-10}$	$7.54\cdot10^{-7}$
9	0.83	4.32	2.31	0.87	8.39	$2.54\cdot10^{-8}$	$3.76\cdot10^{-8}$	$8.68\cdot10^{-11}$	$8.95\cdot10^{-8}$
10	0.67	3.18	2.26	0.96	7.40	$1.39\cdot10^{-8}$	$2.50\cdot10^{-8}$	$1.07\cdot10^{-10}$	$7.91\cdot10^{-8}$
10	0.63	2.99	1.97	0.59	5.95	$4.13\cdot10^{-9}$	$8.65\cdot10^{-9}$	$5.87\cdot10^{-11}$	$2.54\cdot10^{-8}$
10	0.96	4.52	2.65	1.87	10.80	$4.78\cdot10^{-8}$	$8.11\cdot10^{-8}$	$6.96\cdot10^{-11}$	$2.32\cdot10^{-7}$
11	1.58	6.75	3.17	2.61	11.80	$1.42\cdot10^{-7}$	$3.16\cdot10^{-7}$	$1.46\cdot10^{-10}$	$8.76\cdot10^{-7}$
9	1.22	6.39	4.51	0.23	16.30	$1.12\cdot10^{-9}$	$1.04\cdot10^{-9}$	$9.18\cdot10^{-11}$	$2.97\cdot10^{-9}$
13	1.23	4.44	2.38	0.77	8.02	$1.01\cdot10^{-7}$	$3.48\cdot10^{-7}$	$5.61\cdot10^{-11}$	$1.26\cdot10^{-6}$
13	1.74	6.32	3.20	0.86	12.00	$1.30\cdot10^{-8}$	$4.24\cdot10^{-8}$	$7.46\cdot10^{-11}$	$1.54\cdot10^{-7}$
5	0.52	4.87	4.07	0.75	10.70	$2.50\cdot10^{-8}$	$4.47\cdot10^{-8}$	$1.34\cdot10^{-10}$	$1.04\cdot10^{-7}$
6	0.40	3.15	1.89	0.62	6.19	$7.56\cdot10^{-10}$	$6.44\cdot10^{-10}$	$1.17\cdot10^{-10}$	$1.78\cdot10^{-9}$
9	0.61	3.18	3.20	0.07	9.29	$4.00\cdot10^{-8}$	$1.12\cdot10^{-7}$	$1.50\cdot10^{-10}$	$3.37\cdot10^{-7}$
12	1.03	4.05	2.72	0.68	8.36	$1.05\cdot10^{-8}$	$2.27\cdot10^{-8}$	$8.04\cdot10^{-11}$	$6.75\cdot10^{-8}$

Table D.6 Deposition hole #6, "natural fractures"

# of traces	P_{21} [m/m^2]	trace length [m]				Fracture transmissivity [m^2/s]			
		Average	Std dev	Min	Max	Average	Std dev	Min	Max
12	1.23	4.81	4.00	0.22	14.20	$3.84\cdot10^{-9}$	$4.42\cdot10^{-9}$	$5.11\cdot10^{-11}$	$1.18\cdot10^{-8}$
10	1.36	6.40	5.82	0.46	16.10	$1.82\cdot10^{-8}$	$5.47\cdot10^{-8}$	$1.34\cdot10^{-10}$	$1.74\cdot10^{-7}$
11	1.00	4.28	2.10	0.44	6.39	$3.37\cdot10^{-9}$	$4.90\cdot10^{-9}$	$5.25\cdot10^{-11}$	$1.41\cdot10^{-8}$
9	1.18	6.20	4.51	0.03	15.60	$8.88\cdot10^{-10}$	$1.67\cdot10^{-9}$	$8.38\cdot10^{-11}$	$5.06\cdot10^{-9}$
10	0.95	4.49	2.10	0.10	6.76	$4.83\cdot10^{-8}$	$1.11\cdot10^{-7}$	$1.26\cdot10^{-10}$	$3.57\cdot10^{-7}$
7	1.31	8.82	4.46	4.71	15.60	$7.69\cdot10^{-8}$	$1.96\cdot10^{-7}$	$1.13\cdot10^{-10}$	$5.20\cdot10^{-7}$
8	0.72	4.23	4.64	0.22	11.80	$1.36\cdot10^{-8}$	$3.66\cdot10^{-8}$	$5.56\cdot10^{-11}$	$1.04\cdot10^{-7}$
10	0.71	3.34	4.18	0.24	12.90	$1.03\cdot10^{-7}$	$2.38\cdot10^{-7}$	$6.67\cdot10^{-11}$	$7.54\cdot10^{-7}$
12	1.36	5.35	4.55	0.29	16.20	$1.86\cdot10^{-8}$	$4.17\cdot10^{-8}$	$1.08\cdot10^{-10}$	$1.47\cdot10^{-7}$
6	0.59	4.59	3.34	1.35	9.88	$5.89\cdot10^{-9}$	$7.17\cdot10^{-9}$	$5.08\cdot10^{-11}$	$1.50\cdot10^{-8}$
5	0.41	3.85	1.73	2.02	5.95	$3.57\cdot10^{-9}$	$7.44\cdot10^{-9}$	$5.87\cdot10^{-11}$	$1.69\cdot10^{-8}$
9	1.03	5.39	3.72	0.76	10.60	$1.52\cdot10^{-9}$	$2.88\cdot10^{-9}$	$6.02\cdot10^{-11}$	$8.74\cdot10^{-9}$
10	1.01	4.76	4.38	0.35	16.10	$7.31\cdot10^{-8}$	$2.12\cdot10^{-7}$	$1.46\cdot10^{-10}$	$6.75\cdot10^{-7}$
4	0.46	5.38	1.60	3.00	6.50	$9.11\cdot10^{-10}$	$8.62\cdot10^{-10}$	$2.52\cdot10^{-10}$	$2.16\cdot10^{-9}$
7	1.01	6.83	3.90	0.72	11.80	$3.03\cdot10^{-9}$	$3.85\cdot10^{-9}$	$6.04\cdot10^{-11}$	$1.10\cdot10^{-8}$
8	0.91	5.38	3.59	0.41	11.90	$3.25\cdot10^{-8}$	$5.72\cdot10^{-8}$	$7.46\cdot10^{-11}$	$1.54\cdot10^{-7}$
5	0.51	4.77	3.22	1.81	9.23	$1.55\cdot10^{-8}$	$3.06\cdot10^{-8}$	$1.63\cdot10^{-10}$	$7.02\cdot10^{-8}$
11	0.53	2.25	1.97	0.18	5.43	$8.43\cdot10^{-8}$	$2.36\cdot10^{-7}$	$5.14\cdot10^{-11}$	$7.92\cdot10^{-7}$
11	0.96	4.11	2.91	0.00	8.00	$9.12\cdot10^{-9}$	$1.01\cdot10^{-8}$	$1.11\cdot10^{-10}$	$3.23\cdot10^{-8}$
7	0.70	4.71	2.76	1.57	8.61	$9.43\cdot10^{-10}$	$7.63\cdot10^{-10}$	$9.59\cdot10^{-11}$	$1.90\cdot10^{-9}$

Table D.7 Deposition hole #1, "all fractures"

# of traces	P_{21} [m/m^2]	trace length [m]				Fracture transmissivity [m^2/s]			
		Average	Std dev	Min	Max	Average	Std dev	Min	Max
28	2.93	4.93	3.05	0.02	10.00	$2.88 \cdot 10^{-10}$	$8.81 \cdot 10^{-10}$	$9.52 \cdot 10^{-16}$	$4.52 \cdot 10^{-9}$
15	1.62	5.09	2.94	1.40	12.10	$1.56 \cdot 10^{-9}$	$5.16 \cdot 10^{-9}$	$1.27 \cdot 10^{-16}$	$2.00 \cdot 10^{-8}$
31	2.37	3.59	2.58	0.29	9.29	$7.92 \cdot 10^{-9}$	$3.68 \cdot 10^{-8}$	$1.37 \cdot 10^{-14}$	$2.05 \cdot 10^{-7}$
29	2.37	3.85	2.32	0.28	7.27	$5.24 \cdot 10^{-9}$	$2.78 \cdot 10^{-8}$	$2.60 \cdot 10^{-15}$	$1.50 \cdot 10^{-7}$
29	3.00	4.87	3.58	0.21	15.80	$1.08 \cdot 10^{-9}$	$5.16 \cdot 10^{-9}$	$3.69 \cdot 10^{-15}$	$2.78 \cdot 10^{-8}$
31	3.00	4.55	3.56	0.12	15.90	$1.25 \cdot 10^{-9}$	$6.25 \cdot 10^{-9}$	$5.86 \cdot 10^{-17}$	$3.49 \cdot 10^{-8}$
27	2.88	5.02	4.23	0.14	16.00	$1.10 \cdot 10^{-10}$	$4.57 \cdot 10^{-10}$	$1.31 \cdot 10^{-14}$	$2.37 \cdot 10^{-9}$
22	2.37	5.08	3.87	1.54	16.00	$5.29 \cdot 10^{-9}$	$2.33 \cdot 10^{-8}$	$1.34 \cdot 10^{-15}$	$1.10 \cdot 10^{-7}$
32	3.65	5.37	3.27	0.28	15.90	$2.31 \cdot 10^{-8}$	$1.26 \cdot 10^{-7}$	$8.53 \cdot 10^{-15}$	$7.16 \cdot 10^{-7}$
24	2.05	4.02	2.45	0.74	9.43	$1.81 \cdot 10^{-9}$	$4.52 \cdot 10^{-9}$	$3.42 \cdot 10^{-16}$	$1.57 \cdot 10^{-8}$
21	1.73	3.89	2.54	0.07	9.28	$7.85 \cdot 10^{-9}$	$3.44 \cdot 10^{-8}$	$1.65 \cdot 10^{-16}$	$1.58 \cdot 10^{-7}$
29	2.41	3.91	2.65	0.52	11.70	$3.97 \cdot 10^{-9}$	$1.17 \cdot 10^{-8}$	$1.48 \cdot 10^{-16}$	$6.00 \cdot 10^{-8}$
23	2.23	4.57	3.52	0.31	16.00	$4.00 \cdot 10^{-9}$	$1.08 \cdot 10^{-8}$	$1.33 \cdot 10^{-17}$	$4.63 \cdot 10^{-8}$
27	2.17	3.78	3.10	0.36	11.10	$7.06 \cdot 10^{-10}$	$2.80 \cdot 10^{-9}$	$5.01 \cdot 10^{-16}$	$1.43 \cdot 10^{-8}$
34	3.82	5.29	3.44	0.26	14.00	$2.52 \cdot 10^{-10}$	$7.17 \cdot 10^{-10}$	$1.53 \cdot 10^{-16}$	$3.13 \cdot 10^{-9}$
30	3.52	5.52	4.37	0.10	16.70	$3.62 \cdot 10^{-8}$	$1.86 \cdot 10^{-7}$	$8.64 \cdot 10^{-16}$	$1.02 \cdot 10^{-6}$
28	2.54	4.27	3.30	0.39	12.70	$3.65 \cdot 10^{-8}$	$1.73 \cdot 10^{-7}$	$1.39 \cdot 10^{-16}$	$9.16 \cdot 10^{-7}$
26	2.30	4.17	2.57	0.62	11.60	$6.11 \cdot 10^{-9}$	$2.54 \cdot 10^{-8}$	$7.29 \cdot 10^{-17}$	$1.29 \cdot 10^{-7}$
32	3.25	4.78	3.28	0.09	16.00	$1.78 \cdot 10^{-9}$	$7.05 \cdot 10^{-9}$	$4.80 \cdot 10^{-15}$	$3.81 \cdot 10^{-8}$
13	1.34	4.87	3.35	0.96	12.40	$4.98 \cdot 10^{-8}$	$1.24 \cdot 10^{-7}$	$6.40 \cdot 10^{-14}$	$3.90 \cdot 10^{-7}$

Table D.8 Deposition hole #2, "all fractures"

# of traces	P_{21} [m/m^2]	trace length [m]				Fracture transmissivity [m^2/s]			
		Average	Std dev	Min	Max	Average	Std dev	Min	Max
24	2.78	5.46	3.95	0.00	16.90	$6.45 \cdot 10^{-9}$	$2.36 \cdot 10^{-8}$	$2.22 \cdot 10^{-15}$	$1.11 \cdot 10^{-7}$
26	1.90	3.44	2.49	0.38	9.48	$5.00 \cdot 10^{-9}$	$2.40 \cdot 10^{-8}$	$7.17 \cdot 10^{-17}$	$1.23 \cdot 10^{-7}$
21	1.99	4.45	3.49	0.22	12.90	$3.29 \cdot 10^{-10}$	$1.28 \cdot 10^{-9}$	$1.21 \cdot 10^{-16}$	$5.87 \cdot 10^{-9}$
28	3.67	6.18	4.08	0.30	16.00	$8.78 \cdot 10^{-10}$	$3.39 \cdot 10^{-9}$	$2.34 \cdot 10^{-19}$	$1.71 \cdot 10^{-8}$
41	4.36	5.01	3.64	0.13	16.20	$7.04 \cdot 10^{-9}$	$2.54 \cdot 10^{-8}$	$1.38 \cdot 10^{-17}$	$1.36 \cdot 10^{-7}$
35	3.04	4.10	3.26	0.15	16.40	$2.22 \cdot 10^{-10}$	$5.12 \cdot 10^{-10}$	$5.86 \cdot 10^{-17}$	$2.05 \cdot 10^{-9}$
23	2.63	5.39	4.35	0.18	16.30	$1.46 \cdot 10^{-10}$	$4.93 \cdot 10^{-10}$	$1.31 \cdot 10^{-14}$	$2.37 \cdot 10^{-9}$
18	2.24	5.86	4.39	0.60	15.20	$1.63 \cdot 10^{-8}$	$4.10 \cdot 10^{-8}$	$1.34 \cdot 10^{-15}$	$1.50 \cdot 10^{-7}$
25	2.69	5.07	3.70	0.52	14.10	$3.09 \cdot 10^{-9}$	$1.49 \cdot 10^{-8}$	$8.58 \cdot 10^{-15}$	$7.46 \cdot 10^{-8}$
22	2.78	5.95	4.38	0.16	16.20	$1.07 \cdot 10^{-9}$	$2.98 \cdot 10^{-9}$	$3.42 \cdot 10^{-16}$	$1.23 \cdot 10^{-8}$
30	3.26	5.12	3.30	0.48	15.10	$1.59 \cdot 10^{-8}$	$5.07 \cdot 10^{-8}$	$5.49 \cdot 10^{-16}$	$2.32 \cdot 10^{-7}$
26	1.95	3.53	2.48	0.22	9.17	$1.59 \cdot 10^{-9}$	$5.58 \cdot 10^{-9}$	$6.74 \cdot 10^{-17}$	$2.54 \cdot 10^{-8}$
22	2.50	5.34	2.84	0.84	10.70	$3.04 \cdot 10^{-9}$	$1.01 \cdot 10^{-8}$	$5.83 \cdot 10^{-15}$	$4.63 \cdot 10^{-8}$
28	2.81	4.73	3.36	0.59	16.10	$4.40 \cdot 10^{-9}$	$1.66 \cdot 10^{-8}$	$2.28 \cdot 10^{-18}$	$8.42 \cdot 10^{-8}$
17	1.64	4.55	2.26	0.48	8.88	$1.53 \cdot 10^{-9}$	$2.72 \cdot 10^{-9}$	$1.18 \cdot 10^{-16}$	$9.94 \cdot 10^{-9}$
32	2.83	4.16	2.62	0.05	9.16	$5.28 \cdot 10^{-9}$	$2.86 \cdot 10^{-8}$	$4.89 \cdot 10^{-15}$	$1.62 \cdot 10^{-7}$
26	3.29	5.95	4.48	0.00	16.10	$4.52 \cdot 10^{-8}$	$1.75 \cdot 10^{-7}$	$1.60 \cdot 10^{-15}$	$8.51 \cdot 10^{-7}$
24	2.72	5.33	3.42	0.64	15.20	$3.15 \cdot 10^{-10}$	$8.39 \cdot 10^{-10}$	$1.09 \cdot 10^{-17}$	$3.86 \cdot 10^{-9}$
27	2.22	3.88	3.32	0.07	14.00	$1.44 \cdot 10^{-8}$	$6.28 \cdot 10^{-8}$	$3.01 \cdot 10^{-15}$	$3.24 \cdot 10^{-7}$
23	2.68	5.48	3.67	0.48	13.60	$1.26 \cdot 10^{-8}$	$5.83 \cdot 10^{-8}$	$3.48 \cdot 10^{-16}$	$2.80 \cdot 10^{-7}$

Table D.9 Deposition hole #3, "all fractures"

# of traces	P_{21} [m/m^2]	trace length [m]				Fracture transmissivity [m^2/s]			
		Average	Std dev	Min	Max	Average	Std dev	Min	Max
29	2.67	4.33	3.71	0.08	14.90	$5.42 \cdot 10^{-8}$	$2.60 \cdot 10^{-7}$	$1.39 \cdot 10^{-14}$	$1.40 \cdot 10^{-6}$
24	3.09	6.07	4.39	0.42	16.40	$1.34 \cdot 10^{-8}$	$4.44 \cdot 10^{-8}$	$5.03 \cdot 10^{-15}$	$1.86 \cdot 10^{-7}$
22	2.46	5.27	3.85	0.73	15.30	$1.30 \cdot 10^{-9}$	$4.08 \cdot 10^{-9}$	$9.10 \cdot 10^{-16}$	$1.46 \cdot 10^{-8}$
24	2.73	5.36	3.36	0.32	16.00	$1.55 \cdot 10^{-9}$	$6.16 \cdot 10^{-9}$	$7.65 \cdot 10^{-15}$	$2.98 \cdot 10^{-8}$
31	4.56	6.92	4.96	0.66	16.20	$3.32 \cdot 10^{-9}$	$1.55 \cdot 10^{-8}$	$6.45 \cdot 10^{-16}$	$8.64 \cdot 10^{-8}$
29	2.19	3.56	2.70	0.14	9.66	$1.62 \cdot 10^{-9}$	$6.13 \cdot 10^{-9}$	$1.43 \cdot 10^{-16}$	$3.27 \cdot 10^{-8}$
25	2.66	5.00	3.12	0.04	12.10	$4.01 \cdot 10^{-10}$	$1.34 \cdot 10^{-9}$	$6.39 \cdot 10^{-17}$	$6.57 \cdot 10^{-9}$
26	2.54	4.60	3.31	0.63	14.80	$4.70 \cdot 10^{-9}$	$1.84 \cdot 10^{-8}$	$1.65 \cdot 10^{-16}$	$9.02 \cdot 10^{-8}$
27	3.08	5.37	3.85	0.71	16.00	$2.43 \cdot 10^{-7}$	$1.26 \cdot 10^{-6}$	$9.00 \cdot 10^{-16}$	$6.56 \cdot 10^{-6}$
24	2.15	4.22	3.97	0.03	15.20	$2.51 \cdot 10^{-9}$	$6.43 \cdot 10^{-9}$	$3.42 \cdot 10^{-16}$	$2.89 \cdot 10^{-8}$
33	3.41	4.87	3.63	0.53	16.20	$4.19 \cdot 10^{-10}$	$1.59 \cdot 10^{-9}$	$1.95 \cdot 10^{-15}$	$8.74 \cdot 10^{-9}$
17	1.46	4.04	2.20	0.49	8.35	$1.06 \cdot 10^{-9}$	$4.08 \cdot 10^{-9}$	$8.92 \cdot 10^{-14}$	$1.69 \cdot 10^{-8}$
37	3.40	4.32	2.25	0.22	8.04	$2.01 \cdot 10^{-8}$	$1.20 \cdot 10^{-7}$	$2.84 \cdot 10^{-16}$	$7.32 \cdot 10^{-7}$
33	3.65	5.21	3.94	0.45	16.00	$4.69 \cdot 10^{-9}$	$1.82 \cdot 10^{-8}$	$1.59 \cdot 10^{-16}$	$8.42 \cdot 10^{-8}$
24	2.77	5.43	4.04	0.09	16.40	$3.37 \cdot 10^{-9}$	$1.15 \cdot 10^{-8}$	$5.70 \cdot 10^{-15}$	$5.58 \cdot 10^{-8}$
30	3.79	5.95	3.94	0.60	16.20	$3.97 \cdot 10^{-9}$	$1.69 \cdot 10^{-8}$	$2.35 \cdot 10^{-14}$	$8.98 \cdot 10^{-8}$
28	3.49	5.87	4.48	0.12	16.10	$3.72 \cdot 10^{-8}$	$1.63 \cdot 10^{-7}$	$1.60 \cdot 10^{-15}$	$8.51 \cdot 10^{-7}$
31	3.02	4.59	3.40	0.13	11.20	$1.79 \cdot 10^{-8}$	$8.02 \cdot 10^{-8}$	$4.53 \cdot 10^{-16}$	$4.35 \cdot 10^{-7}$
35	4.37	5.88	3.88	1.10	16.20	$4.22 \cdot 10^{-9}$	$1.53 \cdot 10^{-8}$	$1.94 \cdot 10^{-14}$	$8.96 \cdot 10^{-8}$
30	3.60	5.65	3.24	0.97	13.50	$2.51 \cdot 10^{-8}$	$1.36 \cdot 10^{-7}$	$3.85 \cdot 10^{-18}$	$7.47 \cdot 10^{-7}$

Table D.10 Deposition hole #4, "all fractures"

# of traces	P_{21} [m/m^2]	trace length [m]				Fracture transmissivity [m^2/s]			
		Average	Std dev	Min	Max	Average	Std dev	Min	Max
27	2.43	4.23	3.17	0.08	13.30	$3.55 \cdot 10^{-10}$	$7.75 \cdot 10^{-10}$	$1.06 \cdot 10^{-16}$	$2.90 \cdot 10^{-9}$
31	2.69	4.09	2.46	0.38	10.70	$4.89 \cdot 10^{-9}$	$2.21 \cdot 10^{-8}$	$5.03 \cdot 10^{-15}$	$1.23 \cdot 10^{-7}$
31	3.03	4.60	2.80	0.33	11.50	$4.22 \cdot 10^{-9}$	$1.60 \cdot 10^{-8}$	$9.64 \cdot 10^{-17}$	$8.30 \cdot 10^{-8}$
28	2.34	3.94	3.05	0.04	9.90	$1.51 \cdot 10^{-9}$	$3.74 \cdot 10^{-9}$	$1.74 \cdot 10^{-16}$	$1.42 \cdot 10^{-8}$
31	3.11	4.73	2.94	0.09	12.70	$1.53 \cdot 10^{-8}$	$6.21 \cdot 10^{-8}$	$6.45 \cdot 10^{-16}$	$3.39 \cdot 10^{-7}$
27	2.70	4.72	3.27	0.83	14.10	$5.11 \cdot 10^{-9}$	$1.50 \cdot 10^{-8}$	$5.34 \cdot 10^{-19}$	$6.59 \cdot 10^{-8}$
30	3.17	4.98	4.26	0.47	15.70	$8.68 \cdot 10^{-8}$	$4.73 \cdot 10^{-7}$	$1.74 \cdot 10^{-16}$	$2.59 \cdot 10^{-6}$
32	3.36	4.94	3.89	0.22	16.80	$6.98 \cdot 10^{-9}$	$2.70 \cdot 10^{-8}$	$6.62 \cdot 10^{-16}$	$1.27 \cdot 10^{-7}$
36	3.93	5.14	4.37	0.16	16.10	$1.83 \cdot 10^{-7}$	$1.09 \cdot 10^{-6}$	$8.08 \cdot 10^{-15}$	$6.56 \cdot 10^{-6}$
25	3.23	6.09	3.96	0.30	16.20	$3.92 \cdot 10^{-10}$	$1.29 \cdot 10^{-9}$	$2.39 \cdot 10^{-14}$	$6.20 \cdot 10^{-9}$
24	2.46	4.82	3.54	0.78	16.10	$6.84 \cdot 10^{-8}$	$3.32 \cdot 10^{-7}$	$9.37 \cdot 10^{-15}$	$1.63 \cdot 10^{-6}$
22	2.18	4.67	3.90	0.14	15.90	$1.93 \cdot 10^{-8}$	$8.37 \cdot 10^{-8}$	$6.88 \cdot 10^{-16}$	$3.93 \cdot 10^{-7}$
23	2.39	4.89	2.20	0.10	8.06	$1.12 \cdot 10^{-10}$	$2.84 \cdot 10^{-10}$	$8.55 \cdot 10^{-15}$	$1.34 \cdot 10^{-9}$
21	1.88	4.21	3.25	0.43	15.40	$5.27 \cdot 10^{-9}$	$1.86 \cdot 10^{-8}$	$2.17 \cdot 10^{-15}$	$8.42 \cdot 10^{-8}$
20	2.16	5.09	3.79	0.15	13.90	$2.93 \cdot 10^{-9}$	$8.58 \cdot 10^{-9}$	$1.12 \cdot 10^{-14}$	$3.75 \cdot 10^{-8}$
20	2.22	5.23	3.79	0.11	14.00	$2.17 \cdot 10^{-8}$	$6.30 \cdot 10^{-8}$	$7.35 \cdot 10^{-16}$	$2.38 \cdot 10^{-7}$
24	2.78	5.46	4.19	0.78	16.20	$2.54 \cdot 10^{-9}$	$7.64 \cdot 10^{-9}$	$1.60 \cdot 10^{-15}$	$3.55 \cdot 10^{-8}$
21	2.16	4.84	2.66	0.37	10.80	$9.84 \cdot 10^{-10}$	$4.41 \cdot 10^{-9}$	$7.85 \cdot 10^{-15}$	$2.02 \cdot 10^{-8}$
33	3.04	4.34	2.69	0.79	11.50	$3.50 \cdot 10^{-10}$	$7.76 \cdot 10^{-10}$	$2.95 \cdot 10^{-16}$	$3.14 \cdot 10^{-9}$
30	3.07	4.81	3.27	0.33	15.00	$1.48 \cdot 10^{-7}$	$7.68 \cdot 10^{-7}$	$3.48 \cdot 10^{-16}$	$4.21 \cdot 10^{-6}$

Table D.11 Deposition hole #5, "all fractures"

# of traces	P_{21} [m/m^2]	trace length [m]				Fracture transmissivity [m^2/s]			
		Average	Std dev	Min	Max	Average	Std dev	Min	Max
29	3.49	5.66	4.22	0.13	16.00	$4.95 \cdot 10^{-9}$	$2.02 \cdot 10^{-8}$	$1.68 \cdot 10^{-16}$	$1.03 \cdot 10^{-7}$
24	3.18	6.25	4.19	0.45	16.00	$2.11 \cdot 10^{-7}$	$1.03 \cdot 10^{-6}$	$5.61 \cdot 10^{-15}$	$5.03 \cdot 10^{-6}$
32	2.94	4.33	3.66	0.02	14.10	$1.46 \cdot 10^{-9}$	$6.36 \cdot 10^{-9}$	$7.86 \cdot 10^{-16}$	$3.54 \cdot 10^{-8}$
31	4.09	6.21	3.97	0.08	15.50	$2.49 \cdot 10^{-9}$	$7.36 \cdot 10^{-9}$	$2.02 \cdot 10^{-15}$	$3.71 \cdot 10^{-8}$
27	3.18	5.54	3.16	0.84	13.00	$1.51 \cdot 10^{-8}$	$6.88 \cdot 10^{-8}$	$6.91 \cdot 10^{-18}$	$3.57 \cdot 10^{-7}$
22	1.65	3.53	2.55	0.18	9.18	$1.70 \cdot 10^{-10}$	$6.74 \cdot 10^{-10}$	$7.59 \cdot 10^{-16}$	$3.16 \cdot 10^{-9}$
25	2.71	5.10	3.26	1.30	16.00	$2.85 \cdot 10^{-9}$	$1.23 \cdot 10^{-8}$	$2.18 \cdot 10^{-15}$	$6.18 \cdot 10^{-8}$
19	2.22	5.51	3.56	1.00	14.80	$4.00 \cdot 10^{-8}$	$1.73 \cdot 10^{-7}$	$7.79 \cdot 10^{-15}$	$7.54 \cdot 10^{-7}$
34	2.82	3.90	2.57	0.05	9.45	$6.74 \cdot 10^{-9}$	$2.17 \cdot 10^{-8}$	$1.49 \cdot 10^{-15}$	$8.95 \cdot 10^{-8}$
37	3.37	4.29	3.54	0.09	16.00	$3.77 \cdot 10^{-9}$	$1.40 \cdot 10^{-8}$	$2.58 \cdot 10^{-15}$	$7.91 \cdot 10^{-8}$
12	0.64	2.52	2.03	0.21	5.97	$2.05 \cdot 10^{-8}$	$6.99 \cdot 10^{-8}$	$5.18 \cdot 10^{-15}$	$2.42 \cdot 10^{-7}$
29	3.36	5.46	3.35	0.83	12.10	$1.30 \cdot 10^{-7}$	$6.97 \cdot 10^{-7}$	$5.62 \cdot 10^{-18}$	$3.75 \cdot 10^{-6}$
26	2.92	5.29	3.24	0.14	11.80	$6.01 \cdot 10^{-8}$	$2.13 \cdot 10^{-7}$	$9.52 \cdot 10^{-18}$	$8.76 \cdot 10^{-7}$
25	2.98	5.61	3.43	0.23	16.30	$4.09 \cdot 10^{-10}$	$8.11 \cdot 10^{-10}$	$1.07 \cdot 10^{-17}$	$2.97 \cdot 10^{-9}$
30	2.70	4.23	2.53	0.58	9.23	$4.38 \cdot 10^{-8}$	$2.30 \cdot 10^{-7}$	$1.60 \cdot 10^{-14}$	$1.26 \cdot 10^{-6}$
35	4.13	5.55	3.04	0.86	13.80	$4.83 \cdot 10^{-9}$	$2.60 \cdot 10^{-8}$	$6.08 \cdot 10^{-17}$	$1.54 \cdot 10^{-7}$
24	2.12	4.17	2.79	0.33	10.70	$5.22 \cdot 10^{-9}$	$2.13 \cdot 10^{-8}$	$1.90 \cdot 10^{-14}$	$1.04 \cdot 10^{-7}$
25	2.50	4.70	3.51	0.32	16.10	$1.85 \cdot 10^{-10}$	$4.40 \cdot 10^{-10}$	$4.25 \cdot 10^{-17}$	$1.78 \cdot 10^{-9}$
34	2.36	3.28	2.43	0.07	9.29	$1.06 \cdot 10^{-8}$	$5.78 \cdot 10^{-8}$	$1.42 \cdot 10^{-16}$	$3.37 \cdot 10^{-7}$
32	3.47	5.10	4.24	0.15	15.30	$3.94 \cdot 10^{-9}$	$1.45 \cdot 10^{-8}$	$1.90 \cdot 10^{-15}$	$6.75 \cdot 10^{-8}$

Table D.12 Deposition hole #6, "all fractures"

# of traces	P_{21} [m/m^2]	trace length [m]				Fracture transmissivity [m^2/s]			
		Average	Std dev	Min	Max	Average	Std dev	Min	Max
30	2.70	4.24	3.58	0.09	14.20	$1.54 \cdot 10^{-9}$	$3.33 \cdot 10^{-9}$	$4.50 \cdot 10^{-16}$	$1.18 \cdot 10^{-8}$
25	2.59	4.87	4.54	0.34	16.10	$7.30 \cdot 10^{-9}$	$3.47 \cdot 10^{-8}$	$5.61 \cdot 10^{-15}$	$1.74 \cdot 10^{-7}$
42	4.04	4.53	3.22	0.30	16.50	$8.90 \cdot 10^{-10}$	$2.85 \cdot 10^{-9}$	$3.28 \cdot 10^{-15}$	$1.41 \cdot 10^{-8}$
24	2.07	4.07	3.70	0.02	15.60	$3.38 \cdot 10^{-10}$	$1.07 \cdot 10^{-9}$	$5.09 \cdot 10^{-15}$	$5.06 \cdot 10^{-9}$
32	3.15	4.64	2.79	0.10	13.60	$1.51 \cdot 10^{-8}$	$6.39 \cdot 10^{-8}$	$4.31 \cdot 10^{-17}$	$3.57 \cdot 10^{-7}$
25	3.16	5.95	4.20	0.62	15.60	$2.15 \cdot 10^{-8}$	$1.04 \cdot 10^{-7}$	$3.36 \cdot 10^{-15}$	$5.20 \cdot 10^{-7}$
28	2.96	4.98	3.71	0.03	12.20	$3.89 \cdot 10^{-9}$	$1.97 \cdot 10^{-8}$	$3.26 \cdot 10^{-15}$	$1.04 \cdot 10^{-7}$
21	2.14	4.81	4.62	0.23	16.10	$4.89 \cdot 10^{-8}$	$1.68 \cdot 10^{-7}$	$3.04 \cdot 10^{-18}$	$7.54 \cdot 10^{-7}$
29	2.81	4.57	3.74	0.24	16.20	$7.70 \cdot 10^{-9}$	$2.78 \cdot 10^{-8}$	$4.45 \cdot 10^{-17}$	$1.47 \cdot 10^{-7}$
25	2.39	4.50	3.57	0.62	16.40	$1.42 \cdot 10^{-9}$	$4.15 \cdot 10^{-9}$	$1.69 \cdot 10^{-14}$	$1.50 \cdot 10^{-8}$
16	1.70	5.01	3.78	0.55	14.90	$1.80 \cdot 10^{-8}$	$7.02 \cdot 10^{-8}$	$1.41 \cdot 10^{-15}$	$2.81 \cdot 10^{-7}$
21	2.12	4.75	3.19	0.13	12.50	$1.42 \cdot 10^{-9}$	$6.33 \cdot 10^{-9}$	$8.20 \cdot 10^{-17}$	$2.90 \cdot 10^{-8}$
33	3.47	4.96	3.70	0.05	16.10	$2.21 \cdot 10^{-8}$	$1.17 \cdot 10^{-7}$	$1.18 \cdot 10^{-16}$	$6.75 \cdot 10^{-7}$
16	1.92	5.65	3.79	0.46	15.60	$2.35 \cdot 10^{-10}$	$5.58 \cdot 10^{-10}$	$5.62 \cdot 10^{-16}$	$2.16 \cdot 10^{-9}$
27	3.04	5.31	2.71	0.55	11.80	$7.90 \cdot 10^{-10}$	$2.29 \cdot 10^{-9}$	$2.44 \cdot 10^{-15}$	$1.10 \cdot 10^{-8}$
31	3.62	5.50	4.16	0.13	16.00	$8.38 \cdot 10^{-9}$	$3.12 \cdot 10^{-8}$	$5.77 \cdot 10^{-15}$	$1.54 \cdot 10^{-7}$
23	1.75	3.59	2.35	0.34	9.23	$3.37 \cdot 10^{-9}$	$1.46 \cdot 10^{-8}$	$2.36 \cdot 10^{-17}$	$7.02 \cdot 10^{-8}$
37	2.96	3.77	2.83	0.04	10.50	$2.51 \cdot 10^{-8}$	$1.30 \cdot 10^{-7}$	$4.25 \cdot 10^{-17}$	$7.92 \cdot 10^{-7}$
29	2.90	4.71	3.17	0.00	12.90	$3.46 \cdot 10^{-9}$	$7.53 \cdot 10^{-9}$	$1.11 \cdot 10^{-16}$	$3.23 \cdot 10^{-8}$
32	3.34	4.91	3.82	0.20	16.00	$2.09 \cdot 10^{-10}$	$5.18 \cdot 10^{-10}$	$4.25 \cdot 10^{-16}$	$1.90 \cdot 10^{-9}$

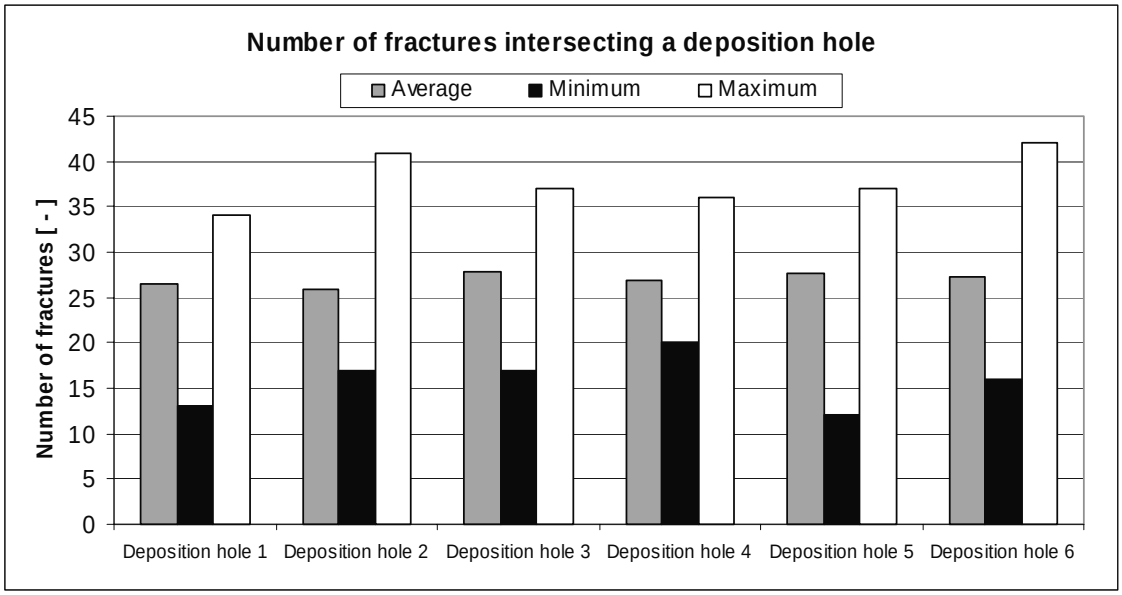

Figure D.1 *Number of fracture traces per deposition hole. Summary statistics based on 20 realisations with all fractures of the calibrated DFN model.*

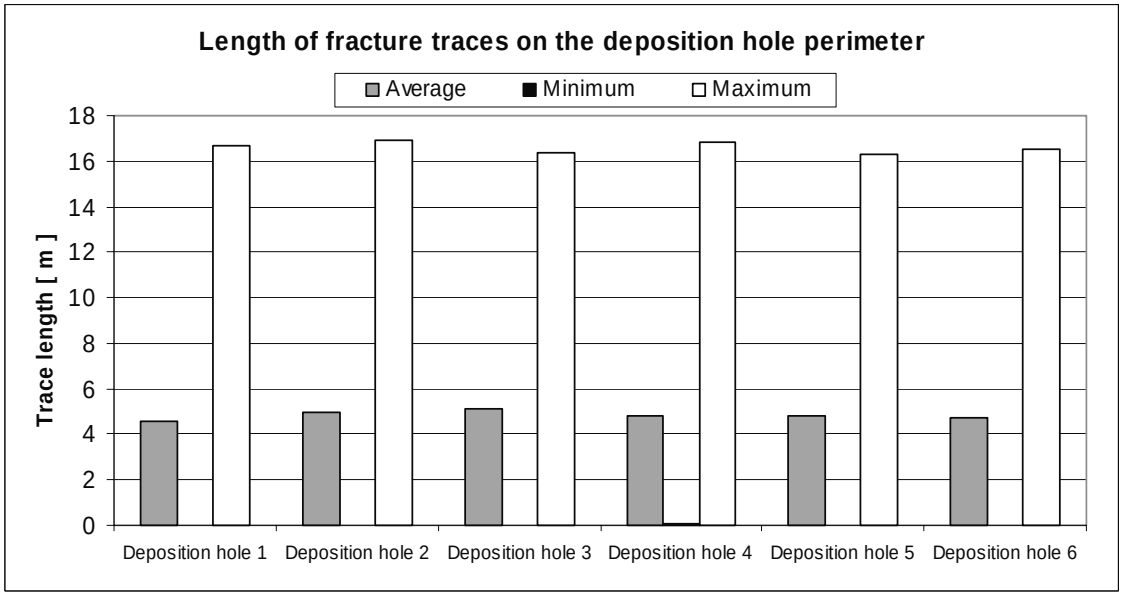

Figure D.2 *Trace length of individual fractures per deposition hole. Summary statistics based on 20 realisations with all fractures of the calibrated DFN model*

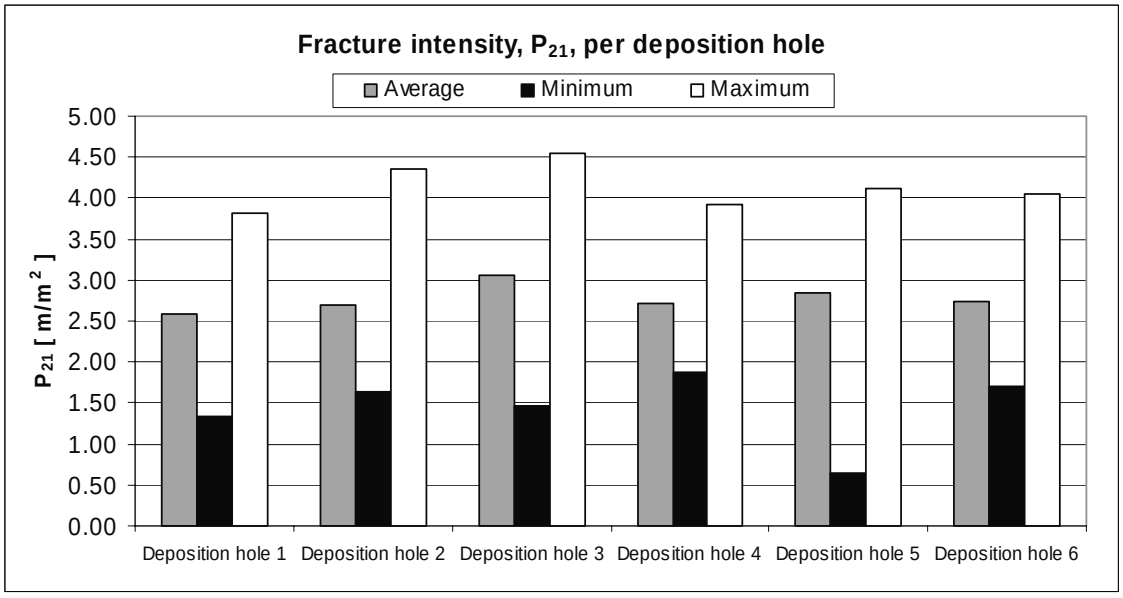

Figure D.3 *Fracture intensity, P_{21} (m/m^2), for all fractures on the deposition hole walls. Summary statistics based on 20 realisations of the calibrated DFN model.*

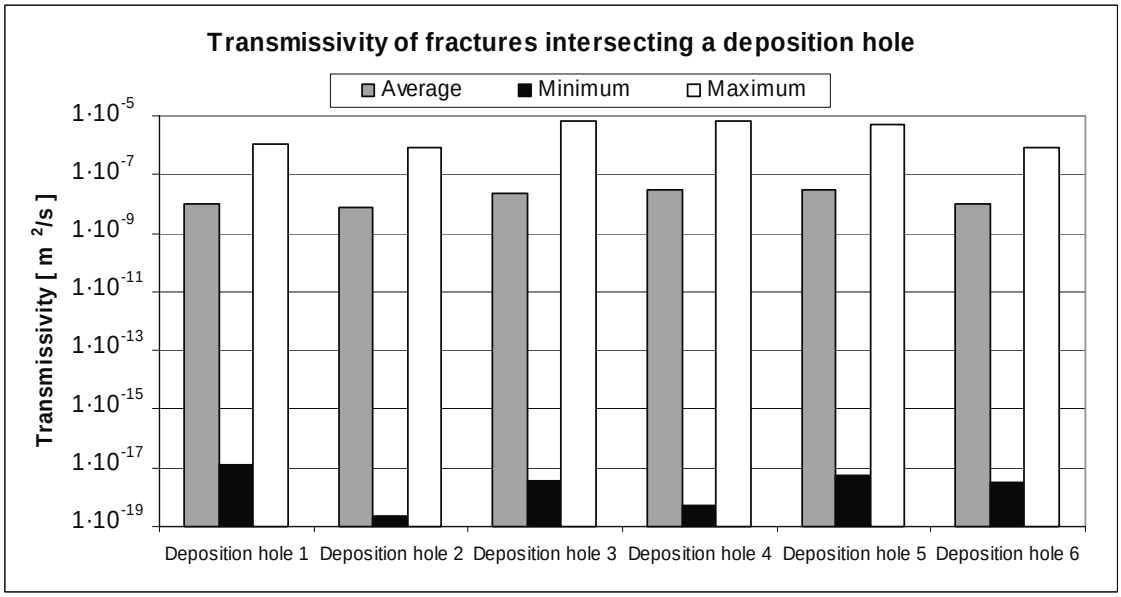

Figure D.4 *Transmissivity of individual fractures intersecting the deposition holes. Summary statistics based on 20 realisations with all fractures of the calibrated DFN model.*

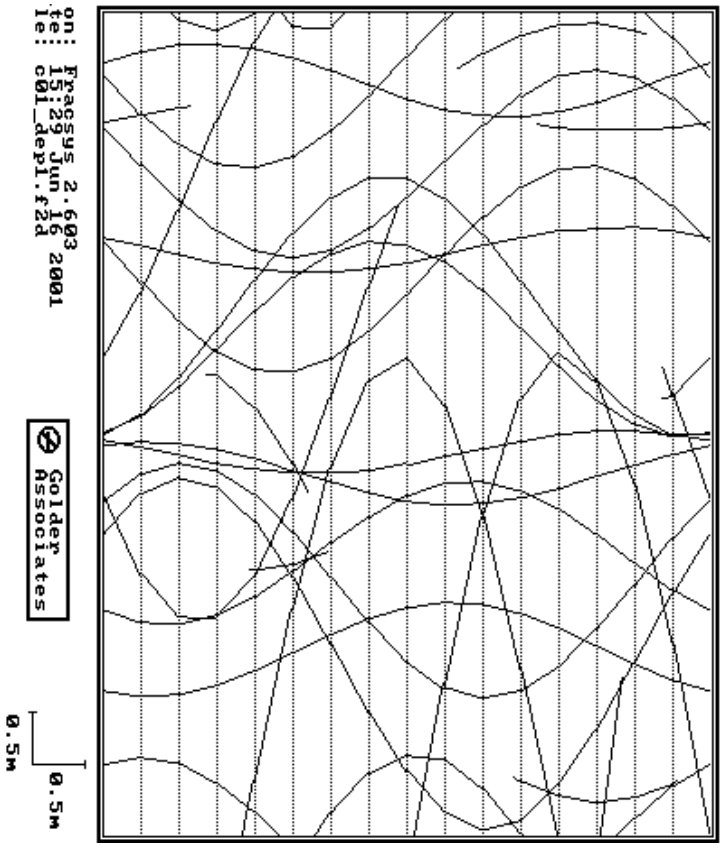

Figure D.5 *Modelled trace map*

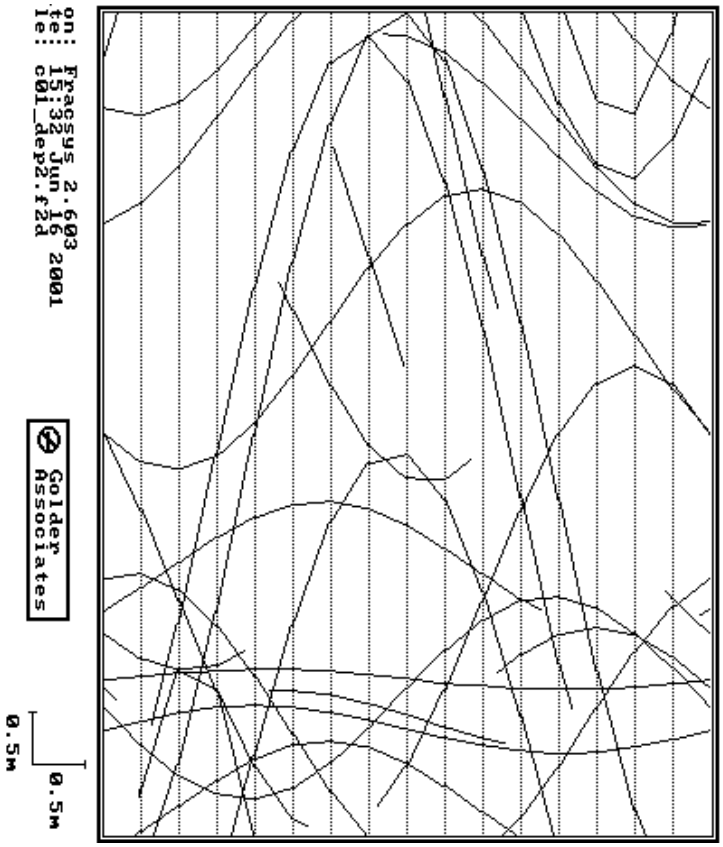

Figure D.6 *Modelled trace map*

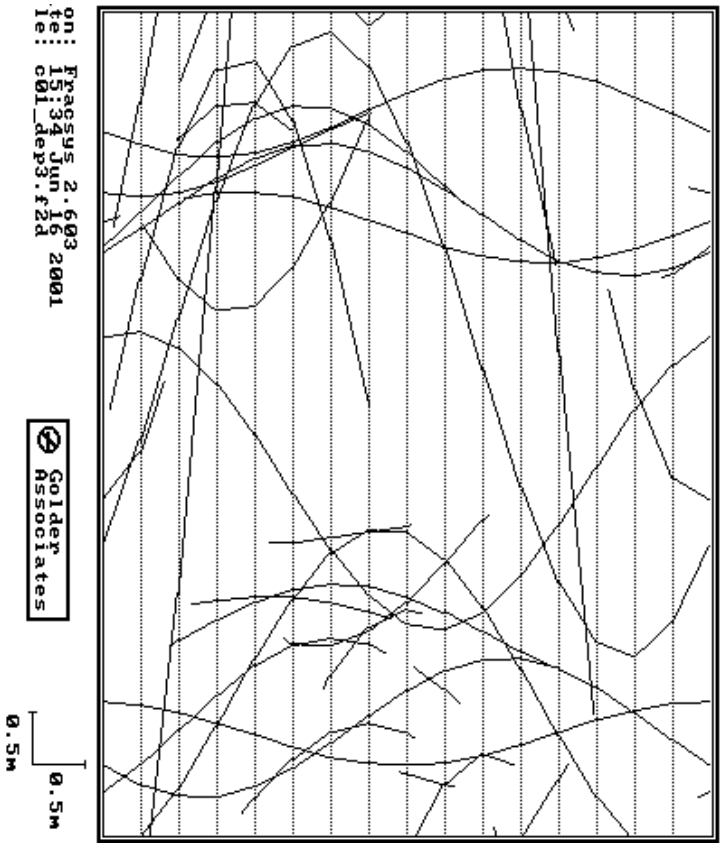

Figure D.7 *Modelled trace map*

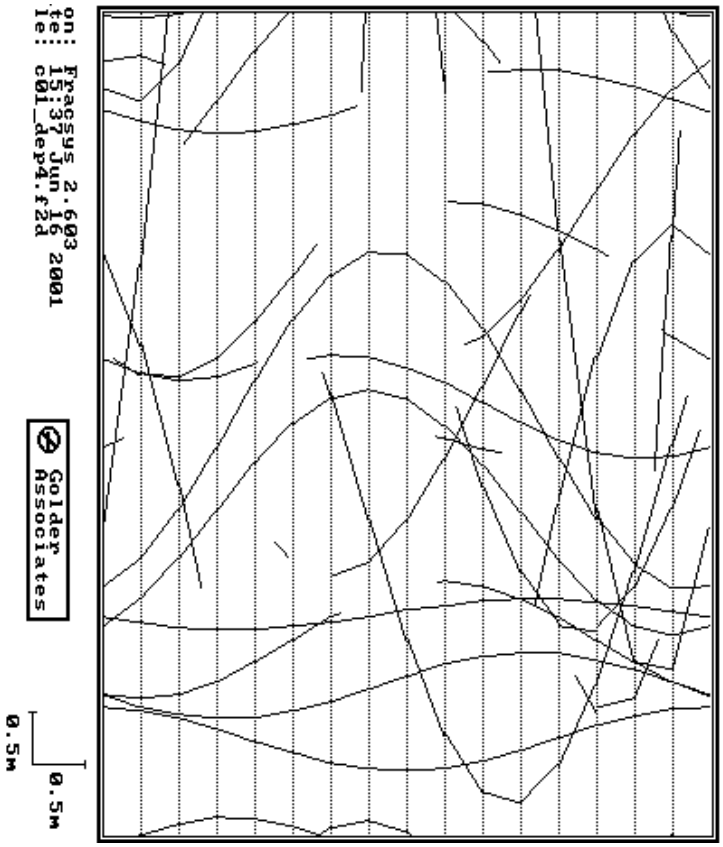

Figure D.8 *Modelled trace map*

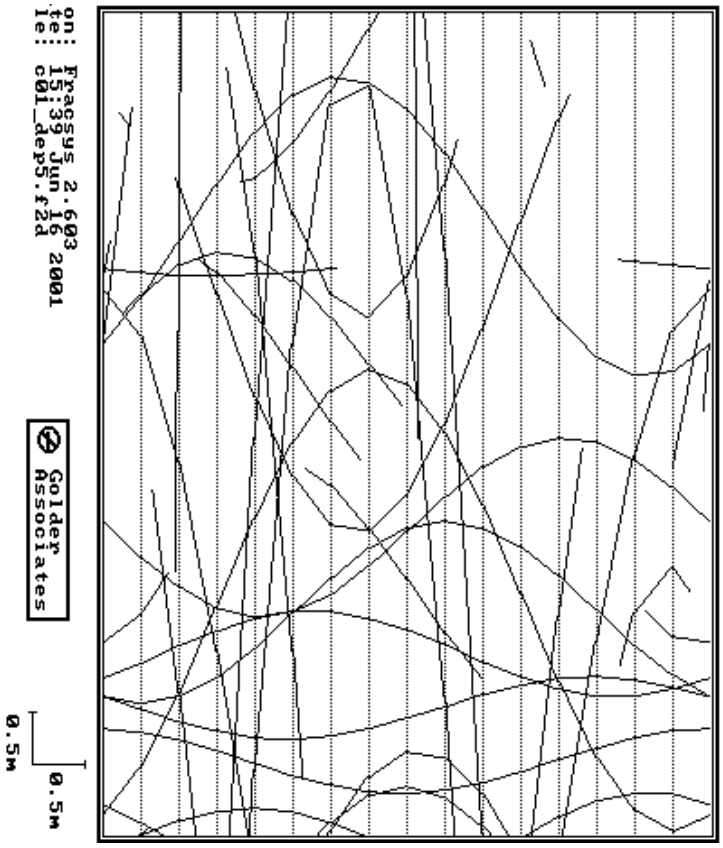

Figure D.9 *Modelled trace map*

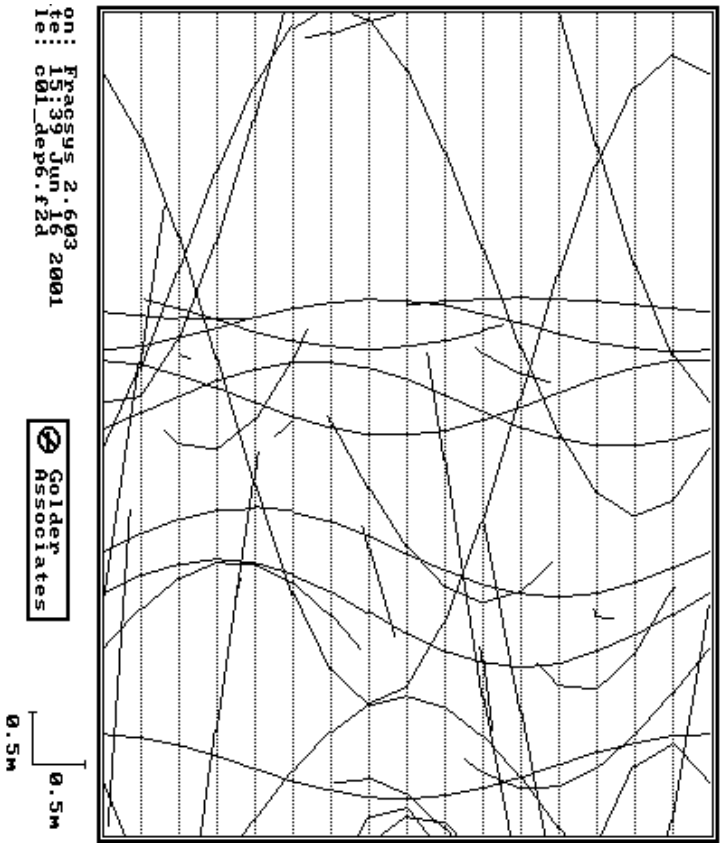

Figure D.10 *Modelled trace map*

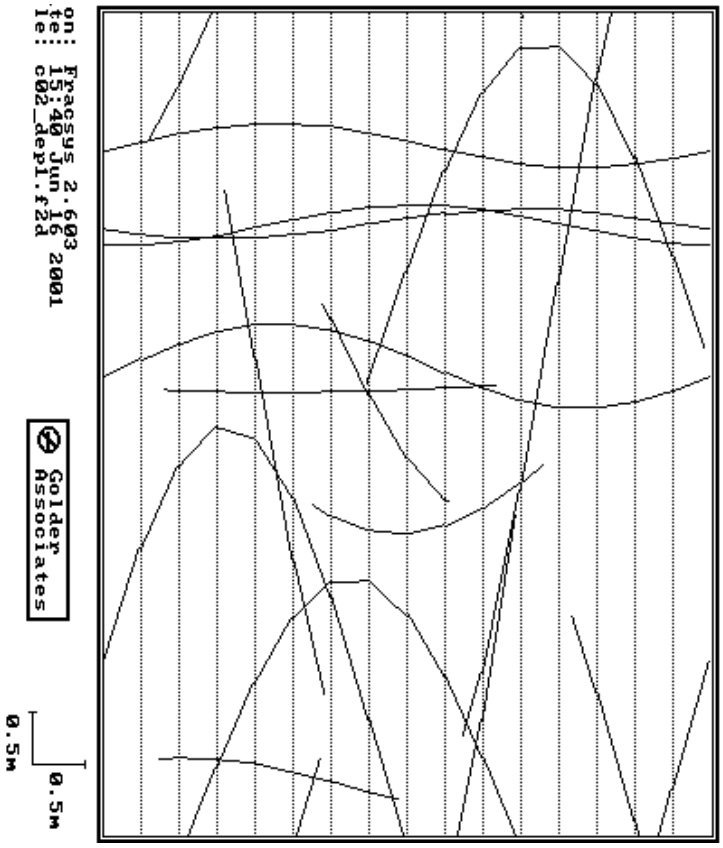

Figure D.11 *Modelled trace map*

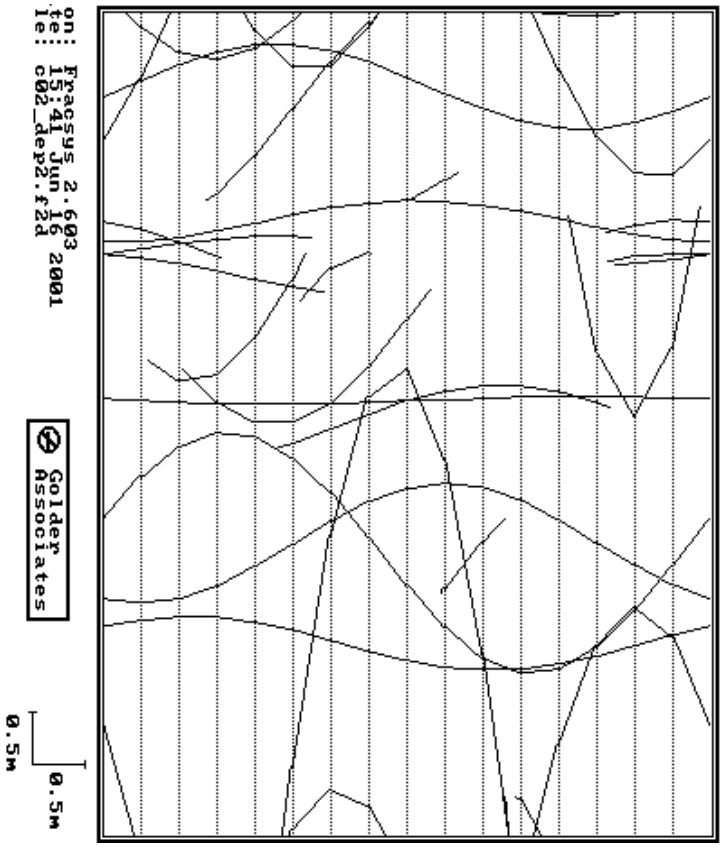

Figure D.12 *Modelled trace map*

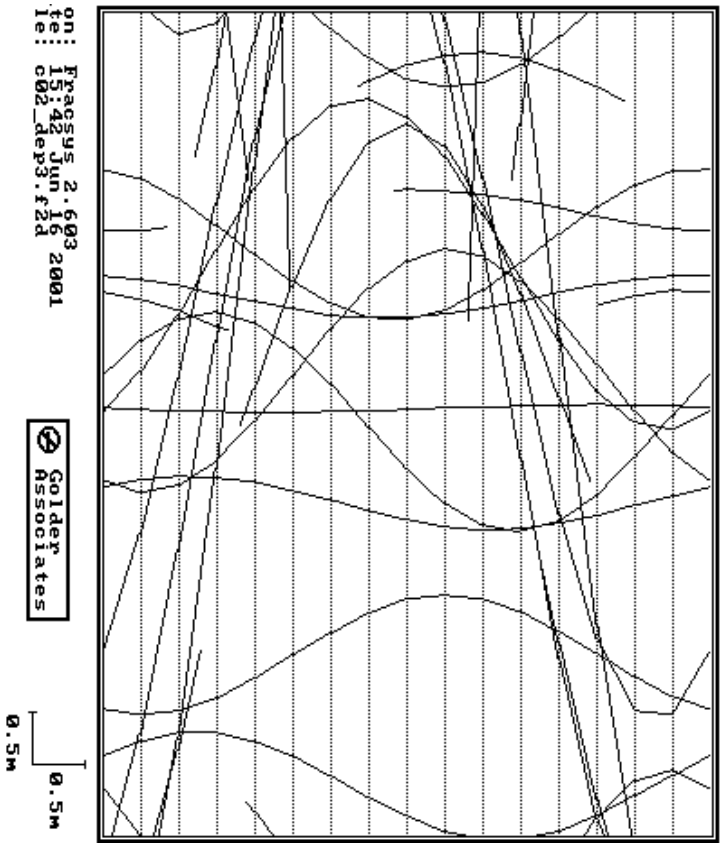

Figure D.13 *Modelled trace map*

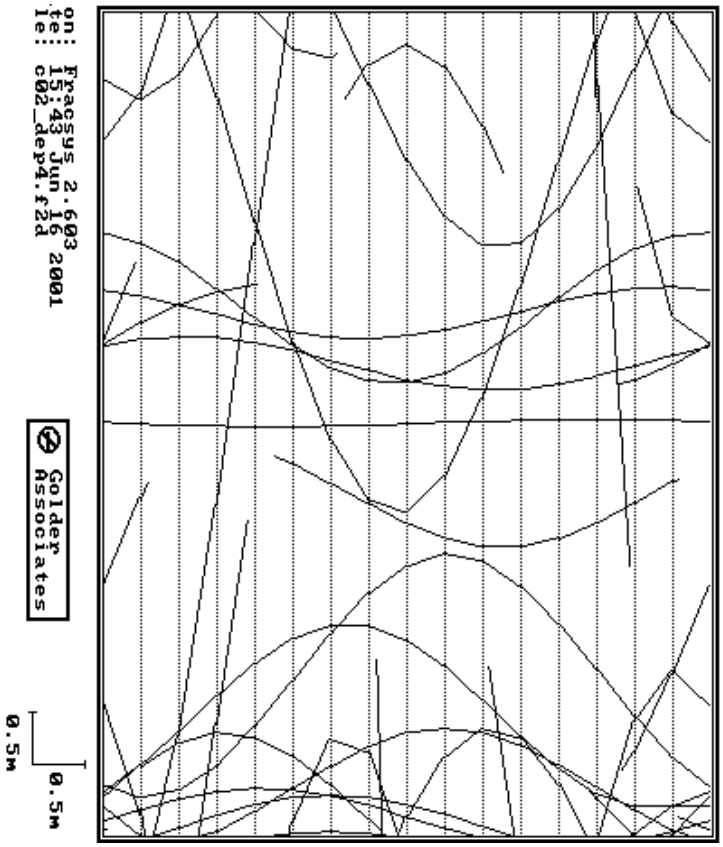

Figure D.14 *Modelled trace map*

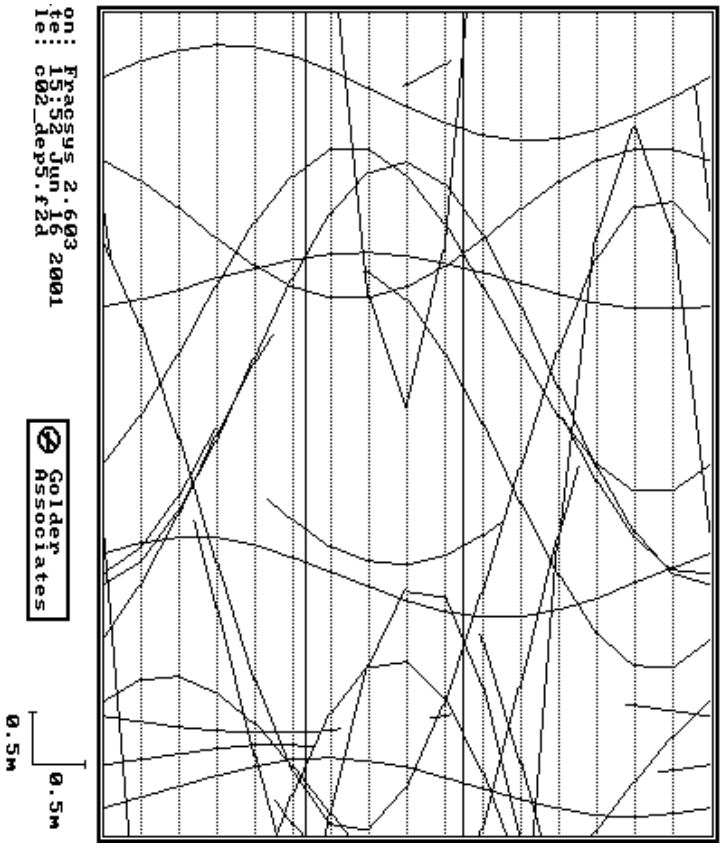

Figure D.15 *Modelled trace map*

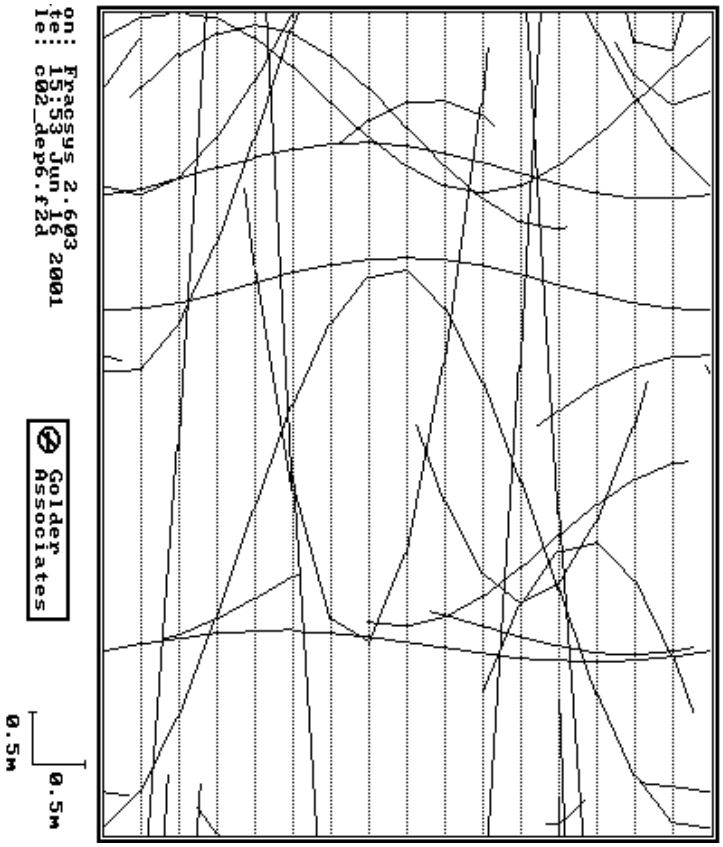

Figure D.16 *Modelled trace map*

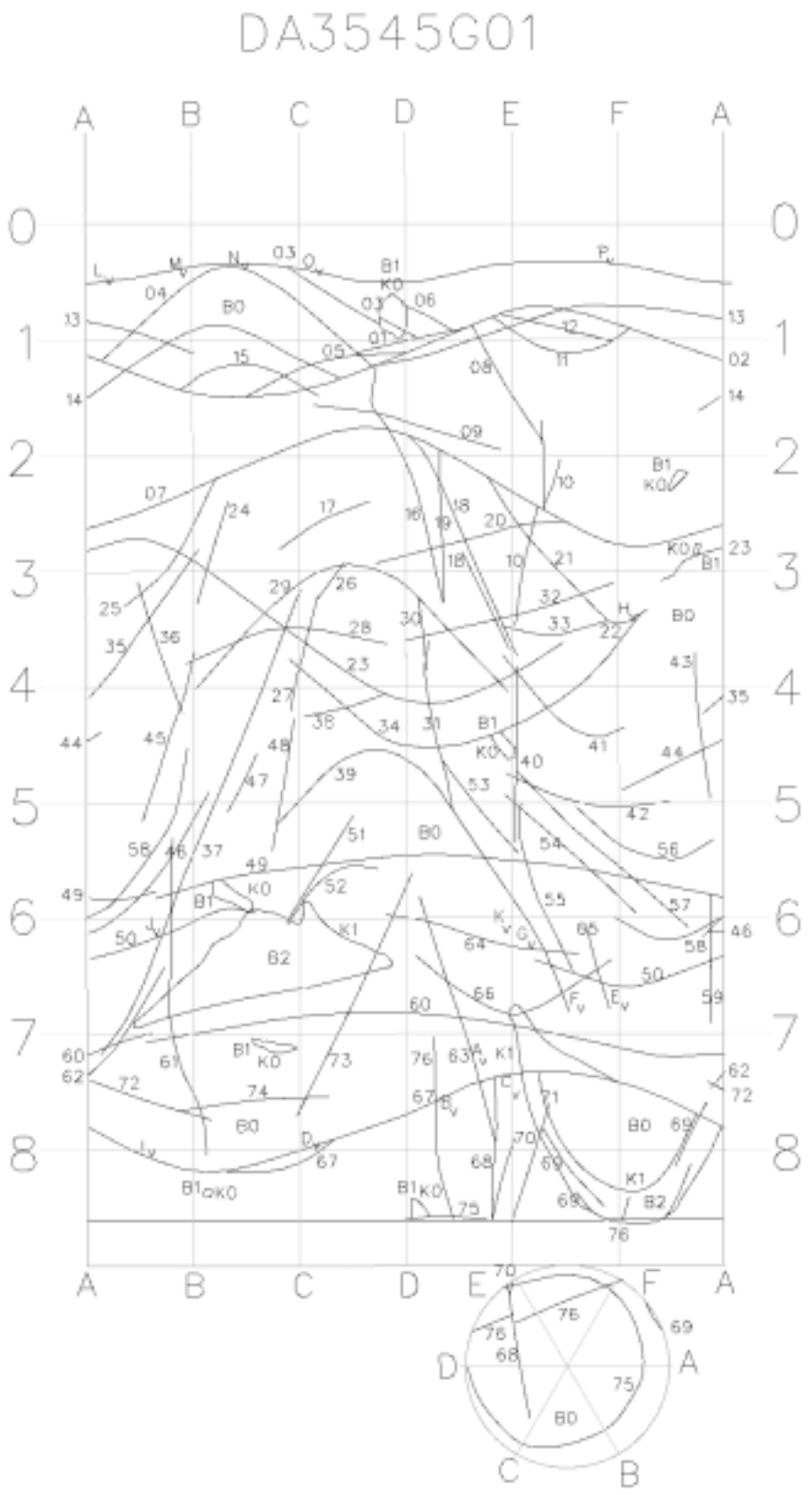

Figure D.17 *Measured trace map*

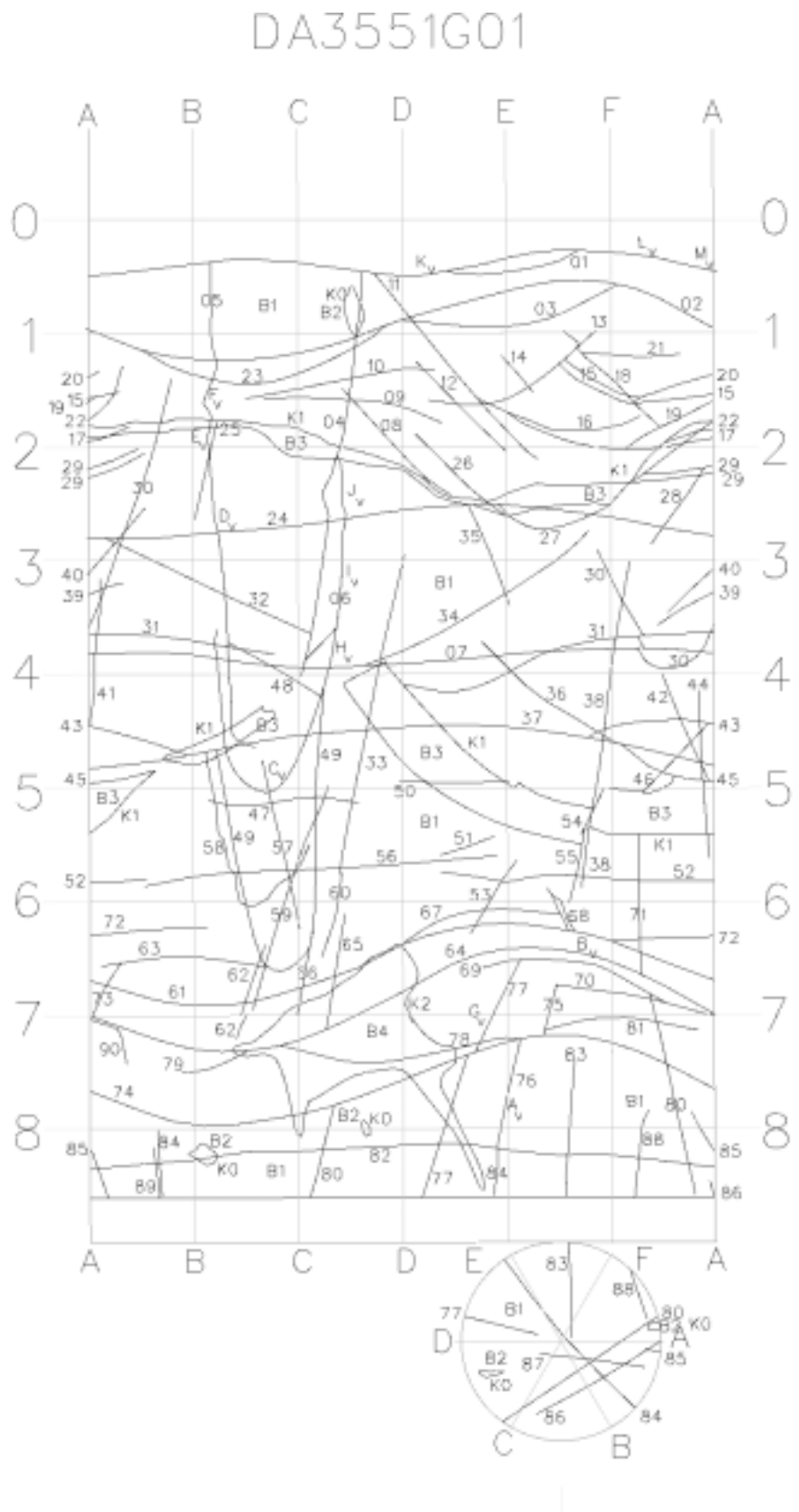

Figure D.18 *Measured trace map*

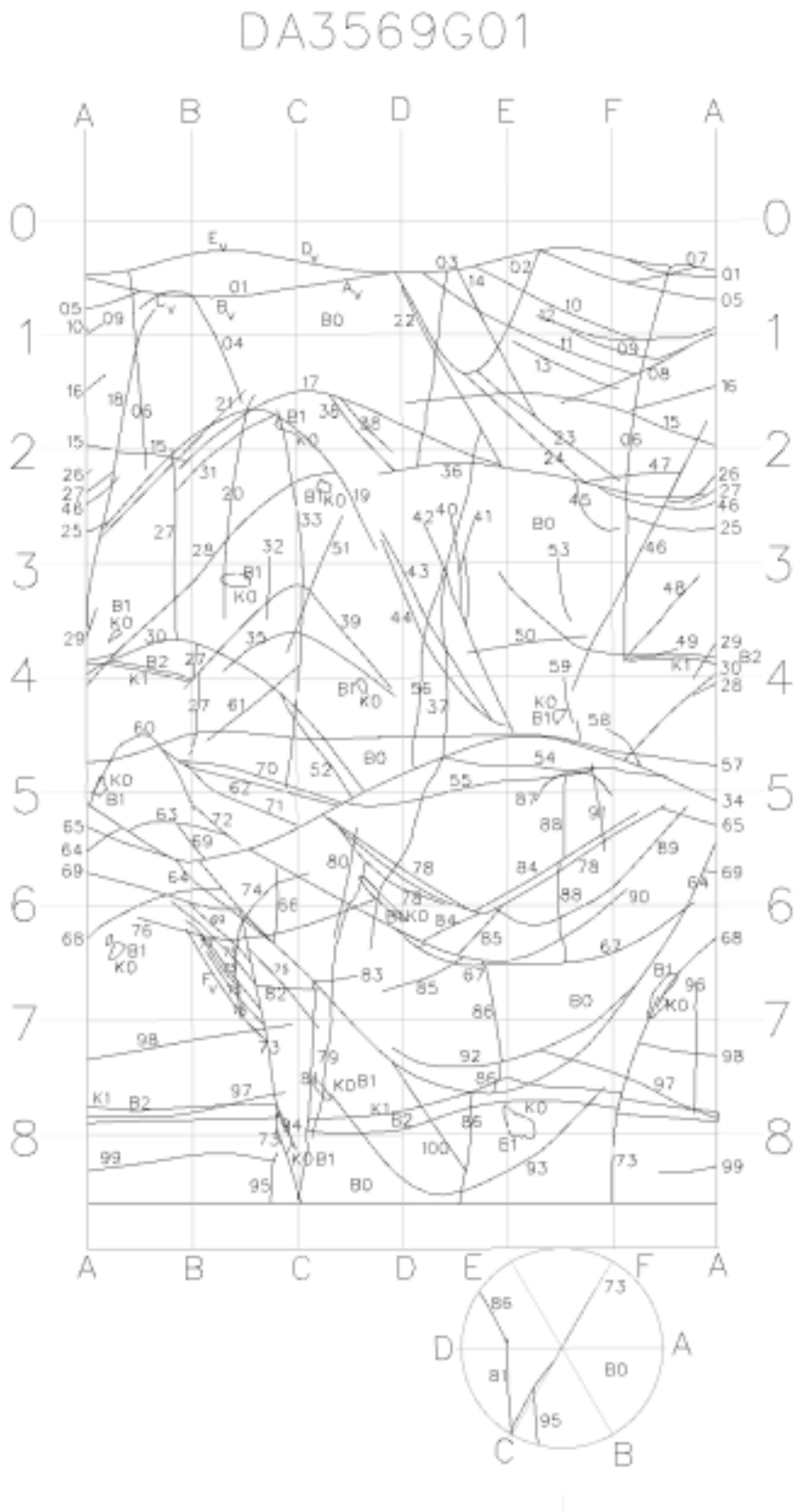

Figure D.19 *Measured trace map*

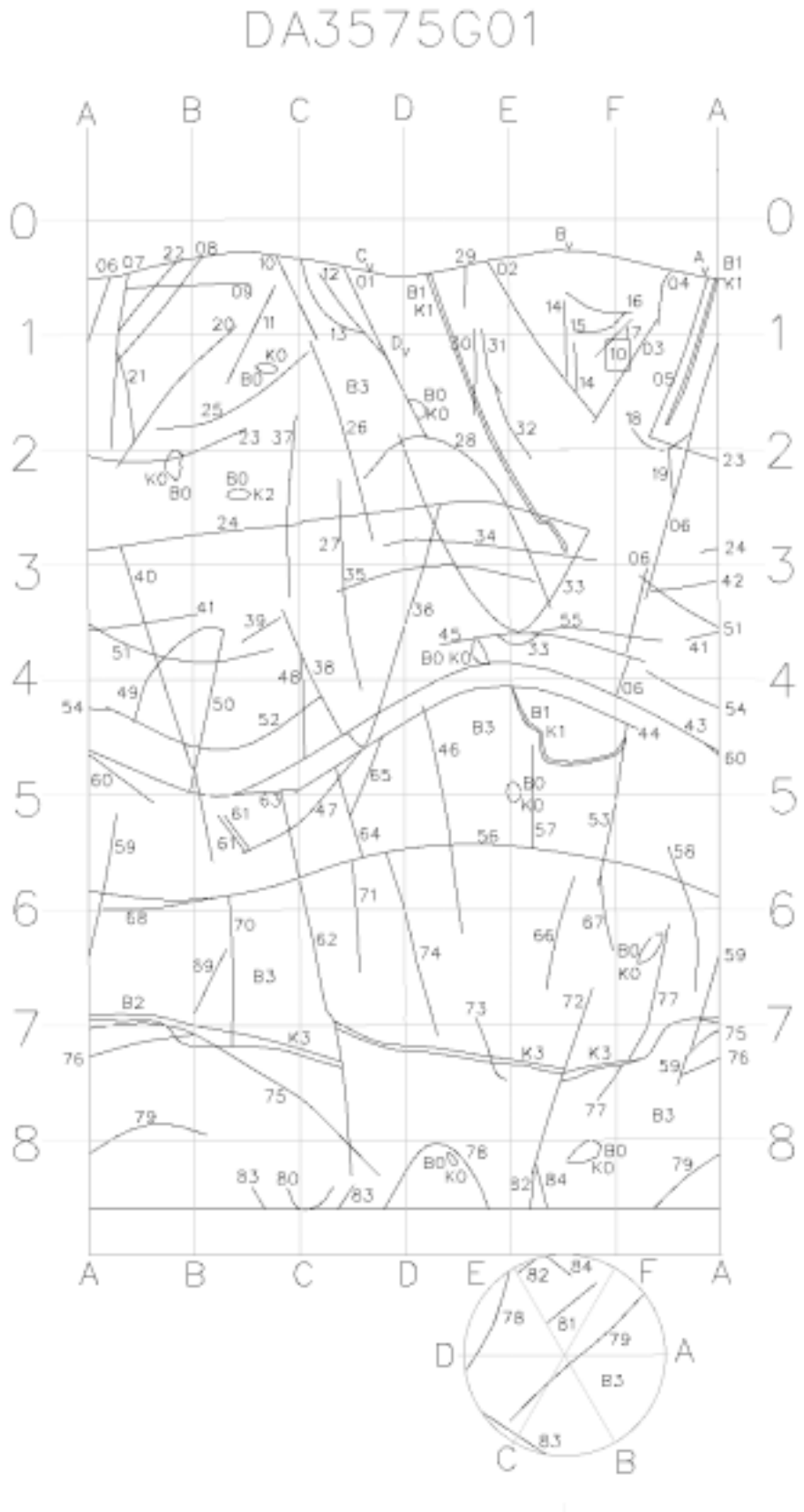

Figure D.20 *Measured trace map*

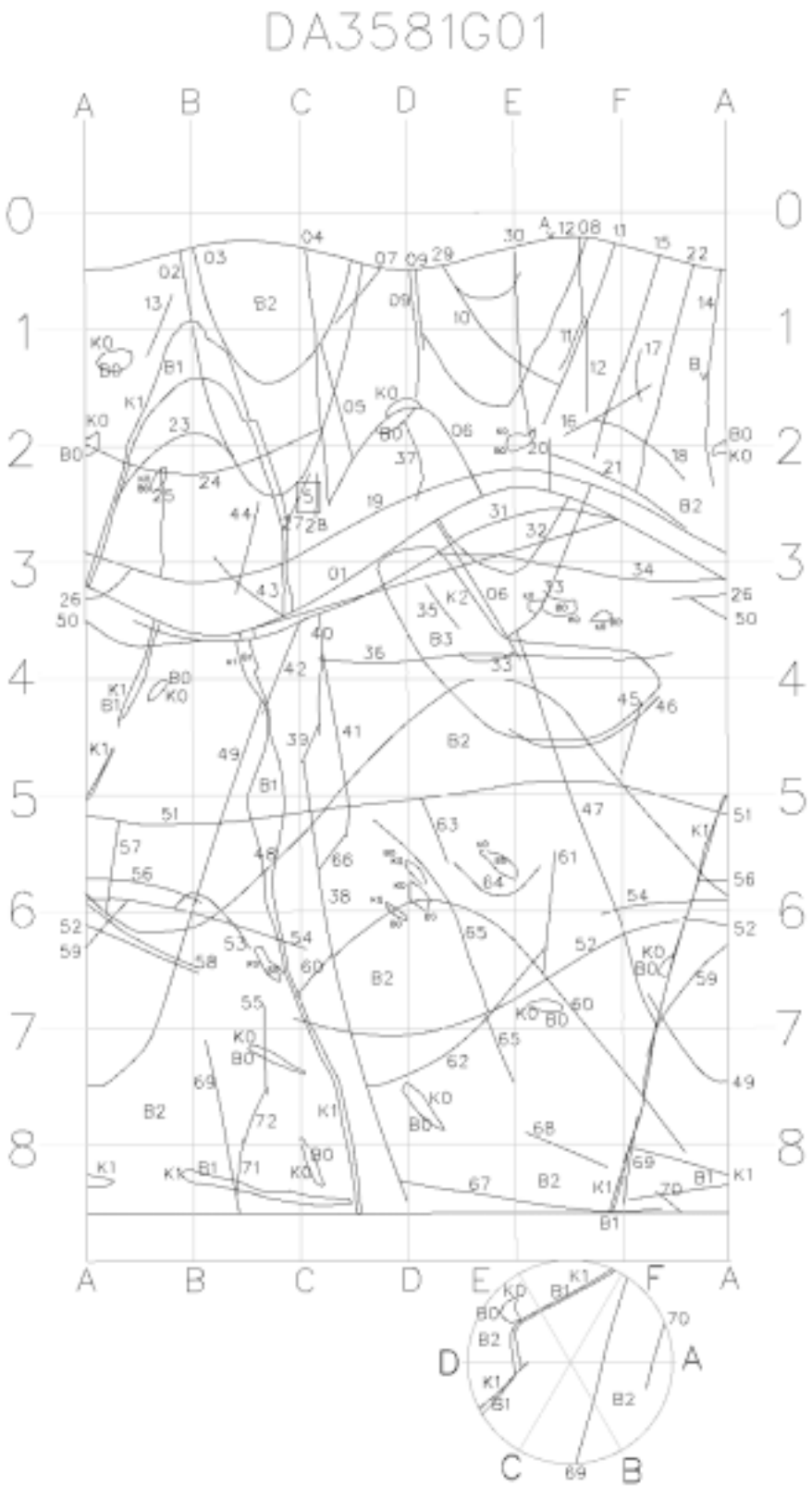

Figure D.21 *Measured trace map*

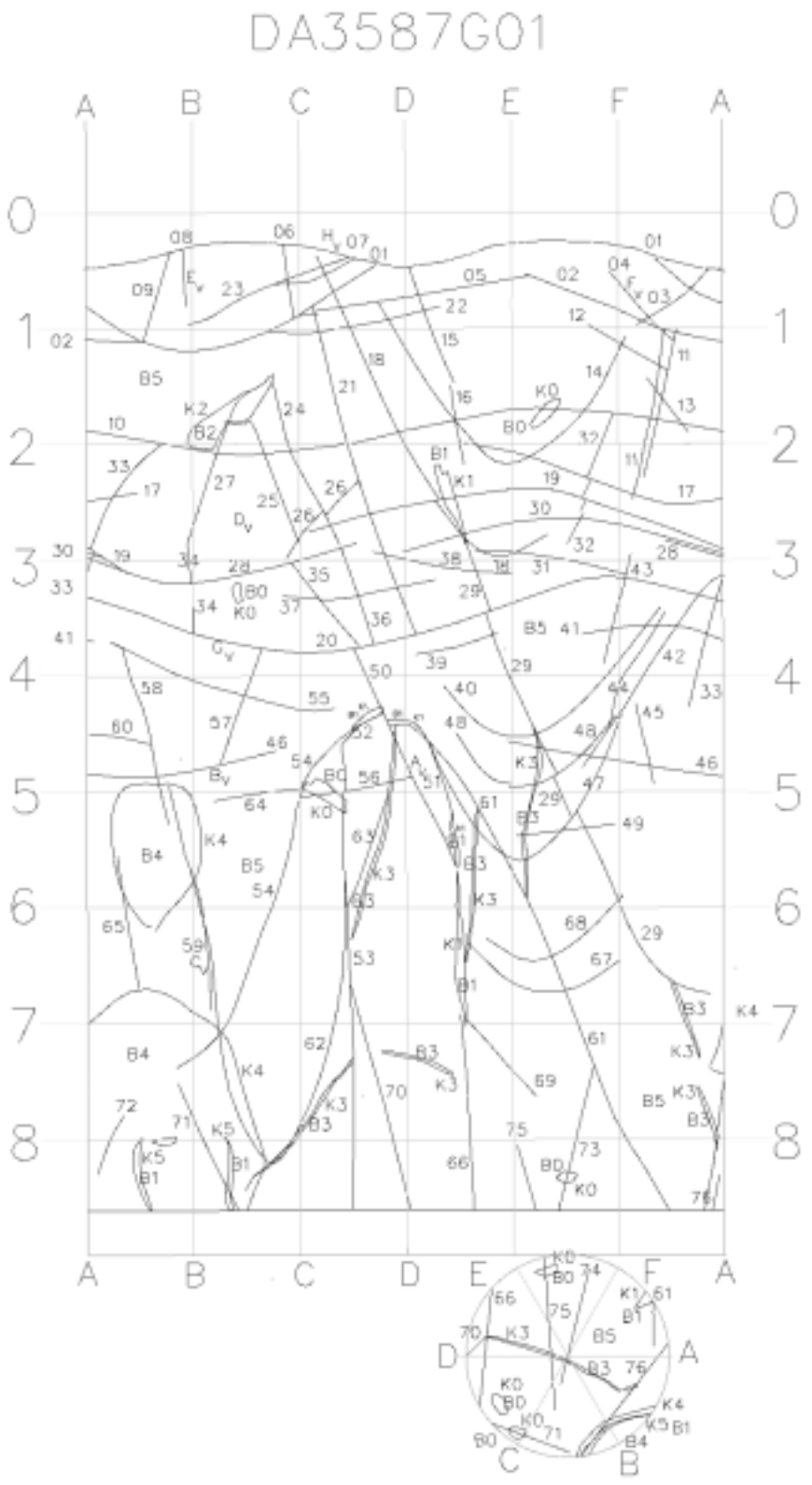

Figure D.22 *Measured trace map*

Appendix E

Inflow to TBM tunnel, G-tunnel and deposition holes

Table E.1 Inflow to tunnels when no deposition holes are excavated

Realization	TBM tunnel	G-tunnel
1	6.816	6.828
2	11.298	1.715
3	3.492	0.794
4	11.664	2.421
5	6.018	11.430
6	7.956	3.893
7	16.530	10.128
8	3.993	5.015
9	9.096	1.516
10	2.045	3.276
11	3.653	2.257
12	6.648	5.042
13	9.126	3.746
14	2.557	4.144
15	4.363	3.265
16	1.721	7.212
17	4.184	10.272
18	13.728	1.088
19	3.288	9.030
20	6.156	1.733

Table E.2 Inflow to tunnels and deposition hole 1 to 4 when the first 4 deposition holes are excavated

Realization	TBM tunnel	G-tunnel	Deposition hole 1	Deposition hole 2	Deposition hole 3	Deposition hole 4
1	6.534	6.822	0.286	0.793	3.541	0.299
2	10.590	1.700	0.771	1.712	2.746	1.813
3	3.405	0.792	0.342	0.189	0.610	1.177
4	11.418	2.410	0.075	0.276	1.196	0.337
5	5.642	11.412	0.372	0.745	1.076	3.107
6	7.158	3.880	0.128	0.136	0.901	2.980
7	14.064	10.032	0.513	0.000	0.008	18.666
8	3.452	4.963	3.211	2.956	0.956	3.391
9	8.466	1.516	1.225	0.000	0.000	0.455
10	1.982	3.270	0.606	0.446	0.848	0.270
11	2.083	2.249	2.126	1.156	0.038	11.202
12	6.264	5.038	3.895	0.048	0.002	0.529
13	8.916	3.745	1.603	1.541	0.268	0.034
14	2.263	4.139	0.308	1.463	1.349	0.265
15	4.150	3.245	0.229	0.715	1.355	1.668
16	1.400	7.176	0.902	3.565	1.608	5.288
17	3.185	10.242	0.248	5.666	1.233	0.266
18	13.326	1.086	0.244	0.028	1.940	0.008
19	2.897	9.024	0.599	0.513	4.087	0.475
20	4.492	1.661	5.653	0.234	0.019	10.680

Table E.3 Inflow to tunnels and deposition holes when all 6 deposition holes are excavated

Realization	TBM tunnel	G-tunnel	Deposition hole 1	Deposition hole 2	Deposition hole 3	Deposition hole 4	Deposition hole 5	Deposition hole 6
1	6.474	6.816	0.285	0.788	3.515	0.295	0.186	1.094
2	8.706	1.658	0.747	1.384	1.703	0.922	13.596	0.128
3	3.371	0.788	0.341	0.188	0.604	1.165	0.418	0.845
4	11.292	2.395	0.075	0.272	1.175	0.328	1.836	0.044
5	5.295	11.370	0.361	0.713	1.006	2.886	2.251	2.555
6	6.690	3.857	0.125	0.133	0.880	2.875	0.182	6.708
7	13.974	10.008	0.510	0.000	0.007	18.168	2.317	0.033
8	3.028	4.774	3.107	2.840	0.837	2.596	9.840	2.576
9	8.232	1.508	1.205	0.000	0.000	0.428	2.684	1.110
10	1.930	3.256	0.596	0.435	0.817	0.254	3.056	0.784
11	1.981	2.244	2.073	1.123	0.037	10.632	0.092	3.652
12	5.991	4.985	3.716	0.045	0.002	0.458	17.664	0.006
13	7.404	3.734	1.557	1.476	0.252	0.030	8.238	2.184
14	2.256	4.137	0.308	1.460	1.344	0.263	0.342	0.056
15	4.113	3.226	0.227	0.707	1.339	1.621	0.629	0.932
16	1.307	7.038	0.884	3.466	1.559	5.107	4.373	3.200
17	3.015	10.200	0.246	5.590	1.193	0.257	1.520	0.937
18	13.158	1.084	0.243	0.028	1.927	0.008	0.251	1.023
19	2.869	9.018	0.597	0.507	4.030	0.467	0.132	0.639
20	4.456	1.657	5.619	0.232	0.019	10.554	0.973	0.109

Appendix F

Drawdown in the monitoring borehole sections, steady state approach

The drawdown is the piezometric head change and it is expressed in metres. It is calculated for a steady state solution, i.e. there are no changes for pressure or flow in time. The head-field is calculated for three stages for the 20 stochastic realisations; in stage 1 are no deposition holes excavated, in stage 2 are holes #1-4 excavated and in stage 3 are all 6 deposition holes excavated. The drawdown is then calculated as the differense in head between stage 1 and 2, stage 1 and 3 and stage 2 and 3. This corresponds to drawdown due to excavation of deposition hole 1 to 4 (Diff 0-4), the drawdown due to excavation of all 6 boreholes (Diff 0-6) and the drawdown from 4 deposition holes to 6 deposition holes (Diff 4-6).

Table F.1. Drawdown in monitoring bore hole section for realisation 1 and 2. "Diff 0-4" is the draw down due to excavation of deposition holes 1 to 4, "Diff 0-6" is draw down due to excavation of all 6 deposition holes, and "Diff 4-6" is the difference in draw down between 4 excavated deposition holes and 6.

	Realisation 1			Realisation 2		
Borehole section	**Diff 0-4**	**Diff 0-6**	**Diff 4-6**	**Diff 0-4**	**Diff 0-6**	**Diff 4-6**
KA3539G (1.3-9.3 m)	-5.98	-115.88	-109.90	-21.85	-116.37	-94.52
KA3539G (9.8-18.3 m)	-	-	-	-27.37	-119.53	-92.15
KA3539G (19.3-30.01 m)	-5.53	-8.38	-2.85	-31.09	-127.84	-96.74
KA3542G01 (1.3-7.8 m)	-8.46	-69.42	-60.96	-60.13	-292.79	-232.66
KA3542G01 (8.8-24.8 m)	-7.52	-28.52	-21.00	-48.85	-227.70	-178.84
KA3542G01 (25.8-30.04 m)	-5.67	-13.25	-7.58	-14.86	-46.84	-31.98
KA3542G02 (1.3-7.8 m)	-5.63	-26.17	-20.54	-13.82	-60.90	-47.09
KA3542G02 (8.8-12.8 m)	-6.79	-15.76	-8.97	-6.79	-15.76	-8.97
KA3542G02 (13.8-21.3 m)	-4.43	-10.65	-6.22	-24.32	-95.39	-71.07
KA3542G02 (22.3-30.01 m)	-3.00	-6.33	-3.33	-5.29	-19.85	-14.55
KA3544G01 (1.3-5.3 m)	-10.51	-285.45	-274.94	-31.51	-264.31	-232.80
KA3544G01 (6.3-12 m)	-10.97	-324.53	-313.56	-37.00	-234.68	-197.68
KA3546G01 (1.3-5.8 m)	-7.83	-171.13	-163.30	-45.61	-363.97	-318.36
KA3546G01 (6.8-12 m)	-9.95	-73.86	-63.92	-49.24	-357.00	-307.76
KA3548A (10-14 m)	-14.50	-19.78	-5.28	-16.28	-45.10	-28.82
KA3548A (15-30 m)	-6.19	-8.14	-1.94	-14.08	-32.98	-18.89
KA3548G01 (0.3-12.01 m)	-10.72	-76.58	-65.86	-49.72	-290.97	-241.24
KA3550G01 (1.3-5.3 m)	-	-	-	-24.66	-135.14	-110.48
KA3550G01 (6.3-12.03 m)	-21.69	-340.68	-319.00	-47.72	-349.95	-302.23
KA3552G01 (0.3-3.05 m)	-	-	-	-	-	-
KA3552G01 (4.05-7.8 m)	-39.03	-332.20	-293.17	-64.50	-341.24	-276.75
KA3552G01 (8.8-12.01 m)	-	-	-	-	-	-
KA3554G01 (1.3-11.3 m)	-43.62	-51.87	-8.25	-83.25	-288.97	-205.72
KA3554G01 (12.3-21.3 m)	-43.13	-49.45	-6.32	-70.82	-252.87	-182.06
KA3554G01 (22.3-30.01 m)	-6.46	-11.63	-5.17	-6.46	-11.63	-5.17
KA3554G02 (1.3-9.3 m)	-27.76	-44.39	-16.63	-57.94	-290.18	-232.24
KA3554G02 (10.3-21.3 m)	-14.01	-20.96	-6.95	-23.94	-88.77	-64.83
KA3554G02 (22.3-30.01 m)	-7.31	-10.52	-3.21	-15.97	-56.77	-40.81
KA3557G (0.30-8 m)	-53.00	-57.21	-4.21	-66.36	-315.69	-249.33
KA3563G (1.3-9.3 m)	-	-	-	-	-	-
KA3563G (MOVED m)	-98.39	-102.64	-4.25	-123.47	-292.89	-169.43
KA3563G (9.3-30.00 m)	-19.57	-21.20	-1.63	-103.94	-285.24	-181.30
KA3566G01 (1.3-6.3 m)	-150.47	-154.17	-3.70	-97.27	-151.15	-53.89
KA3566G01 (7.3-11.3 m)	-98.02	-102.36	-4.34	-107.59	-183.65	-76.07
KA3566G01 (12.3-19.8 m)	-44.43	-48.84	-4.42	-37.32	-51.71	-14.39
KA3566G01 (20.8-30.01 m)	-21.22	-25.79	-4.58	-31.90	-44.65	-12.75
KA3566G02 (1.3-6.8 m)	-102.38	-106.27	-3.89	-105.85	-195.74	-89.89
KA3566G02 (7.8-11.3 m)	-65.03	-69.67	-4.64	-65.03	-69.67	-4.64
KA3566G02 (12.3-18.3 m)	-26.41	-30.54	-4.13	-41.41	-104.48	-63.08
KA3566G02 (19.3-30.01 m)	-8.69	-10.77	-2.08	-25.71	-65.27	-39.57
KA3572G01 (1.3-5.3 m)	-	-	-	-335.61	-355.45	-19.85
KA3572G01 (6.3-12.00 m)	-271.49	-273.05	-1.56	-268.16	-312.17	-44.01
KA3573A (4.5-17.0 m)	-29.41	-31.08	-1.67	-20.94	-30.68	-9.74
KA3573A (18.0-40.07 m)	-17.05	-18.29	-1.24	-8.92	-13.52	-4.60
KA3574G01 (8.8-12.00 m)	-	-	-	-274.20	-311.11	-36.92
KA3576G01 (1.3-2.8 m)	-	-	-	-	-	-
KA3576G01 (3.8-7.8 m)	-306.78	-307.44	-0.66	-353.30	-358.05	-4.75
KA3576G01 (8.8-12.01 m)	-	-	-	-343.19	-354.13	-10.94
KA3578G01 (1.3-5.8 m)	-156.71	-157.56	-0.85	-359.88	-363.31	-3.43
KA3578G01 (6.8-12.58 m)	-288.67	-289.39	-0.72	-332.95	-344.36	-11.41
KA3579G (1.3-4.3 m)	-358.65	-358.90	-0.25	-235.53	-236.70	-1.17
KA3579G (5.3-8.3 m)	-	-	-	-365.70	-367.81	-2.11
KA3579G (9.3-22.65 m)	-303.22	-303.98	-0.76	-299.74	-316.44	-16.70
KA3584G01 (0.3-12.00 m)	-280.07	-280.67	-0.60	-239.99	-250.29	-10.30
KA3590G01 (1.3-6.8 m)	-23.86	-24.53	-0.67	-59.86	-63.46	-3.60
KA3590G01 (7.8-16.3 m)	-22.44	-23.61	-1.18	-47.37	-52.61	-5.24
KA3590G01 (17.3-30.06 m)	-10.27	-11.45	-1.17	-9.20	-13.08	-3.88
KA3590G02 (1.3-7.3 m)	-64.94	-65.89	-0.95	-25.75	-31.30	-5.55
KA3590G02 (8.3-16.3 m)	-34.89	-35.94	-1.05	-78.95	-93.37	-14.42
KA3590G02 (17.3-22.3 m)	-	-	-	-57.44	-78.25	-20.81
KA3590G02 (23.3-30.05 m)	-23.19	-24.26	-1.07	-25.35	-36.59	-11.24
KA3593G (1.3-9.3 m)	-50.64	-52.10	-1.46	-136.24	-144.63	-8.39
KA3593G (MOVED m)	-17.88	-18.50	-0.62	-38.16	-47.34	-9.18
KA3600F (4.5-21.00 m)	-9.83	-10.36	-0.53	-1.08	-1.49	-0.41
KA3600F (22.00-50.10 m)	-0.46	-0.49	-0.03	-0.46	-0.64	-0.19
KA3510a (4.52-113.02 m)	-5.89	-14.29	-8.40	-2.27	-7.43	-5.16
KG0021A01 (4-16 m)	-2.57	-5.22	-2.65	-6.03	-23.12	-17.09
KG0021A01 (17-24 m)	-2.75	-5.57	-2.82	-5.92	-22.71	-16.79
KG0021A01 (25-34 m)	-3.31	-6.97	-3.65	-4.37	-13.58	-9.21
KG0021A01 (35-41.5 m)	-3.96	-8.86	-4.91	-5.51	-16.78	-11.27
KG0021A01 (42.5-48.8 m)	-5.11	-11.17	-6.06	-12.17	-31.18	-19.01
KG0048A01 (4-12 m)	-3.63	-4.94	-1.31	-9.07	-27.94	-18.86
KG0048A01 (13-29 m)	-13.38	-15.22	-1.85	-15.99	-35.57	-19.58
KG0048A01 (30-40 m)	-22.03	-24.12	-2.09	-10.90	-21.88	-10.99
KG0048A01 (41-48 m)	-20.21	-21.92	-1.71	-8.97	-14.87	-5.90
KG0048A01 (49-54.7 m)	-21.77	-23.22	-1.45	-9.45	-14.26	-4.82

Table F.2. Drawdown in monitoring bore hole section for realisation 3 and 4. "Diff 0-4" is the draw down due to excavation of deposition holes 1 to 4, "Diff 0-6" is draw down due to excavation of all 6 deposition holes, and "Diff 4-6" is the difference in draw down between 4 excavated deposition holes and 6.

	Realisation 3			Realisation 4		
Borehole section	**Diff 0-4**	**Diff 0-6**	**Diff 4-6**	**Diff 0-4**	**Diff 0-6**	**Diff 4-6**
KA3539G (1.3-9.3 m)	-2.05	-27.37	-25.32	-1.91	-8.45	-6.55
KA3539G (9.8-18.3 m)	-3.25	-49.70	-46.45	-4.34	-47.08	-42.74
KA3539G (19.3-30.01 m)	-31.09	-127.84	-96.74	-6.17	-62.21	-56.05
KA3542G01 (1.3-7.8 m)	-60.13	-292.79	-232.66	-60.13	-292.79	-232.66
KA3542G01 (8.8-24.8 m)	-10.00	-22.29	-12.29	-4.89	-29.92	-25.02
KA3542G01 (25.8-30.04 m)	-14.86	-46.84	-31.98	-4.15	-14.96	-10.81
KA3542G02 (1.3-7.8 m)	-2.85	-37.22	-34.37	-5.12	-184.51	-179.39
KA3542G02 (8.8-12.8 m)	-2.26	-23.98	-21.72	-4.53	-21.04	-16.52
KA3542G02 (13.8-21.3 m)	-24.32	-95.39	-71.07	-3.10	-11.66	-8.56
KA3542G02 (22.3-30.01 m)	-1.10	-5.36	-4.26	-3.91	-12.03	-8.12
KA3544G01 (1.3-5.3 m)	-	-452.90	-452.90	-6.53	-324.41	-317.88
KA3544G01 (6.3-12 m)	-5.83	-310.75	-304.92	-6.63	-182.41	-175.78
KA3546G01 (1.3-5.8 m)	-4.81	-91.28	-86.47	-3.88	-178.70	-174.82
KA3546G01 (6.8-12 m)	-6.73	-262.00	-255.27	-6.69	-226.97	-220.28
KA3548A (10-14 m)	-12.10	-19.37	-7.27	-5.90	-15.87	-9.97
KA3548A (15-30 m)	-3.54	-4.99	-1.45	-6.35	-10.24	-3.89
KA3548G01 (0.3-12.01 m)	-7.09	-282.65	-275.56	-6.81	-244.56	-237.75
KA3550G01 (1.3-5.3 m)	-24.66	-135.14	-110.48	-24.66	-135.14	-110.48
KA3550G01 (6.3-12.03 m)	-7.40	-301.73	-294.33	-6.90	-328.00	-321.10
KA3552G01 (0.3-3.05 m)	-	-	-	-	-	-
KA3552G01 (4.05-7.8 m)	-8.76	-326.17	-317.42	-8.76	-326.17	-317.42
KA3552G01 (8.8-12.01 m)	-7.76	-176.53	-168.77	-7.76	-176.53	-168.77
KA3554G01 (1.3-11.3 m)	-14.36	-33.94	-19.58	-19.36	-105.70	-86.35
KA3554G01 (12.3-21.3 m)	-10.14	-22.54	-12.40	-16.31	-52.45	-36.14
KA3554G01 (22.3-30.01 m)	-10.99	-15.84	-4.85	-8.03	-16.31	-8.28
KA3554G02 (1.3-9.3 m)	-8.35	-67.90	-59.55	-3.87	-76.18	-72.31
KA3554G02 (10.3-21.3 m)	-4.02	-17.92	-13.90	-6.16	-29.32	-23.16
KA3554G02 (22.3-30.01 m)	-3.47	-11.67	-8.19	-4.03	-12.44	-8.40
KA3557G (0.30-8 m)	-8.99	-30.00	-21.01	-11.72	-74.73	-63.01
KA3563G (1.3-9.3 m)	-8.36	-84.85	-76.49	-8.36	-84.85	-76.49
KA3563G (MOVED m)	-18.63	-44.27	-25.65	-18.63	-44.27	-25.65
KA3563G (9.3-30.00 m)	-103.94	-285.24	-181.30	-24.86	-35.03	-10.16
KA3566G01 (1.3-6.3 m)	-21.12	-23.96	-2.84	-21.12	-23.96	-2.84
KA3566G01 (7.3-11.3 m)	-21.43	-29.04	-7.61	-66.53	-73.72	-7.19
KA3566G01 (12.3-19.8 m)	-23.33	-27.49	-4.16	-27.07	-31.98	-4.91
KA3566G01 (20.8-30.01 m)	-14.88	-18.04	-3.17	-10.29	-16.04	-5.76
KA3566G02 (1.3-6.8 m)	-19.22	-26.14	-6.92	-19.14	-41.99	-22.85
KA3566G02 (7.8-11.3 m)	-15.47	-22.48	-7.01	-15.44	-37.79	-22.35
KA3566G02 (12.3-18.3 m)	-13.02	-20.75	-7.73	-7.91	-29.22	-21.31
KA3566G02 (19.3-30.01 m)	-9.95	-15.40	-5.45	-6.79	-19.78	-12.99
KA3572G01 (1.3-5.3 m)	-291.07	-293.01	-1.94	-291.07	-293.01	-1.94
KA3572G01 (6.3-12.00 m)	-327.95	-328.82	-0.88	-270.61	-272.97	-2.36
KA3573A (4.5-17.0 m)	-12.15	-14.28	-2.13	-20.19	-24.30	-4.10
KA3573A (18.0-40.07 m)	-2.09	-2.52	-0.43	-4.32	-5.82	-1.50
KA3574G01 (8.8-12.00 m)	-293.51	-294.72	-1.20	-34.63	-41.37	-6.74
KA3576G01 (1.3-2.8 m)	-	-	-	-	-	-
KA3576G01 (3.8-7.8 m)	-353.30	-358.05	-4.75	-296.86	-298.23	-1.37
KA3576G01 (8.8-12.01 m)	-343.19	-354.13	-10.94	-135.07	-139.66	-4.58
KA3578G01 (1.3-5.8 m)	-359.88	-363.31	-3.43	-359.88	-363.31	-3.43
KA3578G01 (6.8-12.58 m)	-145.22	-147.70	-2.48	-43.04	-49.45	-6.41
KA3579G (1.3-4.3 m)	-235.53	-236.70	-1.17	-269.57	-269.58	-0.01
KA3579G (5.3-8.3 m)	-365.70	-367.81	-2.11	-224.98	-227.58	-2.59
KA3579G (9.3-22.65 m)	-190.78	-192.70	-1.92	-41.03	-47.37	-6.35
KA3584G01 (0.3-12.00 m)	-49.45	-51.92	-2.48	-455.16	-455.16	0.00
KA3590G01 (1.3-6.8 m)	-15.26	-16.44	-1.19	-67.79	-71.94	-4.14
KA3590G01 (7.8-16.3 m)	-12.06	-13.18	-1.11	-12.06	-13.18	-1.11
KA3590G01 (17.3-30.06 m)	-7.85	-8.64	-0.79	-8.42	-10.64	-2.22
KA3590G02 (1.3-7.3 m)	-46.98	-48.14	-1.17	-30.57	-33.98	-3.40
KA3590G02 (8.3-16.3 m)	-13.20	-15.31	-2.11	-26.52	-30.11	-3.59
KA3590G02 (17.3-22.3 m)	-9.76	-11.90	-2.14	-9.76	-11.90	-2.14
KA3590G02 (23.3-30.05 m)	-13.48	-16.44	-2.96	-8.52	-14.02	-5.51
KA3593G (1.3-9.3 m)	-22.06	-23.44	-1.39	-60.02	-64.02	-4.00
KA3593G (MOVED m)	-11.51	-12.59	-1.08	-10.45	-12.15	-1.70
KA3600F (4.5-21.00 m)	-1.79	-2.01	-0.22	-1.51	-1.90	-0.39
KA3600F (22.00-50.10 m)	-0.52	-0.59	-0.07	-0.79	-1.00	-0.21
KA3510a (4.52-113.02 m)	-3.59	-6.57	-2.99	-3.64	-12.59	-8.96
KG0021A01 (4-16 m)	-0.94	-3.91	-2.98	-1.97	-6.27	-4.30
KG0021A01 (17-24 m)	-1.00	-5.65	-4.64	-2.93	-8.93	-6.00
KG0021A01 (25-34 m)	-3.76	-10.05	-6.28	-3.87	-10.96	-7.09
KG0021A01 (35-41.5 m)	-2.39	-4.17	-1.79	-3.94	-11.07	-7.14
KG0021A01 (42.5-48.8 m)	-3.20	-5.18	-1.97	-4.05	-9.22	-5.17
KG0048A01 (4-12 m)	-2.55	-6.01	-3.47	-3.74	-8.64	-4.90
KG0048A01 (13-29 m)	-5.96	-10.50	-4.54	-5.27	-12.06	-6.78
KG0048A01 (30-40 m)	-5.50	-6.87	-1.37	-6.03	-12.81	-6.79
KG0048A01 (41-48 m)	-6.97	-8.24	-1.27	-7.26	-10.29	-3.04
KG0048A01 (49-54.7 m)	-5.60	-6.51	-0.91	-28.27	-31.45	-3.18

Table F.3. Drawdown in monitoring bore hole section for realisation 5 and 6. "Diff 0-4" is the draw down due to excavation of deposition holes 1 to 4, "Diff 0-6" is draw down due to excavation of all 6 deposition holes, and "Diff 4-6" is the difference in draw down between 4 excavated deposition holes and 6.

	Realisation 5			Realisation 6		
Borehole section	**Diff 0-4**	**Diff 0-6**	**Diff 4-6**	**Diff 0-4**	**Diff 0-6**	**Diff 4-6**
KA3539G (1.3-9.3 m)	-13.88	-167.99	-154.11	-5.43	-160.98	-155.55
KA3539G (9.8-18.3 m)	-15.47	-154.24	-138.77	-4.60	-34.02	-29.42
KA3539G (19.3-30.01 m)	-12.66	-82.29	-69.63	-4.11	-29.76	-25.65
KA3542G01 (1.3-7.8 m)	-17.12	-209.31	-192.19	-6.39	-164.40	-158.00
KA3542G01 (8.8-24.8 m)	-11.25	-80.25	-69.00	-6.77	-94.88	-88.12
KA3542G01 (25.8-30.04 m)	-8.68	-19.38	-10.70	-5.69	-61.47	-55.78
KA3542G02 (1.3-7.8 m)	-8.87	-85.37	-76.51	-7.77	-38.37	-30.61
KA3542G02 (8.8-12.8 m)	-8.55	-71.33	-62.78	-8.55	-71.33	-62.78
KA3542G02 (13.8-21.3 m)	-8.84	-46.16	-37.32	-8.84	-46.16	-37.32
KA3542G02 (22.3-30.01 m)	-3.59	-16.43	-12.84	-3.28	-11.20	-7.92
KA3544G01 (1.3-5.3 m)	-23.61	-346.34	-322.72	-7.50	-330.75	-323.25
KA3544G01 (6.3-12 m)	-22.95	-254.65	-231.70	-22.95	-254.65	-231.70
KA3546G01 (1.3-5.8 m)	-25.06	-366.49	-341.44	-4.01	-155.89	-151.89
KA3546G01 (6.8-12 m)	-26.71	-336.00	-309.29	-6.24	-247.40	-241.16
KA3548A (10-14 m)	-16.38	-33.08	-16.70	-5.89	-36.55	-30.66
KA3548A (15-30 m)	-8.13	-16.39	-8.26	-3.82	-17.99	-14.17
KA3548G01 (0.3-12.01 m)	-27.51	-347.59	-320.08	-6.94	-264.79	-257.85
KA3550G01 (1.3-5.3 m)	-29.76	-336.80	-307.04	-29.76	-336.80	-307.04
KA3550G01 (6.3-12.03 m)	-32.53	-293.91	-261.39	-7.28	-363.89	-356.62
KA3552G01 (0.3-3.05 m)	-	-	-	-	-	-
KA3552G01 (4.05-7.8 m)	-31.85	-364.40	-332.55	-22.62	-211.07	-188.45
KA3552G01 (8.8-12.01 m)	-7.76	-176.53	-168.77	-7.76	-176.53	-168.77
KA3554G01 (1.3-11.3 m)	-36.64	-79.30	-42.66	-24.11	-60.82	-36.71
KA3554G01 (12.3-21.3 m)	-26.42	-59.01	-32.60	-15.92	-67.19	-51.26
KA3554G01 (22.3-30.01 m)	-21.34	-41.01	-19.67	-15.16	-42.46	-27.30
KA3554G02 (1.3-9.3 m)	-31.01	-230.66	-199.65	-8.13	-38.91	-30.79
KA3554G02 (10.3-21.3 m)	-13.29	-71.14	-57.85	-8.30	-31.70	-23.39
KA3554G02 (22.3-30.01 m)	-11.85	-43.90	-32.05	-4.08	-14.70	-10.62
KA3557G (0.30-8 m)	-40.61	-104.45	-63.84	-8.23	-12.49	-4.26
KA3563G (1.3-9.3 m)	-8.36	-84.85	-76.49	-25.45	-32.50	-7.06
KA3563G (MOVED m)	-140.26	-174.31	-34.05	-39.26	-49.54	-10.27
KA3563G (9.3-30.00 m)	-65.51	-116.27	-50.76	-31.31	-37.43	-6.12
KA3566G01 (1.3-6.3 m)	-112.60	-131.75	-19.15	-158.45	-166.47	-8.02
KA3566G01 (7.3-11.3 m)	-66.53	-73.72	-7.19	-36.22	-55.41	-19.19
KA3566G01 (12.3-19.8 m)	-54.44	-70.47	-16.03	-28.11	-41.47	-13.36
KA3566G01 (20.8-30.01 m)	-26.53	-44.04	-17.51	-16.86	-28.58	-11.72
KA3566G02 (1.3-6.8 m)	-112.40	-146.84	-34.44	-33.26	-40.45	-7.19
KA3566G02 (7.8-11.3 m)	-94.31	-147.60	-53.29	-94.31	-147.60	-53.29
KA3566G02 (12.3-18.3 m)	-48.86	-118.92	-70.06	-17.37	-28.64	-11.27
KA3566G02 (19.3-30.01 m)	-44.33	-90.37	-46.04	-8.53	-15.85	-7.32
KA3572G01 (1.3-5.3 m)	-360.44	-363.05	-2.61	-360.44	-363.05	-2.61
KA3572G01 (6.3-12.00 m)	-324.47	-329.94	-5.47	-266.19	-268.62	-2.43
KA3573A (4.5-17.0 m)	-31.20	-46.46	-15.25	-18.03	-28.61	-10.58
KA3573A (18.0-40.07 m)	-3.83	-5.63	-1.80	-8.75	-17.67	-8.92
KA3574G01 (8.8-12.00 m)	-34.63	-41.37	-6.74	-322.75	-323.77	-1.02
KA3576G01 (1.3-2.8 m)	-	-	-	-120.56	-121.46	-0.90
KA3576G01 (3.8-7.8 m)	-340.78	-343.32	-2.54	-328.28	-329.23	-0.94
KA3576G01 (8.8-12.01 m)	-135.07	-139.66	-4.58	-296.60	-298.40	-1.81
KA3578G01 (1.3-5.8 m)	-251.65	-252.74	-1.09	-249.47	-251.41	-1.94
KA3578G01 (6.8-12.58 m)	-43.04	-49.45	-6.41	-43.04	-49.45	-6.41
KA3579G (1.3-4.3 m)	-271.10	-271.84	-0.74	-271.10	-271.84	-0.74
KA3579G (5.3-8.3 m)	-356.77	-358.45	-1.68	-358.84	-359.06	-0.23
KA3579G (9.3-22.65 m)	-184.54	-191.13	-6.59	-72.27	-78.09	-5.82
KA3584G01 (0.3-12.00 m)	-229.73	-235.10	-5.37	-151.89	-155.46	-3.57
KA3590G01 (1.3-6.8 m)	-76.22	-83.40	-7.18	-21.57	-25.18	-3.61
KA3590G01 (7.8-16.3 m)	-12.06	-13.18	-1.11	-25.30	-30.94	-5.64
KA3590G01 (17.3-30.06 m)	-19.51	-22.48	-2.97	-10.52	-15.19	-4.67
KA3590G02 (1.3-7.3 m)	-30.57	-33.98	-3.40	-51.92	-53.22	-1.30
KA3590G02 (8.3-16.3 m)	-84.52	-90.31	-5.79	-62.82	-67.44	-4.61
KA3590G02 (17.3-22.3 m)	-42.57	-52.01	-9.44	-42.57	-52.01	-9.44
KA3590G02 (23.3-30.05 m)	-30.47	-41.41	-10.94	-23.38	-27.88	-4.50
KA3593G (1.3-9.3 m)	-99.28	-108.75	-9.47	-48.43	-56.11	-7.68
KA3593G (MOVED m)	-57.03	-61.69	-4.66	-29.86	-33.43	-3.57
KA3600F (4.5-21.00 m)	-6.94	-8.68	-1.74	-3.16	-4.67	-1.51
KA3600F (22.00-50.10 m)	-1.33	-1.64	-0.31	-0.69	-1.14	-0.45
KA3510a (4.52-113.02 m)	-4.05	-14.62	-10.56	-5.79	-71.92	-66.13
KG0021A01 (4-16 m)	-1.72	-7.44	-5.72	-2.02	-9.38	-7.35
KG0021A01 (17-24 m)	-1.98	-8.45	-6.47	-3.89	-17.27	-13.38
KG0021A01 (25-34 m)	-6.29	-11.85	-5.55	-4.15	-19.40	-15.25
KG0021A01 (35-41.5 m)	-8.58	-15.36	-6.78	-8.58	-15.36	-6.78
KG0021A01 (42.5-48.8 m)	-9.54	-16.18	-6.64	-5.64	-35.67	-30.04
KG0048A01 (4-12 m)	-5.34	-11.00	-5.66	-6.56	-12.79	-6.24
KG0048A01 (13-29 m)	-20.76	-35.82	-15.06	-9.09	-15.45	-6.35
KG0048A01 (30-40 m)	-44.80	-58.25	-13.45	-7.36	-15.88	-8.52
KG0048A01 (41-48 m)	-12.37	-17.05	-4.68	-5.60	-11.76	-6.15
KG0048A01 (49-54.7 m)	-15.06	-21.96	-6.91	-12.03	-20.06	-8.03

Table F.4. Drawdown in monitoring bore hole section for realisation 7 and 8. "Diff 0-4" is the draw down due to excavation of deposition holes 1 to 4, "Diff 0-6" is draw down due to excavation of all 6 deposition holes, and "Diff 4-6" is the difference in draw down between 4 excavated deposition holes and 6.

	Realisation 7			Realisation 8		
Borehole section	**Diff 0-4**	**Diff 0-6**	**Diff 4-6**	**Diff 0-4**	**Diff 0-6**	**Diff 4-6**
KA3539G (1.3-9.3 m)	-43.25	-67.84	-24.58	-24.94	-206.84	-181.91
KA3539G (9.8-18.3 m)	-41.23	-63.71	-22.48	-41.23	-63.71	-22.48
KA3539G (19.3-30.01 m)	-4.11	-29.76	-25.65	-4.11	-29.76	-25.65
KA3542G01 (1.3-7.8 m)	-68.87	-174.32	-105.45	-25.26	-232.26	-207.01
KA3542G01 (8.8-24.8 m)	-72.92	-145.74	-72.82	-28.46	-231.75	-203.29
KA3542G01 (25.8-30.04 m)	-73.02	-80.41	-7.39	-14.84	-63.34	-48.50
KA3542G02 (1.3-7.8 m)	-45.42	-68.32	-22.90	-31.13	-188.30	-157.17
KA3542G02 (8.8-12.8 m)	-46.25	-67.52	-21.27	-29.00	-151.99	-122.98
KA3542G02 (13.8-21.3 m)	-43.76	-61.07	-17.31	-43.76	-61.07	-17.31
KA3542G02 (22.3-30.01 m)	-28.13	-37.46	-9.33	-12.72	-81.72	-69.00
KA3544G01 (1.3-5.3 m)	-60.20	-315.78	-255.58	-18.88	-199.34	-180.46
KA3544G01 (6.3-12 m)	-22.95	-254.65	-231.70	-27.89	-281.56	-253.67
KA3546G01 (1.3-5.8 m)	-4.01	-155.89	-151.89	-31.29	-316.97	-285.68
KA3546G01 (6.8-12 m)	-74.06	-389.76	-315.70	-34.82	-288.54	-253.72
KA3548A (10-14 m)	-58.36	-69.77	-11.41	-18.03	-67.30	-49.27
KA3548A (15-30 m)	-62.18	-71.23	-9.05	-13.70	-50.01	-36.32
KA3548G01 (0.3-12.01 m)	-74.31	-292.47	-218.16	-38.22	-326.91	-288.70
KA3550G01 (1.3-5.3 m)	-29.76	-336.80	-307.04	-39.88	-397.91	-358.03
KA3550G01 (6.3-12.03 m)	-77.49	-385.81	-308.32	-40.34	-372.87	-332.53
KA3552G01 (0.3-3.05 m)	-132.42	-180.78	-48.36	-132.42	-180.78	-48.36
KA3552G01 (4.05-7.8 m)	-98.77	-353.40	-254.63	-98.77	-353.40	-254.63
KA3552G01 (8.8-12.01 m)	-91.75	-170.54	-78.79	-40.37	-384.05	-343.68
KA3554G01 (1.3-11.3 m)	-127.10	-146.99	-19.89	-13.22	-68.65	-55.43
KA3554G01 (12.3-21.3 m)	-161.72	-170.04	-8.31	-57.39	-95.82	-38.43
KA3554G01 (22.3-30.01 m)	-175.31	-179.04	-3.73	-51.85	-80.44	-28.59
KA3554G02 (1.3-9.3 m)	-91.17	-133.11	-41.94	-44.39	-301.74	-257.34
KA3554G02 (10.3-21.3 m)	-53.70	-72.03	-18.33	-38.27	-163.69	-125.42
KA3554G02 (22.3-30.01 m)	-44.94	-59.90	-14.96	-29.86	-122.30	-92.44
KA3557G (0.30-8 m)	-153.12	-167.60	-14.48	-97.90	-177.93	-80.04
KA3563G (1.3-9.3 m)	-27.16	-27.69	-0.52	-89.64	-119.39	-29.75
KA3563G (MOVED m)	-238.85	-246.62	-7.76	-238.85	-246.62	-7.76
KA3563G (9.3-30.00 m)	-329.55	-330.89	-1.35	-110.32	-133.61	-23.29
KA3566G01 (1.3-6.3 m)	-158.45	-166.47	-8.02	-252.10	-274.31	-22.22
KA3566G01 (7.3-11.3 m)	-36.22	-55.41	-19.19	-164.67	-186.73	-22.06
KA3566G01 (12.3-19.8 m)	-117.08	-120.05	-2.97	-87.24	-107.08	-19.84
KA3566G01 (20.8-30.01 m)	-69.39	-72.40	-3.01	-51.50	-64.42	-12.92
KA3566G02 (1.3-6.8 m)	-164.60	-173.31	-8.70	-176.85	-247.60	-70.75
KA3566G02 (7.8-11.3 m)	-110.89	-125.34	-14.45	-105.88	-208.21	-102.32
KA3566G02 (12.3-18.3 m)	-87.13	-105.27	-18.13	-61.14	-145.20	-84.06
KA3566G02 (19.3-30.01 m)	-47.81	-58.80	-10.99	-19.00	-54.21	-35.22
KA3572G01 (1.3-5.3 m)	-31.81	-31.80	0.01	-31.81	-31.80	0.01
KA3572G01 (6.3-12.00 m)	-255.16	-256.90	-1.74	-374.77	-379.76	-5.00
KA3573A (4.5-17.0 m)	-55.54	-58.55	-3.01	-76.91	-93.60	-16.69
KA3573A (18.0-40.07 m)	-12.07	-12.70	-0.63	-23.05	-29.32	-6.28
KA3574G01 (8.8-12.00 m)	-322.75	-323.77	-1.02	-362.65	-368.97	-6.32
KA3576G01 (1.3-2.8 m)	-120.56	-121.46	-0.90	-120.56	-121.46	-0.90
KA3576G01 (3.8-7.8 m)	-328.28	-329.23	-0.94	-395.55	-396.64	-1.09
KA3576G01 (8.8-12.01 m)	-155.08	-157.53	-2.45	-155.08	-157.53	-2.45
KA3578G01 (1.3-5.8 m)	-249.47	-251.41	-1.94	-249.47	-251.41	-1.94
KA3578G01 (6.8-12.58 m)	-130.28	-132.98	-2.70	-363.93	-367.60	-3.67
KA3579G (1.3-4.3 m)	-271.10	-271.84	-0.74	-271.10	-271.84	-0.74
KA3579G (5.3-8.3 m)	-358.84	-359.06	-0.23	-386.25	-387.85	-1.60
KA3579G (9.3-22.65 m)	-138.65	-140.77	-2.12	-179.68	-188.62	-8.94
KA3584G01 (0.3-12.00 m)	-93.93	-95.96	-2.04	-224.88	-230.75	-5.88
KA3590G01 (1.3-6.8 m)	-88.91	-90.40	-1.49	-121.79	-127.45	-5.66
KA3590G01 (7.8-16.3 m)	-52.41	-53.57	-1.16	-166.00	-173.45	-7.44
KA3590G01 (17.3-30.06 m)	-38.76	-39.80	-1.04	-67.20	-72.59	-5.39
KA3590G02 (1.3-7.3 m)	-51.92	-53.22	-1.30	-158.75	-166.70	-7.96
KA3590G02 (8.3-16.3 m)	-61.10	-65.80	-4.70	-141.67	-151.06	-9.39
KA3590G02 (17.3-22.3 m)	-90.50	-95.75	-5.25	-55.05	-78.35	-23.31
KA3590G02 (23.3-30.05 m)	-82.86	-88.34	-5.47	-26.06	-46.40	-20.34
KA3593G (1.3-9.3 m)	-71.26	-72.40	-1.14	-163.55	-171.06	-7.51
KA3593G (MOVED m)	-73.22	-74.40	-1.18	-158.60	-166.45	-7.84
KA3600F (4.5-21.00 m)	-15.47	-16.07	-0.59	-11.76	-13.41	-1.65
KA3600F (22.00-50.10 m)	-3.40	-3.54	-0.15	-5.16	-5.95	-0.79
KA3510a (4.52-113.02 m)	-5.21	-5.47	-0.26	-4.89	-12.26	-7.37
KG0021A01 (4-16 m)	-8.83	-11.61	-2.78	-6.68	-39.68	-33.00
KG0021A01 (17-24 m)	-29.31	-39.89	-10.58	-12.02	-62.14	-50.12
KG0021A01 (25-34 m)	-41.36	-56.21	-14.85	-13.50	-66.81	-53.32
KG0021A01 (35-41.5 m)	-39.69	-51.81	-12.12	-16.83	-80.30	-63.47
KG0021A01 (42.5-48.8 m)	-41.60	-47.86	-6.26	-21.03	-68.77	-47.74
KG0048A01 (4-12 m)	-32.23	-41.65	-9.42	-7.25	-26.22	-18.97
KG0048A01 (13-29 m)	-61.63	-70.09	-8.46	-42.34	-135.39	-93.04
KG0048A01 (30-40 m)	-50.47	-57.17	-6.70	-36.15	-63.26	-27.11
KG0048A01 (41-48 m)	-30.58	-33.34	-2.76	-34.49	-52.34	-17.85
KG0048A01 (49-54.7 m)	-15.76	-16.74	-0.98	-41.22	-55.52	-14.30

Table F.5. Drawdown in monitoring bore hole section for realisation 9 and 10. "Diff 0-4" is the draw down due to excavation of deposition holes 1 to 4, "Diff 0-6" is draw down due to excavation of all 6 deposition holes, and "Diff 4-6" is the difference in draw down between 4 excavated deposition holes and 6.

	Realisation 9			Realisation 10		
Borehole section	**Diff 0-4**	**Diff 0-6**	**Diff 4-6**	**Diff 0-4**	**Diff 0-6**	**Diff 4-6**
KA3539G (1.3-9.3 m)	-1.21	-104.12	-102.91	-2.69	-58.03	-55.34
KA3539G (9.8-18.3 m)	-1.37	-81.14	-79.77	-1.37	-81.14	-79.77
KA3539G (19.3-30.01 m)	-0.89	-23.91	-23.02	-3.49	-89.14	-85.65
KA3542G01 (1.3-7.8 m)	-2.11	-161.94	-159.82	-3.78	-83.24	-79.46
KA3542G01 (8.8-24.8 m)	-2.06	-41.39	-39.32	-4.71	-56.97	-52.26
KA3542G01 (25.8-30.04 m)	-2.47	-31.22	-28.75	-2.47	-31.22	-28.75
KA3542G02 (1.3-7.8 m)	-0.97	-52.37	-51.40	-0.97	-52.37	-51.40
KA3542G02 (8.8-12.8 m)	-0.93	-48.57	-47.64	-0.93	-48.57	-47.64
KA3542G02 (13.8-21.3 m)	-0.86	-42.14	-41.29	-1.56	-9.68	-8.12
KA3542G02 (22.3-30.01 m)	-0.37	-11.88	-11.50	-1.52	-8.84	-7.32
KA3544G01 (1.3-5.3 m)	-1.80	-340.71	-338.92	-5.06	-399.00	-393.93
KA3544G01 (6.3-12 m)	-1.82	-275.08	-273.26	-5.38	-420.96	-415.59
KA3546G01 (1.3-5.8 m)	-2.52	-361.88	-359.36	-2.52	-361.88	-359.36
KA3546G01 (6.8-12 m)	-2.33	-352.51	-350.18	-6.33	-333.91	-327.58
KA3548A (10-14 m)	-2.87	-49.23	-46.36	-2.87	-49.23	-46.36
KA3548A (15-30 m)	-2.87	-27.14	-24.27	-3.79	-14.74	-10.94
KA3548G01 (0.3-12.01 m)	-2.62	-342.29	-339.67	-7.11	-350.82	-343.71
KA3550G01 (1.3-5.3 m)	-1.86	-225.82	-223.96	-10.81	-375.28	-364.46
KA3550G01 (6.3-12.03 m)	-2.72	-380.17	-377.44	-7.31	-394.37	-387.06
KA3552G01 (0.3-3.05 m)	-132.42	-180.78	-48.36	-132.42	-180.78	-48.36
KA3552G01 (4.05-7.8 m)	-3.06	-308.14	-305.08	-8.27	-380.92	-372.65
KA3552G01 (8.8-12.01 m)	-3.05	-269.25	-266.19	-3.05	-269.25	-266.19
KA3554G01 (1.3-11.3 m)	-3.52	-90.71	-87.19	-9.69	-177.97	-168.28
KA3554G01 (12.3-21.3 m)	-3.49	-65.27	-61.77	-9.00	-40.52	-31.52
KA3554G01 (22.3-30.01 m)	-2.33	-25.98	-23.66	-7.22	-34.07	-26.85
KA3554G02 (1.3-9.3 m)	-3.57	-55.92	-52.35	-15.91	-51.04	-35.13
KA3554G02 (10.3-21.3 m)	-2.68	-59.31	-56.63	-10.55	-107.90	-97.35
KA3554G02 (22.3-30.01 m)	-0.77	-15.85	-15.08	-1.92	-10.75	-8.83
KA3557G (0.30-8 m)	-3.04	-95.40	-92.36	-12.16	-116.29	-104.14
KA3563G (1.3-9.3 m)	-2.25	-14.01	-11.76	-16.71	-57.96	-41.25
KA3563G (MOVED m)	-12.93	-74.63	-61.70	-17.12	-71.97	-54.86
KA3563G (9.3-30.00 m)	-12.09	-57.95	-45.86	-17.41	-45.51	-28.10
KA3566G01 (1.3-6.3 m)	-22.96	-22.97	0.00	-22.56	-35.00	-12.44
KA3566G01 (7.3-11.3 m)	-10.89	-39.95	-29.06	-43.91	-57.99	-14.08
KA3566G01 (12.3-19.8 m)	-11.13	-28.83	-17.71	-15.68	-32.73	-17.05
KA3566G01 (20.8-30.01 m)	-3.13	-15.68	-12.55	-10.33	-24.24	-13.91
KA3566G02 (1.3-6.8 m)	-13.05	-73.02	-59.98	-18.14	-48.42	-30.28
KA3566G02 (7.8-11.3 m)	-3.77	-33.25	-29.47	-16.15	-45.00	-28.85
KA3566G02 (12.3-18.3 m)	-3.47	-13.16	-9.69	-12.79	-36.17	-23.38
KA3566G02 (19.3-30.01 m)	-2.00	-9.79	-7.79	-6.34	-17.66	-11.32
KA3572G01 (1.3-5.3 m)	-31.81	-31.80	0.01	-260.74	-267.39	-6.64
KA3572G01 (6.3-12.00 m)	-81.98	-88.94	-6.96	-213.98	-223.92	-9.94
KA3573A (4.5-17.0 m)	-6.99	-24.89	-17.91	-12.53	-24.39	-11.86
KA3573A (18.0-40.07 m)	-3.36	-8.29	-4.94	-5.70	-11.86	-6.16
KA3574G01 (8.8-12.00 m)	-362.65	-368.97	-6.32	-240.27	-247.39	-7.12
KA3576G01 (1.3-2.8 m)	-120.56	-121.46	-0.90	-120.56	-121.46	-0.90
KA3576G01 (3.8-7.8 m)	-395.55	-396.64	-1.09	-341.37	-343.68	-2.31
KA3576G01 (8.8-12.01 m)	-155.08	-157.53	-2.45	-162.88	-171.39	-8.51
KA3578G01 (1.3-5.8 m)	-249.47	-251.41	-1.94	-312.53	-315.48	-2.95
KA3578G01 (6.8-12.58 m)	-363.93	-367.60	-3.67	-125.69	-134.34	-8.65
KA3579G (1.3-4.3 m)	-271.10	-271.84	-0.74	-271.10	-271.84	-0.74
KA3579G (5.3-8.3 m)	-386.25	-387.85	-1.60	-344.37	-346.38	-2.01
KA3579G (9.3-22.65 m)	-31.05	-37.35	-6.30	-71.98	-81.09	-9.11
KA3584G01 (0.3-12.00 m)	-158.30	-161.96	-3.65	-140.45	-146.18	-5.72
KA3590G01 (1.3-6.8 m)	-12.87	-14.91	-2.04	-35.89	-40.85	-4.96
KA3590G01 (7.8-16.3 m)	-10.65	-15.53	-4.88	-23.77	-28.28	-4.51
KA3590G01 (17.3-30.06 m)	-9.08	-13.69	-4.61	-5.74	-8.65	-2.91
KA3590G02 (1.3-7.3 m)	-40.44	-45.03	-4.59	-67.88	-72.71	-4.84
KA3590G02 (8.3-16.3 m)	-24.11	-28.68	-4.57	-23.85	-30.02	-6.17
KA3590G02 (17.3-22.3 m)	-12.37	-18.99	-6.61	-16.09	-22.28	-6.19
KA3590G02 (23.3-30.05 m)	-4.47	-10.93	-6.46	-8.54	-14.53	-5.99
KA3593G (1.3-9.3 m)	-40.27	-47.27	-7.00	-52.62	-57.81	-5.20
KA3593G (MOVED m)	-20.90	-26.14	-5.23	-15.89	-19.46	-3.57
KA3600F (4.5-21.00 m)	-2.13	-3.29	-1.16	-3.89	-5.45	-1.56
KA3600F (22.00-50.10 m)	-0.44	-0.71	-0.27	-0.58	-0.86	-0.28
KA3510a (4.52-113.02 m)	-0.72	-6.11	-5.39	-5.46	-37.85	-32.39
KG0021A01 (4-16 m)	-0.68	-20.55	-19.87	-1.23	-6.57	-5.34
KG0021A01 (17-24 m)	-0.80	-23.91	-23.11	-1.54	-7.26	-5.72
KG0021A01 (25-34 m)	-0.72	-9.24	-8.52	-1.91	-7.33	-5.42
KG0021A01 (35-41.5 m)	-1.35	-13.44	-12.09	-1.92	-8.44	-6.52
KG0021A01 (42.5-48.8 m)	-2.18	-15.12	-12.94	-2.89	-8.12	-5.23
KG0048A01 (4-12 m)	-0.81	-5.88	-5.08	-1.71	-5.85	-4.15
KG0048A01 (13-29 m)	-3.13	-14.26	-11.14	-3.70	-8.54	-4.84
KG0048A01 (30-40 m)	-4.05	-15.69	-11.64	-4.18	-8.42	-4.25
KG0048A01 (41-48 m)	-4.15	-10.77	-6.62	-4.89	-8.93	-4.04
KG0048A01 (49-54.7 m)	-3.02	-8.15	-5.12	-9.05	-17.06	-8.01

Table F.6. Drawdown in monitoring bore hole section for realisation 11 and 12. "Diff 0-4" is the draw down due to excavation of deposition holes 1 to 4, "Diff 0-6" is draw down due to excavation of all 6 deposition holes, and "Diff 4-6" is the difference in draw down between 4 excavated deposition holes and 6.

	Realisation 11			Realisation 12		
Borehole section	**Diff 0-4**	**Diff 0-6**	**Diff 4-6**	**Diff 0-4**	**Diff 0-6**	**Diff 4-6**
KA3539G (1.3-9.3 m)	-39.43	-125.66	-86.24	-39.43	-125.66	-86.24
KA3539G (9.8-18.3 m)	-33.07	-99.73	-66.66	-5.26	-189.50	-184.24
KA3539G (19.3-30.01 m)	-40.88	-112.89	-72.00	-3.84	-97.57	-93.73
KA3542G01 (1.3-7.8 m)	-52.17	-96.08	-43.91	-4.78	-185.32	-180.54
KA3542G01 (8.8-24.8 m)	-64.25	-95.04	-30.79	-4.94	-197.85	-192.91
KA3542G01 (25.8-30.04 m)	-41.23	-50.59	-9.36	-2.98	-53.31	-50.32
KA3542G02 (1.3-7.8 m)	-16.79	-33.93	-17.14	-8.99	-187.68	-178.69
KA3542G02 (8.8-12.8 m)	-14.83	-27.49	-12.66	-5.16	-147.60	-142.44
KA3542G02 (13.8-21.3 m)	-13.10	-23.58	-10.48	-4.60	-109.09	-104.49
KA3542G02 (22.3-30.01 m)	-3.75	-6.38	-2.63	-2.38	-35.55	-33.17
KA3544G01 (1.3-5.3 m)	-57.71	-393.19	-335.48	-9.71	-264.54	-254.83
KA3544G01 (6.3-12 m)	-48.43	-177.33	-128.90	-48.43	-177.33	-128.90
KA3546G01 (1.3-5.8 m)	-57.98	-285.89	-227.91	-57.98	-285.89	-227.91
KA3546G01 (6.8-12 m)	-60.33	-326.02	-265.69	-	-456.84	-456.84
KA3548A (10-14 m)	-97.19	-113.12	-15.93	-6.05	-98.72	-92.67
KA3548A (15-30 m)	-63.03	-71.97	-8.94	-6.36	-27.00	-20.64
KA3548G01 (0.3-12.01 m)	-67.28	-309.10	-241.82	-7.41	-375.45	-368.05
KA3550G01 (1.3-5.3 m)	-10.81	-375.28	-364.46	-9.12	-321.54	-312.42
KA3550G01 (6.3-12.03 m)	-70.71	-376.99	-306.28	-9.07	-328.41	-319.34
KA3552G01 (0.3-3.05 m)	-132.42	-180.78	-48.36	-132.42	-180.78	-48.36
KA3552G01 (4.05-7.8 m)	-8.27	-380.92	-372.65	-8.27	-380.92	-372.65
KA3552G01 (8.8-12.01 m)	-3.05	-269.25	-266.19	-3.05	-269.25	-266.19
KA3554G01 (1.3-11.3 m)	-93.42	-140.50	-47.07	-47.81	-140.88	-93.07
KA3554G01 (12.3-21.3 m)	-133.98	-147.35	-13.38	-6.75	-130.82	-124.07
KA3554G01 (22.3-30.01 m)	-97.92	-107.76	-9.83	-8.87	-94.63	-85.76
KA3554G02 (1.3-9.3 m)	-73.95	-216.04	-142.09	-9.62	-181.47	-171.85
KA3554G02 (10.3-21.3 m)	-20.53	-36.07	-15.54	-6.25	-195.64	-189.39
KA3554G02 (22.3-30.01 m)	-10.98	-18.12	-7.15	-4.02	-56.62	-52.60
KA3557G (0.30-8 m)	-80.69	-144.16	-63.47	-6.75	-52.63	-45.88
KA3563G (1.3-9.3 m)	-16.71	-57.96	-41.25	-209.84	-212.41	-2.57
KA3563G (MOVED m)	-159.31	-196.75	-37.44	-72.75	-131.22	-58.48
KA3563G (9.3-30.00 m)	-90.94	-138.91	-47.97	-12.52	-49.89	-37.37
KA3566G01 (1.3-6.3 m)	-222.08	-224.25	-2.17	-53.42	-82.00	-28.58
KA3566G01 (7.3-11.3 m)	-43.91	-57.99	-14.08	-45.16	-72.84	-27.68
KA3566G01 (12.3-19.8 m)	-256.78	-261.21	-4.43	-27.28	-57.01	-29.74
KA3566G01 (20.8-30.01 m)	-128.14	-132.89	-4.75	-23.78	-54.41	-30.63
KA3566G02 (1.3-6.8 m)	-93.04	-144.31	-51.27	-265.55	-268.23	-2.68
KA3566G02 (7.8-11.3 m)	-82.39	-159.10	-76.71	-26.87	-110.15	-83.28
KA3566G02 (12.3-18.3 m)	-63.36	-103.37	-40.01	-8.92	-113.94	-105.02
KA3566G02 (19.3-30.01 m)	-17.35	-26.53	-9.18	-4.46	-67.24	-62.78
KA3572G01 (1.3-5.3 m)	-260.74	-267.39	-6.64	-65.83	-70.05	-4.21
KA3572G01 (6.3-12.00 m)	-344.89	-347.09	-2.20	-29.58	-61.60	-32.02
KA3573A (4.5-17.0 m)	-180.46	-184.33	-3.87	-22.36	-39.57	-17.20
KA3573A (18.0-40.07 m)	-36.29	-37.92	-1.63	-11.12	-23.72	-12.61
KA3574G01 (8.8-12.00 m)	-319.63	-323.88	-4.24	-319.63	-323.88	-4.24
KA3576G01 (1.3-2.8 m)	-120.56	-121.46	-0.90	-120.56	-121.46	-0.90
KA3576G01 (3.8-7.8 m)	-327.21	-328.51	-1.30	-327.21	-328.51	-1.30
KA3576G01 (8.8-12.01 m)	-162.88	-171.39	-8.51	-98.61	-116.64	-18.03
KA3578G01 (1.3-5.8 m)	-312.53	-315.48	-2.95	-312.53	-315.48	-2.95
KA3578G01 (6.8-12.58 m)	-125.69	-134.34	-8.65	-126.06	-141.68	-15.62
KA3579G (1.3-4.3 m)	-271.10	-271.84	-0.74	-104.11	-116.34	-12.22
KA3579G (5.3-8.3 m)	-344.37	-346.38	-2.01	-344.37	-346.38	-2.01
KA3579G (9.3-22.65 m)	-169.81	-180.09	-10.28	-105.73	-121.62	-15.89
KA3584G01 (0.3-12.00 m)	-300.64	-301.55	-0.92	-211.75	-221.18	-9.43
KA3590G01 (1.3-6.8 m)	-88.97	-90.49	-1.53	-48.35	-54.32	-5.96
KA3590G01 (7.8-16.3 m)	-136.18	-140.45	-4.27	-43.62	-56.27	-12.65
KA3590G01 (17.3-30.06 m)	-63.71	-66.85	-3.14	-20.97	-31.67	-10.70
KA3590G02 (1.3-7.3 m)	-105.49	-115.11	-9.62	-98.77	-106.65	-7.88
KA3590G02 (8.3-16.3 m)	-79.31	-91.07	-11.76	-40.40	-50.48	-10.08
KA3590G02 (17.3-22.3 m)	-30.03	-37.23	-7.20	-18.96	-34.07	-15.11
KA3590G02 (23.3-30.05 m)	-27.11	-35.33	-8.22	-12.78	-34.69	-21.92
KA3593G (1.3-9.3 m)	-201.60	-205.22	-3.62	-106.45	-119.57	-13.12
KA3593G (MOVED m)	-64.02	-68.16	-4.14	-47.09	-57.11	-10.02
KA3600F (4.5-21.00 m)	-15.65	-16.62	-0.97	-8.86	-12.52	-3.66
KA3600F (22.00-50.10 m)	-7.69	-8.16	-0.48	-4.26	-6.15	-1.89
KA3510a (4.52-113.02 m)	-6.55	-9.17	-2.62	-4.95	-138.44	-133.49
KG0021A01 (4-16 m)	-6.64	-11.15	-4.51	-1.05	-15.98	-14.93
KG0021A01 (17-24 m)	-8.81	-14.75	-5.94	-2.24	-38.57	-36.33
KG0021A01 (25-34 m)	-21.79	-30.42	-8.63	-2.23	-37.58	-35.35
KG0021A01 (35-41.5 m)	-27.31	-35.92	-8.61	-6.52	-45.24	-38.72
KG0021A01 (42.5-48.8 m)	-33.98	-40.55	-6.58	-8.02	-34.67	-26.65
KG0048A01 (4-12 m)	-5.67	-9.24	-3.57	-1.58	-18.21	-16.63
KG0048A01 (13-29 m)	-23.15	-34.31	-11.16	-9.47	-43.06	-33.59
KG0048A01 (30-40 m)	-40.19	-56.37	-16.18	-8.32	-26.68	-18.37
KG0048A01 (41-48 m)	-99.34	-103.90	-4.56	-8.55	-21.93	-13.37
KG0048A01 (49-54.7 m)	-100.71	-104.45	-3.75	-15.50	-27.83	-12.34

Table F.7. Drawdown in monitoring bore hole section for realisation 13 and 14. "Diff 0-4" is the draw down due to excavation of deposition holes 1 to 4, "Diff 0-6" is draw down due to excavation of all 6 deposition holes, and "Diff 4-6" is the difference in draw down between 4 excavated deposition holes and 6.

	Realisation 13			Realisation 14		
Borehole section	**Diff 0-4**	**Diff 0-6**	**Diff 4-6**	**Diff 0-4**	**Diff 0-6**	**Diff 4-6**
KA3539G (1.3-9.3 m)	-2.76	-245.92	-243.16	-4.33	-10.97	-6.64
KA3539G (9.8-18.3 m)	-3.29	-144.05	-140.76	-4.58	-10.91	-6.32
KA3539G (19.3-30.01 m)	-2.92	-82.74	-79.82	-4.88	-9.99	-5.11
KA3542G01 (1.3-7.8 m)	-2.71	-179.90	-177.19	-4.55	-12.34	-7.79
KA3542G01 (8.8-24.8 m)	-5.58	-247.56	-241.98	-3.82	-5.73	-1.91
KA3542G01 (25.8-30.04 m)	-4.10	-49.55	-45.46	-4.41	-5.80	-1.39
KA3542G02 (1.3-7.8 m)	-3.02	-74.55	-71.53	-3.13	-16.78	-13.65
KA3542G02 (8.8-12.8 m)	-2.32	-49.15	-46.82	-5.11	-13.01	-7.91
KA3542G02 (13.8-21.3 m)	-2.75	-20.01	-17.26	-3.44	-8.09	-4.65
KA3542G02 (22.3-30.01 m)	-0.87	-7.66	-6.78	-3.02	-6.98	-3.96
KA3544G01 (1.3-5.3 m)	-3.03	-291.24	-288.21	-	-452.89	-452.89
KA3544G01 (6.3-12 m)	-3.10	-302.51	-299.41	-5.09	-13.90	-8.81
KA3546G01 (1.3-5.8 m)	-2.66	-213.08	-210.43	-4.95	-169.32	-164.38
KA3546G01 (6.8-12 m)	-3.48	-308.56	-305.08	-6.44	-261.48	-255.04
KA3548A (10-14 m)	-5.80	-234.16	-228.36	-5.80	-234.16	-228.36
KA3548A (15-30 m)	-3.30	-33.09	-29.80	-5.37	-5.67	-0.30
KA3548G01 (0.3-12.01 m)	-3.44	-319.17	-315.73	-7.24	-195.82	-188.57
KA3550G01 (1.3-5.3 m)	-3.02	-239.26	-236.24	-9.49	-318.31	-308.82
KA3550G01 (6.3-12.03 m)	-5.78	-331.63	-325.85	-9.38	-282.24	-272.86
KA3552G01 (0.3-3.05 m)	-1.88	-120.71	-118.82	-10.37	-180.59	-170.23
KA3552G01 (4.05-7.8 m)	-5.75	-366.49	-360.74	-5.75	-366.49	-360.74
KA3552G01 (8.8-12.01 m)	-6.47	-231.32	-224.85	-12.02	-231.51	-219.50
KA3554G01 (1.3-11.3 m)	-6.41	-233.52	-227.10	-29.74	-31.57	-1.83
KA3554G01 (12.3-21.3 m)	-7.48	-52.01	-44.53	-18.48	-19.99	-1.51
KA3554G01 (22.3-30.01 m)	-8.49	-37.00	-28.51	-19.36	-20.28	-0.92
KA3554G02 (1.3-9.3 m)	-5.94	-53.29	-47.35	-17.38	-82.81	-65.43
KA3554G02 (10.3-21.3 m)	-6.25	-195.64	-189.39	-6.39	-14.64	-8.25
KA3554G02 (22.3-30.01 m)	-2.76	-19.19	-16.42	-4.90	-12.30	-7.40
KA3557G (0.30-8 m)	-7.95	-55.59	-47.64	-15.09	-17.80	-2.71
KA3563G (1.3-9.3 m)	-6.68	-38.60	-31.92	-6.68	-38.60	-31.92
KA3563G (MOVED m)	-72.75	-131.22	-58.48	-34.35	-39.70	-5.35
KA3563G (9.3-30.00 m)	-8.43	-46.40	-37.98	-25.38	-27.85	-2.47
KA3566G01 (1.3-6.3 m)	-53.42	-82.00	-28.58	-153.21	-154.88	-1.68
KA3566G01 (7.3-11.3 m)	-45.16	-72.84	-27.68	-45.16	-72.84	-27.68
KA3566G01 (12.3-19.8 m)	-46.69	-69.10	-22.41	-45.95	-46.63	-0.68
KA3566G01 (20.8-30.01 m)	-20.29	-35.37	-15.08	-31.29	-31.88	-0.60
KA3566G02 (1.3-6.8 m)	-6.69	-38.03	-31.33	-30.96	-36.05	-5.09
KA3566G02 (7.8-11.3 m)	-16.23	-42.21	-25.98	-30.18	-35.68	-5.50
KA3566G02 (12.3-18.3 m)	-6.73	-33.01	-26.28	-20.35	-23.81	-3.46
KA3566G02 (19.3-30.01 m)	-2.90	-19.39	-16.49	-5.03	-6.05	-1.02
KA3572G01 (1.3-5.3 m)	-307.80	-312.98	-5.18	-247.15	-247.74	-0.60
KA3572G01 (6.3-12.00 m)	-321.44	-327.10	-5.66	-204.30	-205.11	-0.81
KA3573A (4.5-17.0 m)	-49.09	-68.07	-18.98	-41.47	-42.04	-0.57
KA3573A (18.0-40.07 m)	-6.61	-16.19	-9.58	-3.22	-3.31	-0.09
KA3574G01 (8.8-12.00 m)	-364.86	-367.51	-2.65	-364.86	-367.51	-2.65
KA3576G01 (1.3-2.8 m)	-120.56	-121.46	-0.90	-120.56	-121.46	-0.90
KA3576G01 (3.8-7.8 m)	-327.36	-331.69	-4.34	-218.71	-219.09	-0.38
KA3576G01 (8.8-12.01 m)	-283.55	-290.33	-6.78	-223.67	-224.12	-0.45
KA3578G01 (1.3-5.8 m)	-342.35	-345.37	-3.02	-199.53	-199.70	-0.17
KA3578G01 (6.8-12.58 m)	-317.29	-322.02	-4.73	-188.76	-189.29	-0.53
KA3579G (1.3-4.3 m)	-345.78	-348.03	-2.25	-234.19	-234.28	-0.08
KA3579G (5.3-8.3 m)	-344.37	-346.38	-2.01	-344.37	-346.38	-2.01
KA3579G (9.3-22.65 m)	-340.69	-344.07	-3.38	-69.07	-69.91	-0.84
KA3584G01 (0.3-12.00 m)	-365.17	-366.53	-1.36	-60.53	-61.06	-0.52
KA3590G01 (1.3-6.8 m)	-44.64	-49.11	-4.47	-32.24	-32.57	-0.32
KA3590G01 (7.8-16.3 m)	-33.91	-42.67	-8.76	-18.36	-18.60	-0.25
KA3590G01 (17.3-30.06 m)	-13.35	-22.88	-9.53	-11.56	-11.78	-0.23
KA3590G02 (1.3-7.3 m)	-133.55	-137.31	-3.76	-36.51	-36.96	-0.44
KA3590G02 (8.3-16.3 m)	-24.26	-31.52	-7.26	-41.46	-42.02	-0.57
KA3590G02 (17.3-22.3 m)	-21.59	-30.36	-8.77	-25.59	-26.30	-0.71
KA3590G02 (23.3-30.05 m)	-9.73	-22.48	-12.75	-20.14	-20.94	-0.81
KA3593G (1.3-9.3 m)	-104.43	-113.15	-8.73	-37.63	-38.03	-0.40
KA3593G (MOVED m)	-24.28	-29.23	-4.96	-29.11	-29.46	-0.35
KA3600F (4.5-21.00 m)	-5.88	-9.44	-3.56	-3.68	-3.76	-0.08
KA3600F (22.00-50.10 m)	-1.28	-1.90	-0.62	-0.36	-0.37	-0.01
KA3510a (4.52-113.02 m)	-3.64	-25.01	-21.37	-3.42	-4.81	-1.40
KG0021A01 (4-16 m)	-0.37	-3.95	-3.58	-1.28	-2.56	-1.28
KG0021A01 (17-24 m)	-1.40	-16.69	-15.29	-2.38	-4.72	-2.34
KG0021A01 (25-34 m)	-2.08	-26.18	-24.10	-2.62	-4.03	-1.41
KG0021A01 (35-41.5 m)	-3.33	-39.34	-36.01	-6.79	-7.62	-0.83
KG0021A01 (42.5-48.8 m)	-3.23	-38.53	-35.30	-6.75	-7.55	-0.80
KG0048A01 (4-12 m)	-2.00	-7.15	-5.14	-1.67	-2.22	-0.55
KG0048A01 (13-29 m)	-9.54	-19.50	-9.97	-11.64	-13.00	-1.36
KG0048A01 (30-40 m)	-11.89	-21.46	-9.57	-13.07	-14.27	-1.20
KG0048A01 (41-48 m)	-10.78	-18.57	-7.80	-12.60	-13.13	-0.53
KG0048A01 (49-54.7 m)	-9.59	-15.68	-6.08	-11.65	-11.89	-0.24

Table F.8. Drawdown in monitoring bore hole section for realisation 15 and 16. "Diff 0-4" is the draw down due to excavation of deposition holes 1 to 4, "Diff 0-6" is draw down due to excavation of all 6 deposition holes, and "Diff 4-6" is the difference in draw down between 4 excavated deposition holes and 6.

	Realisation 15			Realisation 16		
Borehole section	**Diff 0-4**	**Diff 0-6**	**Diff 4-6**	**Diff 0-4**	**Diff 0-6**	**Diff 4-6**
KA3539G (1.3-9.3 m)	-16.09	-141.72	-125.63	-16.09	-141.72	-125.63
KA3539G (9.8-18.3 m)	-14.67	-53.40	-38.73	-12.36	-162.32	-149.96
KA3539G (19.3-30.01 m)	-13.74	-41.94	-28.20	-7.67	-84.43	-76.77
KA3542G01 (1.3-7.8 m)	-4.55	-12.34	-7.79	-12.75	-185.14	-172.39
KA3542G01 (8.8-24.8 m)	-29.79	-59.44	-29.64	-9.37	-79.91	-70.53
KA3542G01 (25.8-30.04 m)	-6.06	-9.72	-3.66	-6.06	-9.72	-3.66
KA3542G02 (1.3-7.8 m)	-3.13	-16.78	-13.65	-5.80	-113.81	-108.01
KA3542G02 (8.8-12.8 m)	-9.63	-23.36	-13.73	-13.75	-110.03	-96.28
KA3542G02 (13.8-21.3 m)	-5.03	-11.87	-6.85	-9.39	-66.08	-56.69
KA3542G02 (22.3-30.01 m)	-2.03	-5.03	-3.00	-6.53	-41.32	-34.79
KA3544G01 (1.3-5.3 m)	-18.10	-398.34	-380.25	-18.23	-398.57	-380.34
KA3544G01 (6.3-12 m)	-16.58	-180.25	-163.67	-14.64	-333.06	-318.42
KA3546G01 (1.3-5.8 m)	-18.43	-373.56	-355.12	-18.56	-378.37	-359.81
KA3546G01 (6.8-12 m)	-18.44	-323.48	-305.05	-15.14	-365.52	-350.38
KA3548A (10-14 m)	-33.76	-39.72	-5.97	-24.65	-59.23	-34.58
KA3548A (15-30 m)	-11.68	-13.43	-1.76	-24.35	-32.45	-8.10
KA3548G01 (0.3-12.01 m)	-18.81	-207.39	-188.57	-19.54	-383.53	-363.99
KA3550G01 (1.3-5.3 m)	-9.49	-318.31	-308.82	-9.49	-318.31	-308.82
KA3550G01 (6.3-12.03 m)	-19.06	-194.86	-175.79	-19.62	-388.77	-369.15
KA3552G01 (0.3-3.05 m)	-10.37	-180.59	-170.23	-10.37	-180.59	-170.23
KA3552G01 (4.05-7.8 m)	-37.42	-312.52	-275.10	-22.74	-393.79	-371.04
KA3552G01 (8.8-12.01 m)	-26.85	-142.38	-115.53	-21.00	-303.47	-282.47
KA3554G01 (1.3-11.3 m)	-77.58	-91.71	-14.13	-26.35	-225.83	-199.48
KA3554G01 (12.3-21.3 m)	-43.49	-58.86	-15.37	-31.88	-80.98	-49.11
KA3554G01 (22.3-30.01 m)	-22.09	-26.95	-4.87	-30.80	-50.32	-19.52
KA3554G02 (1.3-9.3 m)	-12.15	-31.60	-19.45	-22.04	-111.44	-89.40
KA3554G02 (10.3-21.3 m)	-17.82	-31.84	-14.01	-17.50	-100.53	-83.03
KA3554G02 (22.3-30.01 m)	-8.45	-19.67	-11.22	-10.75	-52.96	-42.21
KA3557G (0.30-8 m)	-24.26	-50.93	-26.67	-29.05	-153.04	-123.99
KA3563G (1.3-9.3 m)	-6.68	-38.60	-31.92	-6.68	-38.60	-31.92
KA3563G (MOVED m)	-186.84	-196.99	-10.15	-258.65	-303.17	-44.52
KA3563G (9.3-30.00 m)	-27.50	-47.51	-20.01	-70.48	-92.86	-22.38
KA3566G01 (1.3-6.3 m)	-157.79	-163.52	-5.72	-241.34	-248.82	-7.47
KA3566G01 (7.3-11.3 m)	-96.93	-100.89	-3.96	-104.43	-168.57	-64.14
KA3566G01 (12.3-19.8 m)	-60.74	-64.40	-3.66	-116.27	-123.10	-6.83
KA3566G01 (20.8-30.01 m)	-41.83	-45.18	-3.35	-58.75	-64.89	-6.14
KA3566G02 (1.3-6.8 m)	-230.43	-236.21	-5.79	-148.61	-208.78	-60.18
KA3566G02 (7.8-11.3 m)	-40.23	-58.36	-18.14	-40.23	-58.36	-18.14
KA3566G02 (12.3-18.3 m)	-17.91	-31.89	-13.98	-23.07	-108.31	-85.25
KA3566G02 (19.3-30.01 m)	-9.71	-20.47	-10.76	-22.28	-90.08	-67.79
KA3572G01 (1.3-5.3 m)	-336.88	-337.52	-0.64	-375.19	-376.09	-0.90
KA3572G01 (6.3-12.00 m)	-204.30	-205.11	-0.81	-289.26	-293.51	-4.25
KA3573A (4.5-17.0 m)	-17.59	-18.92	-1.33	-98.76	-105.43	-6.67
KA3573A (18.0-40.07 m)	-8.84	-9.60	-0.76	-44.94	-50.67	-5.72
KA3574G01 (8.8-12.00 m)	-364.86	-367.51	-2.65	-273.77	-278.41	-4.64
KA3576G01 (1.3-2.8 m)	-192.11	-193.20	-1.08	-192.11	-193.20	-1.08
KA3576G01 (3.8-7.8 m)	-314.63	-315.66	-1.04	-283.67	-287.16	-3.50
KA3576G01 (8.8-12.01 m)	-223.67	-224.12	-0.45	-226.19	-231.43	-5.24
KA3578G01 (1.3-5.8 m)	-199.53	-199.70	-0.17	-199.53	-199.70	-0.17
KA3578G01 (6.8-12.58 m)	-271.24	-272.80	-1.56	-212.98	-218.79	-5.81
KA3579G (1.3-4.3 m)	-234.19	-234.28	-0.08	-301.69	-305.10	-3.41
KA3579G (5.3-8.3 m)	-334.95	-335.68	-0.72	-319.28	-322.22	-2.95
KA3579G (9.3-22.65 m)	-138.43	-142.20	-3.77	-171.82	-178.92	-7.10
KA3584G01 (0.3-12.00 m)	-160.87	-163.00	-2.13	-214.89	-219.68	-4.78
KA3590G01 (1.3-6.8 m)	-18.66	-19.53	-0.87	-127.36	-131.93	-4.56
KA3590G01 (7.8-16.3 m)	-21.75	-23.15	-1.40	-109.95	-114.55	-4.60
KA3590G01 (17.3-30.06 m)	-12.04	-13.14	-1.10	-60.43	-64.19	-3.77
KA3590G02 (1.3-7.3 m)	-88.32	-91.19	-2.87	-53.09	-54.28	-1.19
KA3590G02 (8.3-16.3 m)	-51.43	-55.32	-3.89	-82.03	-91.47	-9.44
KA3590G02 (17.3-22.3 m)	-18.44	-22.21	-3.77	-69.39	-77.47	-8.07
KA3590G02 (23.3-30.05 m)	-13.01	-16.40	-3.39	-63.13	-77.64	-14.51
KA3593G (1.3-9.3 m)	-32.64	-34.43	-1.80	-150.35	-155.40	-5.05
KA3593G (MOVED m)	-24.43	-26.00	-1.57	-41.97	-46.29	-4.32
KA3600F (4.5-21.00 m)	-2.60	-2.85	-0.24	-15.89	-17.47	-1.59
KA3600F (22.00-50.10 m)	-1.91	-2.09	-0.18	-3.96	-4.35	-0.39
KA3510a (4.52-113.02 m)	-5.95	-9.45	-3.50	-3.74	-8.30	-4.56
KG0021A01 (4-16 m)	-1.76	-3.66	-1.90	-2.69	-16.02	-13.33
KG0021A01 (17-24 m)	-3.65	-7.75	-4.10	-9.22	-50.11	-40.89
KG0021A01 (25-34 m)	-3.97	-6.93	-2.96	-10.68	-48.84	-38.16
KG0021A01 (35-41.5 m)	-10.50	-13.76	-3.27	-16.09	-42.32	-26.23
KG0021A01 (42.5-48.8 m)	-11.53	-12.88	-1.35	-19.92	-40.90	-20.98
KG0048A01 (4-12 m)	-6.21	-9.29	-3.08	-4.44	-16.06	-11.62
KG0048A01 (13-29 m)	-17.40	-22.80	-5.40	-32.23	-83.65	-51.42
KG0048A01 (30-40 m)	-43.81	-47.57	-3.77	-73.75	-100.58	-26.83
KG0048A01 (41-48 m)	-51.02	-54.14	-3.12	-24.38	-31.02	-6.64
KG0048A01 (49-54.7 m)	-16.87	-18.11	-1.24	-61.06	-67.03	-5.97

Table F.9. Drawdown in monitoring bore hole section for realisation 17 and 18. "Diff 0-4" is the draw down due to excavation of deposition holes 1 to 4, "Diff 0-6" is draw down due to excavation of all 6 deposition holes, and "Diff 4-6" is the difference in draw down between 4 excavated deposition holes and 6.

	Realisation 17			Realisation 18		
Borehole section	**Diff 0-4**	**Diff 0-6**	**Diff 4-6**	**Diff 0-4**	**Diff 0-6**	**Diff 4-6**
KA3539G (1.3-9.3 m)	-12.14	-225.40	-213.26	-1.67	-18.09	-16.41
KA3539G (9.8-18.3 m)	-11.89	-99.66	-87.77	-1.65	-22.54	-20.90
KA3539G (19.3-30.01 m)	-12.13	-70.49	-58.36	-2.85	-19.82	-16.97
KA3542G01 (1.3-7.8 m)	-13.19	-196.78	-183.59	-3.06	-203.18	-200.12
KA3542G01 (8.8-24.8 m)	-11.59	-20.84	-9.25	-2.64	-8.23	-5.59
KA3542G01 (25.8-30.04 m)	-15.03	-23.54	-8.51	-2.58	-7.03	-4.45
KA3542G02 (1.3-7.8 m)	-11.68	-56.11	-44.43	-1.84	-19.72	-17.88
KA3542G02 (8.8-12.8 m)	-9.76	-43.90	-34.14	-9.76	-43.90	-34.14
KA3542G02 (13.8-21.3 m)	-8.98	-38.40	-29.43	-4.54	-9.26	-4.72
KA3542G02 (22.3-30.01 m)	-5.12	-16.21	-11.10	-1.63	-5.04	-3.41
KA3544G01 (1.3-5.3 m)	-11.26	-311.75	-300.49	-1.27	-129.41	-128.15
KA3544G01 (6.3-12 m)	-15.96	-221.63	-205.67	-15.96	-221.63	-205.67
KA3546G01 (1.3-5.8 m)	-15.05	-341.38	-326.33	-15.05	-341.38	-326.33
KA3546G01 (6.8-12 m)	-17.64	-203.46	-185.81	-4.42	-279.23	-274.81
KA3548A (10-14 m)	-16.58	-23.97	-7.39	-16.58	-23.97	-7.39
KA3548A (15-30 m)	-10.99	-13.40	-2.41	-2.03	-4.23	-2.20
KA3548G01 (0.3-12.01 m)	-20.55	-185.17	-164.62	-6.16	-252.02	-245.86
KA3550G01 (1.3-5.3 m)	-9.49	-318.31	-308.82	-8.89	-326.25	-317.36
KA3550G01 (6.3-12.03 m)	-23.38	-181.60	-158.21	-7.36	-270.88	-263.53
KA3552G01 (0.3-3.05 m)	-5.37	-58.57	-53.20	-3.03	-7.27	-4.24
KA3552G01 (4.05-7.8 m)	-22.74	-393.79	-371.04	-9.18	-290.87	-281.69
KA3552G01 (8.8-12.01 m)	-21.00	-303.47	-282.47	-21.00	-303.47	-282.47
KA3554G01 (1.3-11.3 m)	-21.68	-41.49	-19.80	-7.46	-18.15	-10.69
KA3554G01 (12.3-21.3 m)	-28.83	-41.74	-12.91	-4.41	-7.77	-3.37
KA3554G01 (22.3-30.01 m)	-15.79	-24.47	-8.68	-2.53	-5.34	-2.82
KA3554G02 (1.3-9.3 m)	-23.44	-99.99	-76.56	-11.22	-23.54	-12.32
KA3554G02 (10.3-21.3 m)	-15.59	-56.67	-41.07	-11.29	-21.58	-10.29
KA3554G02 (22.3-30.01 m)	-10.77	-27.50	-16.73	-5.38	-8.92	-3.54
KA3557G (0.30-8 m)	-52.03	-71.43	-19.40	-10.42	-23.54	-13.12
KA3563G (1.3-9.3 m)	-6.68	-38.60	-31.92	-6.68	-38.60	-31.92
KA3563G (MOVED m)	-258.65	-303.17	-44.52	-17.60	-25.78	-8.18
KA3563G (9.3-30.00 m)	-80.81	-94.02	-13.21	-12.78	-22.68	-9.91
KA3566G01 (1.3-6.3 m)	-36.21	-37.27	-1.06	-17.40	-25.45	-8.05
KA3566G01 (7.3-11.3 m)	-109.21	-115.79	-6.58	-19.50	-22.02	-2.52
KA3566G01 (12.3-19.8 m)	-109.43	-112.57	-3.14	-3.46	-5.48	-2.02
KA3566G01 (20.8-30.01 m)	-38.89	-41.41	-2.52	-3.41	-5.67	-2.26
KA3566G02 (1.3-6.8 m)	-63.12	-95.41	-32.29	-21.73	-27.84	-6.11
KA3566G02 (7.8-11.3 m)	-40.23	-58.36	-18.14	-16.64	-23.58	-6.94
KA3566G02 (12.3-18.3 m)	-26.26	-78.20	-51.93	-15.42	-20.63	-5.21
KA3566G02 (19.3-30.01 m)	-12.52	-20.29	-7.77	-6.34	-9.76	-3.42
KA3572G01 (1.3-5.3 m)	-285.01	-286.89	-1.88	-328.75	-328.81	-0.06
KA3572G01 (6.3-12.00 m)	-286.65	-289.15	-2.50	-285.23	-286.01	-0.78
KA3573A (4.5-17.0 m)	-93.51	-95.47	-1.96	-3.88	-5.35	-1.47
KA3573A (18.0-40.07 m)	-19.09	-19.96	-0.87	-0.97	-1.46	-0.50
KA3574G01 (8.8-12.00 m)	-273.77	-278.41	-4.64	-273.77	-278.41	-4.64
KA3576G01 (1.3-2.8 m)	-185.74	-185.83	-0.09	-185.74	-185.83	-0.09
KA3576G01 (3.8-7.8 m)	-307.26	-307.45	-0.18	-335.01	-335.01	0.00
KA3576G01 (8.8-12.01 m)	-226.19	-231.43	-5.24	-272.64	-273.26	-0.62
KA3578G01 (1.3-5.8 m)	-199.53	-199.70	-0.17	-199.53	-199.70	-0.17
KA3578G01 (6.8-12.58 m)	-329.90	-330.91	-1.01	-147.69	-149.09	-1.40
KA3579G (1.3-4.3 m)	-331.91	-332.48	-0.57	-331.91	-332.48	-0.57
KA3579G (5.3-8.3 m)	-363.80	-364.00	-0.20	-363.80	-364.00	-0.20
KA3579G (9.3-22.65 m)	-278.60	-280.51	-1.90	-137.12	-138.70	-1.58
KA3584G01 (0.3-12.00 m)	-260.46	-261.74	-1.28	-235.76	-236.29	-0.53
KA3590G01 (1.3-6.8 m)	-86.61	-87.87	-1.26	-5.48	-6.12	-0.64
KA3590G01 (7.8-16.3 m)	-84.42	-85.69	-1.27	-2.35	-2.77	-0.42
KA3590G01 (17.3-30.06 m)	-21.21	-22.02	-0.81	-2.64	-3.25	-0.61
KA3590G02 (1.3-7.3 m)	-110.12	-111.92	-1.80	-58.79	-59.79	-1.01
KA3590G02 (8.3-16.3 m)	-305.78	-306.79	-1.01	-28.35	-28.86	-0.50
KA3590G02 (17.3-22.3 m)	-69.39	-77.47	-8.07	-34.85	-36.86	-2.01
KA3590G02 (23.3-30.05 m)	-20.66	-27.80	-7.14	-16.76	-19.55	-2.78
KA3593G (1.3-9.3 m)	-114.90	-116.48	-1.58	-11.25	-12.47	-1.23
KA3593G (MOVED m)	-85.49	-86.66	-1.17	-7.13	-7.81	-0.68
KA3600F (4.5-21.00 m)	-6.91	-7.21	-0.30	-2.06	-2.31	-0.25
KA3600F (22.00-50.10 m)	-1.13	-1.20	-0.07	-0.27	-0.31	-0.04
KA3510a (4.52-113.02 m)	-10.12	-17.61	-7.49	-2.10	-6.95	-4.85
KG0021A01 (4-16 m)	-3.36	-9.73	-6.38	-1.76	-2.82	-1.07
KG0021A01 (17-24 m)	-6.39	-20.13	-13.74	-4.35	-7.32	-2.97
KG0021A01 (25-34 m)	-9.77	-32.95	-23.18	-5.25	-7.93	-2.68
KG0021A01 (35-41.5 m)	-9.56	-17.56	-8.00	-6.98	-9.73	-2.75
KG0021A01 (42.5-48.8 m)	-14.57	-18.67	-4.09	-2.99	-4.32	-1.33
KG0048A01 (4-12 m)	-6.35	-11.99	-5.64	-4.78	-6.29	-1.51
KG0048A01 (13-29 m)	-14.05	-24.55	-10.50	-13.27	-15.96	-2.68
KG0048A01 (30-40 m)	-43.32	-50.66	-7.34	-23.77	-26.87	-3.10
KG0048A01 (41-48 m)	-46.18	-48.71	-2.53	-8.31	-9.43	-1.11
KG0048A01 (49-54.7 m)	-46.77	-48.90	-2.13	-3.22	-4.11	-0.89

Table F.10. Drawdown in monitoring bore hole section for realisation 19 and 20. "Diff 0-4" is the draw down due to excavation of deposition holes 1 to 4, "Diff 0-6" is draw down due to excavation of all 6 deposition holes, and "Diff 4-6" is the difference in draw down between 4 excavated deposition holes and 6.

	Realisation 19			Realisation 20		
Borehole section	**Diff 0-4**	**Diff 0-6**	**Diff 4-6**	**Diff 0-4**	**Diff 0-6**	**Diff 4-6**
KA3539G (1.3-9.3 m)	-17.68	-51.29	-33.61	-27.36	-120.59	-93.23
KA3539G (9.8-18.3 m)	-25.42	-81.27	-55.85	-28.17	-59.06	-30.89
KA3539G (19.3-30.01 m)	-49.46	-59.86	-10.39	-39.45	-50.23	-10.77
KA3542G01 (1.3-7.8 m)	-22.86	-45.46	-22.60	-27.07	-41.68	-14.61
KA3542G01 (8.8-24.8 m)	-55.65	-63.22	-7.57	-24.56	-29.41	-4.85
KA3542G01 (25.8-30.04 m)	-2.58	-7.03	-4.45	-2.58	-7.03	-4.45
KA3542G02 (1.3-7.8 m)	-14.36	-51.82	-37.46	-64.40	-82.07	-17.67
KA3542G02 (8.8-12.8 m)	-12.90	-31.74	-18.84	-64.61	-78.95	-14.34
KA3542G02 (13.8-21.3 m)	-9.15	-14.34	-5.19	-54.02	-60.57	-6.55
KA3542G02 (22.3-30.01 m)	-1.96	-2.63	-0.66	-47.36	-51.62	-4.25
KA3544G01 (1.3-5.3 m)	-17.19	-274.65	-257.46	-	-452.90	-452.90
KA3544G01 (6.3-12 m)	-34.48	-130.53	-96.06	-33.55	-265.90	-232.35
KA3546G01 (1.3-5.8 m)	-26.00	-155.11	-129.11	-31.61	-268.30	-236.70
KA3546G01 (6.8-12 m)	-49.12	-226.73	-177.61	-42.69	-173.24	-130.54
KA3548A (10-14 m)	-16.58	-23.97	-7.39	-38.49	-41.97	-3.49
KA3548A (15-30 m)	-12.96	-14.44	-1.48	-34.62	-37.51	-2.89
KA3548G01 (0.3-12.01 m)	-48.16	-221.30	-173.13	-42.41	-214.15	-171.74
KA3550G01 (1.3-5.3 m)	-8.89	-326.25	-317.36	-53.65	-324.37	-270.72
KA3550G01 (6.3-12.03 m)	-55.22	-295.39	-240.17	-57.13	-389.78	-332.65
KA3552G01 (0.3-3.05 m)	-3.03	-7.27	-4.24	-3.03	-7.27	-4.24
KA3552G01 (4.05-7.8 m)	-65.28	-309.41	-244.12	-62.13	-305.32	-243.19
KA3552G01 (8.8-12.01 m)	-76.12	-86.75	-10.63	-61.47	-134.94	-73.47
KA3554G01 (1.3-11.3 m)	-85.93	-93.52	-7.59	-85.93	-93.52	-7.59
KA3554G01 (12.3-21.3 m)	-77.03	-82.91	-5.87	-68.70	-75.10	-6.40
KA3554G01 (22.3-30.01 m)	-2.53	-5.34	-2.82	-36.74	-40.45	-3.71
KA3554G02 (1.3-9.3 m)	-36.24	-60.21	-23.97	-73.12	-115.83	-42.71
KA3554G02 (10.3-21.3 m)	-18.81	-21.49	-2.68	-79.05	-83.89	-4.84
KA3554G02 (22.3-30.01 m)	-8.64	-11.02	-2.38	-48.40	-52.14	-3.74
KA3557G (0.30-8 m)	-75.90	-84.32	-8.43	-76.27	-83.96	-7.69
KA3563G (1.3-9.3 m)	-6.68	-38.60	-31.92	-6.68	-38.60	-31.92
KA3563G (MOVED m)	-97.27	-104.35	-7.08	-279.05	-280.42	-1.37
KA3563G (9.3-30.00 m)	-79.08	-84.54	-5.46	-370.77	-371.02	-0.24
KA3566G01 (1.3-6.3 m)	-89.04	-94.88	-5.83	-229.22	-230.94	-1.72
KA3566G01 (7.3-11.3 m)	-102.93	-107.61	-4.69	-102.93	-107.61	-4.69
KA3566G01 (12.3-19.8 m)	-45.28	-47.01	-1.74	-91.51	-95.41	-3.90
KA3566G01 (20.8-30.01 m)	-25.34	-26.71	-1.37	-44.95	-47.88	-2.93
KA3566G02 (1.3-6.8 m)	-73.42	-77.03	-3.62	-126.07	-129.14	-3.07
KA3566G02 (7.8-11.3 m)	-49.20	-51.97	-2.78	-100.96	-104.45	-3.48
KA3566G02 (12.3-18.3 m)	-23.27	-24.98	-1.70	-80.47	-84.14	-3.67
KA3566G02 (19.3-30.01 m)	-15.70	-17.09	-1.39	-62.32	-66.09	-3.77
KA3572G01 (1.3-5.3 m)	-328.75	-328.81	-0.06	-317.14	-317.82	-0.69
KA3572G01 (6.3-12.00 m)	-264.24	-266.87	-2.63	-214.10	-215.70	-1.60
KA3573A (4.5-17.0 m)	-30.91	-32.15	-1.23	-72.89	-75.35	-2.46
KA3573A (18.0-40.07 m)	-3.08	-3.28	-0.20	-29.64	-30.79	-1.16
KA3574G01 (8.8-12.00 m)	-345.88	-346.67	-0.80	-196.13	-197.64	-1.51
KA3576G01 (1.3-2.8 m)	-185.74	-185.83	-0.09	-185.74	-185.83	-0.09
KA3576G01 (3.8-7.8 m)	-332.62	-333.34	-0.73	-290.35	-291.24	-0.89
KA3576G01 (8.8-12.01 m)	-256.45	-258.04	-1.59	-167.79	-169.56	-1.77
KA3578G01 (1.3-5.8 m)	-247.17	-248.38	-1.21	-217.59	-219.03	-1.43
KA3578G01 (6.8-12.58 m)	-222.85	-224.65	-1.80	-119.19	-121.16	-1.96
KA3579G (1.3-4.3 m)	-179.06	-180.55	-1.49	-179.06	-180.55	-1.49
KA3579G (5.3-8.3 m)	-270.18	-271.38	-1.20	-269.44	-269.82	-0.38
KA3579G (9.3-22.65 m)	-151.81	-153.22	-1.41	-115.47	-117.38	-1.91
KA3584G01 (0.3-12.00 m)	-302.61	-303.07	-0.46	-81.58	-81.64	-0.06
KA3590G01 (1.3-6.8 m)	-24.03	-24.53	-0.50	-105.48	-106.16	-0.68
KA3590G01 (7.8-16.3 m)	-16.19	-16.68	-0.49	-142.81	-144.07	-1.26
KA3590G01 (17.3-30.06 m)	-6.92	-7.28	-0.37	-53.75	-55.33	-1.58
KA3590G02 (1.3-7.3 m)	-150.49	-151.17	-0.68	-165.99	-166.69	-0.70
KA3590G02 (8.3-16.3 m)	-69.33	-69.82	-0.49	-78.93	-80.05	-1.12
KA3590G02 (17.3-22.3 m)	-37.57	-38.31	-0.74	-74.78	-76.03	-1.25
KA3590G02 (23.3-30.05 m)	-21.90	-22.71	-0.81	-57.16	-58.26	-1.10
KA3593G (1.3-9.3 m)	-53.38	-54.18	-0.79	-179.14	-180.11	-0.97
KA3593G (MOVED m)	-7.35	-7.56	-0.21	-131.01	-131.91	-0.90
KA3600F (4.5-21.00 m)	-7.23	-7.49	-0.26	-9.93	-10.24	-0.31
KA3600F (22.00-50.10 m)	-0.38	-0.40	-0.02	-0.72	-0.74	-0.02
KA3510a (4.52-113.02 m)	-8.94	-11.37	-2.42	-9.49	-10.80	-1.31
KG0021A01 (4-16 m)	-3.11	-4.69	-1.58	-36.10	-38.55	-2.45
KG0021A01 (17-24 m)	-3.79	-5.54	-1.75	-35.12	-37.07	-1.95
KG0021A01 (25-34 m)	-8.63	-11.04	-2.41	-43.76	-46.72	-2.96
KG0021A01 (35-41.5 m)	-6.98	-9.73	-2.75	-36.19	-38.43	-2.24
KG0021A01 (42.5-48.8 m)	-18.33	-19.77	-1.44	-33.63	-35.53	-1.90
KG0048A01 (4-12 m)	-4.78	-6.29	-1.51	-49.96	-52.46	-2.50
KG0048A01 (13-29 m)	-16.85	-18.09	-1.24	-68.05	-70.80	-2.75
KG0048A01 (30-40 m)	-20.95	-21.93	-0.98	-51.76	-53.72	-1.96
KG0048A01 (41-48 m)	-28.75	-29.27	-0.52	-43.50	-45.06	-1.56
KG0048A01 (49-54.7 m)	-17.04	-17.72	-0.67	-48.63	-50.18	-1.55